The Behaviour of Sheathed Cold-Formed Steel Stud Wall Systems under In-plane and Out-of-plane Loading

by

Fatih Yilmaz

A thesis submitted in fulfilment of the requirements for the degree of
Doctor of Philosophy

The University of Sheffield
Faculty of Engineering
Department of Civil and Structural Engineering

June 2022

Abstract

Cold-formed steel (CFS) stud walls have been used extensively in the construction of low to medium-rise buildings, where they provide advantages of cost and material efficiency, offsite manufacturing, a panelized/modular approach and fast construction speeds. This study aims to develop a better understanding of the structural behaviour and performance of sheathed stud wall panels under in-plane and out-of-plane loadings considering the effects of key design parameters on the performance of these systems. To this end, detailed nonlinear finite element (FE) models of panel were developed to investigate the lateral behaviour of such systems by considering geometric imperfections and nonlinear material properties. The FE models, which were validated against available experimental data from the literature, were employed to conduct comprehensive parametric studies to assess the effects of key design variables, including screw spacing, thickness of Oriented Strand Board (OSB) and CFS members, board configuration, gravity load and single- and double-sheathed systems on the response of sheathed stud wall. The structural performance parameters and seismic characteristics of the studied panels were compared in terms of lateral load capacity, initial stiffness, failure mechanism, deformation capacity, ductility, and energy dissipation. Then, comprehensive experimental testing of sheathed CFS stud wall panels under out-of-plane loading was carried out to investigate the bending behaviour of the wall system by taking into account screw spacing, different material properties (i.e. thickness of OSB and CFS, and plywood), board scenarios and effects of main/auxiliary components. Based on the test results, the structural performance parameters (i.e. bending load capacity, maximum vertical deflection), failure mechanism, rotation of the C-shape studs and end-slips of the stud wall panels were determined for each parameter. In light of the analytical and experimental studies performed in this work, it was observed that the connection point for this type of composite structure plays an important role due to the fact that the capacity of sheathed CFS stud wall systems directly dependent on the behaviour of the fasteners. Therefore, small-scale specimens consisting of CFS stud members attached to wood-based boards were tested to characterise the behaviour of the load-slip response under push-out (shear), pull-out (tension) and rotational actions. The numerical and experimental key results of the work were summarised herein, aiming to provide a better understanding of the behaviour of fasteners and make data available for further analytical/numerical research.

Acknowledgements

Table of Contents

List of Figures

List of Tables

List of Notations

A	Area of the coupon samples
a	Flange dimensions of the CFS cross section (top)
a_1	Location point at the wood-based board (top)
b	Web dimensions of the CFS cross section
b_1	Location point at the wood-based board (middle)
c	Flange dimensions of the CFS cross section (bottom)
$C1$	Coefficient of load-slip relationship for fasteners
c_1	Location point at the wood-based board (bottom)
$C2$	Coefficient of load-slip relationship for fasteners
C_b	Compressive strength of floorboard
d	Lip dimensions of the CFS cross section (top)
E	Energy dissipation capacity
e	Lip dimensions of the CFS cross section (bottom)
$E_{,CFS}$	Elastic modulus of CFS

$E_{0.2}$	Tangent modulus at the 0.2% proof stress
$E_{c,OSB}$	Elastic modulus of OSB in compression
$E_{t,OSB}$	Elastic modulus of OSB in tension
ε_{true}	True strain
$\varepsilon_{c,OSB}$	The strains corresponding to the $\sigma_{c,OSB}$
ε_{u}	The strains corresponding to the σ_{u}
F_{max}	Maximum lateral load capacity
$f_{t,osb}$	Ultimate tensile stress of the OSB
$f_{u.CFS}$	Ultimate strength of the steel
F_{y}	Yielding strength
$f_{y,CFS}$	Yield stress of the steel
K_{o}	Slip modulus of connector
p	Load per connector
P_{b}	Bearing resistance of the board
$P\text{-}s$	Load-slip responses
P_{u}	Ultimate load per connector
P_{ult}	Load ultimate
P_{v}	Shear resistance of connector

R_i	Initial stiffness of each connection
r_{int}	Bending radius of the corner of a steel section
s	Slip
S_b	Sb is the slip corresponding to Pb
S_i	Initial stiffness
s_u	The slip at the ultimate load
t	Thickness
UR_x	Rotation at the X-axis
URy	Rotation at the Y-axis
URz	Rotation at the Z-axis
U_x	Displacement at the X-axis
U_y	Displacement at the Y-axis
U_z	Displacement at the Z-axis
δ_{flange}	The out-of-plane imperfections along the centre line of the flange
Δ_u	Ultimate displacement
δ_{web}	The out-of-plane imperfections along the centre line of the web
$\varepsilon_{f.CFS}$	Strain at fracture of the steel
$\varepsilon_{u.CFS}$	Ultimate strain of the steel
σ_u	Yield stress strength of CFS

σ_y	Tensile strength of CFS
$F_{Max,Exp}$	Maximum lateral strength of the experiment
$F_{Max,FE}$	Maximum lateral strength of the FE model
$S_{i,Exp}$	İnitial secant stiffness of the experiment
$S_{i,FE}$	İnitial secant stiffness of the FE model
$\Delta_{u,Exp}$	Ultimate displacements of the FE model
$\Delta_{u,FE}$	Ultimate displacements of the experiment
μ	Ductility
$\sigma_{c,OSB}$	Compressive stresses of OSB
$\sigma_{t,OSB}$	The ultimate tensile stresses of OSB
σ_{true}	The true stress
υ_{CFS}	The Poisson ratios of the CFS
υ_{OSB}	The Poisson ratios of the OSB materials

List of Abbreviations

AISI   American Iron and Steel Institute

ASTM   American Society for Testing and Materials

CFS   Cold-Formed Steel

CSB   Calcium Silicate Board

EEEP   Equivalent Energy Elastic-Plastic

ESM   Effective Strip Method

FCB   Fibre-Cement Board

FE   Finite Element

FGD   Flue Gas Desulphurisation

ICBO   International Council of Building Officials

LRFD   Load and Resistance Factor Design

NRCC   National Republican Congressional Committee

OSB   Oriented Strand Board

PBSD   Performance-Based Seismic Design

PGA	Peak Ground Acceleration
R	The Seismic Response Reduction Factor
SPR	Self-Piercing Riveted
TCB	Tension Control Bolt
WSP	Wood Sheathing Panel

Chapter 1: Introduction

1.1. Background

Cold-formed steel (CFS) is identified as a lightweight structural material manufactured at room temperature by bending thin steel sheets into different cross-sections such as C, Z and Σ profiles, as depicted in Fig. 1.1. The thickness of CFS usually varies from 0.5 to 6 mm and, roofing and wall cladding are made of sheets of profiled with thicknesses of up to 1.5 mm (Dubina et al., 2012).
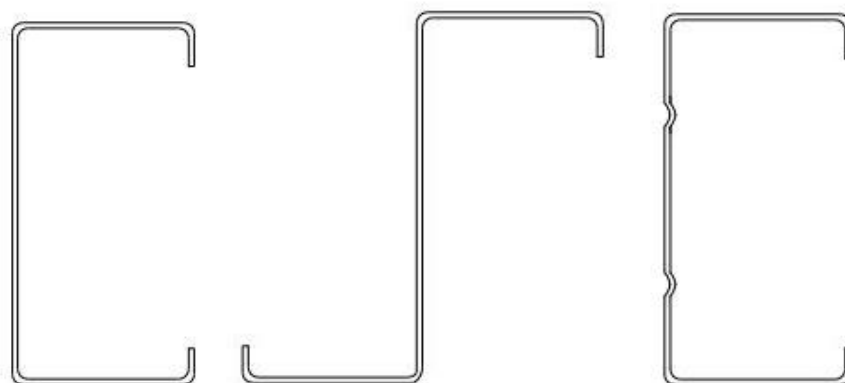
Figure 1.1 Typical popular cross-sectional shapes of cold-formed steel members

CFS section members are manufactured by a press-braking or a rolling process. These procedures provide flexibility in cross-sectional shapes as well as adapt to use different applications for the CFS material. Despite CFS started to be used in the UK and America during the 1850s (Allen, 2006), the CFS has especially gained popularity in the modern construction industry in recent years as secondary load-carrying systems (i.e. wall girts and roof purlins (Hancock et al., 1990)) due to its uniform quality, ease of mass production and prefabrication, lightweight designs, quick and straightforward installations and more accessible transportation and handling compared to other construction materials (Schafer et al., 2016). With the growth in use of CFS elements in constructions, the cold-formed steel wall systems sheathed with boards are generally being preferred for the lateral load resisting systems in low- to medium-rise steel-framed buildings because modular construction systems of sheathed cold-formed steel frames offer an elegant, fast and versatile solution for building low to medium-rise structures. It should be noted that sheathed panels have advantages over the braced ones in terms of lateral stiffness and load-bearing capacity as well as seismic characteristics (i.e. energy dissipation) (Accorti et al., 2016). Therefore, this increase in use of structure was exerting an increased demand on sheathed wall systems in terms of developing more reliable and resilient CFS wall systems.

The using of sheathed CFS shear wall systems was started as early as 1970. CFS stud wall systems are basically designed to resist lateral forces on buildings and also to support the gravity and axial loads. Sheathed CFS wall systems are composed of the CFS framing elements (i.e. studs and track) which are connected to the sheathing boards or braces by using self-drilling screws. A typical CFS sheathing system configuration is shown in Fig. 1.2. Given the structural benefits of sheathed CFS wall panels, extensive numerical and experimental research studies were dedicated to investigate the behaviour and design of such systems (Schafer et al., 2016). While several parameters play roles in determining the behaviour and failure mechanism of the sheathed wall panels, including sheathing types and thickness (Mowrtage et al., 2012; Ye et al., 2015), CFS slenderness, aspect ratios of the panels (DaBreo et al., 2014) and loading conditions (Nithyadharan and Kalyanaraman, 2012), there is a general consensus that the global performance of these structural systems is significantly dependent on the behaviour of fasteners (Bian et al., 2014; Buonopane et al., 2014; Fiorino et al., 2017). However, the current design

guidelines (i.e. Eurocode and AISI S400-15) still provide limited provisions for this type of structure.

Figure 1.2 Typical CFS framed building with steel sheathed shear walls (photo courtesy of J.Ellis, Simpson-Tie Co. Inc.)

Although the body of extensive numerical and experimental studies conducted on the lateral and bending behaviour of sheathed stud wall systems, there was still a lack of comprehensive investigations on the performance and failure mechanisms of the sheathed wall panels by considering the effects of key design parameters of these system to develop an in-depth understanding of the structural behaviour.

1.2. Aim and objectives

The main aim of this study was to contribute towards developing a better understanding of the structural behaviour of the sheathed CFS stud wall systems and to provide insight into the failure mechanism under in-plane and out-of-plane loading conditions. The effect of key design parameters such as screw spacing, the thickness of CFS studs or sheathing board, board configuration, gravity load ratio, the wood-based board material (OSB and plywood), board scenarios (unsheathed, one-sheathed and double-sheathed) and effects of main/auxiliary components on the system (i.e. seam, noggins, pinned no rack) on the performance of these structure systems were examined.

Objectives

The following objectives were set out to achieve the aim of the work:

- ❖ **Sheathed wall systems were investigated under lateral (in-plane) loading.**
    1. To study the lateral structural performance parameters and behaviour (i.e. maximum lateral load capacity, initial stiffness and failure mechanism) of the sheathed CFS wall systems under in-plane loading by developing detailed FE models.
    2. To provide recommendations for more efficient design of the sheathed CFS wall systems by considering the influence of various key design parameters, including screws spacing, the thickness of the OSB and CFS, board configuration, gravity load ratio, and board single- and double-sheathed systems on the response of structural performance.
    3. To assess the seismic characteristics of the sheathed wall panels (i.e. ultimate displacement, ductility and energy dissipation) using the developed Equivalent Energy Elastic-Plastic (EEEP) design methodology and providing the efficiency of these systems with various design variables leading to more efficient design solutions.

- ❖ **Sheathed wall systems were investigated under bending (out-of-plane) loading.**
    4. To examine the structural performance parameters (i.e. maximum bending load capacity, initial stiffness and failure mechanism) of sheathed CFS wall systems under bending (out-of-plane) loading by conducting comprehensive experimental programme.
    5. To investigate the influence of various key design parameters, including screw spacing, the thickness of CFS and sheathing, different board material, the board scenarios (unsheathed, single-sheathed and double-sheathed), drift ratio and the main/auxiliary components (seam, noggins, pinned no track) on the response of structural performance for sheathed stud wall systems.
    6. To determine the rotation of the CFS studs and end-slip between stud and wood-based board of the OSB sheathed stud wall panels when subjected to out-of-plane loading.

❖ **The connection behaviour was investigated under push-out, pull-out and rotation actions.**

7. To investigate the characteristic behaviour of the fasteners (load-slip response) and provide insight into failure mechanism of fasteners at the connection point by considering the effects of various key design parameters such as the thickness of CFS and wood-based sheathing, different board material (i.e. OSB and plywood), presence/absence of washers and screw spacing under push-out (shear), pull-out (tension) and rotation actions.

1.3. Tasks and methodology

The following methodology was implemented to reach the objectives.

1. To examine the strength, stiffness, and seismic behaviour of sheathed CFS wall systems, an overall review was performed on the design provisions for CFS structural members, such as the Eurocode 3 and AISI-S400 guidelines [Objectives 1, 2, 3, 4, 5, 6 and 7].

2. To simulate lateral behaviour of sheathed CFS wall systems under monotonic loading, detailed non-linear FE models were validated using the results of experiment [Objectives 1, 2, 3].

3. The possibility of the axial compressive capacity of the lipped-CFS stud members was calculated according to the Eurocode 3 (EC3) Effective Width Method [Objectives 1, 2, 3].

4. To investigate the bending behaviour and capacity of CFS sheathed with wood-based stud wall panels, four-point test protocol were conducted [Objectives 4, 5 and 6].

5. EN ISO 6892-1 (CEN, 2009), EN 789 (CEN, 2004), ASTM D-3500 standards was used to determine dimensions of the tensile and compression coupon specimens and tensile and compression loading protocols [Objectives 4, 5 and 6].

6. The laser displacement sensor, which was a Keyence LK-G82 sensor with a beam spot diameter of 70 μm, a measurement range between 65 and 95 mm and an

accuracy of ±0.0075 mm, used for the measurement of the geometric imperfections of the CFS stud members [Objectives 4, 5 and 6].

7. Small-scale specimens consisting of cold-formed steel (CFS) stud segments attached to wood-based boards were designed to identify the response of fasteners under monotonic push-out (shear), pull-out (tension) and rotate loadings.

1.4. Thesis layout

In this introduction chapter of the dissertation, a brief overview on the history of the CFS members is presented widespread structural wall system elements are highlighted. Following to these, the research aims and objectives are stated and then the thesis outline is presented. This thesis is divided into seven chapters. In Chapter 2, a general overview of various numerical and experimental research investigating the structural behaviour and design CFS member wall systems are reviewed by taking into in-plane, out-of-plane and axial loading.

In Chapter 3, the lateral structural performance parameters of sheathed CFS wall systems were examined under in-plane loading by developing detailed FE models. After its validation, the developed FE models were employed for parametric studies, the results of which were reported and analysed to assess the seismic characteristics (i.e. ultimate displacement, ductility and energy dissipation) of the CFS shear wall panels with various design variables leading to more efficient design solutions. This chapter, which addresses objectives 1-3, was ready for submission as a journal paper: F. Yilmaz, S.M. Mojtabaei, I. Hajirasouliha, J. Becque. "Behaviour and performance of OSB-sheathed cold-formed steel shear wall panels under combined vertical and seismic loading".

An experimental investigation was performed as part of this study to identify the structural performance parameters (i.e. bending load capacity, initial stiffness), failure mechanism, rotate of the C-shape studs and end-slips of the studied OSB sheathed stud wall panels. The results of this study were presented in Chapters 4 and 5 for face-up and face-down specimens, respectively. The wall system was loaded in face-up and face-down directions, which means the face of the wooden board looked up and down, respectively. The implemented experimental test setup as well as the key results obtained are fully described. These chapters, which

addresses objectives 4-6, were ready for submission as two journal papers: F. Yilmaz, J. Becque. I. Hajirasouliha, S.M. Mojtabaei. "Out-of-plane bending behaviour and capacity of sheathed face-up cold-formed steel stud walls: experimental investigation" and F. Yilmaz, J. Becque. I. Hajirasouliha, S.M. Mojtabaei. "Out-of-plane bending behaviour and capacity of sheathed face-down cold-formed steel stud walls: experimental investigation".

In Chapter 6, an experimental study including a series of connection tests conducted in order to describe the characterise the behaviour of the load-slip response at the connection point under push-out, pull-out and rotation loading. Besides, the connection failure mechanism was provided by taking into account the effects of key design parameters. This chapter, which addresses objectives 7, was ready for submission as a conference paper: F. Yilmaz, J. Becque. I. Hajirasouliha, S.M. Mojtabaei. "Behaviour of fasteners in sheathed cold-formed steel studs under push-out, pull-out and rotational actions".

In the last chapter of the dissertation, the main findings of this research project were summarised and then recommendations for future research works were provided.

The tensile tests were conducted according to EN ISO 6892-1 (CEN, 2009) in a displacement control manner for CFS members in this work. The measured CFS material stress-strain curves of coupon specimens were illustrated in Appendix A.

In Appendix B, the result of the recording initial geometric imperfection was represented for CFS C-section members.

An experimental study including a series of four-point bending tests conducted in order to the structural performance parameters (i.e. bending load capacity, initial stiffness), failure mechanism, rotate of the C-shape studs and end-slips of the studied OSB sheathed stud wall panels in Chapter 4 and 5. The results of strain gauges, rotation of studs and end-slip versus the applied load for face-up and face-down specimens were reported in Appendix C.

In Appendix D, the investigation into the slip load of 12M Tension Control Bolts (TCB) connecting 3 mm steel plates with galvanized surfaces in a double shear configuration was

conducted in order to describe the characterise the behaviour of the load-slip response at the connection point.

An experimental investigation was performed as part of this study to identify the lateral behaviour of eaves connection specimens under a specially designed monotonic in-plane loading protocol. The results of this experimental work were presented in Appendix E.

Chapter 2: Literature review

2.1. Introduction

In this chapter, a number of extensive numerical and experimental investigations into structural behaviour and performance of sheathed CFS wall systems have been carried out. The sheathed CFS wall panel systems basically consisted of the CFS framing elements (i.e. trucks, studs and hold-downs), sheathing panels and self-drilling screws (see Fig. 2.1). The testing of sheathed CFS shear wall systems was initiated as early as 1970 by Tarpy (Tarpy and Hauenstein, 1978; McCreeless and Tarpy, 1978)). From this initial research program and subsequent studies by researchers Tissell (1993), Serrette et al. (1996a, 1996b, 1997a, 1997b), Serrette and Ogunfunmi (1996), Serrette (1997), Selenikovich and Dolan (1999), Selenikovich et al. (2000a), Zhao (2002), Branston (2004), Blais (2004), Chen (2004) and Boudreault (2005) conducted experimental research for sheathed CFS wall structure. The design values for CFS sheathed with wood-based panel wall systems was published in the 1997 version of the UBC (ICBO, 1997). Then, it has been developed in the 1998 Shear Wall Design Guide (AISI, 1998), the 2000 International Building Code (ICC, 2000), and the 2002 version of the Standard for Cold-Formed Steel Framing (Design Provisions Lateral Resistance (AISI, 2002)). Extensive studies have been carried out on the performance of the CFS wall systems several parameters

which play a significant role in determining the failure mechanism and behaviour of the wall panels, including the behaviour of screws (Ye et al., 2016; Fiorino et al., 2017; Xie et al., 2018), types of the sheathing (i.e. plywood, oriented strand board (Blais and Rogers, 2006)), calcium silicate panel, corrugated steel sheet (Zhang et al., 2018), steel sheet (Niari et al., 2015), cement-based panel and gypsum boards (Selvaraj and Madhavan, 2018)), the thickness of sheeting board and frame members, the loading conditions (i.e. the monotonic and reversed cyclic loading) (Gao and Xiao, 2017; Vieira and Schafer, 2012), the aspect ratio of the panels (Yu and Chen, 2011), sheathing board scenarios (i.e. one-sheathed or double-sheathed) (Attari et al., 2016) and screw spacing (Balh et al., 2014).

Mid-Stud

Sheathing Board

Chord Studs (back-to-back)

Track
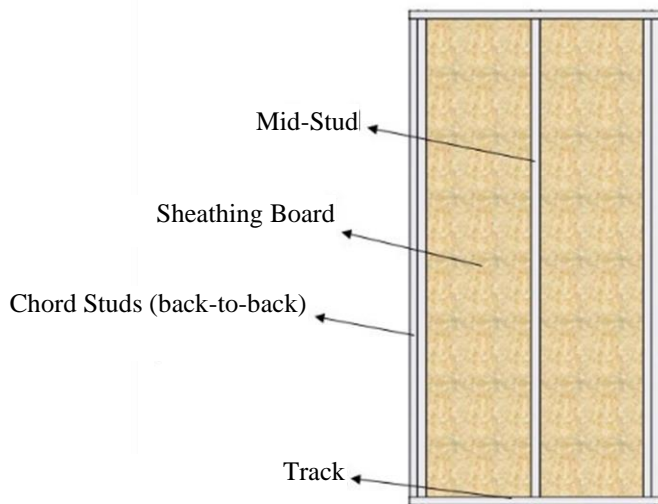
Figure 2.1 A sheathed CFS stud wall panel systems

Tissell (1993) carried out a series of experimental works on sheathed with plywood and Oriented Strand Board (OSB) wall systems to examine the effect of screw spacing and sizes on the behaviour of such structures. The primary purpose of these tests was to examine the effect of CFS with different thicknesses. Serrette et al. (1996a, b) and Serrette (1997) conducted a series of tests to investigate the behaviour of light gauge steel framed shear walls sheathed with OSB, gypsum wallboard and plywood. The intent of the research program performed by Serrette and Ogunfunmi (1996) was to test 13 wall systems with different lateral bracing systems, including gypsum sheathing board, X-bracing, gypsum wallboard and the combination of X-bracing, gypsum sheathing board and gypsum wallboard. Serrette et al. (1997a) tested a series of small-scale and full-scale wall specimens to consider the behaviour of the fasteners

and sheathing materials. OSB, gypsum wallboard, plywood and fiber bond wallboards were fastened to the steel studs on one or both sides under in-plane loading. Serrette et al. (2002) also conducted a series of experiments to assess the behaviour of sheathed shear wall specimens under monotonic and cyc1ic motions to examine the performance of such systems with configurations not covered by the 1997 Uniform Building Code (lCBO, 1997) and the 2000 International Building Code (lCC, 2000).

Branston (2004) revised various methods to evaluate the structural performance parameters; Equivalent Energy Elastic-Plastic (EEEP) bi-linear model was used considering the analysis results in summarised by relied on to develop the Canadian shear wall design method (NRCC, 2005) and found in AISI S400 (2015). The main theory of this method relies on the fact that the area represents the energy dissipated during cyclic or monotonic tests under the load-displacement curve. The energy dissipated represented by the area under the bilinear curve obtained using the EEEP method and experimental test results were equal. The model was modified and improved by Foliente (1996) after its first improvement by Park (1989). Boudreault (2005) provided extensive reversed cyc1ic loading protocols to use with shear wall systems such as the sequential phased displacement (SPD) (Porter, 1987), Applied Technology Council ATC-24 (1992), CUREE ordinary ground motions (Krawinkler et al., 2000; ASTM E2126, 2005) and International Organization for Standardization ISO 16670 (2002). Boudreault (2005) also illustrated a procedure to obtain test-based ductility-related and over strength-related values according to NBCC 2005 (NRCC, 2005). Blais and Rogers (2006) performed experimental tests on a CFS shear wall system sheathed with 9 mm OSB under monotonic and cyclic loadings. The EEEP analysis technique was implemented to estimate design parameters, including nominal elastic stiffness, system ductility and shear strength. Yu and Chen (2011) conducted experiments on the CFS shear wall systems sheathed with steel board under lateral monotonic and cyclic loadings, including four different wall configurations. It was observed that the shear strength and ductility of the CFS shear wall systems could be improved by using blocking and strapping and preventing lateral buckling of interior studs.

This chapter was split into three main parts to summarise the behaviour of sheathed wall systems under in-plane, out-of-plane and axial loading (see Fig. 2.2). Then, in concluding

remarks of the literature review chapter, it was presented the relevant outcomes from the literature review on the structural behaviour of the CFS wall systems to look into the lack of research.
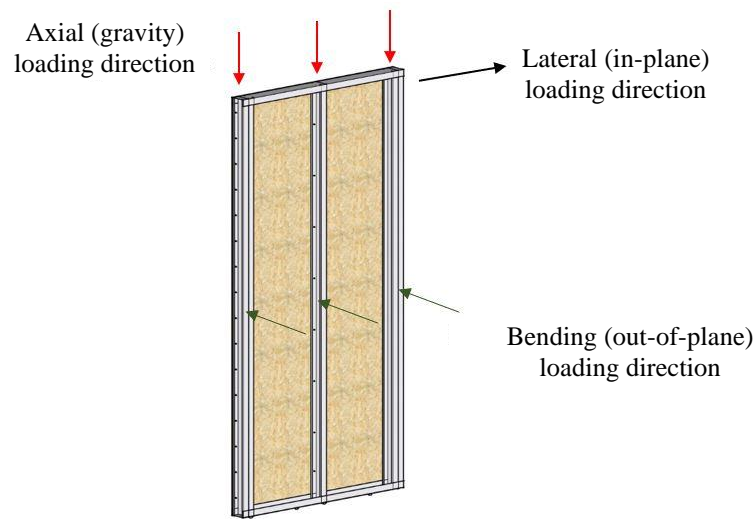
Figure 2.2 Sheathed wall systems under different loading directions

2.2. In-plane (lateral) loading

In recent years, the lateral behaviour and performance of the CFS wall systems used in the construction industry were examined in many research studies. A CFS wall system is composed of CFS framing elements (i.e. studs and track) connected to the sheathing boards or braces using self-drilling screws. The previous research studies on sheathed panels revealed that such panels have advantages over braced ones in terms of load-bearing capacity and lateral stiffness as well as seismic characteristics (i.e. energy dissipation capacity) (Accorti et al. 2016). A general overview of the studies considering various design parameter effects on the sheathed CFS wall systems under in-plane loading was presented in the following subsections.

2.2.1. Behaviour of fasteners

The overall performance of sheathed CFS wall structural systems was significantly dependent on the behaviour of fasteners. Previous experimental research has shown that fasteners used between the CFS frame and OSB panels were one of the critical components when subjected to in-plane monotonic loading and played a crucial role in determining the overall lateral

performance and failure mode of such walls (Bian et al. 2014). In the literature, the behaviour of fasteners under shear forces was investigated through several numerical and experimental studies. Peterman and Schafer (2013) identified the monotonic and hysteretic responses of the fastener between CFS studs and sheathing panel under in-plane lateral loading. It was reported that the connection point of the system provides bracing to the CFS studs under out-of-plane and gravity loads and provides critical energy dissipating mechanism for CFS shear walls sheathed with panels. In this work, the sheathing types (i.e. gypsum and OSB), screw spacing, the thickness of CFS, and fastener type were varied to assess the performance of the fasteners. In addition, the Pinching4 model was created by taking into the hysteretic characterization of the stud-fastener-sheathing response.

Kyvelou et al. (2017) performed several push-out tests considering various design parameters, including CFS thickness, screws spacing, wood adhesive at board joints, and epoxy resin at the beam-board interface. The test results showed that the spacing of the screw had negligible effect on the behaviour of the fasteners. Moreover, it was reported that the thickness of the CFS did not affect the behaviour of the fasteners for this type of system. Since the wood-based material is significantly softer than the CFS, the deformation of the structure was dominated by that of the wood board.

The effect of wood-based board thickness on the behaviour of the fasteners was investigated by Selvaraj and Madhavan (2020). This research work showed that both stiffness and strength of the fasteners increased almost linearly with the increase in the thickness of the plywood board. It should be noted that the aforementioned finding is used to establish the fastener behaviour in the parametric study.

Kyprianou et al. (2021a) conducted a series of pull-through tests to assess the interaction between the various components of a sheathed CFS wall system. In this work, the different type of sheathing boards (i.e. plasterboards and OSB), single- and double-layer and different type of screws were examined. It was observed that the use of double-layer of plasterboard resulted in increases of 30% and 60% in strength and stiffness, respectively, in comparison to those of single-layer of plasterboard. Furthermore, the ultimate load capacity of sheathed with OSB specimens reached to three times compare with those attained by the sheathed with

plasterboard. In another study led by Kyprianou et al. (2021b) also developed an analytical model for analysis of the connection and material behaviour of the key components of sheathed CFS wall systems.

Vieira and Schafer (2012) provided the strength and stiffness characteristics value for structure systems consisting of CFS studs stabilised by sheathing. It was reported that the primary stability resistance for these systems was provided by lateral stiffness supplied by the sheathing at the stud-to-sheathing fastener locations. This study was separated into two parts to the source of translational stiffness: local and diaphragm. The various design parameter (i.e. the sheathing type, stud spacing, edge distance, fastener spacing, construction flaws and environmental parameters) were examined in this research to effect on the structure performance. In addition, analytical formulations were verified for the shear diaphragm stiffness and local translational stiffness to provide for composite systems.

The behaviour of the fasteners used in CFS studs sheathed with cement-based or gypsum boards was also investigated by Fiorino et al. (2017). To identify the mechanical properties of the screws, the experimental investigations were conducted by taking into the effect of sheeting types, the thickness of the CFS, screw diameter and a number of panel layers. It was observed that the edge distance of the corner fasteners at the structure plays an important role in the shear resistance. The increment of the screw diameter from 3.5 to 3.9 mm did not significantly strengthen the response of the CFS wall sheathed with a single layer of gypsum fibre boards. In addition, the shear strength of the system with 3.9 mm diameter screws obtained in this work was almost equal to the theoretical prediction given by EN 1995.

The behaviour of the fasteners for four different sheathing types, calcium silicate board, gypsum wallboard, Bolivian magnesium board and OSB, was investigated by Ye et al. (2015). The thickness of CFS stud, sheathing types, edge distance of the screws, diameter of the screws, loading conditions and sheathing orientations were varied to assess their effect on the response of structural performance. It was reported the edge distance of the fastener took a more critical role in shear capacity of the screw than thickness of stud and screw diameter. Moreover, when the edge distance of the system was increased, the shear capacity of the screw under tension can be enhanced. In this work, a degradation model (four-line) was applied to adopt skeleton

curves for connections, and then a hysteretic model was created depending on a pivot model. The verified numerical method was showed a good agreement with the test results. For four different sheathing types, the ultimate capacity of the screws could be ordered OSB, calcium silicate board, Bolivian magnesium board and gypsum board, respectively. It has been clearly concluded that OSB is a more durable board in terms of performance of the fasteners.

In addition to self-drilling screws, the behaviour of other types of fasteners have also been investigated. For instance, Xie et al. (2018) conducted an experimental study on the CFS shear wall systems screwed with self-piercing riveted (SPR) under lateral monotonic and reversed cyclic loadings. Furthermore, the effects of rivet spacing at the steel sheet edges, loading type (monotonic and cyclic), axial compression ratio, rivet number at CFS framing joints, failure modes and the steel sheathing types (steel sheet sheathing and corrugated steel sheathing) of CFS shear walls were examined. The experimental results indicated that CFS shear walls screwed with SPR had higher stiffness and shear strength compared to the wall systems screwed with self-drilling screws. However, it was observed that the SPR reduced ductility and deformability of the structure. In another work led by Macillo et al. (2017), the behaviour of the ballistic nails, which comprise compressed air-driven, used in the connection between gypsum panels to CFS frame members in shear wall investigated under monotonic and cyclic loading. The main observed deformation of ballistically nailed connections was formed by an excessive pull through of the nail head into the gypsum panel. The test results revealed that the cyclic loads caused a reduction in the wall lateral strength by 20%, whereas the change in the aspect ratio from 1 to 0.5 resulted in an increase in the strength by 35%. Moreover, it was reported that an incorrect assembling condition could cause a decrease of up to 40% of the strength of connection with a total decrease of the wall strength of nearly 15% according to the experimental test results.

In addition, Rignas et al. (2021) described composite action between calcium silicate board and light-gauge steel stud framing under pull-out and push-out loading actions. Key failure modes were identified based on push-out and pull-out tests for these types of structures. It was observed that significant pinching behaviour occurred under cyclic excitations.

2.2.2. Sheathing boards

The several sheathing boards have been used in the CFS stud wall structures to increase the performance of the system. For this reason, their effects on the structure performance have been investigated in many studies. Pan and Shan (2011) studied the lateral behaviour of shear wall panel systems by taking into different key design parameters such as aspect ratios, board thickness and board scenarios (i.e. unsheathed, one-side and double-side panels) under lateral monotonic loading. The structural performance of unsheathed shear wall systems was compared with different sheathed board systems (i.e. Calcium Silicate Board (CSB), Oriented-Strand Board (OSB) and gypsum boards structures) to assess sheathing effect on the system. It was taking into account the same configuration, the sheathed with OSBs systems could provide the highest lateral strength in proportion to other board materials. However, the highest ductility was captured in gypsum board systems due to fact that the gypsum board was softer and less stiff as compared to both other materials OSB and calcium silicate. In addition, by comparing the ductility of the system in the same board material, while the double-side sheathed CFS shear wall had the smallest ductility ratio, the one-side half ratio CFS shear wall systems had the greatest ductility. Besides, the preponderance of the walls experienced separation of sheathing and bearing failure at the locations of the screws.

The shear performance of the CFS system sheathed with anti-fire boards (Bolivian magnesium boards, autoclaved lightweight concrete slabs and gypsum wallboard) were examined by Wang and Ye (2015). The effects of the size and position of the openings (window) and different board scenarios considered in the experimental study. It was observed that one-side sheathed with autoclaved lightweight concrete slabs had a lower shear strength compared to other board types. As expected, the shear capacity of the perforated wall system decreased when increasing the size of the openings in the wall.

Accorti et al. (2016), the different type of boards such as fibre-board (gyproc and cellulose fibres), cement board with fibre, wood-fibre cement, cement-bonded panels reinforced with a glass fibre mesh and gypsum fibre-board were tested. The test results showed that these types of boards had negligible difference on the performance of the sheathed CFS wall systems. In another research to investigate cement-based boards led by Karabulut and Soyoz (2017), a

series of experimental tests were conducted on CFS wall systems sheathed with two different type of boards (white gypsum-based board and gypsum-based board) under lateral and vertical cycled loading. It was observed that the sheathed with gypsum-based board CFS systems could provide the highest lateral strength. In addition, when increasing the screw spacing of the system, the lateral load capacity of the systems significantly reduced under axial loads. The CFS sheathed with corrugated steel board systems were experimentally tested under monotonic and cyclic in-plane loading by Zhang et al. (2018). The analytical studied also conducted followed experimental works.

Mowrtage et al. (2012) aimed to enhance the stability and the lateral load-carrying capacities of the CFS systems to get a much more durable system using the new sheathing technique under monotonic in-plane and axial loadings. While gypsum mortars or cement were sheathed one the side of the system, the shotcrete ribbed steel sheet was sheathed on the other side. Indeed, some specimens were sheathed with the proposed technique (shotcrete ribbed steel sheet) while the other specimens were sheathed with the gypsum boards or traditional fiber cement boards with mat reinforcement. The experimental test results showed that the lateral load-carrying capacities of the system sheathed with the proposed new technique were more than nearly two times compared with the walls sheathed with traditional boards. Besides, local failure modes commonly occurred in the structure rather than overall buckling failure modes.

In another research, sixteen CFS shear wall sheathed with glued laminated bamboo (glubam ply-bamboo) panel systems with two types of aspect ratios were tested under monotonic and cyclic lateral loadings by Gao and Xiao (2017). The shear capacity and failure mechanism of the ply-bamboo sheathed wall systems were examined under four seismic equivalency parameters by taking AISI-RP-4 2010. It was shown that glubam ply-bamboo board was adequately qualified as a seismic-resistant structure with regards to deformability and strength capacity.

2.2.3. Different board scenarios

Various studies showed that the main role of the sheathing was not only to enhance strength and stiffness of the structure but also to improve system dissipative (Accorti et al. (2016),

Pourabdollah et al. (2017)). The different board scenarios (i.e. bracing, drift ratio and unsheathed, double-side sheathed panel) of CFS shear wall systems have been investigated to assess their effect on the performance of systems. Accorti et al. (2016) conducted an experimental work on the sheathing board effect. The sheathed CFS wall specimens were subjected to monotonic in-plane and axial loading considering the bracing and the sheathing scenarios effects (unsheathed and one-side sheathed). The performance of the shear walls was evaluated under monotonic and reversed cyclic loading in terms of stiffness, resistance, energy dissipation capacity and ductility parameters. Based on the test results, using a X-type bracing with the sheathing board at the structure showed a well-thought-of performance regarding resistance and stiffness of the systems.

Since the CFS shear frame system was taken a vital role in ductility and energy-absorbing of the structure, Pourabdollah et al. (2017) examined the performance of the K-braced CFS shear wall systems under cyclic loading conducting experimental works. It was presented that the K-brace-stud connection details had a significant effect on the systems performance with regards to ductility factor, energy dissipation and lateral stiffness. The CFS walls systems sheathed with boards could improve their performance significantly, by increasing its ultimate shear resistance up to 7 times more. Also, it was reported that using a gusset plate in the braced to stud connection of the panel system has indicated considerably remain their ductility capacities, energy dissipation and shear strength compared with using regular connections in the systems.

The lateral behaviour of the CFS shear wall systems with sheathed with one and double-side boards was evaluated by Mohebbi et al. (2015). As expected, the elastic stiffness, shear strength and energy dissipation of CSF wall system sheathed with double-sided board increased by up to 115%, 63% and 70%, respectively, compared to the single-side sheathed CFS walls. It was also reported that the buckle in chord stud did not occur in double-side sheathed specimens. double-side sheathed wall systems was more than twice of one-side sheathed board systems.

Esmaeili et al. (2015) also conducted an experimental work to identify the lateral behaviour of CFS wall systems with one and double-side steel sheathing under reversed cyclic loading by taking into consideration the thickness of the CFS members and steel sheet and various aspect ratios of the structure. The test result demonstrated that sheathed double-side steel plate wall

systems could provide nearly double lateral strength compared to sheathed one-side steel sheathing as mentioned in previous studies. It was also reported that the thickness of the boundary stud element and the steel sheet was a significant aspect in identifying the failure mechanism in structural systems.

Nithyadharan and Kalyanaraman (2012) investigated the behaviour of the CFS shear wall panel systems sheathed with a calcium silicate board under monotonic and reversed cyclic lateral loadings. The board thickness was investigated in terms of the on the strength and behaviour of the structure and the distance of the fasteners from the nearest edge on the walls system were identified. Besides, the load-deformation behaviour of the CFS wall system considering different design parameters and the limit state values in the failure mode of the fasteners were examined

In another study conducted by Brière et al. (2018), the shear performance of the centre-sheathed (mid-ply) board in the CFS wall systems was investigated to improve the energy-absorbing. This innovative configuration for CFS shear wall systems which was board positioned at the mid-line of the framing was tested under monotonic and cyclic loading to the requirement of resistance and ductility. The test result illustrated that the shear wall was able to reach shear resistances higher than the capacity of the system listed in the AISI S400 Standard, whereas, in the optimal case, the reached storey drift values greater than 6%. The equation for the nominal shear strength approach was developed, which could be depicted as a perfect agreement.

2.2.4. Finite element (FE) method

The Finite Element (FE) Analysis was a valuable methodology to capture the complex buckling behaviour of CFS elements. However, the results of the numerical study should have been noteworthy if the simulation determines accurately the load capacities and displacement, buckling behaviour and stiffness. It is shown that detailed FE models followed a more realistic approach by simulating the non-linear response of the system which were the main energy dissipating mechanisms such as including individual sheathing connections and modelling structural member properties. Following studies highlighted the modelling approach used in developed numerical models for sheathed CFS shear wall systems. Besides, the existence of the

reliable FE model could allow a parametric study to be performed that covers a wide variety of alternatives that cannot be carried out by experiments due to economic reasons or testing limitations. Esmaeili et al. (2015) conducted an experimental and numerical study on CFS shear wall sheathing with steel board. The number of sheathing layers and the board thickness were considered in this research. The non-linear FE programme (ABAQUS, 2017) was used to create numerical model to investigate the seismic behaviour of the CFS shear wall systems. The FE model included material and geometric non-linearity to obtain a good agreement between the experimental and numerical results. Then, the failure modes and maximum lateral load capacity of the structure were compared with the experimental test result to validate analytical results. It was concluded that the FE model was dependable enough to be used to undertake a parametric study for examining the effects of different parameters on the behaviour and performance of sheathed steel board systems which were beyond the scope of this study. In another numerical study led by Atari et al. (2016), the numerical models were simulated using the non-linear FE software (ABAQUS). The height to width aspect ratios of the system, the nominal thickness of CFS and board scenarios (one and double-sided) steel sheet panel parameters were performed under monotonic pushover loading. The failure modes, lateral load-story drift response and ultimate strength of shear walls were validated. A linear relationship between the drift ratio and steel sheet thickness in the strength of the specimens obtained from the numerical test results.

Fiorino et al. (2018a) carried out a numerical investigation on the seismic behaviour of the CFS shear wall system sheathed with the nailed gypsum-based board. The numerical models were simulated with the ability possessing capability and non-linear hysteretic behaviour. Based on the experimental test results on individual sheathing connections, detailed FE models were developed in SAP2000 software for the cyclic and monotonic envelope the shear wall response.

In another research led by Ye et al. (2016), the enhanced FE model was created using the nonlinear FE software (ANSYS) in order to investigate the behaviour of the system under axial compression loading. Various parameters such as the different types of sheathed panels (OSB, Bolivian magnesium board, calcium silicate board and, including fire-resistant gypsum plasterboard), screw spacing, and effects of the board configurations (stud was sheathed on

unsheathed, one and double-sided) wall panels were assessed. A two-node non-linear spring element was assigned for connection behaviour between the CFS and sheathing board.

Badr et al. (2019) investigated the behaviour of CFS shear wall systems sheathed with the combined fibre-cement board (FCB) and X-bracing considering the effects of noggin members and screws spacing under monotonic loading. In the non-linear analysis executed in this study, the material stress-strain curves were converted to true plastic stress-strain to be input into the finite element software.

Pehlivan et al. (2018) conducted a series of experimental tests on CFS shear wall systems sheathed with OSB panels to carry out the effect of the hold-down part under the static lateral load. It was reported that the hold-down attachment and bottom track adjacent faced extensive damage under in-plane loading. The seven different hold-downs were analysed to ensure satisfy stiffness and strength as well as cost and easy fabrication under monotonic and cyclic tensile loadings. The numerical models were created using FE software (ANSYS) to make perform an analysis. Then, the numerical results were validated comparing with experimental test results. Baran and Alica (2012) also selected hold-down was assembled on the CFS system to improve better yield points and more effective geometries capable of providing lateral force resisting wall systems to enhance stiffness, strength and energy dissipation.

The development of CFS sections could result in a considerable reduction in material costs if the CFS sections are optimised in terms of performance, considering difference of material properties due to cold working during the production process and the effect of shapes. Qadir et al. (2022) created FE models of Z- and C- sections. The numerical model included both difference of material properties due to cold working, and geometric shapes. Strength of both Z- and C- sections were examined by numerical modelling integrated with design of experiments and response surface. Multi-objective genetic algorithm optimisation used to achieve in optimal sections. In addition, Nguyen et al. (2017) developed new cold roll formed zed section and channel for purlin systems. Direct Strength Method was employed for design of new cold roll formed purlin elements. The new sections were defined in terms of the structural performance (i.e. maximum bending load capacity and failure mechanism) under bending loading. Also, numerical model created and numerical test result compared with

experimental test result and direct strength method. This study obviously illustrated that the expected strength for direct strength method correlated well with both numerical and experimental test results.

2.2.5. Design methodology

One of the well-established methods was the Equivalent Energy Elastic-Plastic (EEEP) analysis model, which was first proposed by Park (1989) and also recommended by the AISI S400 (American Iron and Steel Institute, 2016). To evaluate the structural performance parameters, EEEP bi-linear model was used considering the analysis results summarised by DaBreo et al. (2014), which relied on developing the Canadian shear wall design method found in AISI S400. The main theory of this methodology depends on the fact that the energy dissipated during cyclic or monotonic tests was represented by the area under the load-displacement curve, which was also equal to the energy dissipated represented by the area under the bilinear curve obtained using the EEEP method. The considered dissipated energy here was obtained by the specimen until reaching 80% of the ultimate load after the latter $(0.8 \times Fu)$; once this post-peak load is reached, failure of the specimen (ultimate displacement) is considered to have occurred. The wall resistance at yield point, ductility and elastic stiffness of the wall systems were identified by using the EEEP analysis approach. In addition, Branston et al. (2006) reported that the EEEP model perfect exemplified the behaviour of CFS framed-wood sheathed shear walls tested using reversed cyclic and monotonic loading protocols. With respect to the computation of ductility ratio, it was common practice to convert the load-displacement curves into equivalent bi-linear curves. Based on this method, as can be seen in Fig. 2.3, the load-displacement response was idealised by two straight lines, where the first line representing the secant stiffness (S_i) determined by connecting the origin to the load equal to $0.4\ F_{max}$, and the second horizontal line starting from the yield point $(\Delta_y,\ F_y)$ to the ultimate displacement (Δ_u), was then determined in such a way that the enclosed areas under the equivalent and the actual curves are equal.
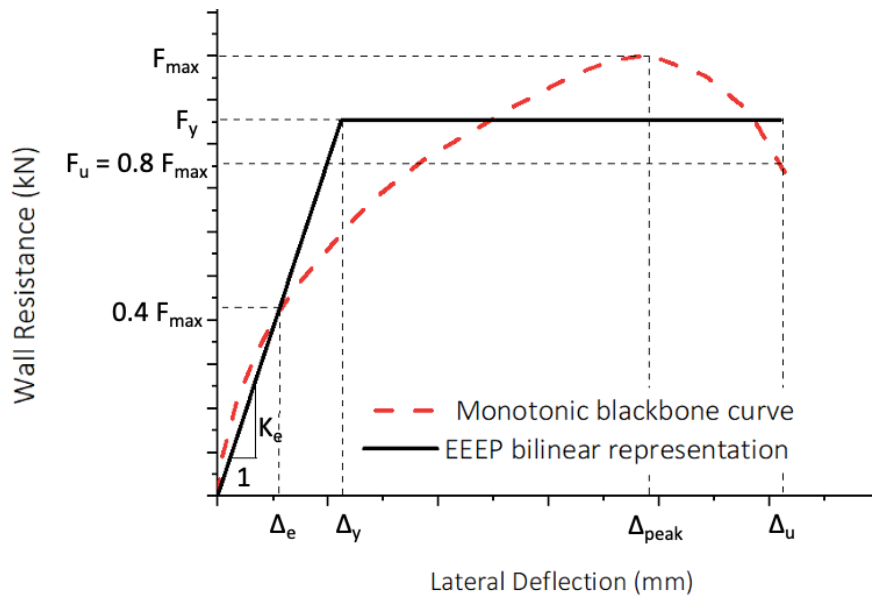
Figure 2.3 EEEP design methodology

Alaee et al. (2012) focussed on predicting the CFS frame and wood-based panel system behaviour using with a new semi-empirical method based on experimental test results obtained from the fastener connection. The simple analytical approach was proposed for the estimate of the displacement of the system corresponding to limit states. The semi-empirical model was performed on a series of wall systems with different fastener and aspect ratios. It was shown that the predicted wall resistance and displacement agree well with the test results.

Yanagi and Yu (2014) provided an analytical effective strip model to define the load-bearing mechanism of the sheathed steel sheet CFS shear wall system subject to lateral load, which was developed to calculate the nominal strength. The statistical analysis showed that the design approach provides accurate and reliable results, in which a uniform LRFD resistance factor was obtained from trustworthiness analysis for the design equation. Indeed, the proposed design method provided designers with an analytical tool to determine the nominal strength of the sheathing with steel panels without conducting full-scale shear wall tests.

Brière et al. (2018) reported that the existing Effective Strip Method derived by Yanagi and Yu (2014) and contained in AISI S400 was inadequate for the new design of these centre-sheathed (mid-ply) board centre-sheathed walls, although it is adequate for the one-sheathed shear wall structure as per the configurations that were used in its calibration. In addition, the bearing

resistance of the (mid-ply) board in a three-ply sheathing connection and tension field that incorporates the entire sheathing member is substantially higher than that estimated using the screw bearing/tilting design rules found in CSA S136 and AISI S100.

Fiorino et al. (2018b) conducted an analytical study about the performance-based seismic design (PBSD). It was aimed to better understanding the seismic behaviour of CFS shear walls in this research. The enhanced PBSD could achieve a level of damage in a structure, which was simulated through non-linear dynamic analysis of computational models having the capability to represent the deteriorating structural behaviour.

2.2.6. Seismic performance

Javaheri-Tafti et al. (2014) conducted cyclic experimental tests on the CFS walls sheathed with thin galvanised steel plates to evaluate their seismic responses in terms of maximum lateral load capacity and seismic response modification factor. Experimental and numerical studies led by Pehlivan et al. (2018; 2020) showed that the hold-down devices which were generally used to control the uplift forces are capable of dissipating noticeable energy generated by the lateral load (i.e. wind and earthquake).

Balh et al., (2014) considered a new method for the design of CFS shear walls differed in terms of screw fastener schedule and framing reinforcement, wall framing and sheathing thickness and aspect ratio. The EEEP method was used to generate key designs from the experimental test result including a resistance factor, nominal shear resistance, seismic force modification factors over-strength and ductility an over-strength factor for capacity based seismic design. According to the research, nominal shear resistance values used monotonic and reversed cyclic shear wall tests, *Sy*, for the blocked and un-blocked systems were decided. A resistance factor, $\phi = 0.7$ was recommended along with an over-strength factor of 1.4 for capacity based seismic design calculations. Test-based seismic force modification factors were decided; interim values of $R_d = 2.5$ and $R_o = 1.7$. The ductility-related force modification factor (R_d) was a measure of the "fuse" element's ability to dissipate energy through inelastic deformation. Also, the overstrength-related force modification factor ($R_{o)}$ was used in limit states design. The factored resistance was required to be greater than the factored applied loads based on the critical load.

Fiorino et al. (2017a) carried out tests on a full-scale two-storey building with gypsum sheathing braced structure which is called the ''ELISSA mockup''. The mockup was made with two different experimental tests for various conditions. The first situation was that the mockup included structural components of the roof, floors and walls, whereas, in the other state, it was completed with all non-structural parts. This study identified results with regards to dynamic identification (damping ratio and fundamental period) and earthquake performance (building drift, global lateral response, diaphragm response, observed damage and acceleration amplification). The building was designed according to European seismic intensity areas with the medium seismic hazard (PGA of 0.25g) with an over-strength factor equal to 1.8 and a behaviour factor equal to 3.0. The structure of the full-scale two-storey building was uploaded to make earthquake tests and white-noise tests by applying the AQV 2009 Aquila (Central Italy) earthquake with scaling factors in the range from 5 to 150%. The effect of sheathing material outcome in a go down of the main period of about 20% corresponding to an go up of the lateral stiffness of the system nearly 4.5 times. The damping ratio was in the range from 1% to 3% for the bare structure to make the earthquake tests and from 1% to 2% for the whole construction, whereas higher values, in the range from 2% to 5%, were evaluated after earthquake tests on the entire structure. The drift of maximum inter-story was minimal (0.52% for the 2nd level and 0.80% for the 1st level) and the drifts of residual inter-story could be negligible (under 0.05%). The amplification of maximum acceleration was in between from 1.11 to 2.23 (second floor) and from 1.60 to 3.10 (roof floor). The failure of the structure occurred very small in both finishing materials and CFS structural parts and was qualified by the presence of gypsum and a small detachment of board at corner joints on the internal faces of walls observed only after earthquake tests with higher scaling factors.

Badr et al. (2019) conducted an experimental work followed by numerical modelling for CFS shear wall system sheathed with the fibre-cement board (FCB) under the lateral monotonic loading. The numerical parametric study was performed taking into account different factors affecting the ductility of CFS wall systems. Based on the experimental and parametric studies results, the seismic response reduction factor (R) was identified by using EEEP. It was reported that the X-strap bracing in the walls system increased the R values as well as the lateral load

capacity of the sheathed CFS shear wall systems. Besides, the R factor was recommended depending on the experimental test result to use in arranging between 2.2 and 3.3.

2.3. Out-of-plane loading

Fiorino et al. (2018) examined the seismic performance of the lightweight steel wall systems sheathed with the gypsum-based panel under out-of-plane quasi-static monotonic (three-point bending) and dynamic loading by considering various design variables, including screw types (i.e. self-piercing or self-drilling screws), frame drift ratio (stud spacing), panel-to-steel joint types (i.e. fixed joint and sliding joint) and sheathing panel effects. They showed that the strength and stiffness of the wall panels can be doubled by reducing the spacing between the studs from 600 to 300 mm. Besides, it was found that the ultimate post-peak response can be significantly affected by the type of joint points in the wall panels while the type of dowel influenced the maximum strength of the system.

Selvaraj and Madhavan (2019) conducted a comprehensive experimental investigation on the CFS wall sheathing double-side with gypsum panels to address the effect of sheathing under 4-point bending loading. The effect of the different sheathing configurations (i.e. unsheathed and double-sheathed board), the thickness of the board and screw spacing were investigated in the system. It was observed that the ultimate moment capacity of the system significantly increased by 126% due to the sheathing restraining effect compared to the design strength of the unsheathed CFS stud walls. It was also reported that the AISI design regulation for sheathed wall panels requires modification on the strength prediction of the CFS member with sheathing. Selvaraj and Madhavan (2018) assessed the bracing effects of the gypsum sheathing in CFS stud wall panels through a comprehensive experimental programme under out-of-plane bending loading. It was shown that the bracing effect of sheathing depends on the global and local slenderness of the CFS stud elements. Moreover, the results of experimental tests proved that the fastener spacing limitations proposed by the AISI guideline are sufficient for the connection of the CFS elements and the gypsum boards. In a follow-up study, Selvaraj and Madhavan (2020) examined the bracing effect of plywood sheathing against the slenderness of the double-sided sheathed CFS wall panels under out-of-plane loading. It was demonstrated that the

bracing effect of sheathing boards mainly depends on the key factors of the sheathing connections, including the type of self-drilling screws and the material properties of the panel board. They also found that the experimentally captured failure modes differ significantly compared to those predicted by the AISI design specification. Mowrtage et al. (2012) examined the maximum out-of-plane load-carrying capacity of the CFS wall systems with steel sheets shotcreted by the cement or the gypsum mortar. It was reported that the out-of-plane strength of the aforementioned wall panels was higher by almost three times compared to the foreseeable maximum wind pressure stipulated by the Turkish code for Design Loads for Buildings (TS498, 2003).

The sheathed CFS wall systems were investigated under out-of-plane and in-plane loading as seen above research; in addition to these, the flooring panels comprising CFS members and the wood-based particle were also carried out to clarify the behaviour of the system. Kyvelou et al. (2017) conducted a series of four-point bending tests for the flooring panels; in other words, the effect of the adhesives, shear connection and featuring fasteners on the system have been investigated. It was found that the adhesive used at the board-beam interface and the spacing of the fasteners had a significant effect on the flexural stiffness and moment capacity of these systems. Based on the test result, the design method was provided for the commonly used principles for steel-concrete composite beams, and the load-slip curve for the fasteners in wood-based floor-board has been produced. Besides, the finite element model was created by Kyvelou et al. (2018), comprising all the components of the CFS flooring system using the non-linear interaction between each other. The model included geometric and material non-linearities, initial geometric imperfections, and the load-slip response of the fasteners employed to achieve the shear connection. Then, the effect of critical parameters on the structural behaviour of the system was examined, including the thickness and depth of the CFS section and the screw spacing. The effect of different types of fasteners (coach screws, self-drilling screws, and bolt and nut) on the load-slip behaviour of CFS-plywood connections in flooring systems was investigated by Karki et al. (2022). It was observed that while bolt and nut connections outperformed self-drilling screws, the size of the bolts and nuts should be designed based on the strength of the wood in order to prevent from being crushed. Moreover, they proposed a

new simple analytical expression for the load-slip response of the connections in flooring systems.

2.4. Axial loading

Based on the extensive experimental test results, a design procedure was developed that allows performance capacity for the design of walls under horizontal and vertical loads. Wang et al. (2019) carried out a series of experimental works followed by numerical analysis to evaluate the structural performance of the CFS tube truss shear walls. The full-scale unsheathed CFS shear wall system with tube truss skeleton frame system and double-side sheathed CFS shear wall systems sheathing with oriented strand board (OSB) panels were tested under in-plane and combining constant axial compression loading. The load-displacement response, ductility and failure pattern of the test specimens were assessed under axial (horizontal) loading. The experimental test result showed that the CFS truss tube shear wall contributed to energy dissipation, hysteretic behaviour and ductility of the system, as expected. Based the parametric study results, the effect of sheathing type, OSB panel thickness, X-shaped bracing number on the elastic stiffness and shear bearing capacities of the CFS tube truss shear walls were examined. It was also observed that elastic stiffness and the shear bearing capacity of the CFS tube truss shear wall were significantly affected by four-limb lattice stud, the number of X-shaped bracing, the type of sheathing and thickness of the OSB panel. Lange and Naujoks (2007) also investigated the behaviour of the CFS shear wall systems under axial and in-plane loading. Four different board types (chipboard with polyurethane polyurea glued panels, gypsum fibre-board, cement-bonded fibre-board and trapezoidal sheet) were tested in the experimental work.

Shamim et al. (2013) conducted shake table tests for single and double-storey sheathed steel board CFS shear walls to examine the natural period and damping of the system and also the consistency between the results of seismic behaviour obtained from static and dynamic tests. In the main conclusion, it was demonstrated that the load-displacement hysteretic response and the failure mode obtained from the test result did not differ noticeably from that captured by the reversed-cyclic loading on the identical shear wall. Furthermore, an account should be taken

of the effects of eccentric loads applied on the CFS framing elements to avoid the loss of the capacity of gravity load. In another study conducted by Shamim and Rogers (2013), the tested sheathed wall systems under dynamic and static cyclic loading conditions were modelled in the Finite Element (FE) OpenSees software, and recommendations were consequently given for element types, modelling of topology and calibration of parameters.

Wu et al. (2018) investigated the innovative CFS shear wall sheathing with lightweight flue gas desulphurisation (FGD) gypsum panel under axial (compressive) behaviour. The axial load-deformation responses, failure modes, axial bearing capacity, axial compressive stiffness and axial load-strain responses of the wall were defined for sheathed wall systems. The full-scale unsheathed and sheathed CFS wall specimens were performed considering sheathing type, configuration and layer of wall panels, stud spacing and different section, and joint details of wall panels. The tested nominal axial bearing capacities of the wall system compared to the design rules of AISI S100-12. It was illustrated that the failure modes of the walls system were quite different from each other in the experimental test result and AISI regulations, which means the AISI rules were inadequate for the shear walls system.

DaBreo et al. (2014) investigated the CFS shear wall systems with different screw spacing, sheathing thickness, sheathing material and thickness and aspect ratio under combined lateral and gravity loading, and in-plane loading. The performance of the system was precisely associated with the sheathing connection pattern. However, the chord studs were faced with significant damage when the CFS frame system was not blocked by tension forces.

2.5. Concluding Remark

The findings of this literature review of CFS wall systems in this study presented with an initial emphasis into discuss shape the main and preliminary behaviour of the system as well as influence of their key design properties. This chapter was categorized by a general overview of loading actions, in-plane, out-of-plane and axial loading. The extensive empirical and numerical research carried out so far on alternative loading actions was summarized above. Indeed, attention has been drawn to loading actions and design parameters of sheathed CFS wall systems as structural components, which is the main topic of this thesis. Despite the

extensive body of experimental and numerical studies conducted on the lateral behaviour of sheathed wall panels, there was still a need to further develop an in-depth understanding of the seismic behaviour and the failure mechanisms of wall panels sheathed with OSB, giving due consideration to the effects of key design parameters on the system performance. This involves more accurate numerical simulations taking into account actual fastener behaviour and subsequently comprehensive investigations on structural performance and seismic characteristics of a wide range of sheathed wall panels considering all potential design variables. To this end, detailed nonlinear FE models of OSB-sheathed CFS wall panels were developed in this study, accounting for nonlinear material properties, geometric nonlinearity and geometric imperfections. In addition, comprehensive experimental investigations were performed to develop a better understanding of the structural behaviour of the sheathed CFS stud wall systems. Moreover, the failure mechanisms of the sheathed CFS wall panels under out-of-plane loading of were assessed by considering all possible key design variables such as screw spacing, different material properties (i.e. the thickness of CFS studs and boards), the board material (OSB vs. plywood), board scenarios (i.e. unsheathed, one-sheathed and double-sheathed) and effects of component parts on the system. To determine the stress-strain behaviour of the boards and CFS elements, material coupon tests were carried out. Besides, a series of axillary push-out, pull-out and rotation tests were performed to investigate the composite action between light-gauge steel stud framing and wood-based materials.

Chapter 3: Behaviour and performance of OSB-sheathed CFS stud wall panels under combined vertical and seismic loading

3.1. Introduction

This chapter describes the numerical investigations into the lateral and seismic behaviour of CFS sheathed with wood-based stud wall panels and provides insight into the failure mechanism and seismic characteristics of such structural systems. Although extensive experimental and numerical studies have been conducted on the lateral behaviour of sheathed stud wall panels in the literature, there was still a lack of comprehensive investigations into the seismic behaviour and failure mechanisms of the wall panels sheathed with popular and practical OSB by considering all possible key design variables. Therefore, in this study, detailed nonlinear FE models of OSB sheathed CFS stud wall panels were developed in this study by considering nonlinear material properties and geometric imperfections of the wall systems. The load-displacement response and failure modes of the systems were validated against those obtained from experimental tests. The validated models were then employed for parametric

studies to investigate the influence of various key design parameters, including screws spacing, thickness of the OSB and CFS, board configuration, gravity load and sheathing on the response of structures. Based on the test results, the structural performance parameters (maximum lateral load capacity and initial stiffness) and the seismic characteristics (ultimate displacement, ductility and energy dissipation) of the OSB sheathed CFS stud wall panels were examined to assess the efficiency of the system with various design variables.

3.2. Description of FE model

It has been previously proved that the FE simulations were capable of predicting the in-plane global behaviour and failure mechanism of sheathed CFS shear wall panels with a high level of accuracy (Esmaeili et al., 2015; Kyvelou et al., 2018). In this section, detailed nonlinear FE models of the wall and floor systems were developed using ABAQUS software (ABAQUS, 2017) by taking into account material nonlinearity, initial geometric imperfections and the interaction between constituent elements of the panel and the nonlinear behaviour of the fasteners. The results were validated against the experimental data reported by Blais and Rogers (2006) pertaining to three CFS wall panels cladded on one side with OSB (see Fig. 3.1). The OSB was connected to the framing elements with self-drilling screws at spacings of 75, 100 and 152 mm around the panel perimeter in the three different tests respectively, while a screw spacing of 305 mm was maintained to connect the sheathing to the inner studs. The overall dimensions of the shear walls were 1220×2440 mm^2. The CFS framing elements were composed of U-shaped tracks and lipped-C studs with dimensions of $92.1 \times 31.8 \times 1.09$ (mm) and $92.1 \times 41.3 \times 12.7 \times 1.09$ (mm), respectively, both rolled from 230 MPa steel sheets. No. 8×1-1/2" Grabber SuperDrive self-drilling screws were used to connect the 9 mm thick OSB sheathing to the framing, while Simpson Strong-Tie S/HD10 hold-down devices were put in place to control overturning moments on the shear wall. The top CFS track was subjected to a uniform in-plane lateral displacement during the test to generate the loading.

Figure 3.1 Reference experimental tests conducted by Blais and Roger (2006)

3.2.1. Modelling of screws

Previous experimental studies have demonstrated that the behaviour of the screws between the CFS framing members and the OSB, reflected in their slip modulus, has a considerable influence on the overall lateral performance and failure mode of the sheathed panels Schafer et al. (2016).

To establish the in-plane load-slip *(P-s)* response of the screws for the purpose of the model validation and the parametric studies described in Section 3.3, the empirical equations proposed by Kyvelou et al. (2017) were implemented:

$$s = \frac{P}{K_0} + C_1 (\frac{P}{P_5})^{C_2} \qquad (3.1)$$

where K_0 is the slip modulus of the screws which was experimentally determined by Peterman and Schafer [36] to be 1.9 kN/mm, and C_1 and C_2 are the coefficients given by:

$$C_1 = s_5 - \frac{P_5}{K_0} \qquad (3.2)$$

$$C_2 = \frac{ln\left(S_b - \frac{P_b}{K_0}\right) - ln(C_1)}{ln\left(\frac{P_b}{P_5}\right)}$$

(3.3)

In the above equations, S_5 was taken as 5 mm, as suggested by Kyprianou et al. (2020), and P_5 was the slip load corresponding to S_5. P_b was the bearing resistance of the board in contact with the fastener, which is calculated as the product of the compressive strength of the board and the area of the board in contact with the fastener, and S_b is the slip corresponding to P_b. The values of the aforementioned parameters were obtained from push-out tests conducted by Peterman and Schafer (2013), who tested No. 8 × 1-1/2" Grabber SuperDrive self-drilling screws connecting 11 mm OSB to 1.37 mm CFS studs, and were listed in Table 3.1. The in-plane load-slip response of these fasteners, as calculated from Eqs. (3.1-3.3), was plotted range up to the peak capacity in Fig. 3.2 and compared to the test results. It was seen that the overall response predicted by the equations proposed by Kyvelou et al. (2017) agrees very well with that obtained from the test over the whole loading range up to the peak capacity.

Table 3.1 Values of parameters required for describing the load-slip response of the fastener (Kyprianou et al., 2020)

Material	K_0 (kN/mm)	P_b (kN)	S_b (mm)	P_5 (kN)	S_5 (mm)	P_v (kN)
OSB	1.90	0.67	0.37	1.90	5	2.03
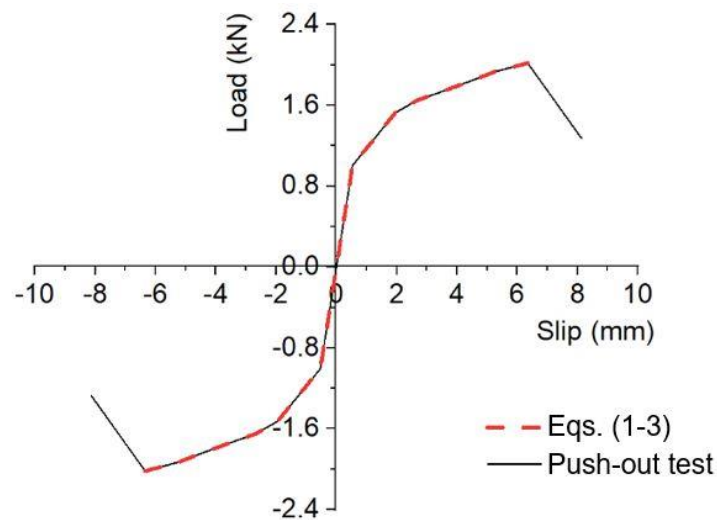
Figure 3.2 Comparison between load-slip response of the fasteners obtained from push-out tests Peterman and Schafer (2013) and the numerical prediction (Kyprianou et al., 2020)

However, the numerical prediction of the load-slip relationship shown in Fig. 3.2 needs to be adjusted for use in the FE models of the tested wall panels, as the thicknesses of their elements (i.e. the CFS and the OSB) are different from those used in Peterman and Schafer (2013). It is worth mentioning that previous studies have revealed that the screw spacing and the thickness of the CFS elements have a negligible effect on the behaviour of the fasteners ((Kyprianou et al., 2020)). The latter is attributed to the fact that damage is always initiated in the board material rather than in the CFS, and therefore, the global deformations of the panel are governed by the deformations in the board. An experimental study conducted by Selvaraj and Madhavan (2020) has shown that both the slip modulus and the strength of the fasteners increase almost linearly with increasing thickness of the board. This information was used to adjust the load-slip relationship of the screws in wall panels with different OSB thicknesses, resulting in the graphs in Fig. 3. Since the empirical equations proposed by Kyvelou et al. (2020) only predict the in-plane load-slip response of the fastener up to the peak load, the experimentally measured post-peak response of the fasteners was added to the pre-peak behaviour obtained from the equations (Fig. 3.3).
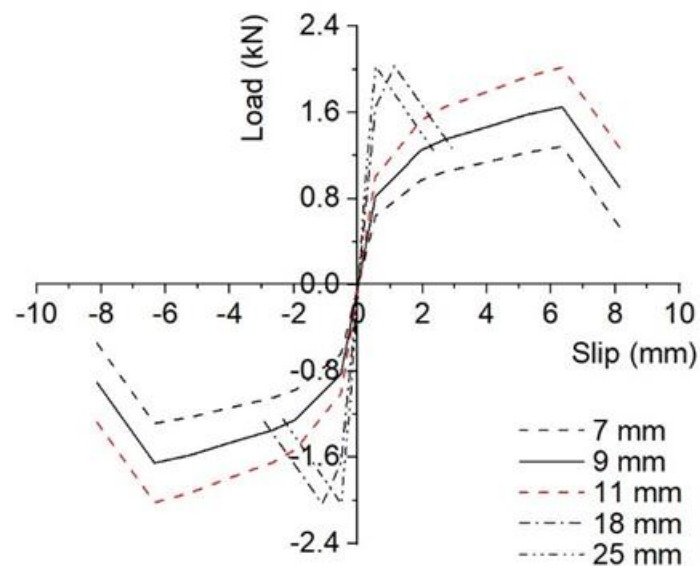
Figure 3.3 Behaviour of the screws connecting CFS to OSB with different thicknesses

The self-drilling screw used to fasten the CFS framing system (i.e. studs and tracks) and the wood-based board was modelled using discrete fastener elements from the Abaqus library (2017), which permitted the input of the actual inelastic bearing and pull-out behaviour.

Discrete fastener elements make use of attachment lines to create connections between the fastening points on the connected surfaces. A radius of influence was assigned to each attachment line, whereby the rotations and displacements of the nodes within the radius of influence were coupled to the rotations and displacements of the fastening point (Papargyriou et al., 2022; Mojtabaei et al., 2021), respectively. This radius was taken equal to half of the screw's shank. In this study, the load-slip response is shown in Fig. 3.3. was incorporated in FE models to establish the screws' behaviour in the validation and further parametric studies (Section 3.3).

3.2.2. Element type and mesh density

In general, shell element type with reduced integration and hourglass control is chosen for the modelling of thin-walled structural members in ABAQUS software (2017), which leads to accurate predictions of flexural and membrane behaviour of the elements (Sabbagh et al., 2012; Sabbagh et al., 2013). The constituent components of the sheathed stud wall panels (i.e. studs, tracks, OSBs and hold-downs) were therefore modelled using general-purpose quadrilateral four-nodded S4R shell elements (Abaqus, 2017), as shown in Fig. 3.4. It was previously proved that mesh density can significantly affect the accuracy of the simulations (Schafer et al., 2016), therefore, following a mesh sensitivity analysis, the size of 15×15 mm^2 was assigned as the component of the model.

(a)　　　　　(b)　　　　　(c)
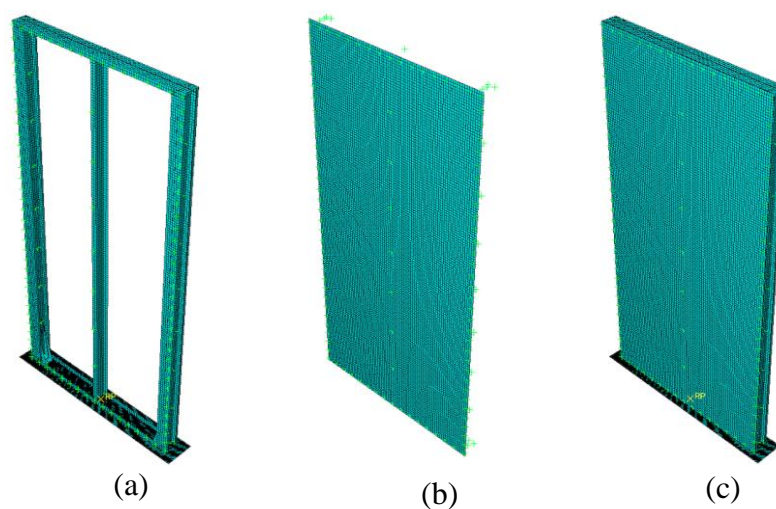
Figure 3.4 Mesh density of: (a) framing elements, (b) OSBs, and (c) whole shear wall panel

3.2.3. Material modelling

Unlike hot-rolled steel counterparts, CFS materials generally indicate a noticeable ductility with a gradual development of yield lines and strain hardening (Kyvelou et al., 2018). The measured stress-strain curves of the CFS and the OSB obtained from the coupon tests (Blais and Rogers, 2006; Zhu et al., 2005) were used in the FE models (Elastic-Plastic material model). Tables 3.2 and 3.3 lists the measured values, where E_{CFS} and E_{OSB} were Young's modulus of CFS and OSB and σ_y and σ_u were the yield stress and the tensile strength of CFS, respectively. In addition, $\sigma_{t,OSB}$ and $\sigma_{c,OSB}$ were denoted as the ultimate tensile and compressive stresses of OSB, ε_u and $\varepsilon_{c,OSB}$ were took as the strains corresponding to the σ_u and $\sigma_{c,OSB}$, and υ_{CFS} and υ_{OSB} were the Poisson ratios of the CFS and OSB materials, respectively. To properly account for the effects of large inelastic strains, the engineering stress (σ)-strain (ε) curve was converted to the true stress versus true plastic strain curve. To take into account the actual cross-sectional area (the changing cross-sectional area with respect to time) of the specimen during material testing to the true stress and logarithmic plastic strain curve. The true stress (σ_{true}) and true strain (ε_{true}) required by ABAQUS (2017) were defined as:

$$\sigma_{true} = \sigma \, (1 + \varepsilon) \tag{3.4}$$

$$\varepsilon_{true} = ln \, (1 + \varepsilon) \tag{3.5}$$

Fig. 3.5 compares the engineering and the true stress-strain curves of CFS material. Besides, as the OSB material does not exhibit plasticity, thus only the engineering stress-strain behaviour of the OSB was shown in Fig. 3.5 (b). The plastic components of the true stress-strain curve shown in Fig. 3.5 were employed as input for the material model in ABAQUS (2017). It should be noted that the effects of cold-working (i.e. strain hardening and residual stress) in the rounded corner zones of the CFS studs and tracks were neglected in this study. These effects are usually quite moderate in CFS and, to some extent, negate each other.

Table 3.2 Measured material properties of the CFS (Blais and Rogers, 2006)

Specimens	E_{CFS} (GPa)	υ_{CFS}	σ_y (MPa)	σ_u (MPa)	ε_u
CFS	199	0.3	264	345	0.315

Table 3.3 Measured material properties of the OSB (Zhu et al., 2005)

Specimens	$E_{t,OSB}$ (MPa)	υ_{OSB}	$\sigma_{t,OSB}$ (MPa)	$\sigma_{c,OSB}$ (MPa)	$\varepsilon_{c,OSB}$
OSB	3650	0.2	11.9	14.1	0.006
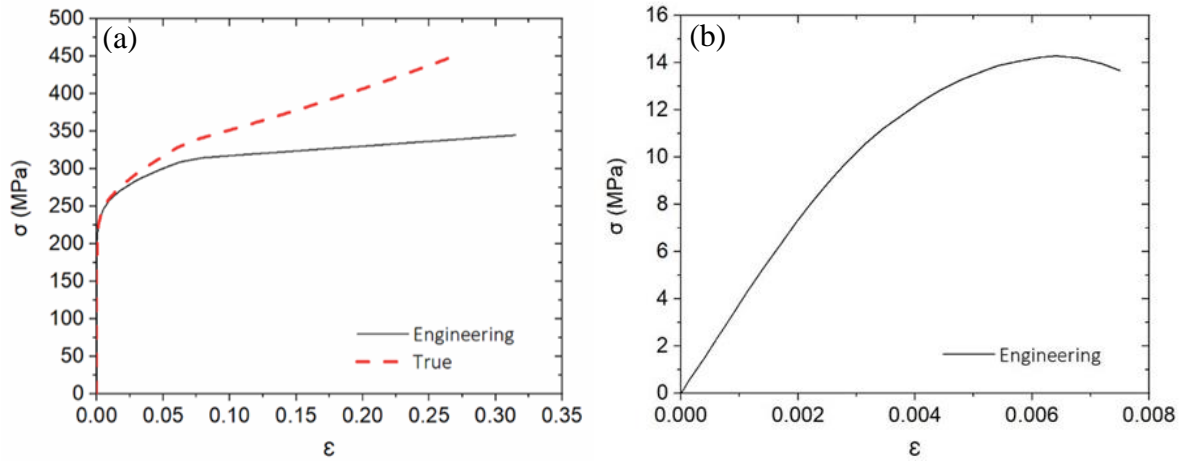
Figure 3.5 (a) Engineering and true stress-strain curves used in the FE modelling for CFS materials and (b) engineering stress-strain for OSB materials

3.2.4. Geometric imperfections

The experimental tests conducted by Blais and Rogers (2006), out-of-plane deformations of the test specimens were prevented and no global buckling of CFS elements was reported. The dominant failure mode was governed by the cross-sectional instabilities. Therefore, either a distortional or a local imperfection was incorporated into the model, depending on which buckling mode had the lower critical buckling stress. It was accomplished by implementing an elastic buckling analysis on the sheathed shear wall panel in FE software and using the scaled first eigenmode as the shape of the initial geometric imperfections. Fig. 3.6 shows the critical buckled shape of the shear wall panel. The amplitude of the imperfection was determined based on the work by Schafer and Peköz (1998), whereby the 50% value of the cumulative distribution function of the imperfection magnitudes was adopted. This represents the 'most likely' imperfection and amounts to a magnitude of 0.34t and 0.94t for the local and distortional imperfections, respectively. It can be noticed that the aforementioned work was based on data pertaining to CFS sections with thicknesses below 3 mm (Schafer and Pekoz, 1998). Therefore,

it directly applies to the model of the experimental schedule conducted by Blais and Rogers (2006).
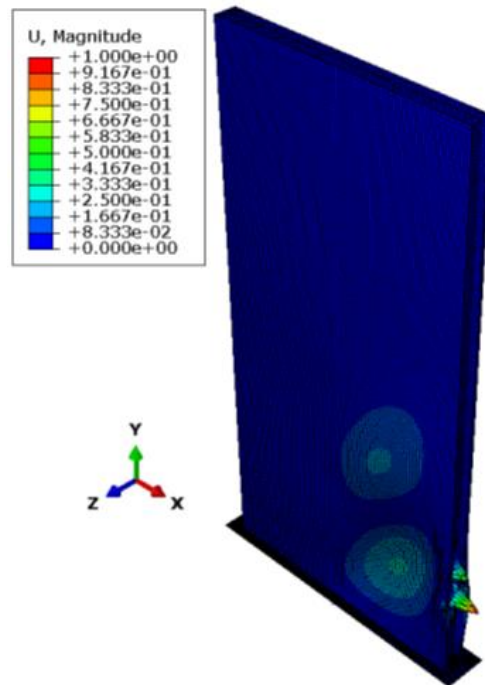
Figure 3.6 First buckling mode shape of the benchmark CFS shear wall panel

3.2.5. Boundary and loading conditions

Fig. 3.7 showed the boundary conditions and loading in FE models. To avoid out of plane deformation of the wall panel, the edge of the top track web along the whole length were restrained in an out-of-plane direction, and the lateral in-plane load was applied to that edge in a displacement control manner. A fixed discrete rigid shell element available in the ABAQUS library (2007) was put in place to simulate the support beam which was used in the experiments. The bottom track at the locations of the four anchor bolts was tied to the discrete rigid plate. In addition, both legs of the hold-downs were tied to the chord and track elements. It should be noted that to avoid penetration of the elements into each other, a surface-to-surface hard contact was defined in a normal direction while a friction coefficient of 0.2 was assigned in the tangential direction using penalty formulation in ABAQUS (2007).
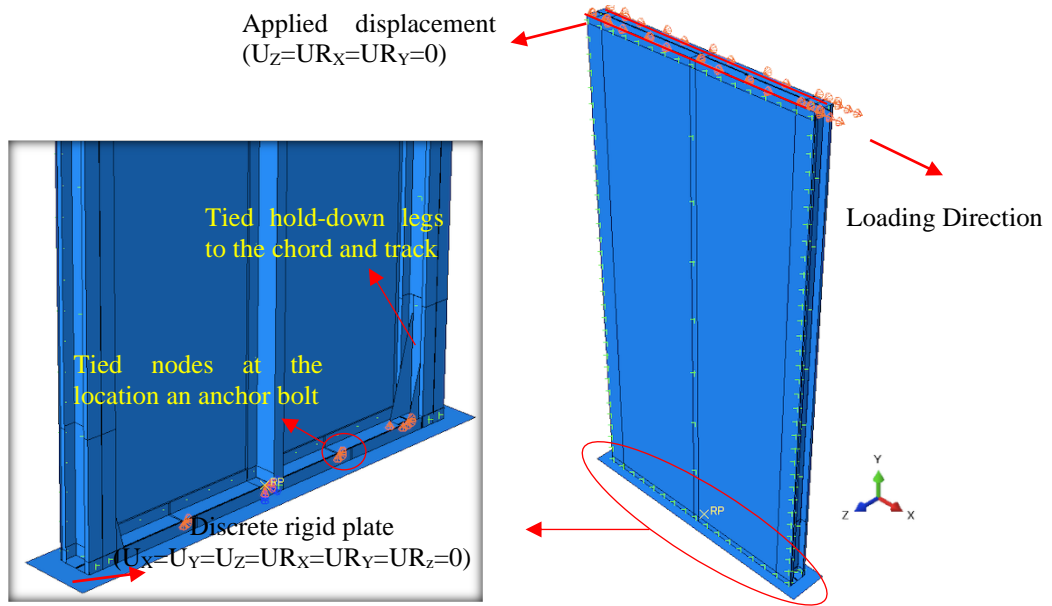
Figure 3.7 Boundary and loading conditions

3.2.6. Validations

Nonlinear FE analyses were conducted using Static General Analysis (available in the ABAQUS library) by applying a displacement at top of the stud wall panels. The load-displacement results of the stud wall panels sheathed with different screw spacings of 75, 100 and 152 mm, were shown in Fig. 3.8 obtained from the FE models and the experimental tests conducted by Roger and Blais (2006). In addition, the ratios of maximum lateral strength of the FE model and the experiment ($F_{Max,FE}/F_{Max,Exp}$) and their corresponding initial stiffness ($S_{i,FE}/S_{i,Exp}$) and ultimate displacements ($\Delta_{u,FE}/\Delta_{u,Exp}$) were listed in Table 3.4 along with their statistical indicators. It should be noted that the ultimate displacement was taken at 80% of the post-peak load. In general, it can be seen that very good agreements between the results of FE and experiments over the whole range of loading were achieved (on average 3% error). The failure modes predicted by the FE models were also consistent with those observed in the experiments. In particular, fastener failure was identified in the FE models, based on the extracted internal fastener forces. As an example, Fig. 3.9 presented the in-plane load-slip response of the fasteners located at all four corners of the wall with 75 mm screw spacing up to failure of the wall. It was seen that the fastener in the bottom right corner has exceeded the displacement associated with its peak load and has entered the descending branch of the curve, indicating failure. In addition, the fasteners in the other corners were approaching their ultimate

capacity and have very little stiffness left in their behaviour. Furthermore, the Von Mises stresses in the boards at failure was showed in following section. The red zones indicate material failure (crushing) in the boards, based on the stress-strain curve in Fig. 3.5b and a Von Mises criterion. These areas were mainly located around the fasteners, result from bearing action, and in some cases extend all the way from the fastener area to the edge of the board, suggesting possible block/plug tear-out. This was entirely consistent with the experimental investigation, which reports a combination of fastener pull-through and block/plug tear-out at the corners as the observed failure mechanisms. It was noted that local buckling of the bottom track close to the hold-downs was also observed in the FE model. However, no mention of this was found in the experimental report.

Table 3.4 Comparison between the results of tests (Blais and Rogers, 2006) and FE models for shear wall panels with different screw spacing

Specimens	$F_{Max,FE}/F_{Max,Exp}$	$\Delta_{u,FE}/\Delta_{u,Exp}$	$S_{i,FE}/S_{i,Exp}$
75 mm screw spacing	0.99	1.00	0.99
100 mm screw spacing	0.93	0.97	0.92
152 mm screw spacing	1.01	0.95	0.94
Average of error	3%	3%	5%
St. dev	0.042	0.025	0.036
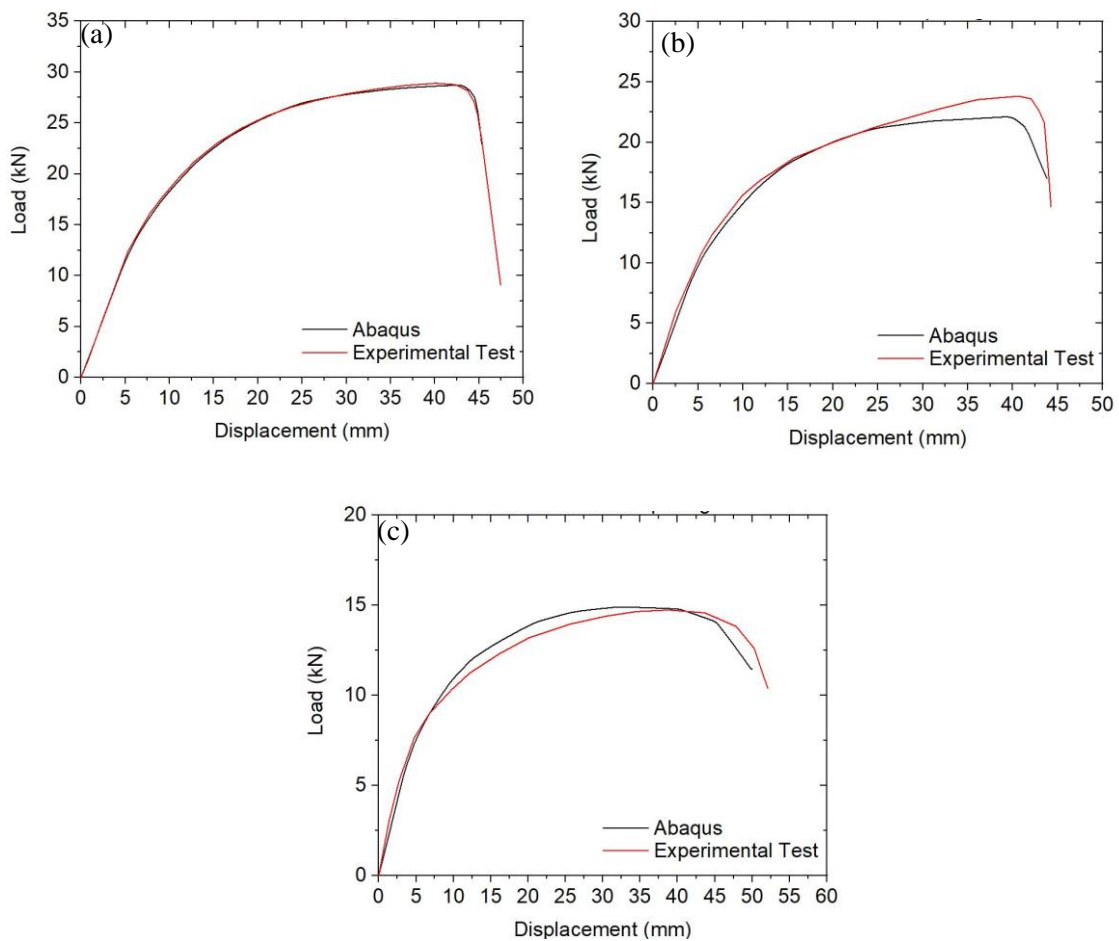
Figure 3.8 Load-displacement curves of shear wall panels with a) 75 mm, b) 100 mm and c)152 mm screw spacing obtained from FE ABAQUS model and experimental tests (Blais and Rogers, 2006)
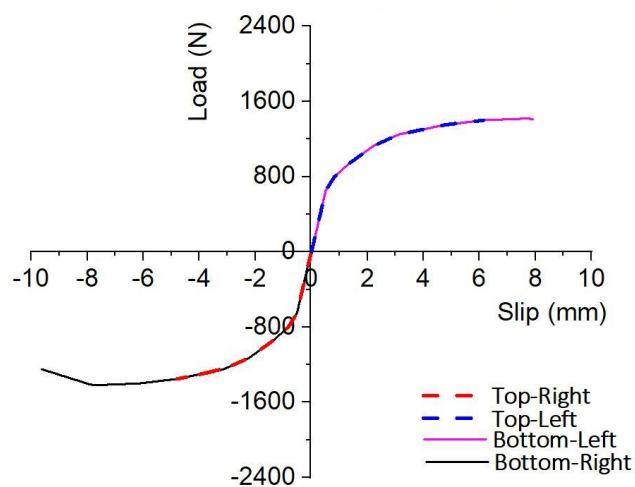
Figure 3.8 FE in-plane load-slip response of the fasteners located at corners of the tested wall with 75 mm screw spacing

3.3. Structural performance assessment

The validated FE models were employed in this section to conduct parametric studies on the effects of the key design parameters of the OSB sheathed shear wall systems screw spacing, board configuration, OSB and CFS thicknesses, the presence and magnitude of gravity load and sheathing system on the lateral seismic behaviour.

3.3.1. Design variables

Table 3.5 lists the details of the parametric studies and the selected design parameters. Four different screw spacing values (75, 100, 150 and 200 mm) were selected for the connections between the OSB and the CFS elements over the panel perimeter, while the screw spacing of the OSB and the middle stud was kept constant during the parametric studies (i.e. 305 mm). Four plate thicknesses (i.e. 1.09, 1.5, 2 and 3 mm) were chosen for the CFS elements, however, five different thicknesses were taken for OSB (i.e. 7, 9, 11, 18, 25 mm). To study the effects of the dimensions and number of the boards, five different board configurations were selected in this study, namely configurations A to E, as shown in Fig. 3.10. Seven different gravity load levels were imposed on the shear wall panels, which were determined as a fracture of the total cross-sectional compressive capacities of the vertical CFS elements (i.e. 0, 10, 20, 30, 40, 50 and 60%). In this study, the axial compressive capacity of the lipped channel section with the dimensions of $92.1 \times 41.3 \times 12.7$ mm and thickness of 1.09 mm was calculated to equal to 39.71 kN according to the Effective Width Method presented in Eurocode 3 (2005). To assess the effect of sheathing system, the behaviour of CFS shear walls with single-sheathed OSB was compared to that of shear walls with unsheathed and double-sheathed OSB. It should be noted that the reference test specimen with the characteristics of board configuration A and 75 mm screw spacing (see Section 3.2) were taken as the 'benchmark specimen' in this study.

Table 3.5 Design parameters used in parametric studies

Variables	Value
Screw spacing	75, 100, 150, 200 mm
OSB thickness	7, 9, 11, 18, 25 mm
CFS thickness	1.09, 1.5, 2, 3 mm
Board configuration	A, B, C, D, E
Gravity load	0, 10, 20, 30, 40, 50, 60 %
Sheathing	Unsheathed, Single-sheathed, Double-Sheathed

(Configuration A) (Configuration B) (Configuration C) (Configuration D) (Configuration E)
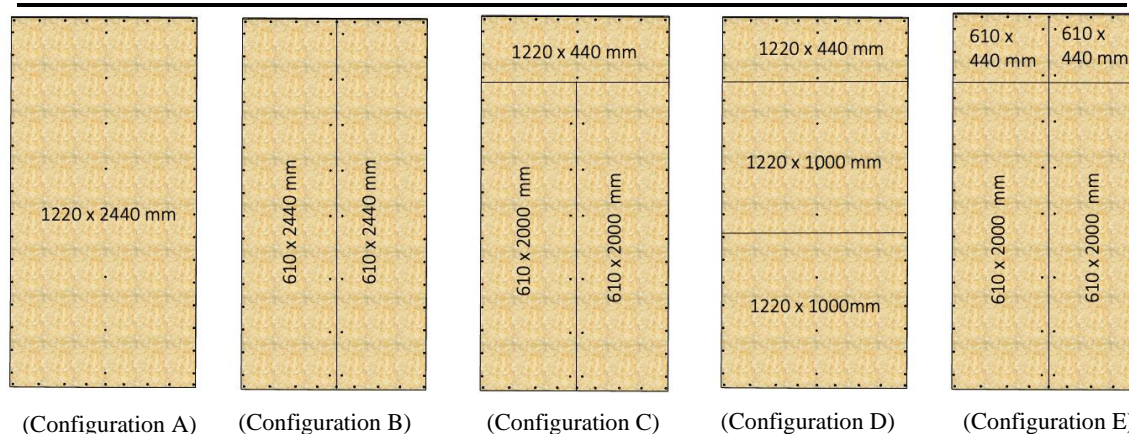
Figure 3.9 Board configurations used in the parametric study

3.3.2. Results

A series of parametric studies were carried out by performing FE analyses on the selected CFS shear wall panels specified in Section 3.3.1 when subjected to in-plane loading. In this subsection, the results of load-displacement responses, as shown in Fig. 3.11, were compared with the benchmark specimen in terms of structural performance parameters (i.e. maximum lateral load capacity and initial stiffness). Besides, the failure mechanisms of the selected shear wall panels listed in Table 3.6 were explained in detail for comparison purposes. It should be noted that the failure was considered as pull-out and tear-out failures or a 80% of post-peak load, depending on whichever happens first. The Eurocode terminology was followed, where failure of the 'fastening' includes pull-out and tear-out failures.
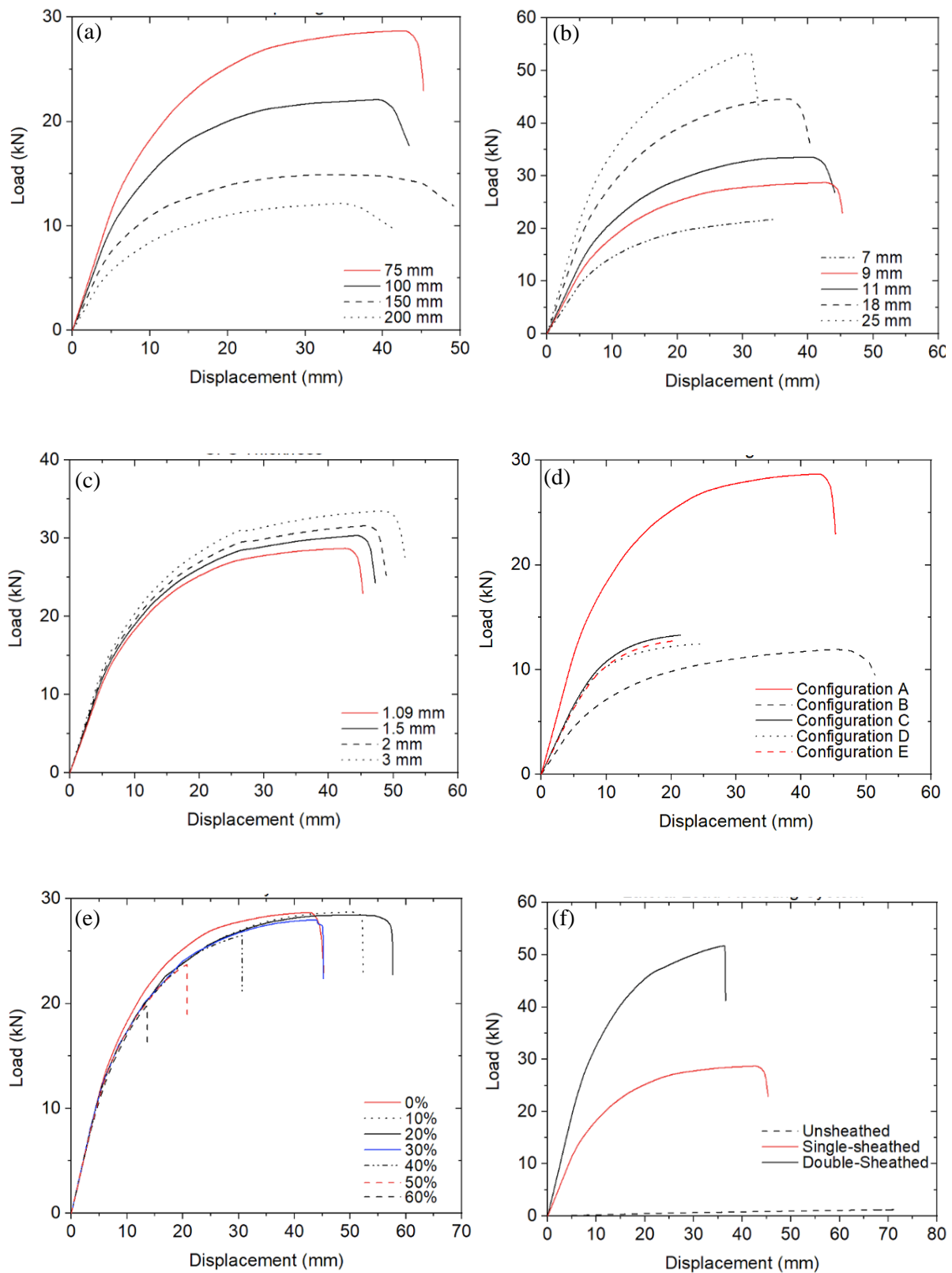
Figure 3.10 Load-displacement responses of the selected shear wall panels with a) screw spacing, b) OSB thickness, c) CFS thickness, d) board configuration, e) gravity load and f) sheathing plotted up to the failure point

Table 3.6 Failure mechanism captured for each parametric study at the failure point

Variables	Value	Failure mode
Screw spacing	75 mm	Fastening failure, Local buckling of bottom track & OSB
	100 mm	Fastening failure, Local buckling of bottom track & OSB
	150 mm	Fastening failure, Local buckling of bottom track & OSB
	200 mm	Fastening failure, Local buckling of bottom track & OSB, Board failure
OSB thickness	7 mm	Board failure
	9 mm	Fastening failure, Local buckling of bottom track & OSB
	11 mm	Fastening failure, Local buckling of bottom track & OSB
	18 mm	Fastening failure, Local buckling of bottom & top tracks & OSB
	25 mm	Fastening failure, Local buckling of compressive chord stud
CFS thickness	1.09 mm	Fastening failure, Local buckling of bottom track & OSB
	1.5 mm	Fastening failure, Local buckling of bottom track & OSB, Board failure
	2 mm	Fastening failure, Local buckling of bottom track & OSB, Board failure
	3 mm	Fastening failure, Yielding of bottom track, Board failure
Board configuration	A	Fastening failure, Local buckling of bottom track & OSB
	B	Fastening failure, Local buckling of bottom track & mid-stud, Board failure
	C	Fastening failure, Local buckling of mid-stud & chord studs, Board failure
	D	Fastening failure, Local buckling of mid-stud & chord studs, Board failure
	E	Fastening failure, Local buckling of mid-stud & chord studs, Board failure
Gravity load	0%	Fastening failure, Local buckling of bottom track & OSB
	10%	Fastening failure, Local buckling of bottom & top tracks & OSB
	20%	Fastening failure, Local buckling of top track & mid-stud & OSB
	30%	Fastening failure, Local buckling of mid-stud & compressive chord stud, Board failure
	40%	Fastening failure, Local buckling of mid-stud & compressive chord stud, Board failure
	50%	Fastening failure, Local buckling of mid-stud & compressive chord stud, Board failure
	60%	Fastening failure, Local buckling of mid-stud & compressive chord stud, Board failure
Sheathing	Unsheathed	Local buckling of top track & mid-stud
	Single-sheathed	Fastening failure, Local buckling of bottom track & OSB
	Double-sheathed	Fastening failure, Local buckling of bottom & top tracks & mid-stud, Board failure

3.3.2.a. Screw spacing

As shown in Fig. 3.11 (a), screw spacing considerably affected the overall structural behaviour of the OSB sheathed CFS shear wall panels. In this study, the maximum lateral load capacity (F_{max}) and initial stiffness (S_i) were used as structural performance parameters to compare the behaviour of the panels (see Fig. 3.12). Based on EEEP method, the load-displacement response is idealised by two straight lines, where the first line represents the initial stiffness (S_i) determined by connecting the origin to the load equal to $0.4F_{max}$ and the corresponding displacement, $\Delta 0.4max$. The initial stiffness (S_i) was calculated using (0.4 F_{max}-0.1 F_{max})/(0.4 Δ_{max}-0.1 Δ_{max}) formulation. In general, reducing the screw spacing significantly increased the maximum lateral load capacity and initial stiffness of the shear-wall panels by up to 136% and 84%, respectively. In comparison to, the benchmark specimen with 75 mm screw spacing exhibited higher lateral load capacity and stiffness by 93% and 40%, respectively. Based on the results of the overall lateral deformation and the internal forces of the fasteners, the failure mechanism in the key specimen was started with the bearing failure of the OSB and pull-through of the screws at the corners of the wall, as shown in Fig. 3.13 (a). It was followed by a significant deformation in the OSB (i.e. OSB buckling) and buckling of the bottom track which eventually led to a drop in the load-displacement curve. If the screw spacing was increased from 75 mm to 200 mm, the dominant failure mode remained the same (i.e. buckling of the bottom track), more significant deformation was observed in the OSB (Fig. 3.13 (b)). In addition, von Mises stress distributions in the OSB board were shown in Fig. 3.13 (b), where the grey colour indicates the failure in the boards. It can be seen that for the specimen with increased screw spacing the board reached their capacity limit (i.e. 14.1 MPa) at the location of the screws in the wall perimeter.

Figure 3.11 The variation of a) maximum load capacity and b) initial stiffness of OSB sheathed CFS shear wall panels with screw spacing of 75, 100, 150 and 200 mm (*benchmark specimen)

(a) 75 mm (benchmark specimen)
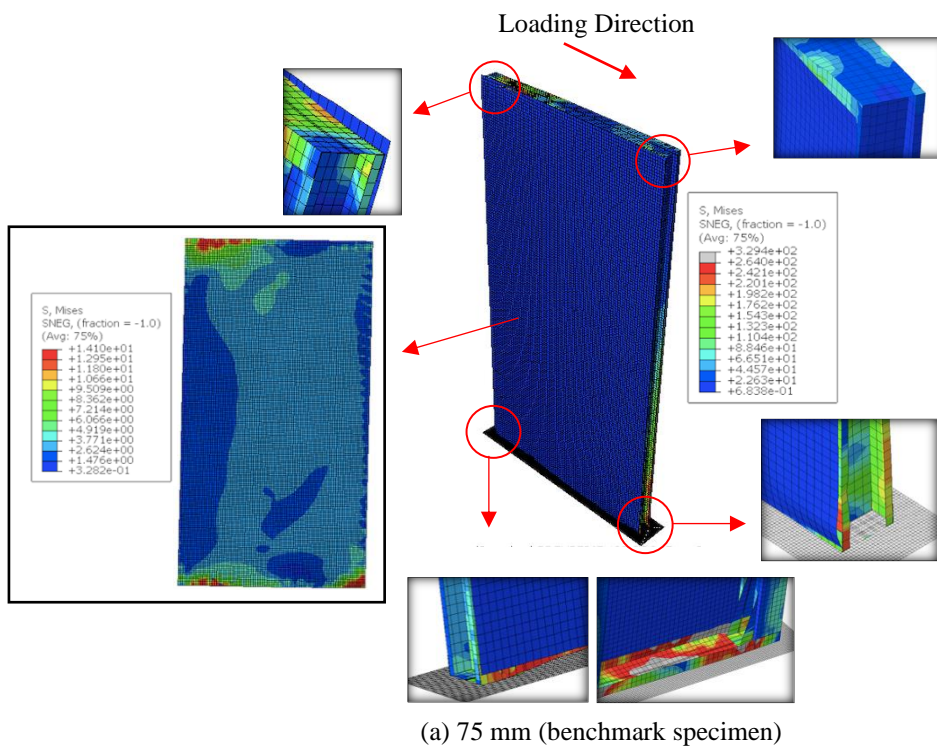
Figure 3.12 von-Mises stress distribution of OSB sheathed CFS shear wall panels with screw spacing of a) 75 and b) 200 mm at the failure point
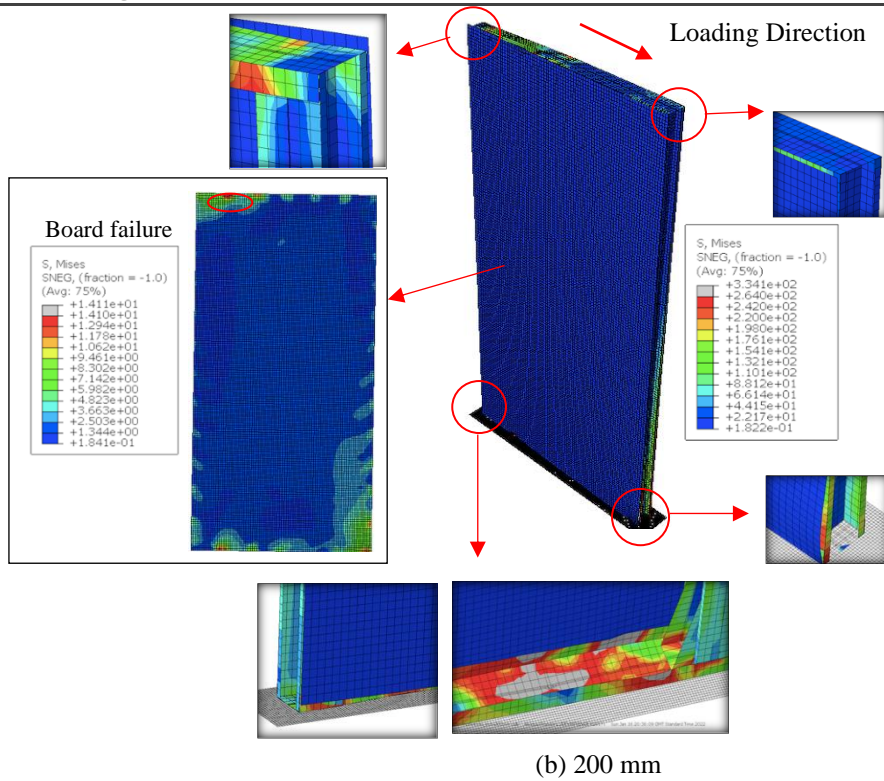
(b) 200 mm

Figure 3.13 von-Mises stress distribution of OSB sheathed CFS shear wall panels with screw spacing of a) 75 and b) 200 mm at the failure point

3.3.2.b. OSB thickness

While the benchmark specimen was sheathed with 9 mm OSB, numerically the response of sheathed CFS wall systems with a range of different OSB thicknesses (i.e. 7, 11, 18 and 25 mm) were also investigated. As shown in Fig. 3.11 (b), changing the OSB thickness could significantly affect the overall load-displacement response of the CFS shear wall panels. The structural performance of variation of OSB sheathed CFS shear wall panels (Fig. 3.14), where maximum load capacity (F_{max}) and initial stiffness (S_i) were improved up to 55% by doubling the OSB thickness from 9 to 18 mm. Fig. 3.15 showed the failure mechanism and the von-Mises stress distribution of OSB sheathed CFS wall panels with various OSB thicknesses presented at the failure point, where the grey colour indicates yielding of CFS and capacity limit of OSB. The failure was observed in the 7 mm OSB prior to the buckling of CFS elements (Fig. 3.15 (a)), on the contrary, no failure was captured in thicker boards. While the dominant failure mode of the panel with 11 mm OSB happened in the bottom track similar to the key specimen (see Section 3.2.1.a), increasing the OSB thickness to 18 mm resulted in buckling of both top and

bottom tracks (Fig. 3.15 (b)). Further increasing OSB thickness (i.e. 25 mm) led to a shift in the dominant failure mode from the tracks to the compressive chord stud (Fig. 3.15 (c)).

Figure 3.13 The variation of a) maximum load capacity and b) initial stiffness of OSB sheathed CFS shear wall panels with OSB thickness of 7, 9, 11, 18 and 25 mm (*benchmark specimen)
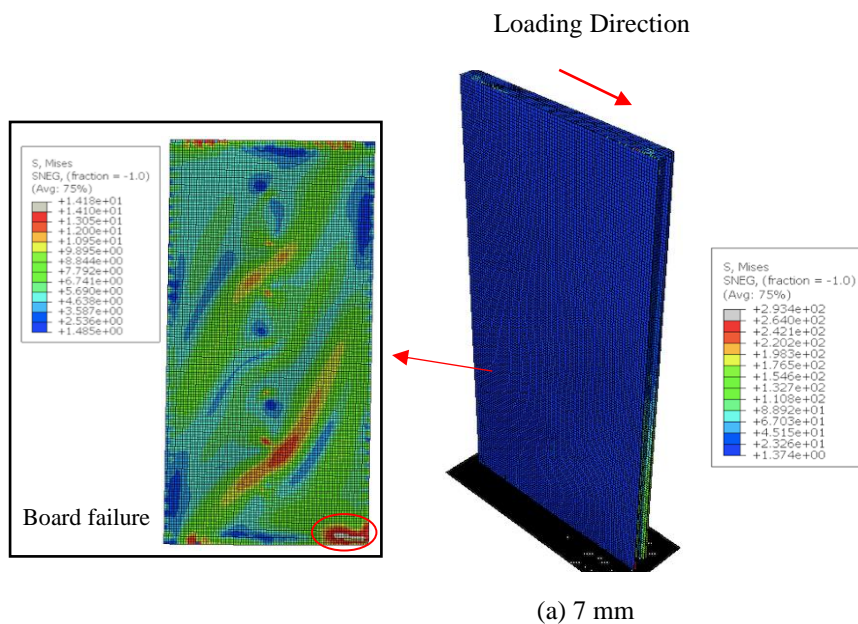
(a) 7 mm

Figure 3.14 von-Mises stress distribution of OSB sheathed CFS shear wall panels with a) 7 mm, b) 18 mm and c) 25 mm OSB thickness at the failure point
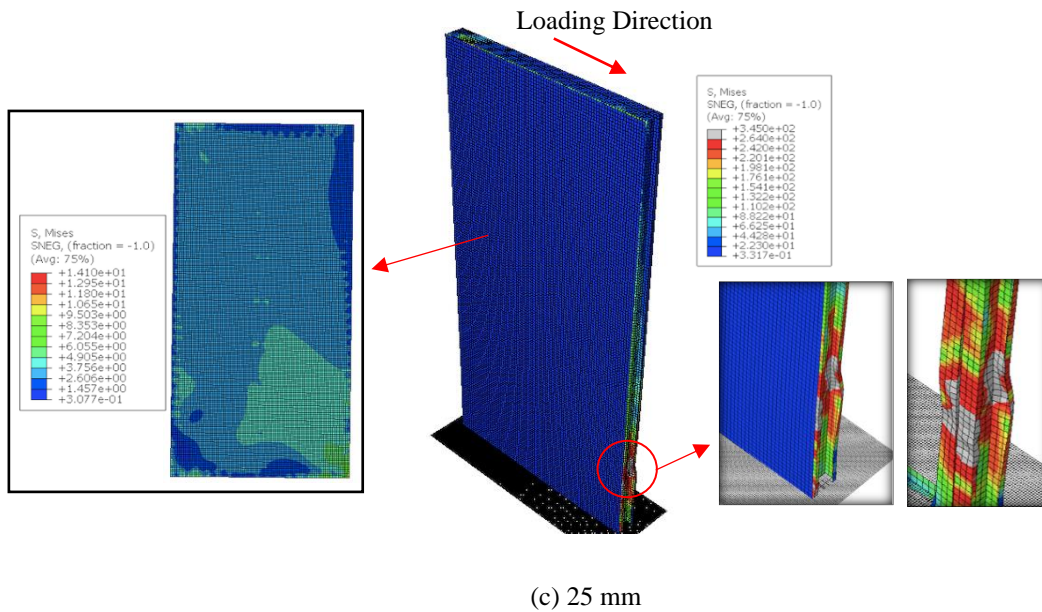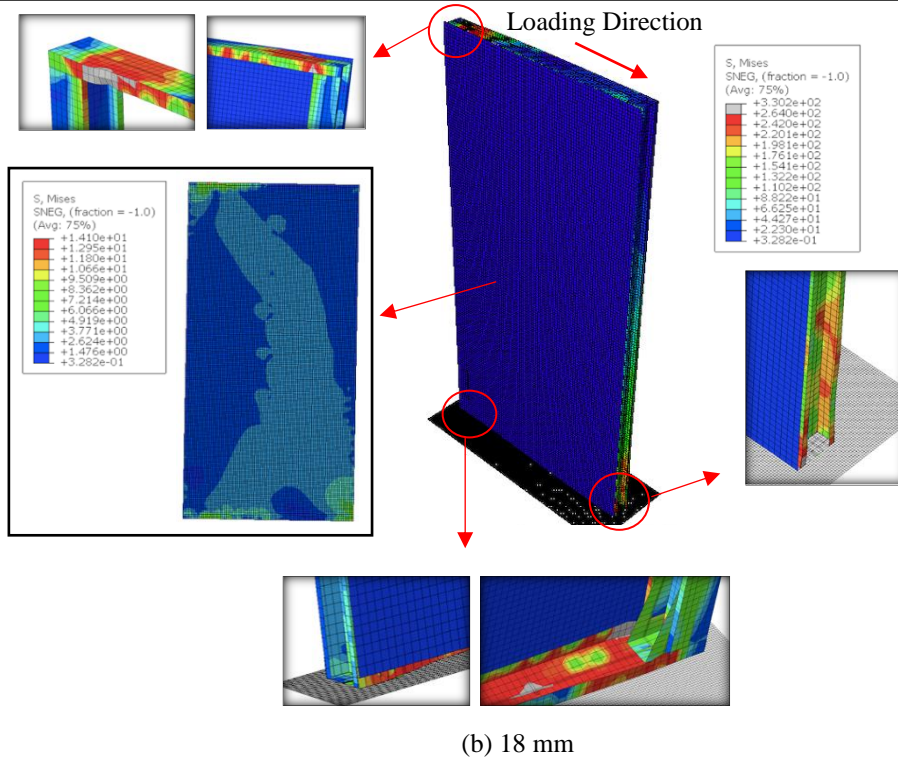
(b) 18 mm

(c) 25 mm

Figure 3.15 von-Mises stress distribution of OSB sheathed CFS shear wall panels with a) 7 mm, b) 18 mm and c) 25 mm OSB thickness at the failure point

3.3.2.c. CFS thickness

As shown in Fig. 3.11 (c), unlike OSB thickness, the contribution of CFS thickness to the lateral behaviour of shear wall panels was found to be negligible. This can be clearly seen in Fig. 3.16 in which the benchmark specimen panel with approximately doubled CFS thickness (i.e. 2 mm) provided only a 10% enhancement in lateral load capacity and initial stiffness of the wall systems. The von-Mises stress distribution shown in Fig. 3.17 indicated that increasing the thickness of the key specimen's framing members from 1.09 mm to 1.5 mm or 2 mm resulted in the development of the failure in the board element in addition to buckling of the bottom track. Besides, using relatively thicker CFS elements (i.e. 3 mm) postponed the buckling of the bottom track, and alternatively yielding of the bottom track was captured at the location of the anchor bolts subject to uplift force (see Fig. 3.17 (b)).
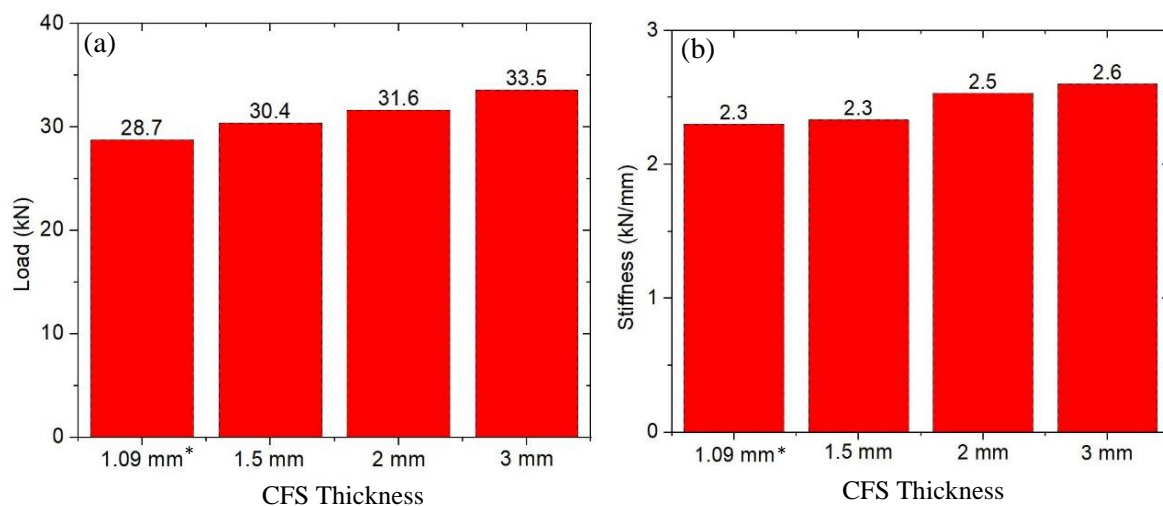
Figure 3.15 The variation of a) maximum load capacity and b) initial stiffness of OSB sheathed CFS shear wall panels with CFS thicknesses of 1.09, 1.5, 2, 3 mm (*benchmark specimen)
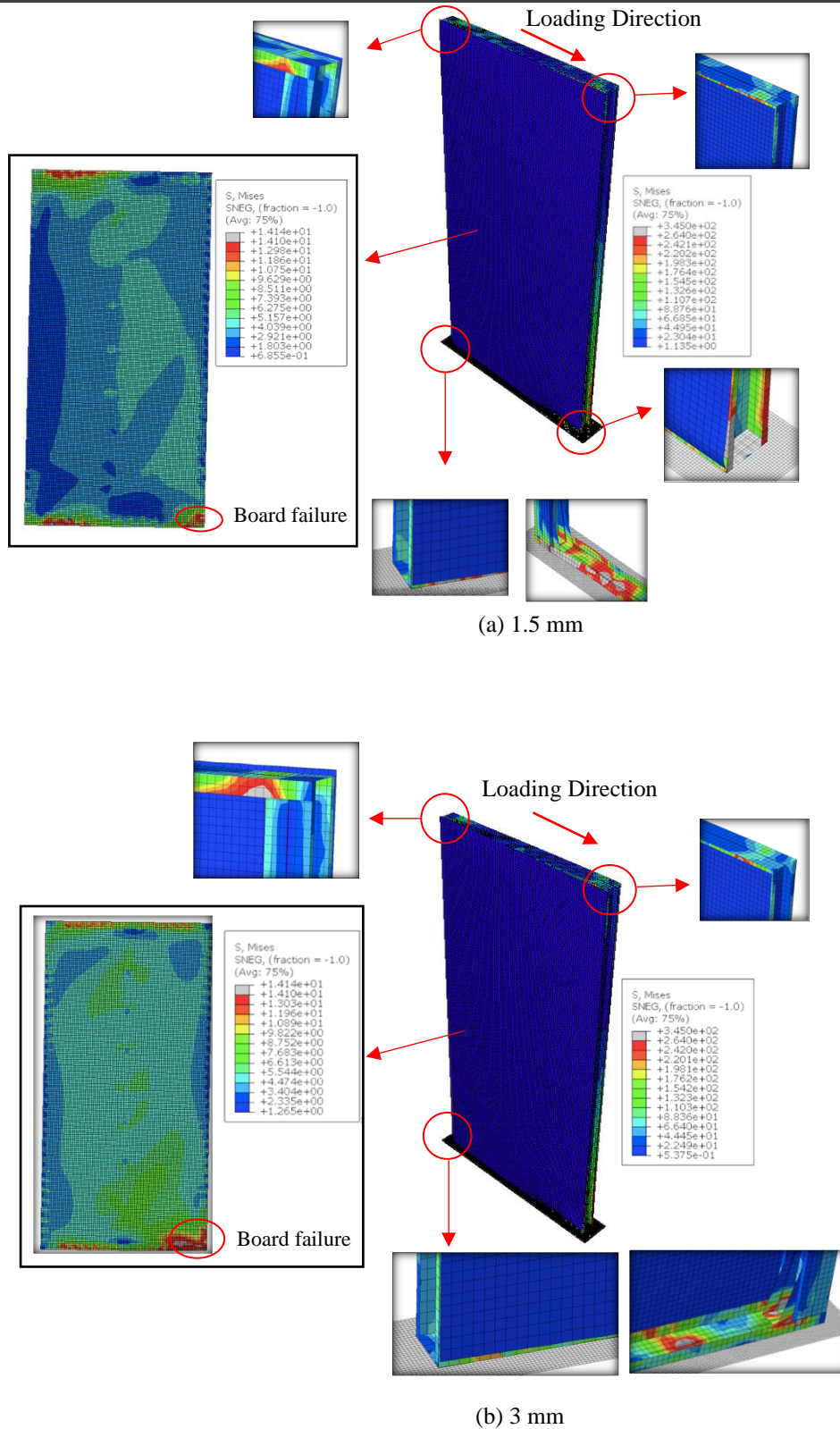
(a) 1.5 mm

(b) 3 mm

Figure 3.16 von-Mises stress distribution of OSB sheathed CFS shear wall panels with CFS thicknesses of a) 1.5 mm and b) 3 mm at the failure point

3.3.2.d. Board configuration

The results presented in Fig. 3.11 (d) indicate a significant dependence of the lateral load-displacement response of the OSB-sheathed panels on the way the OSB boards were installed (Fig. 3.1). This can be also seen in Fig. 3.18 where the shear wall panels with no horizontal/vertical seam (i.e. configuration A) showed the highest maximum lateral load capacity and initial stiffness in comparison to other configurations. However, the existence of horizontal/vertical seam resulted in a significant reduction up to 150% in both lateral strength and stiffness of the system The least favourable structural performance was taken from the panel with a vertical seam throughout the height of the wall at the location of the mid-stud (i.e. configuration B). This can be attributed to localized failure at the bottom of the board on the left-hand side of the panel by local buckling and crushing, and an associated failure at the bottom of the mid-stud by local buckling and yielding (see Fig. 3.19 (a)). As shown in the von-Mises stress distribution of the wall configurations C and D at the failure point (Fig. 3.19 (b) and (c)), the boards and the vertical elements experienced localised failure at the location of the horizontal seam. It should be noted that further discretization of the boards and a combination of horizontal and vertical seams (i.e. configuration E) resulted in a negligible change in the lateral behaviour and failure mechanism of the wall.
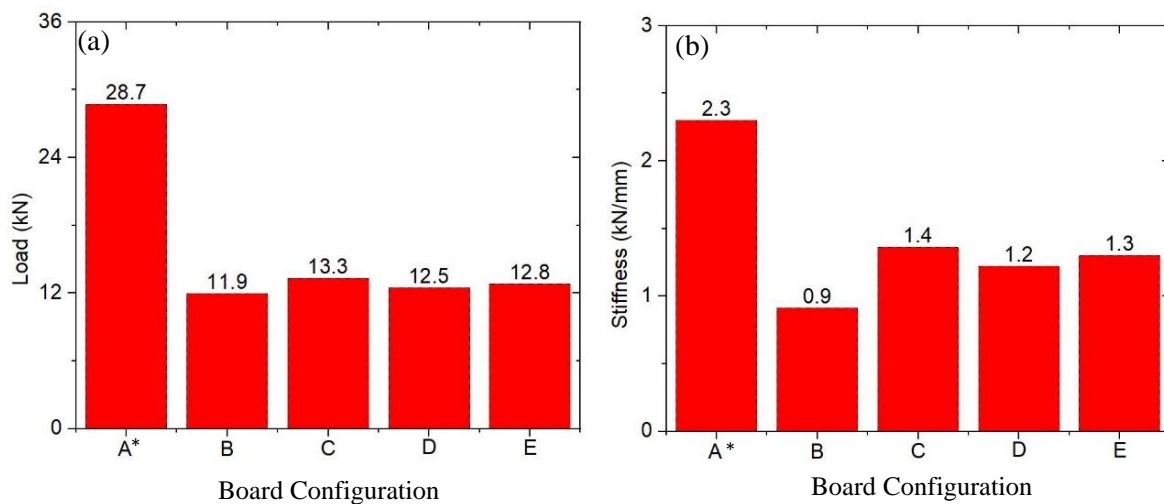
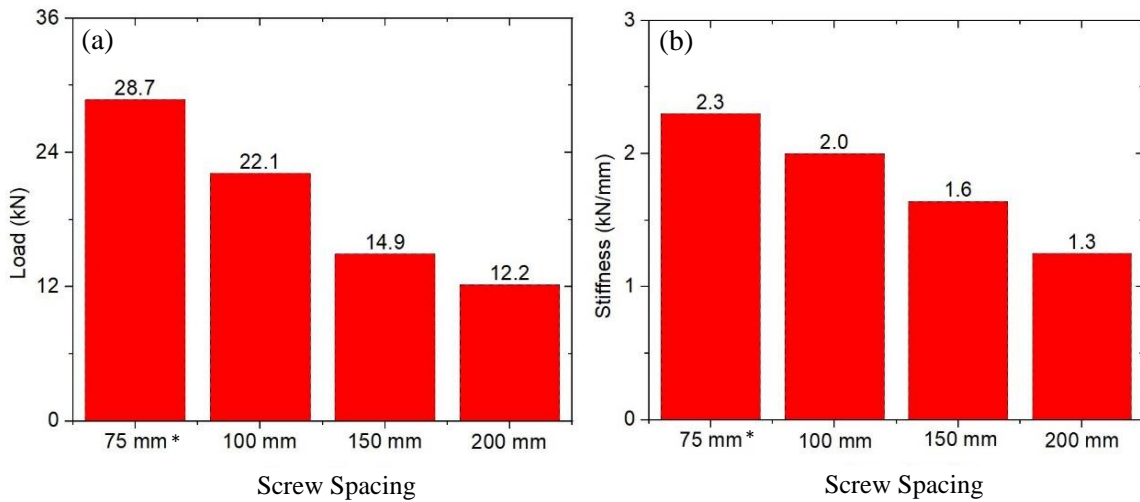**Figure 3.17 The variation of a) maximum load capacity and b) initial stiffness of OSB sheathed CFS shear wall panels with A, B, C, D and E board configurations (*benchmark specimen)**
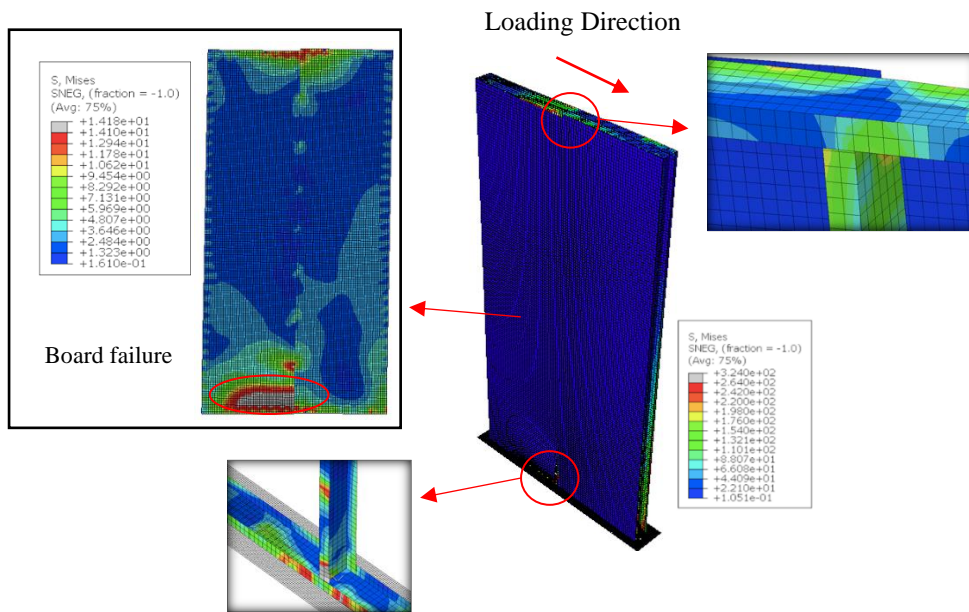
(a) Configuration B
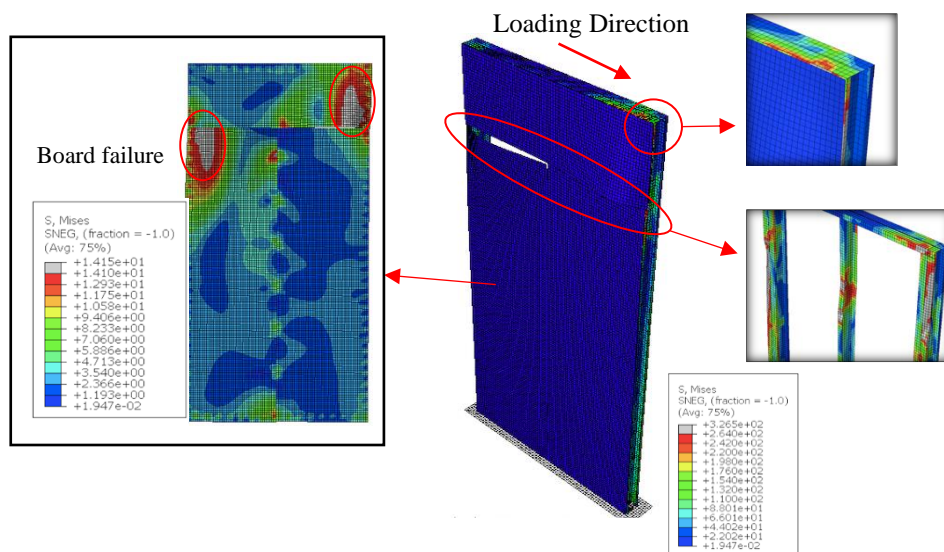
(b) Configuration C

Figure 3.18 von-Mises stress distribution of OSB sheathed CFS shear wall panels with board configurations of a) B, b) C and c) D at the failure point
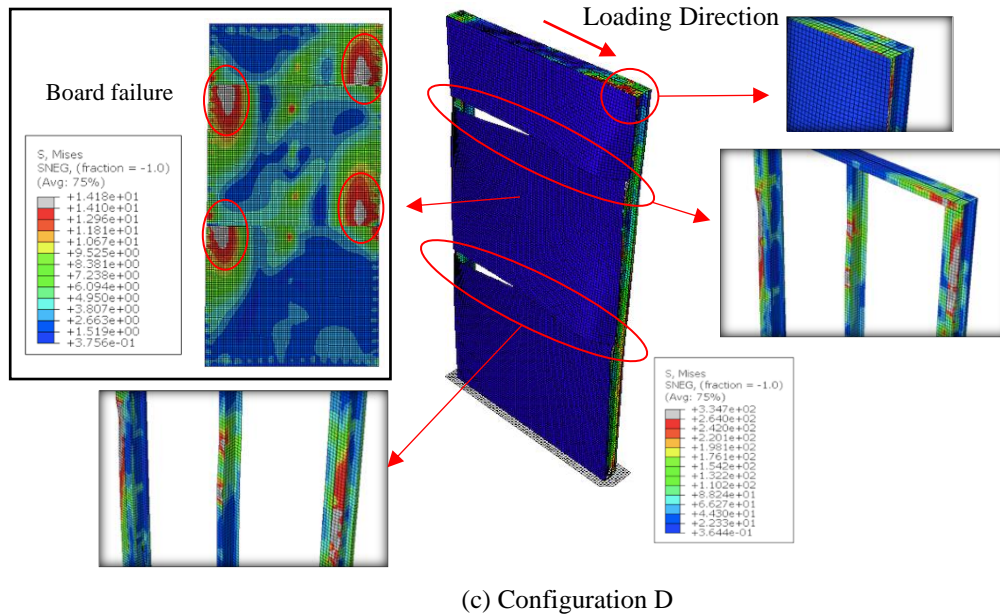
(c) Configuration D

Figure 3.19 von-Mises stress distribution of OSB sheathed CFS shear wall panels with board configurations of a) B, b) C and c) D at the failure point

3.3.2.e. Gravity load

The maximum lateral load capacities (F_{max}) and initial stiffnesses (S_i) of the panels with different gravity load levels was examined in Fig. 3.20. In general, the effects of gravity load on the initial stiffness of the system were approximately negligible regardless of the amount of gravity load. In addition, the influence of gravity load was found to be negligible for loads of up to 40% of the total compressive capacity of the stud cross-sections. On the other hand, when the vertical load was increased to 60% of the total compressive capacity, the lateral strength of the shear wall panel was dramatically reduced (see Fig. 3.20), which was due to localised buckling of the compressive chord stud. It can be seen from Fig. 3.11 (e) that the load-displacement response of the key specimen showed more ductile behaviour by increasing the gravity load up to 20%, however, further enhancement of the gravity load resulted in a more brittle failure of the system. This inconsistency can be attributed to the change in the failure mode of the panels. Since the dominant failure of the key specimen occurred in the bottom track due to the uplift force (see Fig. 3.13 (a)), the application of vertical load can in turn reduce the amount of uplift force and consequently postpone the failure in the bottom track. On the other hand, increasing the gravity load from 20% to 30% of the total compressive capacity resulted in a shift of the failure from fastener to the vertical elements (i.e. mid-stud and compressive

chord stud), as shown in Fig. 3.21. Therefore, further enhancement of the gravity load led to signify the second-order effects (i.e. P-Delta) and reduce the strength and displacement. Similar observations on the second-order effects were reported by Papargyriou et al. (2021) and Papargyriou and Hajirasouliha (Papargyriou and Hajirasouliha, 2021) for strap-braced shear wall systems under high axial load levels.
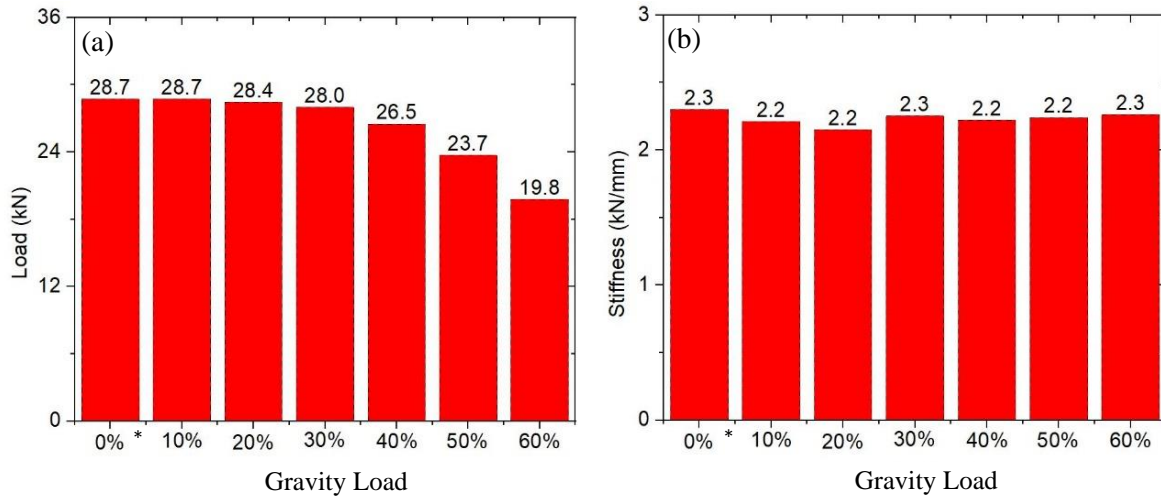
Figure 3.19 The variation of a) maximum load capacity and b) initial stiffness of OSB sheathed CFS shear wall panels with gravity loads of 0%, 10%, 20%, 30%, 40%, 50% and 60% (*benchmark specimen)

(a)   Load ratio 10%
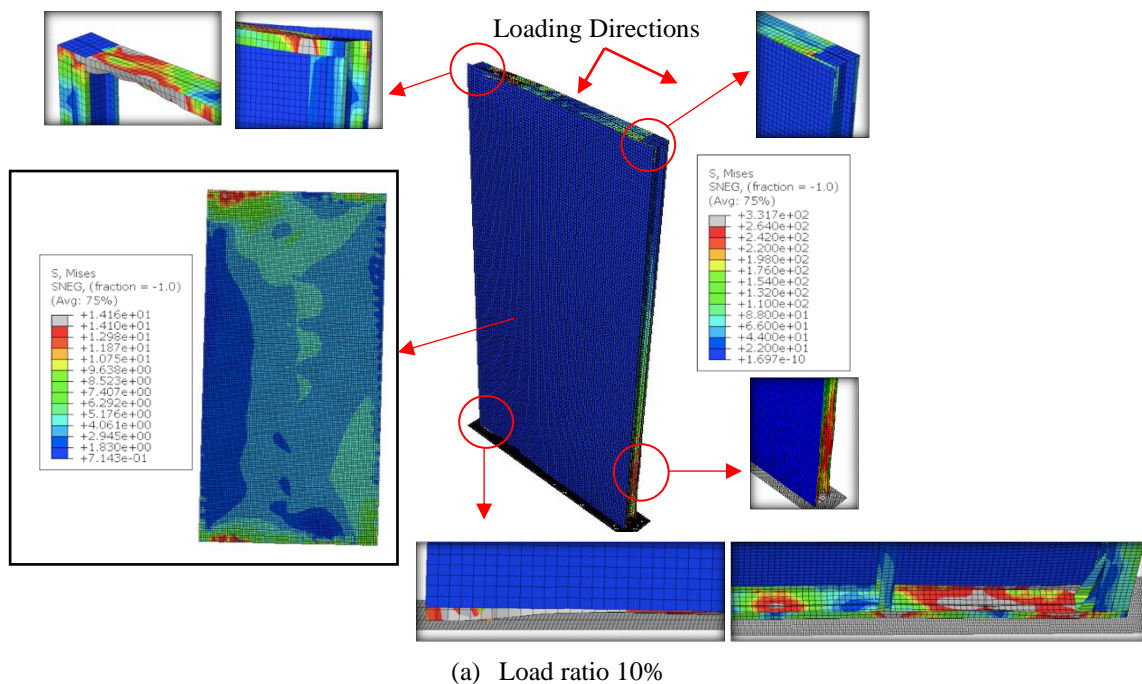
Figure 3.20 von-Mises stress distribution of OSB sheathed CFS shear wall panels with gravity loads of a) 10%, b) 20% and c) 30% at the failure point

(b) Load ratio 20%

(c) Load ratio 30%
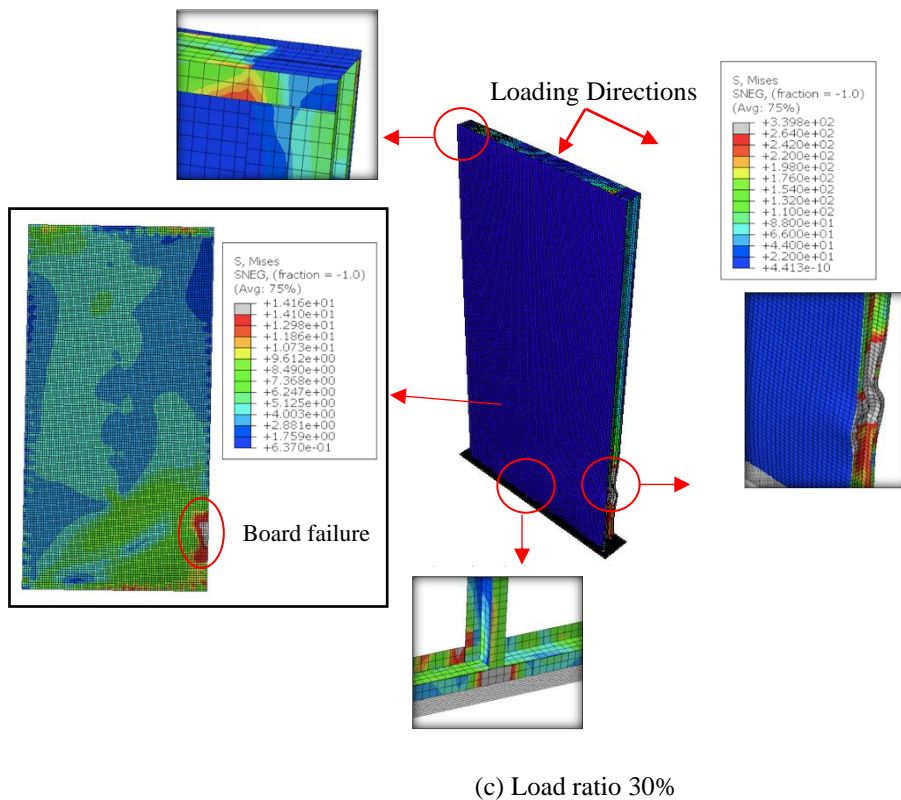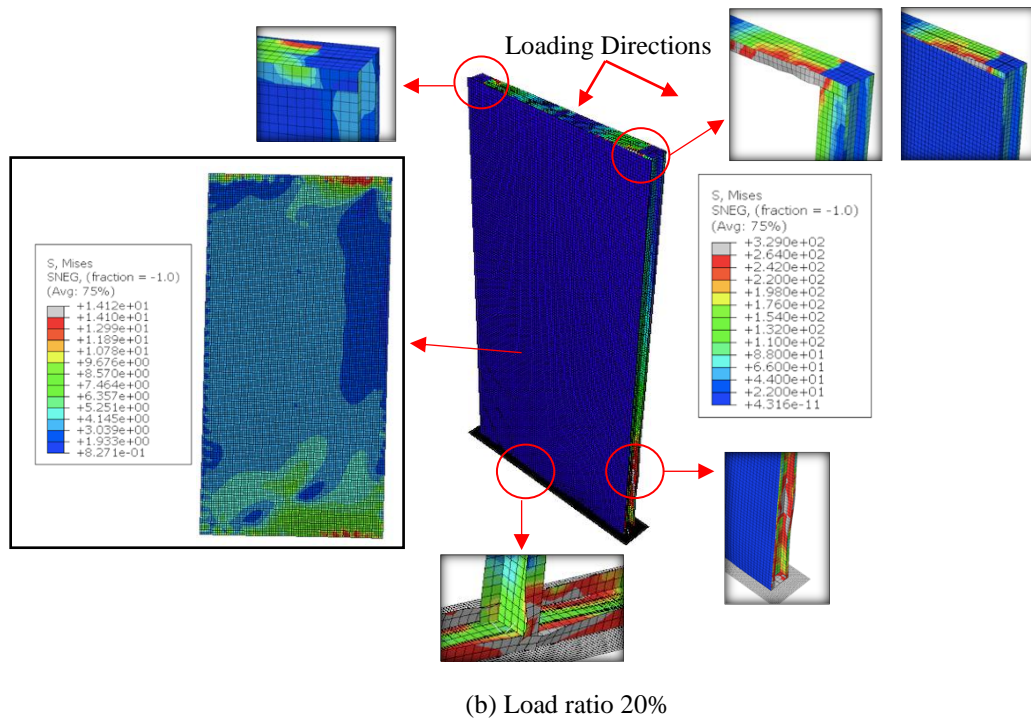
Figure 3.21 von-Mises stress distribution of OSB sheathed CFS shear wall panels with gravity loads of a) 10%, b) 20% and c) 30% at the failure point

3.3.2.f. Sheathing

The lateral load resistance and stiffness of unsheathed CFS shear wall panels with those with single and double OSB sheathing was reported in Fig. 3.22. The comparison of the results for the single sheathed and unsheathed specimens indicated that the contribution of the CFS shear wall panel in providing lateral load resistance and stiffness was less than 5% and 1%, respectively.

In addition, Fig. 3.22 showed that the lateral strength and stiffness of the double-sheathed wall panel were slightly less than twice those of single-sheathed walls. Fig. 3.23 illustrates the von-Mises stress distribution of unsheathed and double-sheathed CFS shear wall panels. It can be clearly seen that significant premature failure occurred in the CFS elements of the unsheathed wall, which justifies its low lateral load resistance as discussed above. Furthermore, compared to the wall with single sheathing, using double-sheathed shear wall panels resulted in an additional failure in the top track and the boards close to the corner zones.
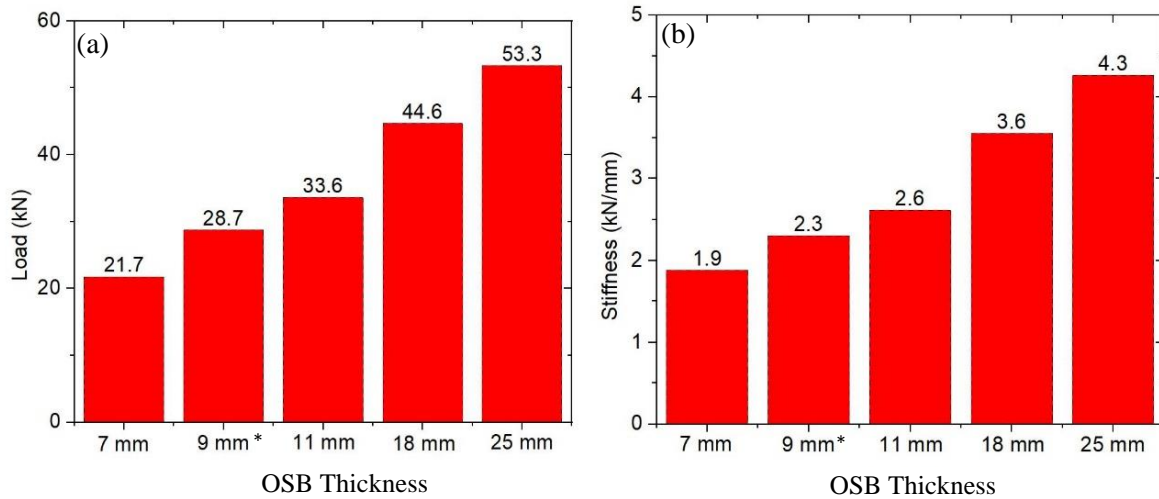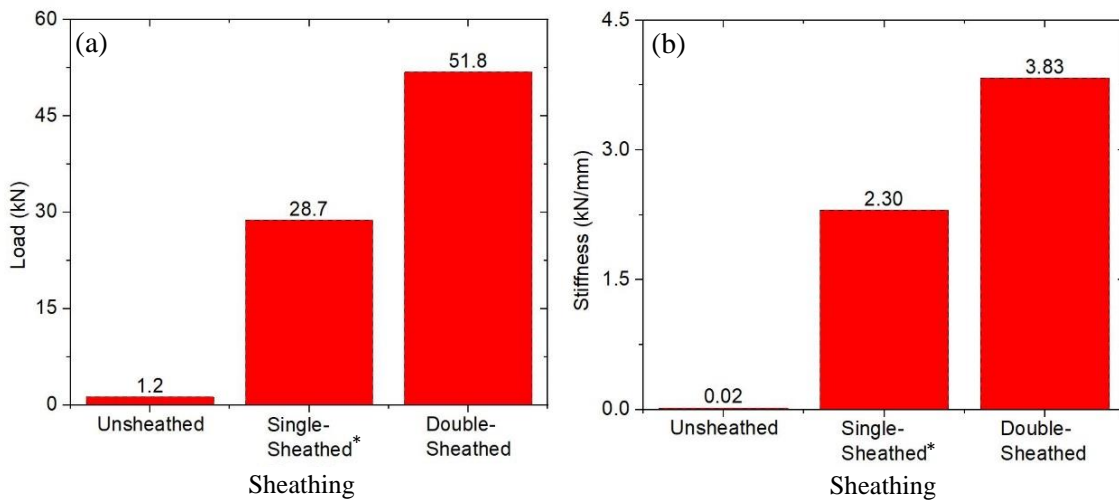

Figure 3.21 The variation of a) maximum load capacity and b) initial stiffness of OSB sheathed CFS shear wall panels with sheathing systems of unsheathed, single- and double-sheathed (*benchmark specimen)

(a) Unsheathed
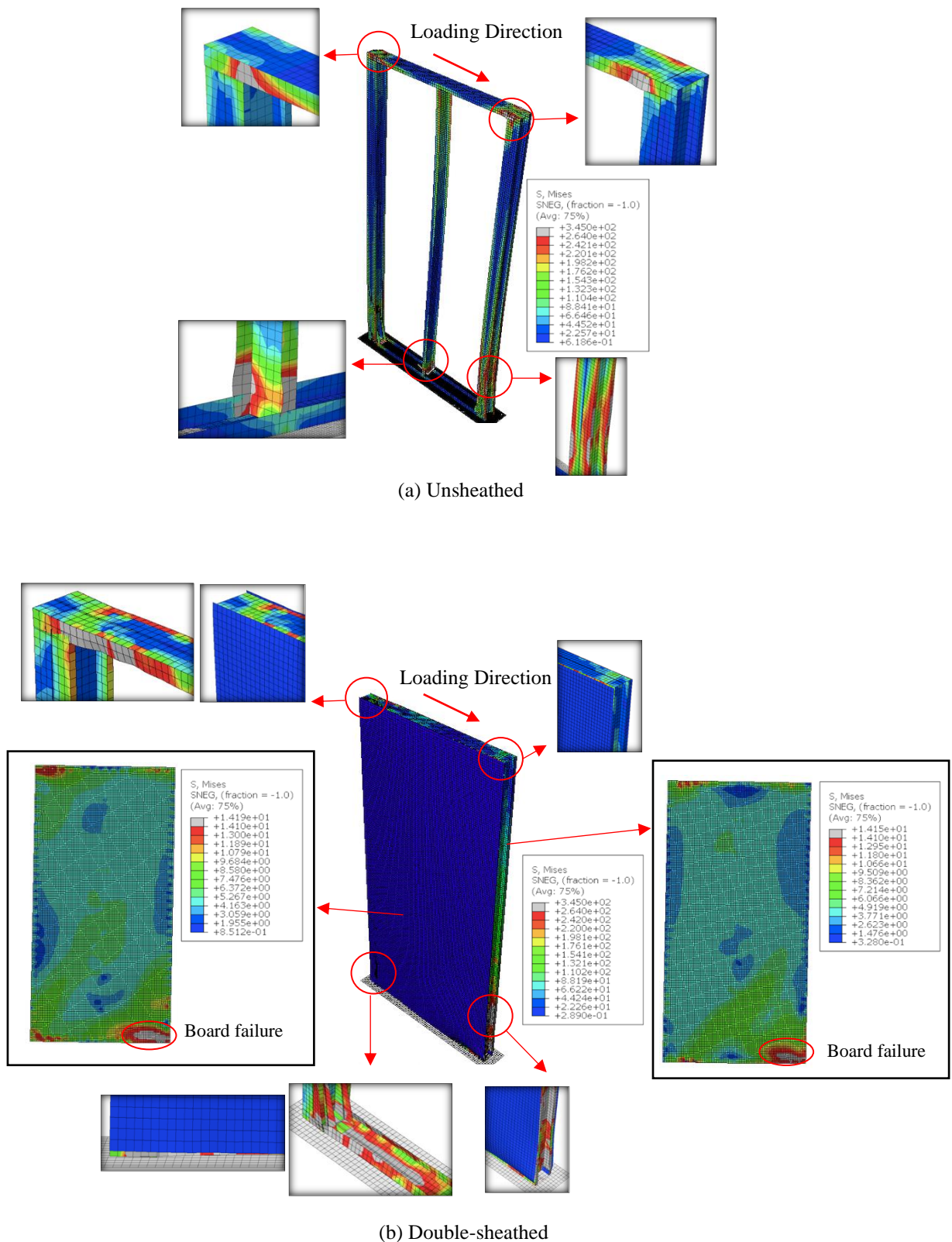
(b) Double-sheathed

Figure 3.22 Failure mechanism and von-Mises stress distribution of OSB sheathed CFS shear wall panels with sheathing systems of a) unsheathed and b) double-sheathed at the failure point

3.4. Seismic assessment of the wall systems and discussions

The results of the parametric studies were further used to evaluate the seismic performance characteristics of CFS OSB-sheathed wall panels and investigate the effects of key design variables on the following parameters:

- The deformation capacity is expressed as the ultimate displacement (Δ_u), corresponding to the failure point (i.e. board failure or an 80% of post-peak load, depending on whichever happens first).

- Ductility is the ability of a structure to undergo large plastic deformations without significant reduction in ultimate strength (Gioncu, 2000). The fundamental definition of ductility ratio (μ) is the ratio of ultimate displacement (Δ_u) and the yield displacement (Δ_y), as follows:

$$\mu = \frac{\Delta_u}{\Delta_y} > 1.0 \tag{3.6}$$

- With respect to the computation of ductility ratio, it is common practice to convert load-displacement curves into equivalent bi-linear curves. One of the well-established methods to assess performance of the CFS wall systems was the Equivalent Energy Elastic-Plastic (EEEP) analysis model which was first proposed by Park (1989) and also recommended by the AISI S400 (American Iron and Steel Institute, 2016). In this method, as can be seen in Fig. 3.24, the load-displacement response is idealised by two straight lines, where the first line represents the secant stiffness (S_i) determined by connecting the origin to the load equal to $0.4F_{max}$, and the second horizontal line starting from the yield point (Δ_y, F_y) to the ultimate displacement (Δ_u), is then determined in such a way that the enclosed areas under the equivalent and the actual curves are equal.

- The energy dissipation capacity (E), is defined as the area under the equivalent bi-linear load-displacement curve up to the ultimate displacement (Δ_u).
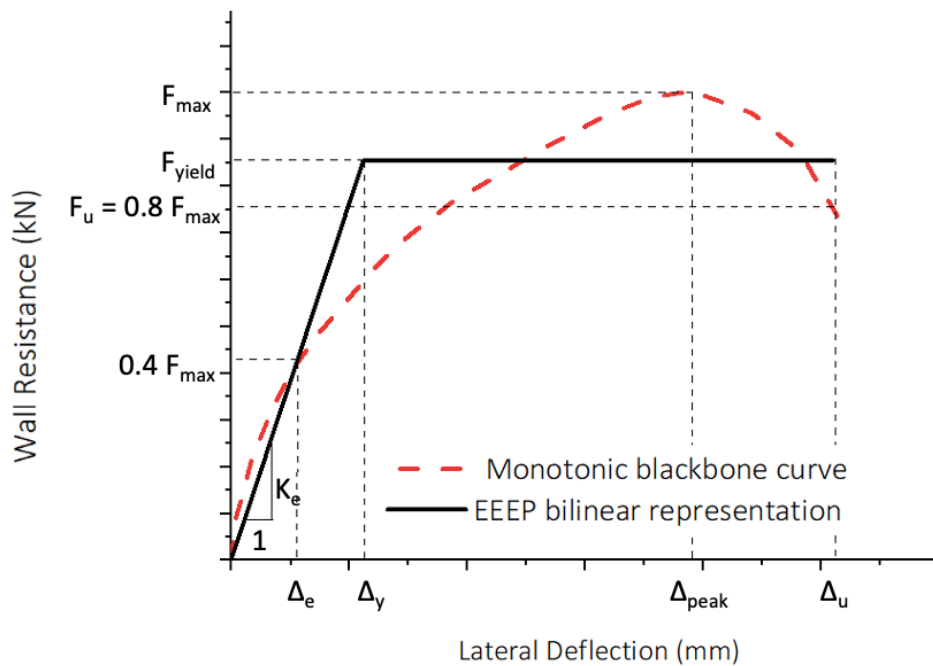
Figure 3.23 EEEP design methodology

Figs. 3.25, 3.26 and 3.27 show the results of ultimate displacement (Δ_u), ductility (μ) and energy dissipation capacity (E) for the shear wall panels with various design variables, respectively. The results demonstrated that increasing screw spacing resulted in an increase (up to 48%) in the ductility of the shear wall panel as long as no failure occurred in the board element (i.e. 75, 100 and 150 mm). As can be seen in Fig. 3.26 (a), the ductility of the system reached the highest value at 150 mm screw spacing specimen. This implies that the maximum structural capacity of the board was exploited, which in turn led to the highest ultimate displacement in the structural system (see Fig. 3.23 (a)). On the contrary, initiation of the failure in the board elements can reduce the ductility and ultimate displacement of the wall due to a reduction in the deformation capacity of the board. It can be therefore concluded that the screw spacing can be adjusted in order to provide a maximum ductility for the CFS OSB sheathed shear wall panels. However, Fig. 3.27 (a) clearly indicates a downward trend in energy dissipation capacity of the CFS shear wall panels (E) by increasing the screw spacing regardless of the type of failure.

Figs. 3.25 (b) and 3.26 (b) showed that using thinner OSB led to higher ductility and ultimate displacements. A difference of 40% in both variables was observed between configurations with thicknesses of 9 and 25 mm. An exception is noted for 7 mm thick OSB, where failure

happened in the board. It can be also seen in Fig. 3.27 (b) that the energy dissipation capacity of the system with different OSB thicknesses was mainly controlled by the failure mechanism. While energy dissipation was increased by increasing the board thickness, shifting the failure to the compressive chord led to a reduction in the energy dissipation capacity. On the other hand, using thicker CFS elements could always improve the seismic characteristics of the OSB sheathed shear wall panels (see Figs. 3.25 (c), 3.26 (c) and 3.27 (c)).

The seismic characteristics of the shear wall panels can be significantly affected by the board configurations (up to 5 times), as shown in Figs. 3.25 (d), 3.26 (d) and 3.27 (d). The results demonstrated that the presence of horizontal seams in the sheathing (i.e. configurations C, D and E) resulted in the least favourable seismic characteristics due to the development of localised failure in the vertical CFS elements at the location of horizontal seams (see Section 3.3.2). On the other hand, the existence of the vertical seam (i.e. configuration B) improved the ultimate displacement and ductility of the system, while the energy dissipation capacity of the shear wall panel with the vertical seam was considerably reduced in comparison to that with no seam (i.e. configuration A).

As discussed in Section 3.3.2, increasing the gravity load up to 20% of the axial compressive capacity of the vertical elements can reduce the uplift force and consequently postpone the failure in the bottom track. Therefore, as long as the failure remained on the bottom track the seismic characteristics of the shear wall panel were improved by increasing the gravity load. However, when the failure shifts to the compressive chord stud, the seismic characteristics were dramatically dropped by increasing the gravity load (see Figs. 3.25 (e), 3.26 (e) and 3.27 (e)).

Fig. 3.25 (f) shows that the unsheathed CFS wall panel exhibited considerably higher lateral deformation capacity compared to its single- and double-sheathed wall panel counterparts (by 58% and 92%, respectively). However, as shown in Fig. 3.26 (f), the ductility of the unsheathed system was around 58% and 45% lower than that of the single- and double-sheathed OSB wall panels. This can be attributed to the considerably higher yield displacement of the unsheathed CFS wall panel due to its lower lateral stiffness. The results in Fig. 3.27 (g) also show that the energy dissipation capacity of the unsheathed CFS wall panel is negligible compared to the OSB sheathed wall panel systems. Double-sheathed shear wall panel outperformed the single-

sheathed wall in terms of energy dissipation capacity by 36 %; however, the single-sheathed wall panel showed around 22% and 30% higher deformation capacity and ductility when compared to the double-sheathed system. This indicated that while the presence of OSB sheathing can considerably improve the seismic performance of the CFS wall panel (as long as the screw connections do not fail), adding the second OSB board does not necessarily enhance the seismic characteristics of the system.
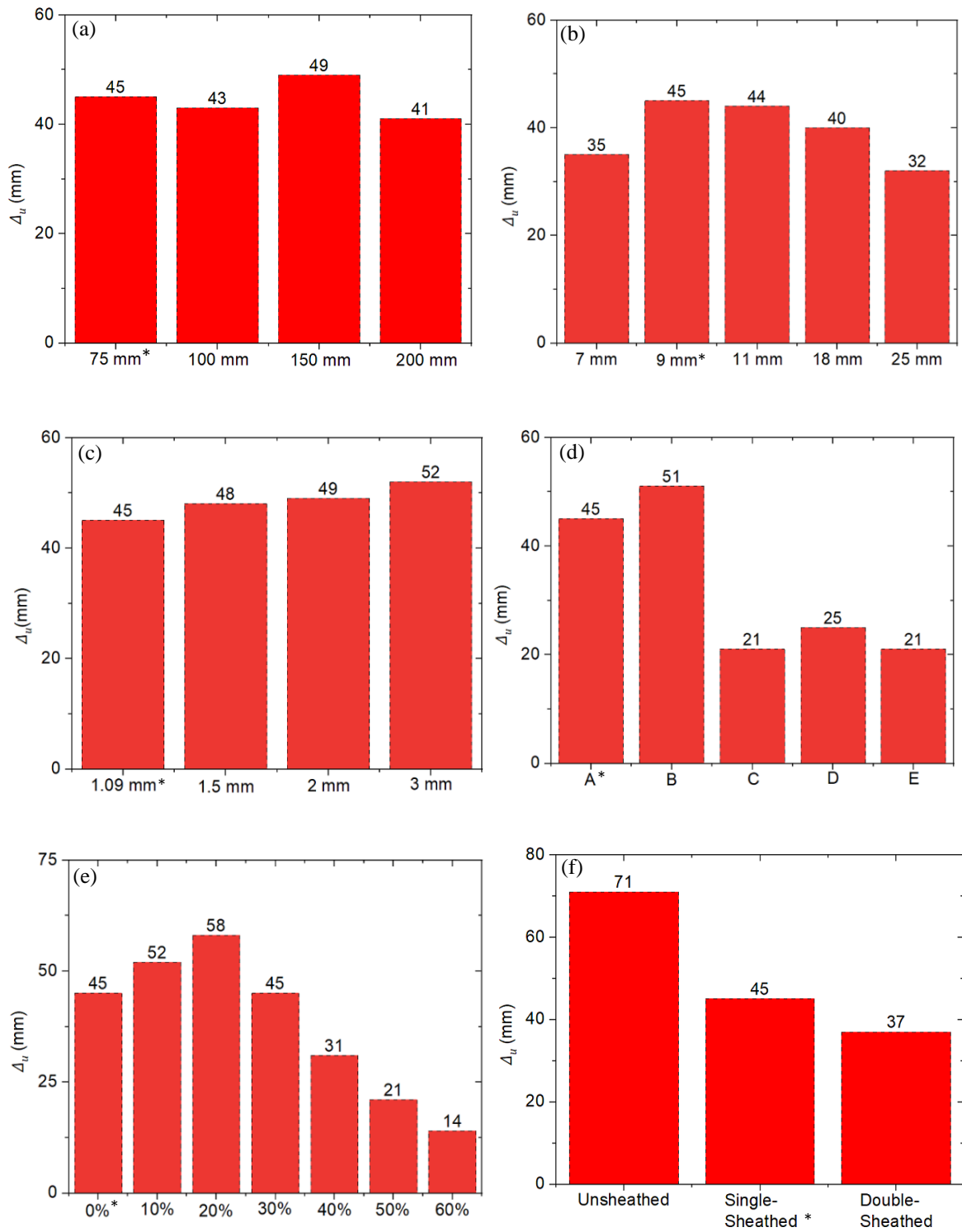
Figure 3.25 Deformation capacity of OSB sheathed CFS shear wall panels with various design parameters (*benchmark specimen)
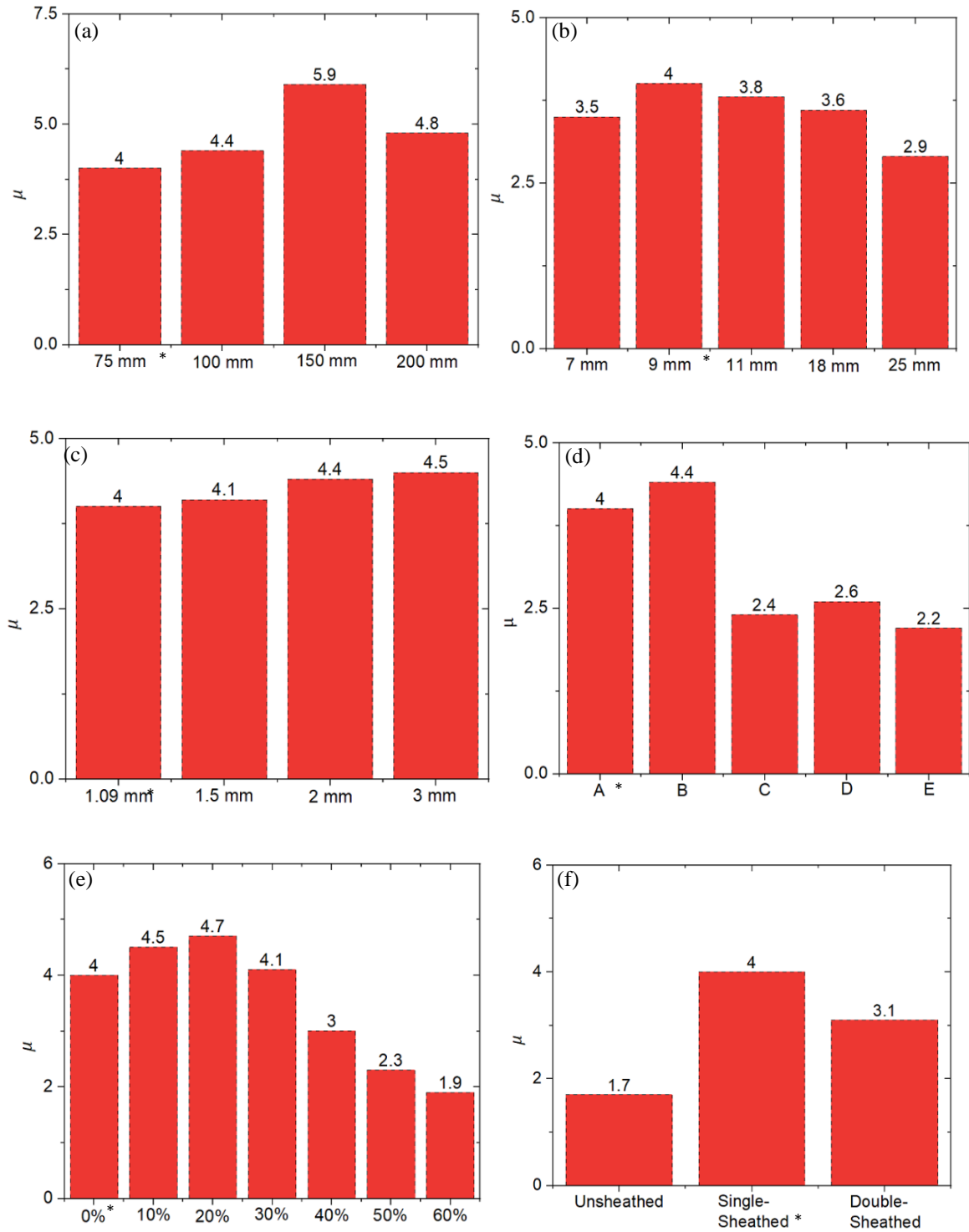
Figure 3.26 Ductility ratios of OSB sheathed CFS shear wall panels with various design parameters (*benchmark specimen)
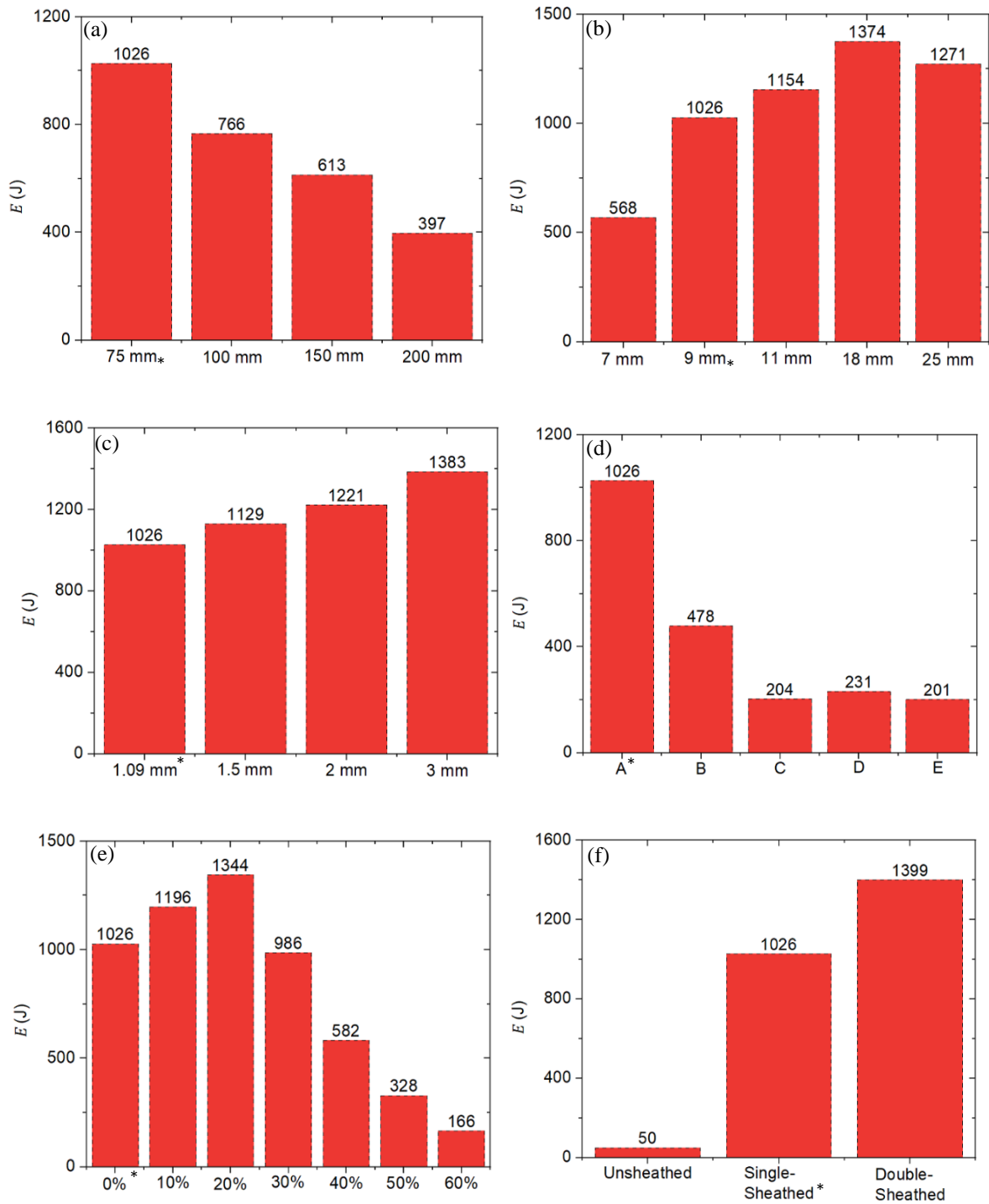
Figure 3.27 Energy dissipation capacity of OSB sheathed CFS shear wall panels with various design parameters (*benchmark specimen)

3.5. Summary and conclusions

In this chapter, the lateral seismic behaviour and failure mechanism of the CFS shear wall panels sheathed with OSB was investigated using detailed nonlinear FE models of OSB sheathed CFS shear wall panels nonlinear material properties and geometric imperfections were taken into account, and the results of load-displacement responses and failure mechanisms were validated against those obtained from the experimental data. The model was subsequently employed in comprehensive parametric studies aimed at investigating the effects of various key design variables on the structural performance parameters and the seismic characteristics of the system. The variables considered were the screw spacing, the thicknesses of the OSB and the CFS members, the board lay-out configuration, the gravity load ratio, and the number of boards (single- vs. double-sheathed systems). Based on the obtained results, the following conclusions can be drawn:

- In general, reduction in the screw spacing could significantly improve the maximum lateral load capacity and initial stiffness of the shear-wall panels by up to 136% and 84%, respectively. In addition, while using a short screw spacing can postpone the failure of the board at the location of the screws, increasing screw spacing results in significant deformation of the OSB and consequently failure in the board. The results demonstrated that increasing screw spacing resulted in an increase (up to 48%) in the ductility of the shear wall panel as long as no failure occurred in the board element. However, a downward trend was seen in the energy dissipation capacity of the CFS shear wall panels with the increasing in the screw spacing regardless of the type of failure.

- The overall load-displacement responses of the CFS shear wall panels were significantly affected by the OSB thickness. Use of thicker OSB could increase the maximum load capacity and initial stiffness of the shear wall panels almost proportionally. Shear wall panels with thin OSB elements experienced failure in the board, however, this failure was shifted to the compressive chord stud by utilising thicker OSB. Overall, using thinner OSB provided higher ductility and ultimate displacement for the system by up to 40%, however, energy dissipation was increased by increasing the board thickness. The contribution of CFS thickness to the lateral strength and stiffness of shear wall

panels was found to be negligible (less than 10%). It was shown that increasing the thickness of CFS elements could potentially result in the development of failure in the board element, while using thicker CFS elements could always improve the seismic characteristics of the OSB sheathed shear wall panels.

- Unlike OSB thickness, the contribution of CFS thickness to the lateral strength and stiffness of shear wall panels was found to be negligible (less than 10%). In general, the increase in the thickness of CFS elements can potentially result in the development of failure in the board element. The results showed that the use of thicker CFS elements could always improve the seismic characteristics of the OSB sheathed shear wall panels.

- The shear wall panels with no horizontal/vertical seam could provide the highest maximum lateral load capacity and initial stiffness, while the existence of the horizontal/vertical seam resulted in a significant reduction in both lateral strength and stiffness of the system (up to 50%). The failure mechanism demonstrated that the boards and the vertical elements in the shear wall panel experienced localised failure at the location of the horizontal seam, which significantly decrease the seismic characteristics of the shear wall panel (up to 5 times). In addition, further discretization of the boards and a combination of horizontal and vertical seams could provide a negligible change in the lateral behaviour and failure mechanism of the wall.

- In general, the effect of gravity load on the initial stiffness of the system was approximately negligible regardless of the amount of gravity load. In addition, the influence of gravity load was found to be negligible for loads of up to 40% of the total compressive capacity of the stud cross-sections. On the other hand, when the vertical load was increased to 60% of the total compressive capacity, the lateral strength of the shear wall panel was dramatically reduced, which was due to localised buckling of the compressive chord stud. The second-order effect was governed in the shear wall panels under high axial load levels, and consequently the failure happened in the compressive chord stud, which led to a significant reduction in the seismic characteristics.

- The contribution of unsheathed panels in providing lateral load resistance was found to be generally negligible. In addition, CFS wall panel sheathed with double OSB sheathing was found to be over twice that with single-sided OSB. The failure mechanism showed that, compared to the wall with single sheathing, using double-

sheathed shear wall panels resulted in an additional failure in the top track and the boards close to the corner zones. Double-sheathed shear wall panels outperform single-sheathed shear wall panels in terms of energy dissipation capacity by 36 %, however, single-sheathed wall panels indicated more ductile behaviour than double-sheathed ones.

The overall outcomes of this study and the developed numerical models provided useful information on the more efficient design of CFS shear wall panels sheathed with OSB for both seismic and non-seismic applications.

Chapter 4: Out-of-plane bending behaviour and capacity of sheathed face-up CFS stud walls: experimental investigation

4.1. Introduction

This chapter describes the experimental investigation into the bending behaviour and capacity of face-up CFS sheathed with wood-based stud wall panels and provides insight into the failure mechanism under out-of-plane loading. Despite extensive experimental and numerical studies conducted for sheathed CFS stud wall systems, there was still a lack of comprehensive investigations on the out-of-plane structural behaviour of the sheathed stud wall panels by considering the effects of key design parameters on the performance of such systems. For this purpose, a comprehensive experimental investigation of sheathed CFS stud wall panels were conducted by considering the effects of screw spacing, the thickness of CFS and sheathing, the board scenarios and the main/auxiliary components. Based on the results and observations made during experiments, the structural performance parameters (i.e. bending load capacity, vertical displacement, initial stiffness), failure mechanism, rotation of the C-shape studs and end-slips of the tested stud wall panels were investigated in detail for each parameter. A total of 15 stud

walls sheathed with either Oriented Strand Board (OSB) or plywood specimens were tested under four-point bending loading which was applied directly to the board. To determine the stress-strain behaviour of the boards and CFS elements, material coupon tests were carried out. Besides, a series of axillary push-out and pull-out tests were performed to investigate the composite action between light-gauge steel stud framing and wood-based materials. It was observed that the out-of-plane behaviour of the CFS stud-wall sheathed with wood-based materials can be altered by changing the key design variables of the system.

4.2. Specimen geometry

The purpose of this experimental investigation was to determine the bending behaviour and capacity of sheathed CFS stud walls for various parameters. In this experimental test schedule, a total of 15 full-scale stud wall systems consisting of the CFS frame elements and a wood-based board were subjected to 4-point bending loading. In this study, the experimental program can be classified into four general design parameters (see Fig.4.1);

- Four different screws spacing, 75, 100, 150 and 300 mm, were used for the connections between the CFS frame elements and the wood-based board over the panel perimeter and inner stud to investigate the effects of the screw spacing on the system.
- The specimens were designed to consider the effects of different thicknesses of materials; OSB 9 and 18 mm, Plywood 9 mm, CFS 1.2 and 2 mm.
- The effect of the board configuration on the response of structural performance was examined by testing the panel specimens with unsheathed, single- and double-sheathed. In addition, two different centres spacing of 305 and 610 mm were taken into account.
- Effects of main/auxiliary components on the system were investigated seam, noggins, pinned no track.

A summary of the test matrix was presented in Table 4.1.
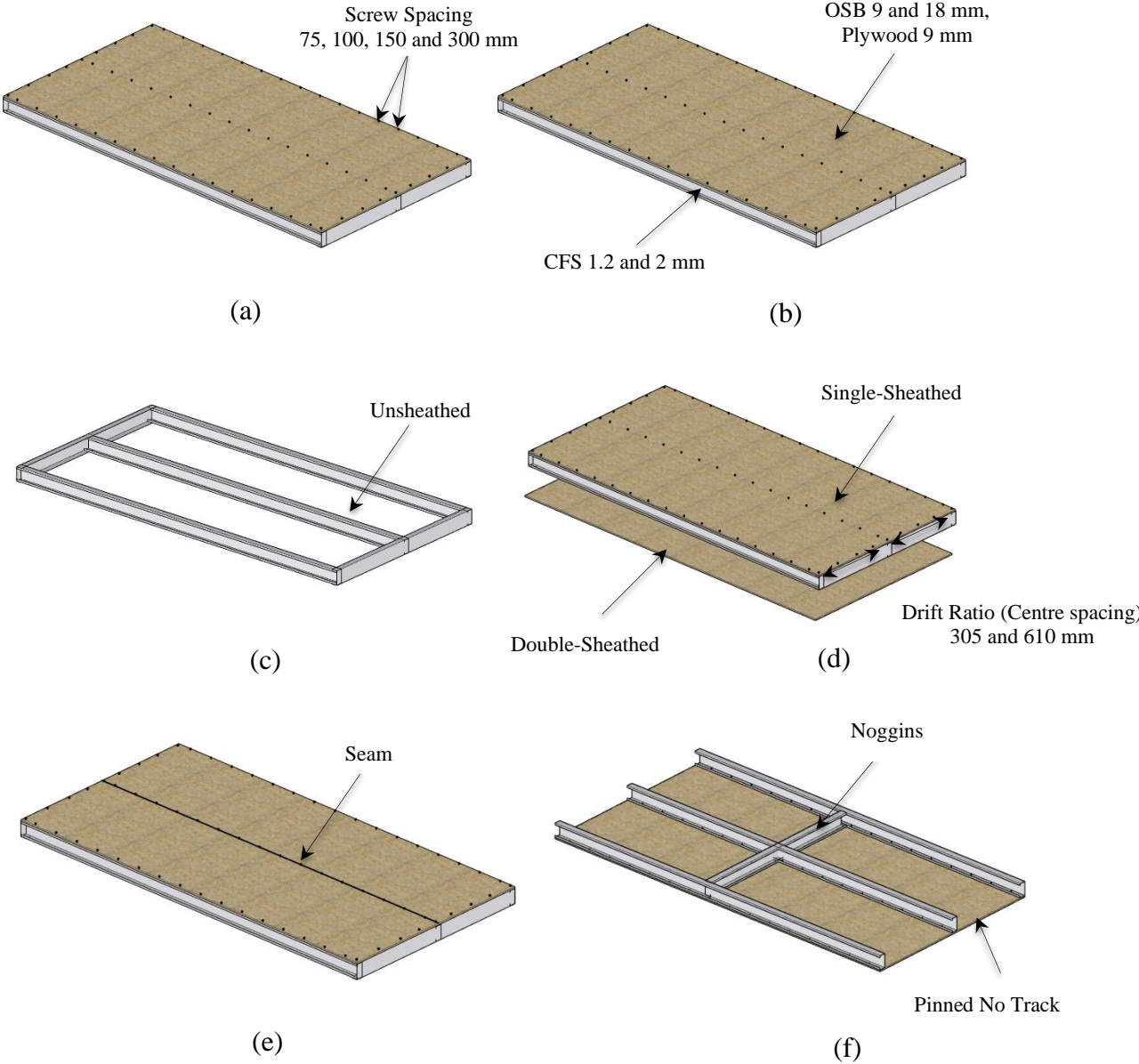
Figure 4.1 Design parameter; (a) screw spacing, (b) materials and thicknesses, (c), (d) board configurations: unsheathed-, single-, and double-sheathed walls, (e) and (f) effects of main/auxiliary components on the system

Table 4.1 The experimental parametric test matrix of the CFS shear wall panels

	Specimens	Test Code	Width x Length (mm x mm)	Test Numbers
Benchmark Test	Key Specimens	K1	1220 × 2440	2 Tests
		K2	1220 × 2440	
Screw Spacing	100 mm	S100	1220 × 2440	3 Tests
	150 mm	S150	1220 × 2440	
	300 mm	S300	1220 × 2440	
Materials and thicknesses	Plywood (9 mm)	P9	1220 × 2440	3 Tests
	OSB (18 mm)	OSB18	1220 × 2440	
	CFS (2 mm)	CFS2	1220 × 2440	
Board Configurations	Unsheathed	UB	1220 × 2440	4 Tests
	Double-Sided	DB1	1220 × 2440	
		DB2	1220 × 2440	
	Centre Spacing(305mm)	DR	610 × 2440	
Effects of main/auxiliary components on the system	Seam	S	1220 × 2440	3 Tests
	Noggings	N	1220 × 2440	
	Pinned no Track	PT	1220 × 2440	

The overall dimensions of the key stud wall specimens were 1220×2440 mm. The CFS framing elements were composed of C-unlipped channel and C-lipped channel for track and stud elements, respectively, as illustrated in Fig. 4.2. To accurately measure the dimensions of the wall components, the micro millimetre calliper was used. The average out-to-out cross-sectional dimensions of all 1.2 and 2 mm CFS members were reported in Table 4.2. Besides, the average thickness of the wood-based board at three different locations; top, middle and bottom (see Fig. 4.3); was listed in Table 4.3.

(a)   (b)
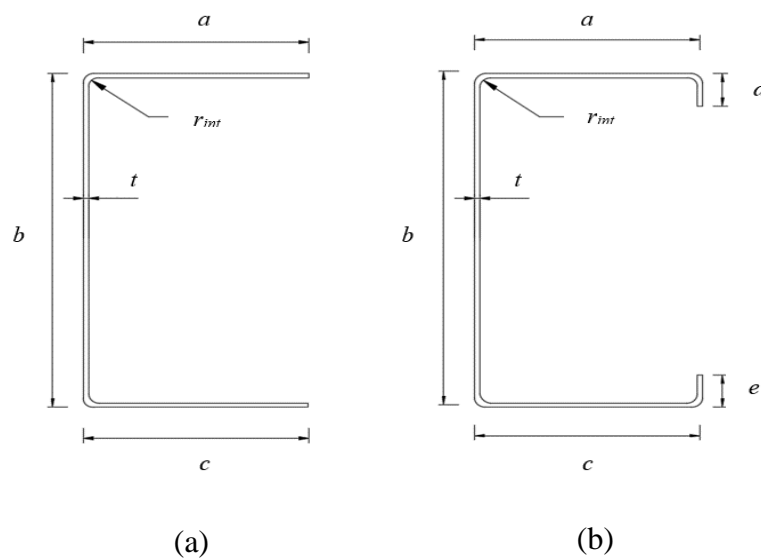
Figure 4.2 Cross-sectional (a) C-unlipped channel track, (b) C-lipped channel stud and labelling of dimensions of tested CFS members

Table 4.2 Average dimensions (out-to-out) of the tested CFS members (in mm)

Specimen Batch	t	r_{int}	C-unlipped channel CFS (tracks)			C-lipped channel CFS (studs)				
			a (flange)	*b* (web)	*c* (flange)	*a* (flange)	*b* (web)	*c* (flange)	*d* (lip)	*e* (lip)
1.2 mm CFS	1.19	2.8	57.57	99.66	57.43	50.57	99.73	50.64	8.93	11.11
2 mm CFS	1.92	3.2	56.76	103.20	57.38	49.19	100.64	49.31	13.93	15.16
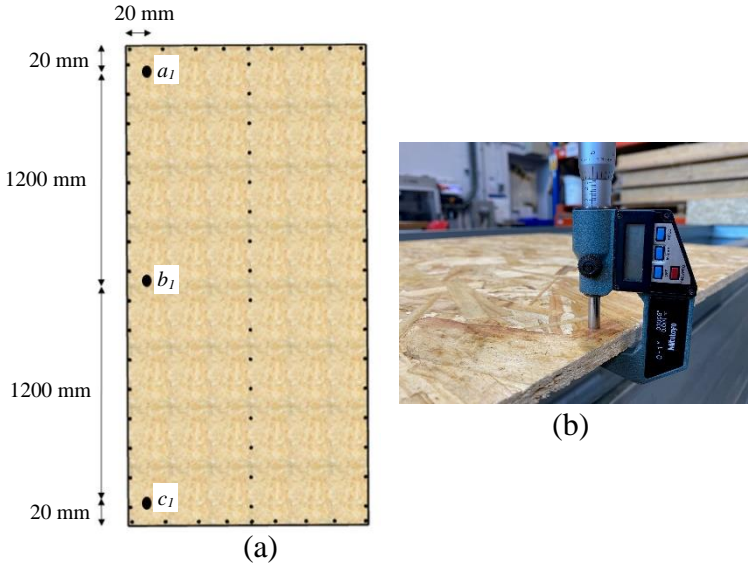
Figure 4.3 (a) Three points for average thickness of tested wood-based boards (b) micrometre calliper

Table 4.3 Average thickness of the tested wood-based boards (in mm)

Specimen Batch	The thickness of the wood-based board			
	a_1	b_1	c_1	Average thickness
9 mm OSB	8.94	8.92	8.84	8.90
18 mm OSB	17.62	17.59	17.64	17.62
9 mm Plywood	9.66	9.59	9.69	9.65

In this study, the benchmark test specimen was called 'key specimen' which was used to evaluate the behaviour of the other tested specimens with different design parameters. The key specimens consisted of 1.2 mm CFS framing members (i.e. studs and tracks) with stud spacing of 75 mm connected to 9 mm thick single OSB sheathing using 6.3 mm diameter self-drilling

screws with a bonded washer screw (see Fig. 4.4). It should be noted that the seam and noggins were not incorporated in the key specimen.

Figure 4.4 The 6.3 mm diameter of the self-drilling screws with a bonded washer

4.3. Material tests

4.3.1. CFS members

In total, six flat tensile coupons were tested to determine the characteristics of the CFS material. It should be also noted that only one coupon specimen was tested for each test configurations. Four coupons were cut along the centrelines of the web and flanges of an intact channel stud, as depicted in Fig. 4.5 (a). The remaining two coupons were sampled from the stud and track webs of actual wall specimens after the test. The detailed drawing of the tensile coupons is given in Fig. 4.5 (b). The dimensions of all tensile coupons were the same with a nominal gauge width of 12.5 mm as recommended by EN ISO 6892-1 (CEN, 2009). The detailed drawing of the tensile coupons was given in Fig. 4.5. Each flat coupon was instrumented using an extensometer with a 50 mm gauge length. Two 10 mm strain gauges were mounted, one on either side, to accurately record longitudinal strains in the early stages of testing, as depicted in Fig. 4.5. In order to capture the realistic values of the strain gauge data, the zinc coating was removed from the coupons before attaching strain gauges.

(a)

(b)

(c)
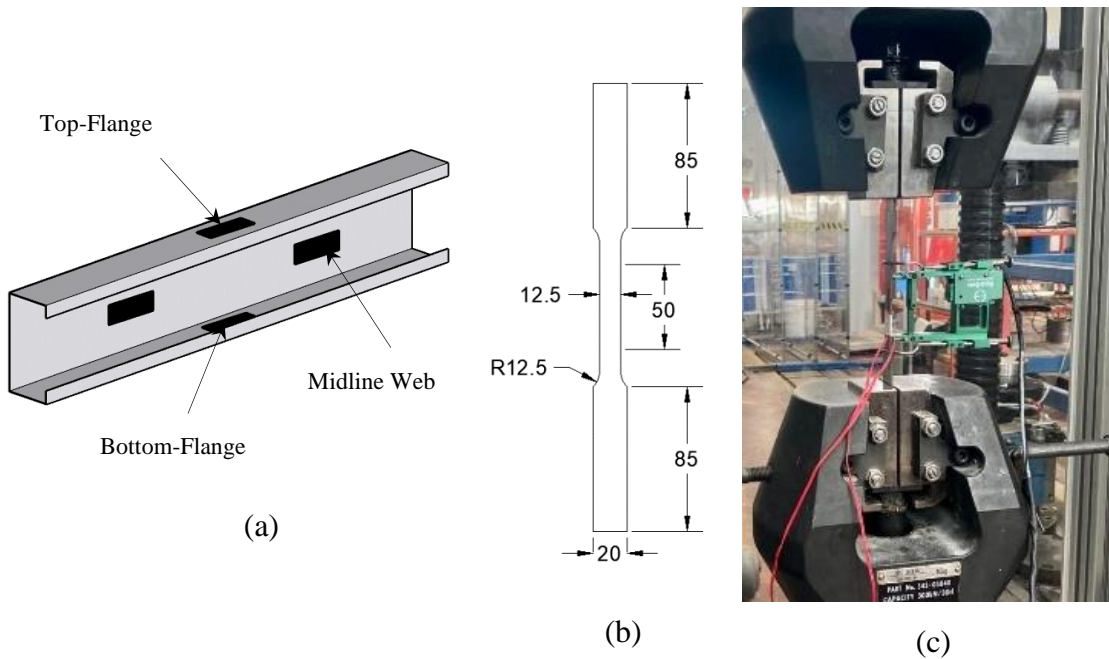
Figure 4.5 (a) Sampling locations of CFS tensile coupons, (b) dimensions of coupon (in mm) and (c) test set-up

The tensile tests were conducted according to EN ISO 6892-1 (CEN, 2009) in a displacement control manner using a 300 kN Shimadzu testing machine. The loading protocol was applied with a displacement rate of 0.50 mm/min. To eliminate the effect of the loading/strain rate on the mechanical properties of the CFS (Huang and Young, 2014), the tensile test was halted two times at the 2 min.; once the yield was reached, and when the ultimate strength was almost achieved. The measured CFS material stress-strain curves of CFS-1 of the coupons taken from the web of the stud element as well as the failures of all coupons were illustrated in Fig. 4.6. The static curve was obtained by reducing the stress values to be consistent with the levels observed during the pauses of loading. The test results of all six CFS flat coupons are presented in Table 4.4, which lists Young's modulus (E_{CFS}), yield stress ($f_{y,CFS}$), ultimate strength ($f_{u,CFS}$), ultimate strain ($\varepsilon_{u,CFS}$) and strain at fracture ($\varepsilon_{f,CFS}$). The measured CFS material stress-strain curves of Side-1, Side-2 and bottom coupons were illustrated in Fig. A.1 in Appendix A.
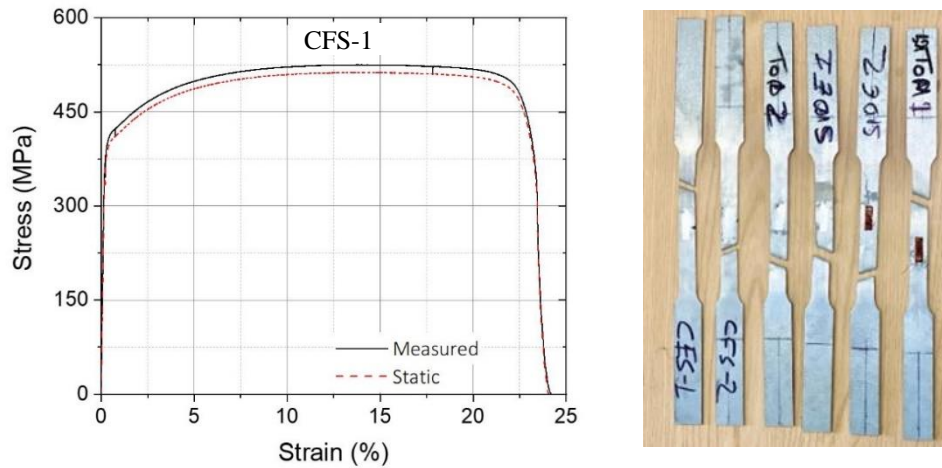
Figure 4.6 Stress-strain curve for CFS-1 and failure mode of all coupon specimens

Table 4.4 Material properties of the CFS

Coupons	$E_{,CFS}$ (GPa)	$f_{y,CFS}$ (Mpa)	$f_{u,CFS}$ (Mpa)	$\varepsilon_{u,CFS}$ (%)	$\varepsilon_{f,CFS}$ (%)
CFS-1	182	410	525	15	24
CFS-2	210	415	517	12	19
Top	214	480	520	8	13
Bottom	239	480	520	5	7
Side-1	226	490	529	7	13
Side-2	235	504	536	7	7
Average	218	463	525	9	14

4.3.2. OSB panel

Since the material properties of OSB are different in tension and compression, separate experiments were conducted to determine its tensile and compressive properties. The tests were conducted according to EN 789 (CEN, 2004). For each loading condition, in total three coupons, one in each direction α = 0°, 45°, and 90°, were cut from the OSB boards for tensile and compression specimens, as shown in Fig. 4.7.
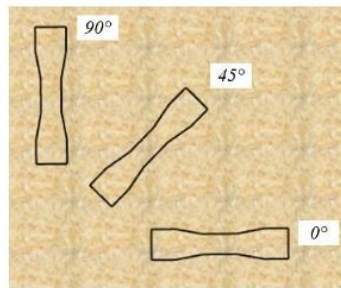
Figure 4.7 Direction of the cut made on the OSB board

4.3.2.a. Tensile coupon test

The dimension of the tensile coupon 9 mm thickness chosen was specified according to EN 789 (CEN, 2004), as presented in Fig. 4.8. The load was applied using a 300 kN Shimadzu universal testing machine employed in a displacement control manner with a constant axial rate of 0.25 mm/min, obeyed EN 789 (CEN, 2004). Each tensile coupon was instrumented using four 10 mm strain gauges mounted to the middle of the specimen. Table 4.5 lists the measured module of elasticity ($E_{t,OSB}$), ultimate tensile stress ($f_{t,osb}$) and its corresponding ultimate strain ($\varepsilon_{t,osb}$) for the tensile coupons. The stress-strain curves of the tensile tests for all specimens were presented in Fig. 4.9.
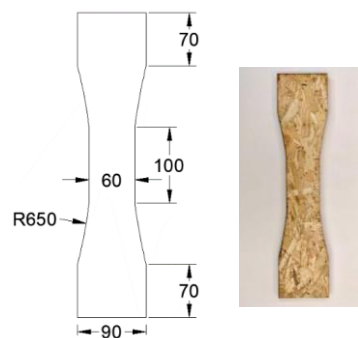
Figure 4.8 OSB tensile coupons dimensions in mm

Table 4.5 Measured of the tested tensile OSB coupon specimens

Specimens	$E_{t,OSB}$ (GPa)	$f_{t,OSB}$ (Mpa)	$\varepsilon_{t,OSB}$
OSB-1$_{ten}$ (α=0)	2.1	13.1	0.009
OSB-2$_{ten}$ (α=45)	2.2	10.18	0.005
OSB-3$_{ten}$ (α=90)	2.1	11.30	0.008
Average	2.1	11.53	0.007
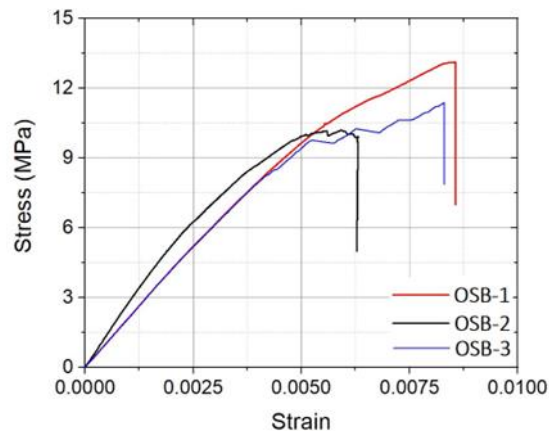
Figure 4.9 The stress-strain curves of the tensile tests for OSB board

4.3.2.b. Compression test

Compressive coupons were extracted from the 9 mm OSB in order to obtain its compressive mechanical properties in the direction parallel to the faces. Each compressive coupon consisted of five rectangular pieces of the board with the dimensions of 50 mm × 240 mm (see Fig. 4.10), in line with BS EN 789 (CEN, 2004). To form the compressive coupon, the five pieces were glued together using outdoor epoxy adhesive and subsequently, as shown in Fig. 4.10. It should be noted that each coupon was cut from the OSB board in three different directions ($\alpha = 0°$, 45°, and 90°). According to (CEN, 2004), the compressive load was applied using a 300 kN Shimadzu universal testing machine in a displacement control manner. A constant displacement rate of 0.50mm/min was applied until failure. In addition, each specimen was instrumented using four 10 mm strain gauges, as depicted in Fig. 4.10.

(a)   (b)
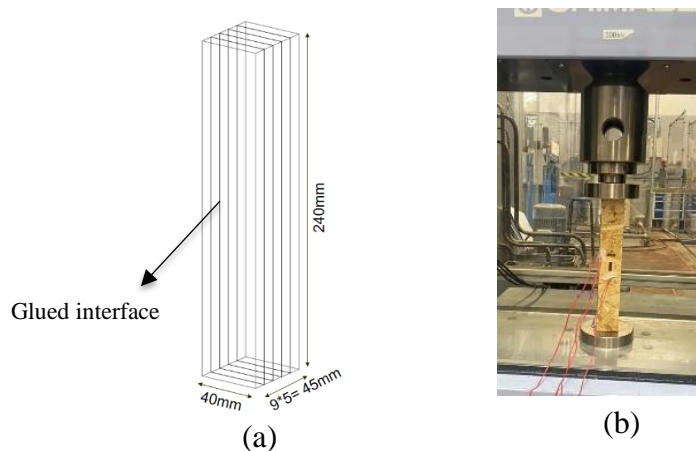
Figure 4.10 OSB compressive coupons: (a) dimensions in mm and (b) test set-up

The measured properties of the OSB material for compressive coupons are presented in Table 4.6, where $E_{c,OSB}$ represents the module of elasticity of the OSB in compression, and $f_{c,OSB}$ and $\varepsilon_{c,OSB}$ are the ultimate compressive stress and strain of the OSB material. The stress-strain curves of the compression tests for all specimens were presented in Fig. 4.11.

Table 4.6 Measured dimensions of the tested compression OSB specimens

Specimens	$E_{c,OSB}$ (GPa)	$f_{c,OSB}$ (MPa)	$\varepsilon_{c,OSB}$
OSB-1$_{com}$ (α=0)	2.3	14.4	0.011
OSB-2$_{com}$ (α=45)	2.4	13.6	0.009
OSB-3$_{com}$ (α=90)	2.3	14.5	0.010
Average	2.3	14.17	0.010
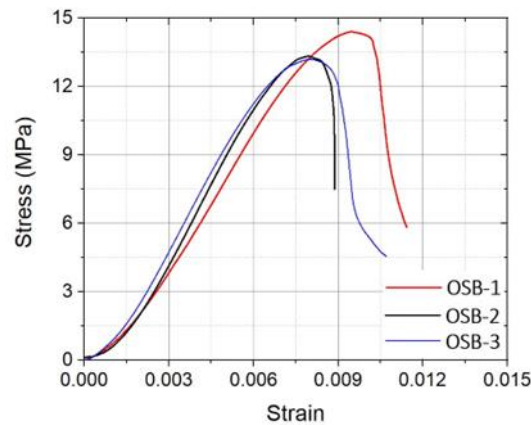
Figure 4.11 The stress-strain curves of the compression tests for OSB boards

4.4. Small-scale connection tests

It was demonstrated in the literature that the capacity and failure mode of the sheathed CFS stud wall systems were directly dependent on the behaviour of the fasteners. To obtain an insight into the behaviour and load-slip response of the CFS-to-sheathing connection, push-out and pull-out tests were conducted on a total of 11 small-scale board-to-CFS connection subassemblies. The summary of the parametric test matrix was presented in Table 4.7. It should be noted that each connection subassembly test was designed to be a representative of the connections in the actual sheal wall panel listed in Table 4.1. As an instance, K1$_{Push}$ represents the push-out test on the key specimen connections, where five self-drilling screws with the spacing of 75 mm were used to connect the 9 mm thick OSB board on each flange of 1.2 mm CFS stud. For both pull-out and push-out tests, the load was applied using a 300 kN Shimadzu

testing machine employed in displacement control mode, and the loading protocol applied a displacement rate of 1 mm/min for push-out tests and 0.5 mm/min for pull-out tests. The data acquisition system was controlled by the National Instrument LabView software, which produced data with a sampling rate of 1 Hz. The small-scale connection tests were discussed in more detail in Chapter 6.

Table 4.7 Small-scale connection test matrix

	Specimen representation	Test Code	Width × Length (mm x mm)	Number of tests
Push-out (Shear) Tests	Key specimens Plywood (9 mm) OSB (18 mm) CFS (2 mm) Washer effect Screw Spacing (300 mm)	$K1_{Push}$-$K2_{Push}$-$K3_{Push}$ $P9_{Push}$ $OSB18_{Push}$ $CFS2_{Push}$ UW_{Push} $S300_{Push}$	200×500	8
Pull-out Tests	Key Specimens	$K1_{Pull}$-$K2_{Pull}$-$K3_{Pull}$	300×300	3

4.4.1. Push-out tests

Fig. 4.12 showed the schematic view of the push-out test arrangement in which both flanges of the CFS section were connected to the wood-based boards to ensure a stable and symmetric system during testing. The eight specimens with various design parameters, including different wood-based boards (i.e. OSB and plywood), OSB and CFS thicknesses, washer effect and screw spacing, were tested under shear loading to identify the load-slip behaviour. The shear load was applied by a 300 kN Shimadzu universal testing machine in a displacement control manner at a rate of 1 mm/min. Two linear variable displacement transducers (LVDTs) were employed to measure the slip at the beginning and ends of connected points.
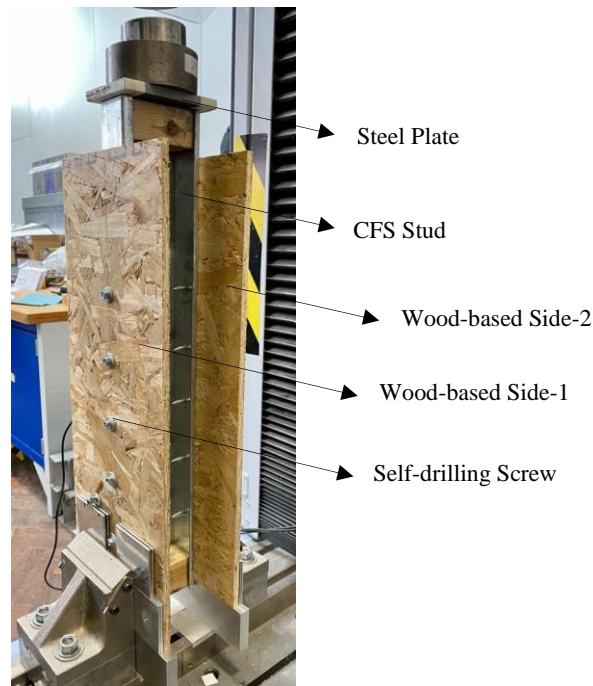
Figure 4.12 Test set-up for the push-out tests

The load-slip (P-s) responses for all specimens were presented in Fig. 4.13, where P is the load per screw under shear force and s is the average slip. The whole load obtained from the actuator was divided ten to obtain the load for per screw under shear force. Besides, a summary of the ultimate load per connector (P_u), the slip at the ultimate load (s_u) and the initial stiffness of each connection (R_i) was reported in Table 4.8. It was observed that all push-out test specimens failed by the significant bearing of the wood-based boards as well as tilting of their screws, as shown in see Fig. 4.14. It can be seen from Fig. 4.13 that increasing the OSB thickness from 9 to 18 mm resulted in significantly higher in-plane strength in connection by up to double. On the contrary, while increasing the CFS thickness had a negligible influence on the in-plane strength of the connection, it is likely to reduce the connection stiffness by down to 1%. The results demonstrated that the presence of a washer in the connection can generally improve the load-slip response obtained from the push-out test, however, increasing the screw spacing from 75 to 300 mm can diminish both in-plane strength and stiffness of the connections. In addition, by comparing the response of plywood and OSB in the same connection configuration, it can be concluded that using plywood provides lower in-plane stiffness and strength for the connection.

Table 4.8 Main performance parameters in push-out test results

Specimen Batch	P_u (kN)	S_u (mm)	R_i (kN/mm)
K1$_{Push}$	3.42	13.70	2.39
K2$_{Push}$	3.48	12.67	2.16
K3$_{Push}$	2.85	7.25	2.20
P9$_{Push}$	2.61	18.04	1.95
OSB18$_{Push}$	5.79	18.77	2.36
CFS2$_{Push}$	3.69	19.18	2.18
UW$_{Push}$	2.59	8.26	2.22
S300$_{Push}$	2.73	12.30	2.05

Figure 4.13 The load-slip (P-s) response obtained from the push-out tests
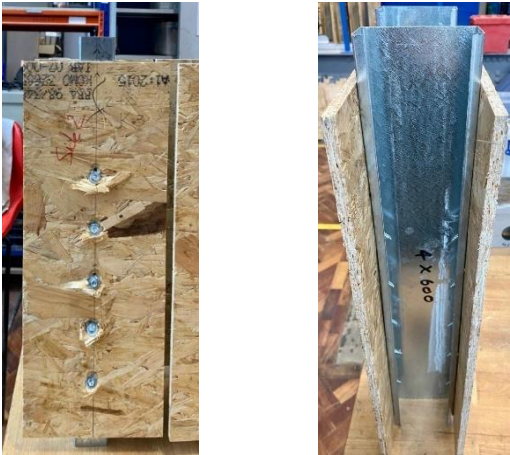
Figure 4.14 Typical failure mode captured from the push-out tests

4.4.2. Pull-out tests

The small-scale specimens were tested to identify the load-slip response of the CFS-to-board connections in an out-of-plane direction. The schematic view of the pull-out test arrangement is shown in Fig. 4.15. To directly pulled down the wood-based board, a steel yoke was used to transfer the applied load to the board. The vertical load was applied by a 300 kN Shimadzu universal testing machine in a displacement control manner at a rate of 0.50 mm/min.
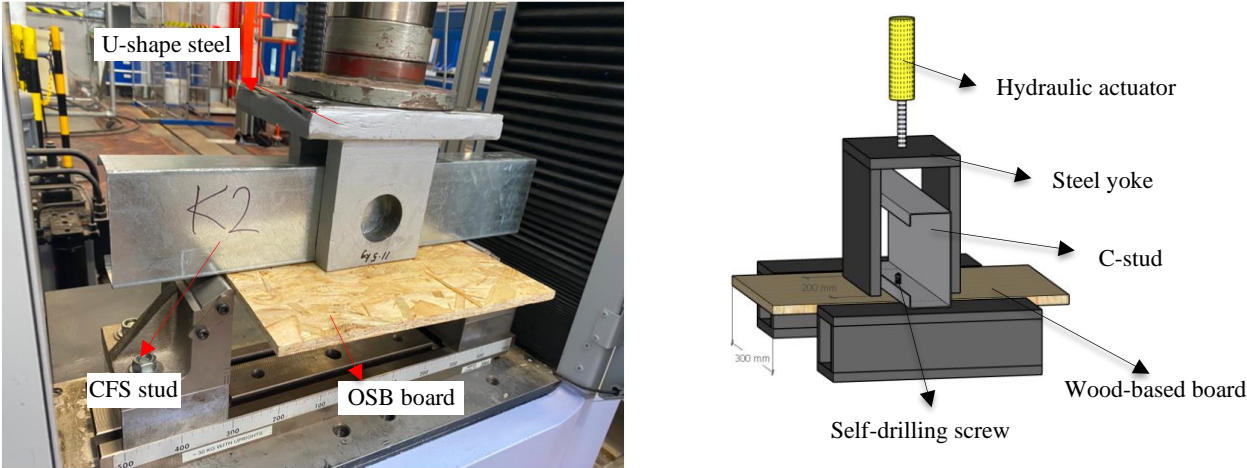
Figure 4.15 Test set-up of the pull-out tests

The load-slip *(P-s)* responses for all specimens were depicted in Fig. 4.16, where *P* is the load per screw and s_u is the average slip. Moreover, a summary of the main performance parameters was reported in Table 4.9, where P_u is the ultimate load per connector, s_u is the slip at the ultimate load and R_i is the initial stiffness. In general, all pull-out specimens showed similar load-slip responses over the whole range of loading (see Fig. 4.16). Pull-thought of screws were observed as a dominant failure mode in all specimens, as depicted in Fig. 4.17.

Table 4.9 Main performance parameters in pull-out test results

Specimen Batch	*Pu* (kN)	*Su* (mm)	*Ri (*kN/mm*)*
K1$_{pull}$	1.98	10.74	0.24
K2$_{pull}$	1.73	9.60	0.21
K3$_{pull}$	1.86	8.45	0.26
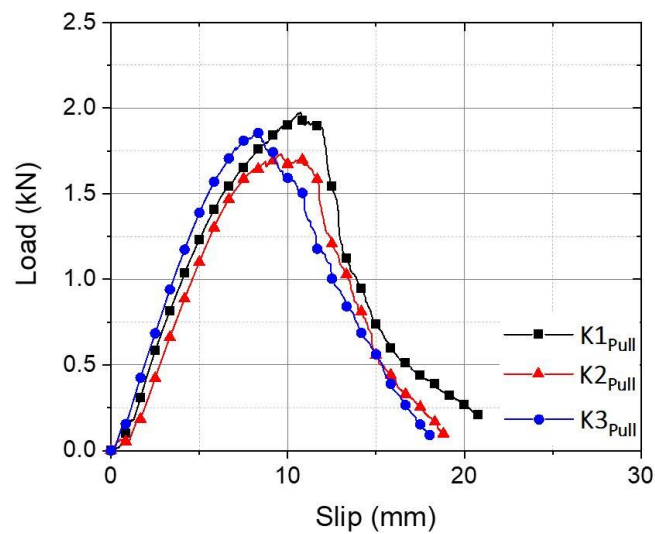
Figure 4.16 The load-slip (P-s) response of the pull-out tests

Figure 4.17 Typical failure mode captured from the pull-out tests

4.5. Initial imperfection measurements

Imperfections could have a significant impact on structure stability, especially on thin-walled structural members when coupled instabilities are involved (van der Neut, 1969; Becque, 2014). Therefore, the geometric imperfections of initial C-shape studs were measured using a specially designed imperfection measuring rig, as shown in Fig. 4.18. The rig consisted of a traverse system with two electric motors in order to move a Keyence LK-G82 laser sensor in two orthogonal directions. During the measuring process, the laser sensor was moved longitudinally at a speed of 5 mm/s while readings were taken at a sampling rate of 5 Hz resulting in one reading every millimetre. Based on the sensitivity assessment conducted on the frame, it was found that the accuracy of the frame is in the order of ±0.07 mm. millimetre.
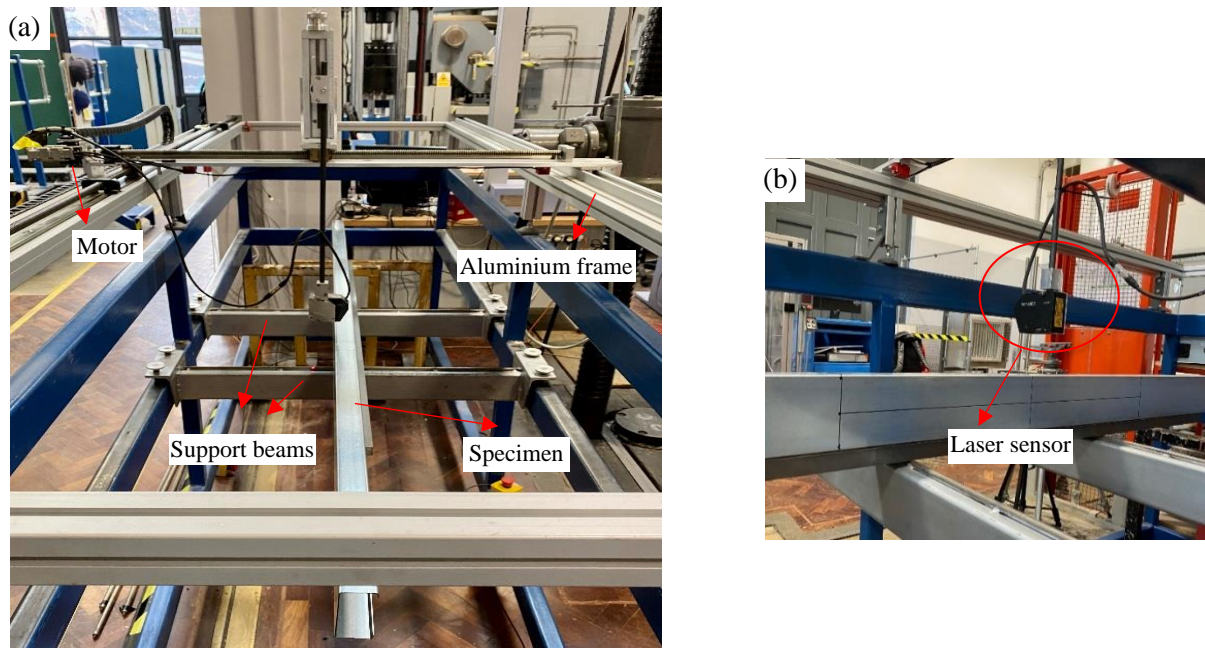
Figure 4.18 (a) Test set-up, (b) laser sensor

As a result, the imperfections were measured along seven longitudinal lines of CFS members, as shown in Fig. 4.19, where three lines were recorded on the web and two lines on both flanges. The imperfection data was further employed to determine representative magnitudes of the cross-sectional out-of-plane imperfections. To this end, the out-of-plane imperfections along the centre line of the web (δ_{web}) and the flange edge (δ_{flange}) were measured relative to their corners. While the readings along lines 1, 2, 6 and 7 were used to identify the distortional imperfections, lines 3, 4 and 5 provided information about the imperfections in overall flexural buckling and local buckling of the web. The distortional imperfection was calculated by subtracting reading along lines 1 to 2, 6 to 7, while the local imperfection was calculated by subtracting the average reading along lines 3 and 5 from the readings taken along line 4 (see *Eq. 4.1, Eq. 4.2* and *Eq. 4.3*).
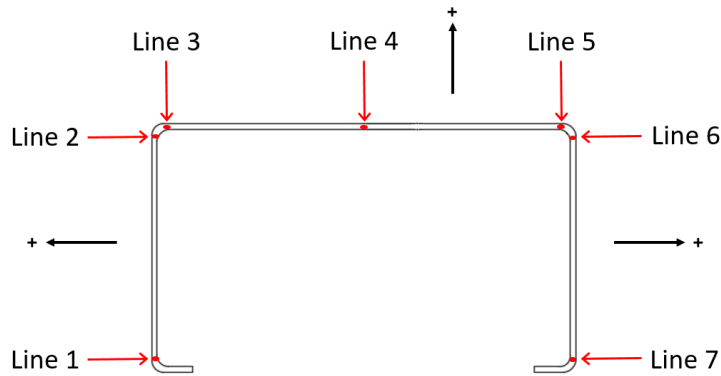
Figure 4.19 Location of imperfection measurements in the initial C-shape

$$Distortional\text{-}1 = \delta\ flange\ (x) = Line\ 1 - Line\ 2$$

$$Average\ \delta\ flange\ (x) = 0 \qquad\qquad (4.1)$$

$$Distortional\text{-}2 = \delta\ flange\ (x) = Line\ 7 - Line\ 6$$

$$Average\ \delta\ flange\ (x) = 0 \qquad\qquad (4.2)$$

$$Local = \delta\ web\ (x) = Line\ 4 - \left(\frac{Line\ 3 - Line\ 5}{2}\right) \qquad\qquad (4.3)$$

The maximum amplitudes of the recorded local and distortional imperfections in the six initial C-shaped elements are provided in Table 4.10. The results indicate that the maximum out-of-plane imperfections encountered in the webs of the channels were of the order of 0.81 mm, while the flange of the C-lipped channels exhibited imperfections of up to 0.36 mm. (see Table 4.10). Fig. 4.20 was represented the result of the recording imperfection at the C1 and C3 specimens.

Table 4.10 Maximum amplitudes of local, distortional-1 and distortional-2 (in mm)

Specimen	Local	Distortional-1	Distortional-2
C1	0.35	0.07	0.17
C2	0.58	0.14	0.22
C3	0.34	0.11	0.24
C4	0.49	0.17	0.36
C5	0.81	0.26	0.13
C6	0.36	0.22	0.21
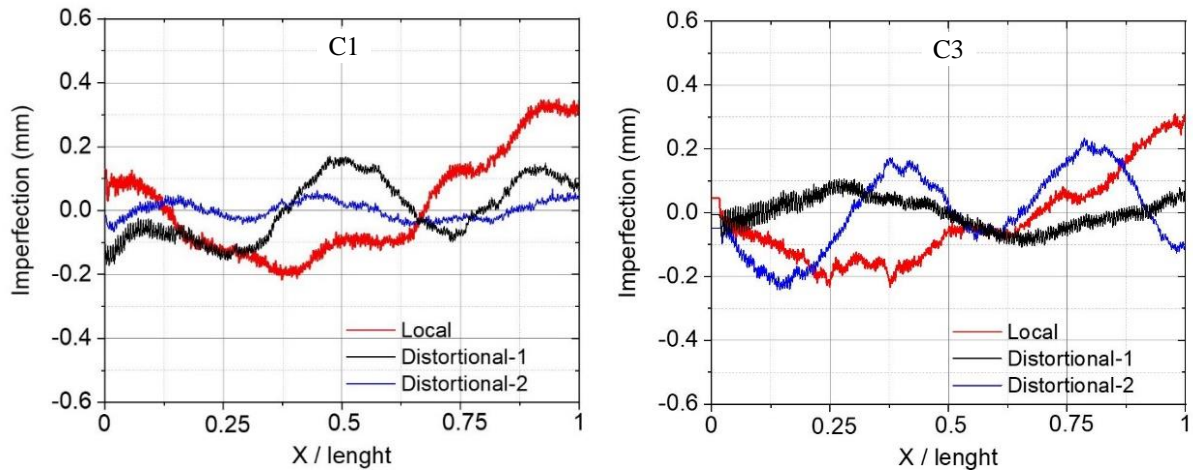
Figure 4.20 Typical recorded imperfections for two different CFS lipped channel members

Fig. B.1 was represented the result of the recording imperfection at the C2 and C4 specimens in Appendix B.

4.6. Four-point bending test set-up

CFS sheathed wall panel specimens were tested under a specially designed four-point bending loading protocol to obtain their out-of-plane bending behaviour. All specimens were lied down in a way that the loading was applied directly to the board of the wall panels. The test set-up was as illustrated in Fig. 4.21. A spreader I-shape beam was used to transfer the load from the 150-kN hydraulic jack through two loading tubes running across the width of the board. The distance between the two intermediate loading points was fixed as equal to 746.67 mm, which was one-third of the total span, with a 100 mm overhanging from each support point (see Fig. 4.22). The data acquisition system was controlled by the National Instrument LabView software, which produced data with a sampling rate of 1 Hz. The loading protocol applied a displacement rate of 2 mm/min. To provide interpretation of the results, the CFS studs were denoted by "B" and "F" for the boundary elements and "C" for the middle one.
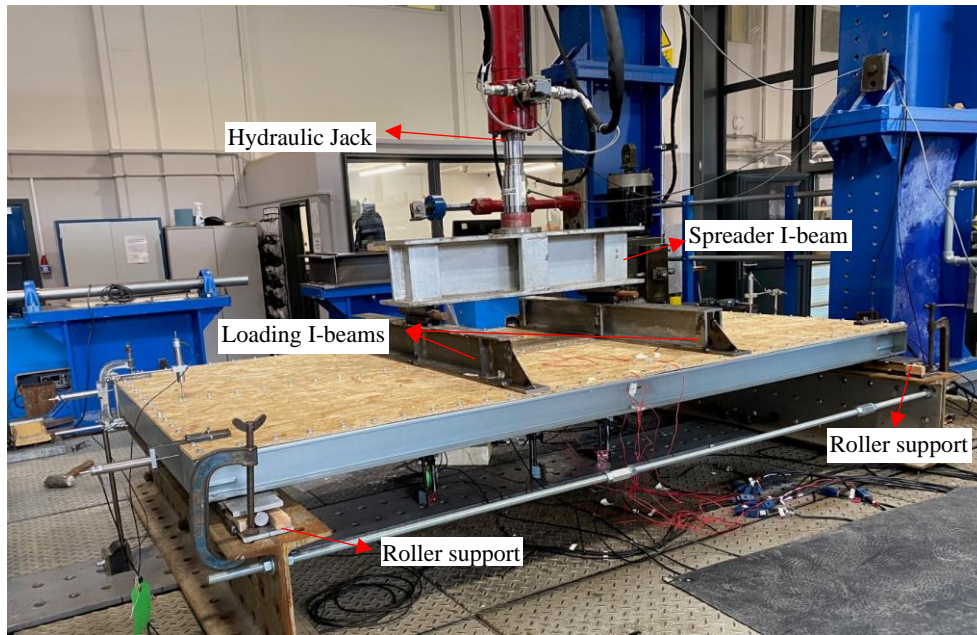
Figure 4.21 Test set-up
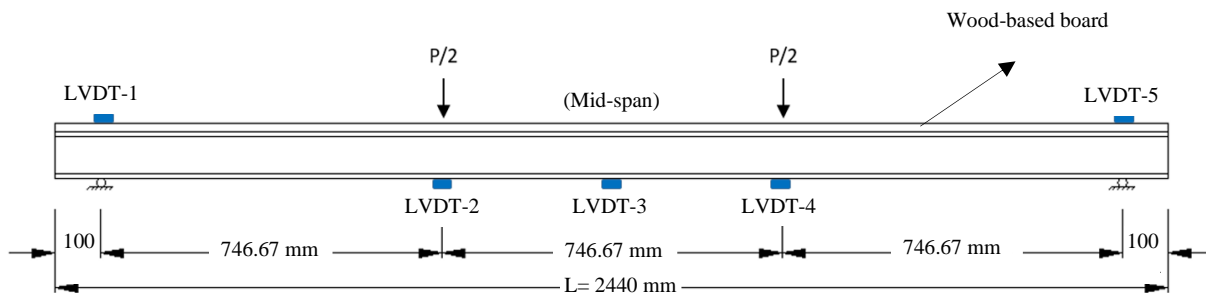
Figure 4.22 Schematic 2D view of the test set-up and the locations of LVDTs

Strain gauges were attached to the board and CFS sections at the mid-span of the shear wall panel, as shown in Fig. 4.23. It should be noted that these strain gauge readings were employed to determine the position of the neutral axis within the CFS elements. To determine the rotation of each CFS stud where one of their flanges was restrained by the wood-based board, an inclinometer was installed to the CFS web at the mid-span of the system (see Fig. 4.23). An extra inclinometer was also mounted to each loading tube in order to measure the longitudinal rotation of the stud wall system, as illustrated in Fig. 4.24. To measure out-of-plane deformations of the wall panels, five LVDTs were installed on top of the supports and along the length of the mid-stud bottom flange at the locations of mid-span and loading points (see Figs. 4.22 and 4.25). In addition, the end-slip between the CFS tracks and wood-based board at

the four corners of the specimens was measured using other four LVDTs readings placed horizontally at four corners of the wall panel (End-slip 1, End-slip 2, End-slip 3 and End-slip 4), as shown in Fig. 4.26.
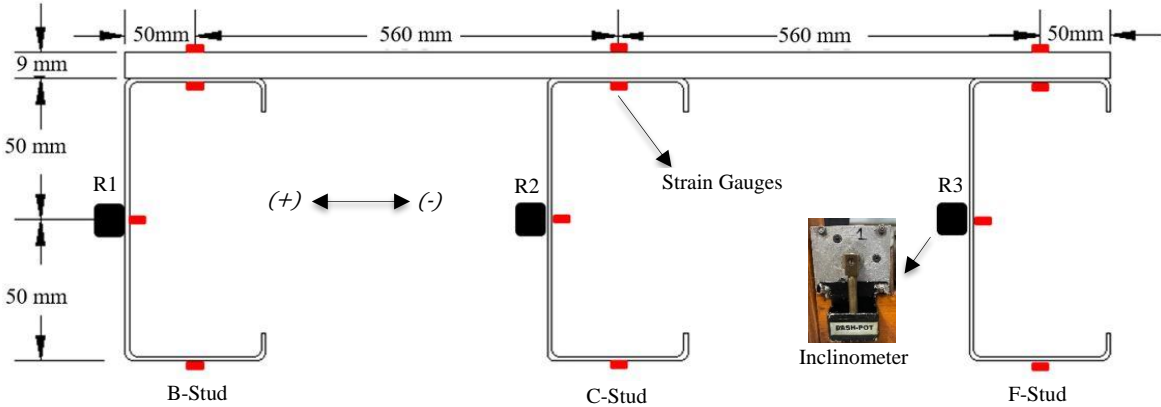
Figure 4.23 Positions of inclinometers and strain gauges in the midspan of the panel
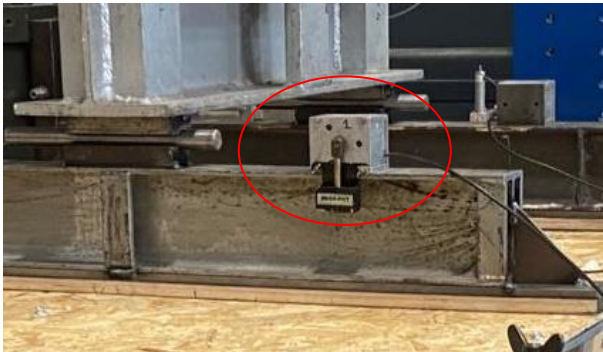
Figure 4.24 Position of inclinometers on the loading tubes
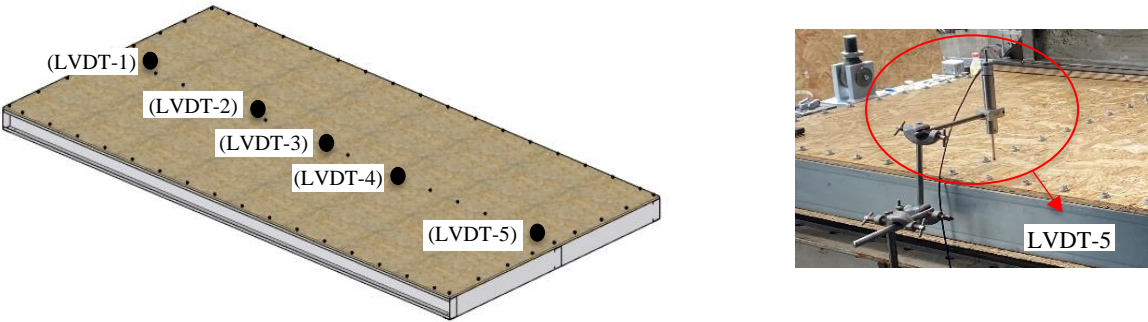
Figure 4.25 Positions of five LVDTs at mid-stud of the system
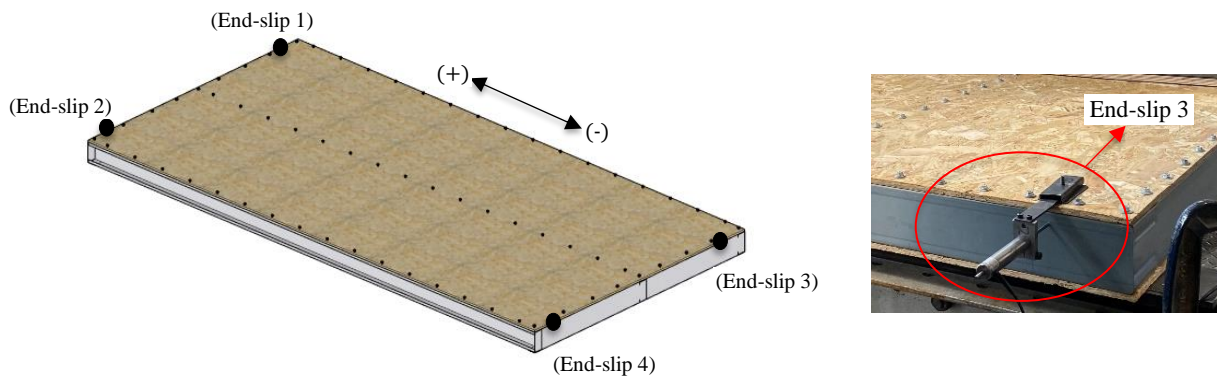
Figure 4.26 Positions of four LVDTs for end-slip measurement up

4.7. Four-point bending test results

A summary of the main structural performance parameters obtained from four-point bending tests on the CFS stud wall panels were listed in Table 4.11, including maximum out-of-plane load capacities and their corresponding displacements, ultimate displacements at which the out-of-plane capacity of the wall was dropped by 20% and the dominant failure modes. In addition, Tables 4.12 and 4.13 reported a series of complementary results consisting of the values of end-slip measured at four corners of the wall in the longitudinal direction and the rotation of the studs for each tested specimen. Based on the aforementioned results, the behaviour of the CFS stud walls was discussed in the following sub-sections by taking into account various design variables.

Table 4.11 Main structural performance parameters and failure mode for each specimen

Specimens	Maximum load capacity (kN)	Displacement at peak load (mm)	Ultimate displacement (mm)	Out-of-plane stiffness (kN/mm)	Failure mode
K1	29.2	33.3	41.6	1.1	Distortional Buckling-wood crushing/bearing
K2	30.6	36.9	43.6	1.1	Distortional Buckling-wood crushing/bearing
S100	29.9	38.4	54.6	1.1	Distortional Buckling-wood crushing/bearing
S150	25.6	30.5	56.7	1.1	Distortional Buckling- wood crushing/bearing
S300	22.8	30.8	72.4	1.0	Distortional Buckling-wood crushing/bearing/tilting
P9	30.7	44.9	54.1	1.0	Distortional Buckling-wood cracking
OSB18	38.9	68.3	83.4	1.2	Lateral torsional Buckling- wood crushing/bearing
CFS2	54.5	48.6	59.6	1.6	Local Buckling wood crushing/bearing
UB	8.0	50.5	67.9	0.5	Lateral-torsional Buckling
DB1	33.7	23.4	37.8	1.6	Distortional Buckling wood crushing/bearing
DB2	35.4	26.4	38.5	1.6	Distortional Buckling wood crushing/bearing
DR	29.3	35.0	37.5	1.0	Distortional Buckling wood crushing/bearing
S	31.3	38.3	59.9	1.1	Distortional Buckling wood crushing/bearing/tilting
N	31.1	42.0	46.7	1.3	Distortional Buckling wood crushing/bearing/tilting
PT	25.8	28.9	30.0	1.1	Lateral-torsional Buckling wood crushing/bearing/tilting

Table 4.12 End-slip readings measured in the longitudinal direction at four corners of each tested specimen (in mm)

Specimens	At Peak Load				At Ultimate Displacement			
	End-slip 1	End-slip 2	End-slip 3	End-slip 4	End-slip 1	End-slip 2	End-slip 3	End-slip 4
K1	0.36	0.22	0.15	0.12	0.63	0.43	0.16	0.14
K2	0.22	0.43	0.28	0.39	0.34	0.53	0.34	0.45
S100	0.31	0.36	0.33	0.42	0.53	0.45	0.49	0.53
S150	0.37	0.57	0.53	0.71	2.11	1.07	1.10	2.11
S300	0.95	1.38	0.85	1.50	1.73	7.13	1.90	9.18
P9	0.78	0.50	0.73	0.25	1.14	0.55	0.97	0.29
OSB18	0.97	1.33	0.75	1.26	1.38	1.59	1.12	1.53
CFS2	0.53	0.40	0.24	0.40	0.79	0.41	0.34	0.42
DB1	0.04	0.29	0.09	0.33	0.17	0.37	0.21	0.36
DB2	0.11	0.25	0.14	0.32	0.22	0.28	0.27	0.33
DR	0.29	0.50	0.25	0.54	0.34	0.58	0.33	0.68
S	0.32	0.60	0.35	0.56	0.57	0.69	0.41	0.75
N	0.42	0.65	0.50	0.65	0.43	0.69	0.51	0.70

Table 4.13 Measured rotation at the three studs of each tested specimen (in Deg•)

Specimens	At Peak Load			At Ultimate Displacement		
	R1 (Deg°)	R2 (Deg°)	R3 (Deg°)	R1 (Deg°)	R2 (Deg°)	R3 (Deg°)
K1	7.89	6.98	12.00	8.17	8.10	12.10
K2	8.34	8.24	12.00	8.89	10.48	11.95
S100	8.73	9.29	14.05	9.87	9.40	14.07
S150	6.29	8.26	10.59	7.33	8.48	13.42
S300	7.55	10.26	11.19	9.09	10.47	13.00
P9	11.94	11.19	24.6	12.43	11.68	37.68
OSB18	9.2	10.55	17.27	14.36	10.69	49.11
CFS2	14.09	-	12.05	14.25	-	12.35
UB	20.76	-	32.37	32.67	-	57.21
DB1	0.15	-	-	7.02	-	-
DB2	-0.43	-	-	4.39	-	-
DR	6.68	8.5	10.65	9.92	10.73	12.00
S	8.18	9.24	15.14	10.07	12.08	24.10
N	3.17	1.18	0.48	6.31	3.22	1.64
PT	6.12	4.42	3.36	3.41	5.62	6.28

*Some data was not recorded due to the sudden drop of the inclinometers

4.7.1. Key specimens (benchmark specimens)

Fig. 4.27 illustrates the load versus vertical displacement measured at the centre of the wall (LVDT-3) for the key specimens (K1 and K2). As expected, the K1 and K2 key specimens exhibited very similar out-of-plane behaviour (see Fig. 4.27). The maximum load capacity reached approximately 30 kN and the out-of-plane deflection of the wall centre point at the peak load was about 35 mm. At the maximum capacity of the specimens, the distortional buckling started to happen in the top flanges of the left and middle studs (i.e. B-stud and C-stud), and by further increasing the load a localised failure occurred in the web of the left stud, as shown in Fig. 4.28 (a). In addition, the OSB material was damaged mainly at the centre point

of the wall where the board experienced maximum deflection and at the location of the localised failure in the left stud due to the loss of load-bearing capability of the stud at that point and subsequently excessive compressive stresses in the board. The results of strain gauges versus the applied load were reported in Fig. 4.29 for the key specimen K1. It was obviously observed that the strains developed in the studs and the OSB board were in good agreement before the initiation of the buckling at a load of approximately 29 kN. Besides, while almost similar stresses were developed at locations of the strain gauges attached to the boundary CFS studs (i.e. B-stud and F-stud), the strain gauges attached to the OSB showed different stress behaviour. This implies that the out-of-plane flexural behaviour of the system was unsymmetric. This was confirmed by extracting the results of inclinometers mounted on the loading tubes, in which the stud wall system was found rotated towards the B-stud in the order of 3 degrees.
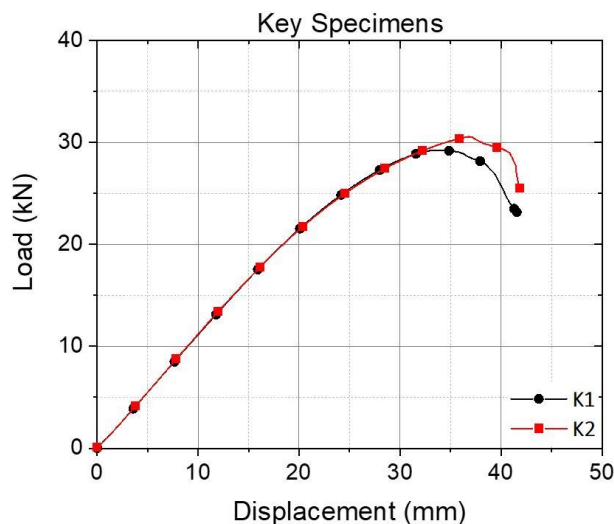
Figure 4.27 Load-displacement responses of key specimens
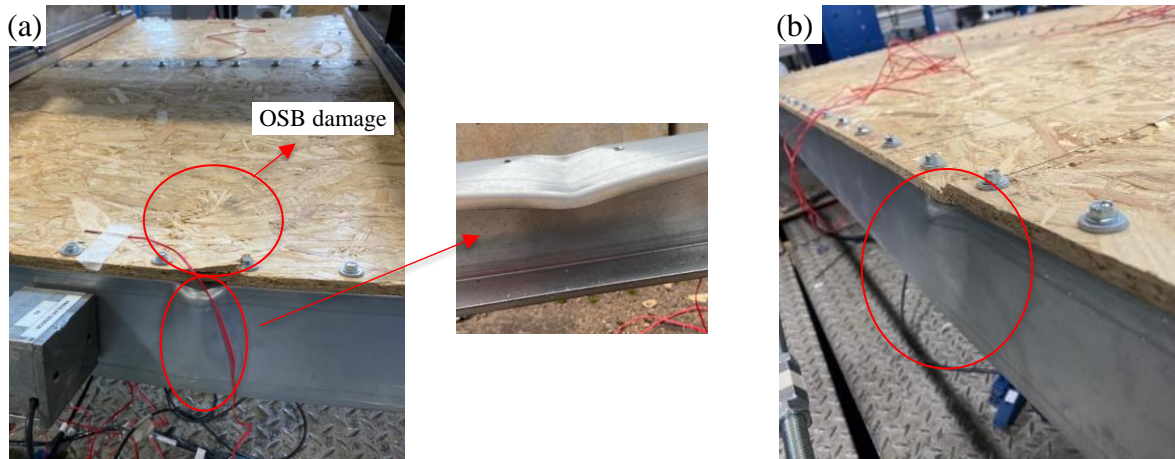
Figure 4.28 Failure modes of: (a) K1 and (b) K2 specimens
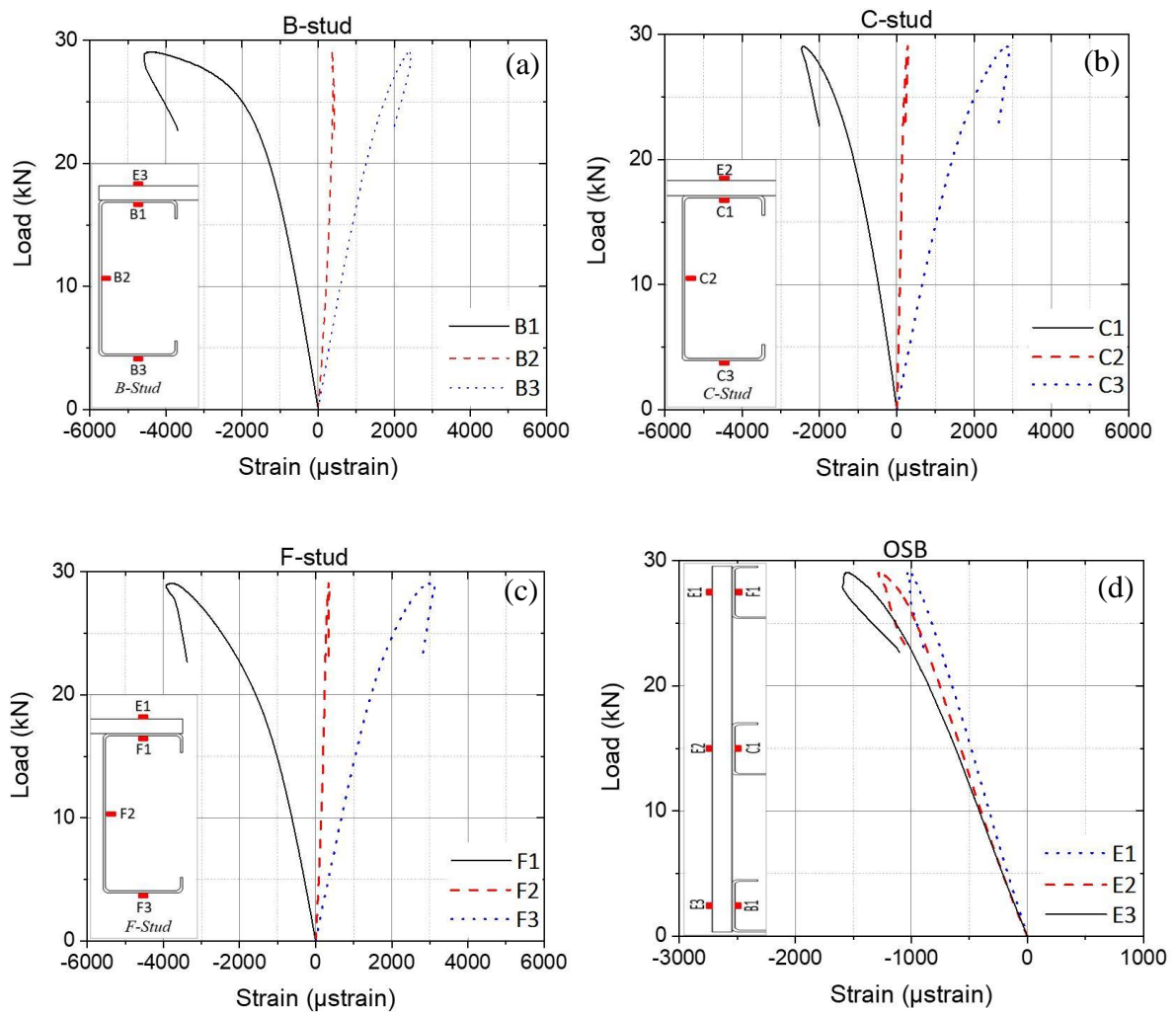
Figure 4.29 Load-strain curve for (a) B-stud, (b) C-stud, (c) F-stud and (d) OSB of K1 specimens

4.7.2. Screw spacing

Fig. 4.30 compared the responses of the key specimen K1 with 75 mm screw spacing and those with 100 mm, 150 mm and 300 mm screw spacing. It was observed that increasing the screw spacing resulted in a reduction in the out-of-plane strength of the stud wall by up to 75%. The results also demonstrated that the initial out-of-plane stiffness of the wall remained almost constant by increasing the screw spacing from 75 mm to 150 mm, however further enhancement of the screw spacing (i.e. 300 mm) reduced the initial out-of-plane stiffness by 9% (see Table 4.11). The ultimate displacement of the key specimen (K1) with 75 mm screw spacing reached 44 mm, on the contrary, it reached 72 mm for the S300 specimen. This implies that in general increasing the screw spacing led to a more ductile stud-wall system. The failure mechanism of the stud wall systems with various screw spacing was found almost similar, where the distortional buckling of studs along with the localised failure of their webs was combined with some damage in the OSB, as depicted in Fig. 4.31. However, for the stud wall system with 300 mm screw spacing additional OSB bearing was observed at the corners of the wall. The stud rotation and end-slips readings were shown in Fig. 4.32 and 4.33, respectively, for K1 and S300 stud walls. It can be concluded that increasing screw spacing can significantly increase the end-slips of the stud wall system and consequently increased the torsional flexibility of the wall, however, it has a slight influence on the rotation of studs. The results of strain gauges versus the applied load were reported in Figs. 4.34 and 4.35 for the S100 and S300 specimens, respectively. It could be concluded that almost similar stresses were developed in the stud walls with different screw spacing.
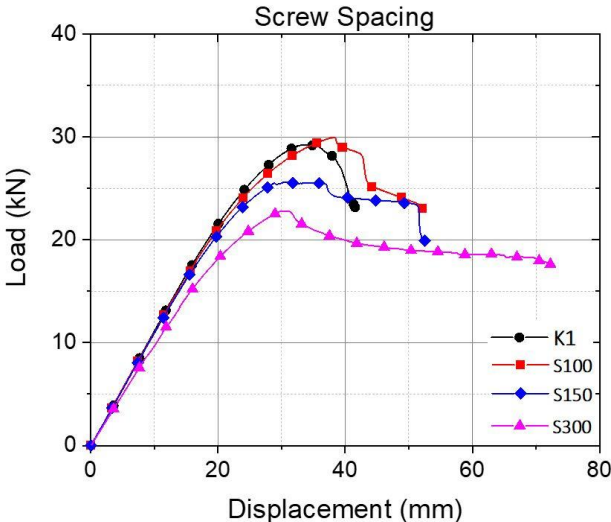
Figure 4.30 Load-displacement responses of stud walls with varied screw spacing
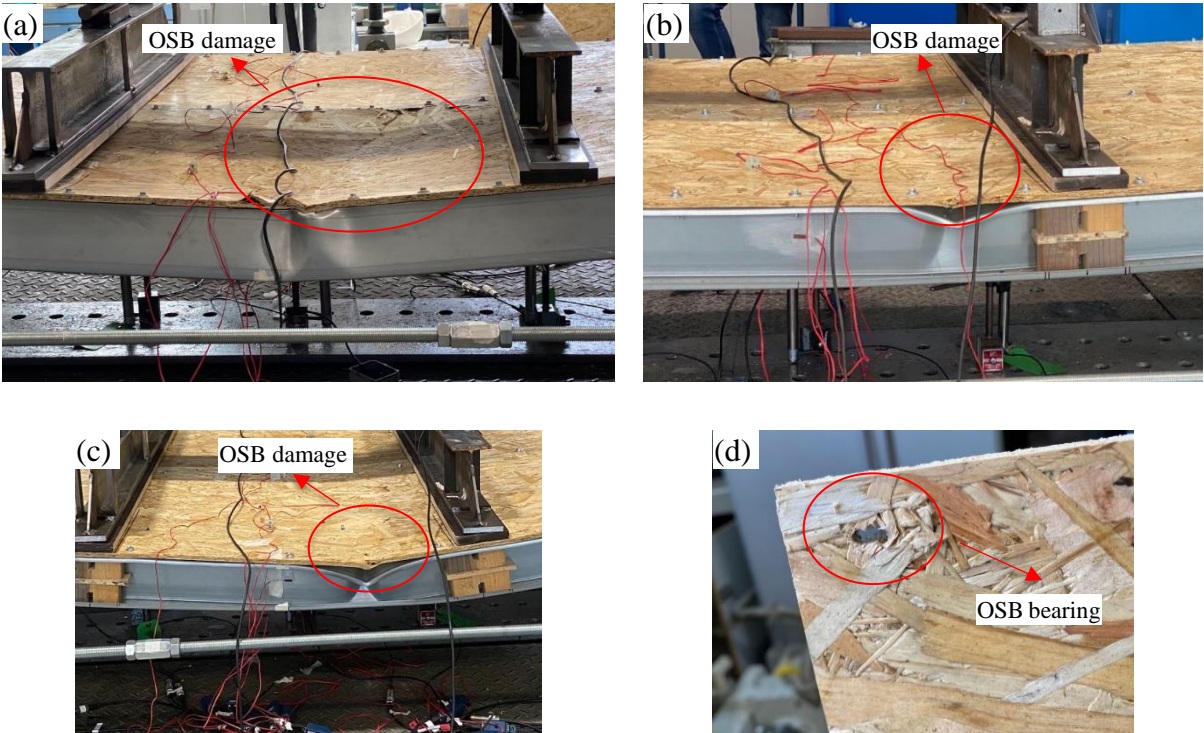
Figure 4.31 Failure modes of (a) S100, (b) S150, (c) and (d) S300 specimens
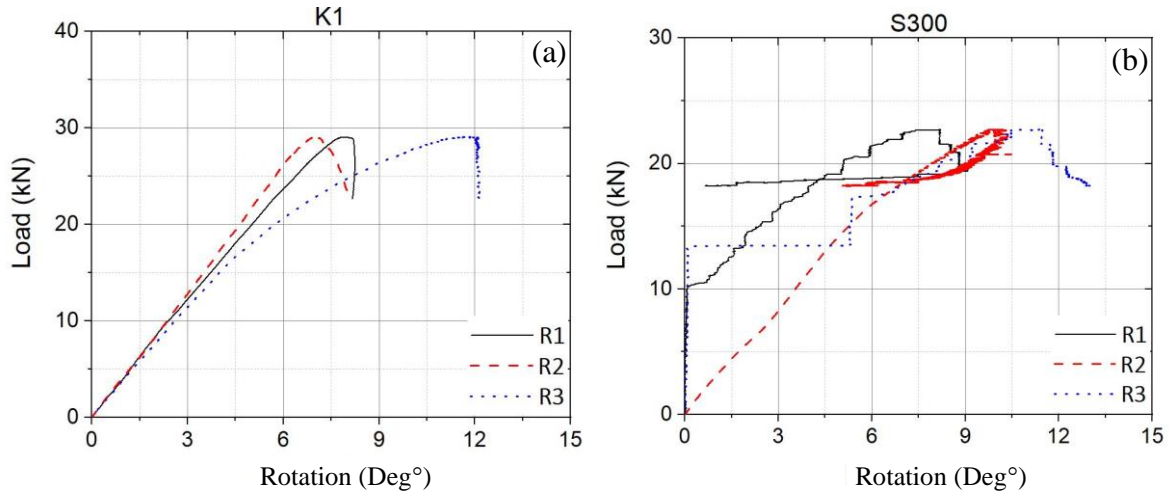
Figure 4.32 Rotation of studs along their major axis for: (a) K1 and (b) S300 specimens
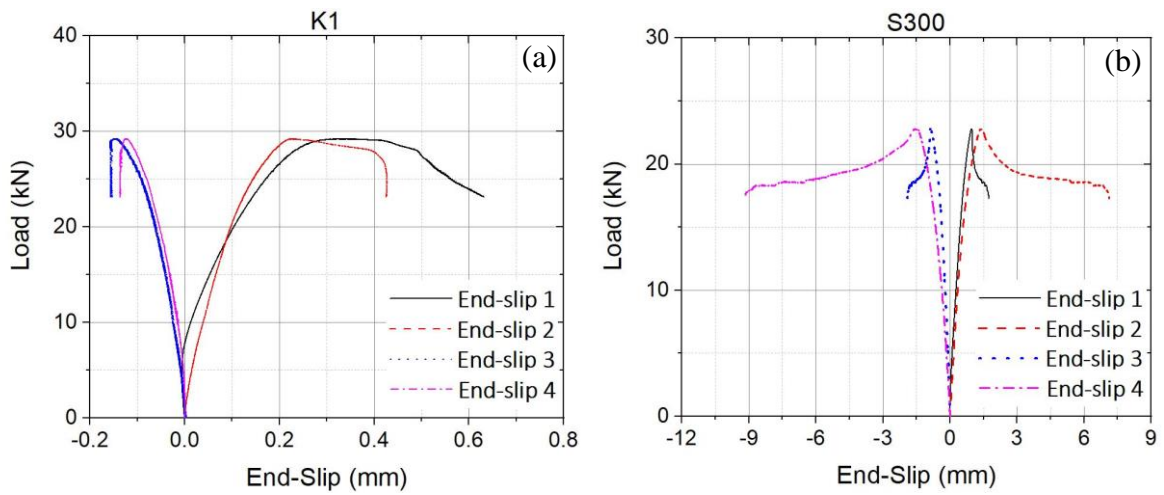
Figure 4.33 End-slip measurement histories of: (a) K1 and (b) S300 specimens

***Figure 4.34** Load-strain curve for (a) B-stud, (b) C-stud, (c) F-stud and (d) OSB of S100 specimen*
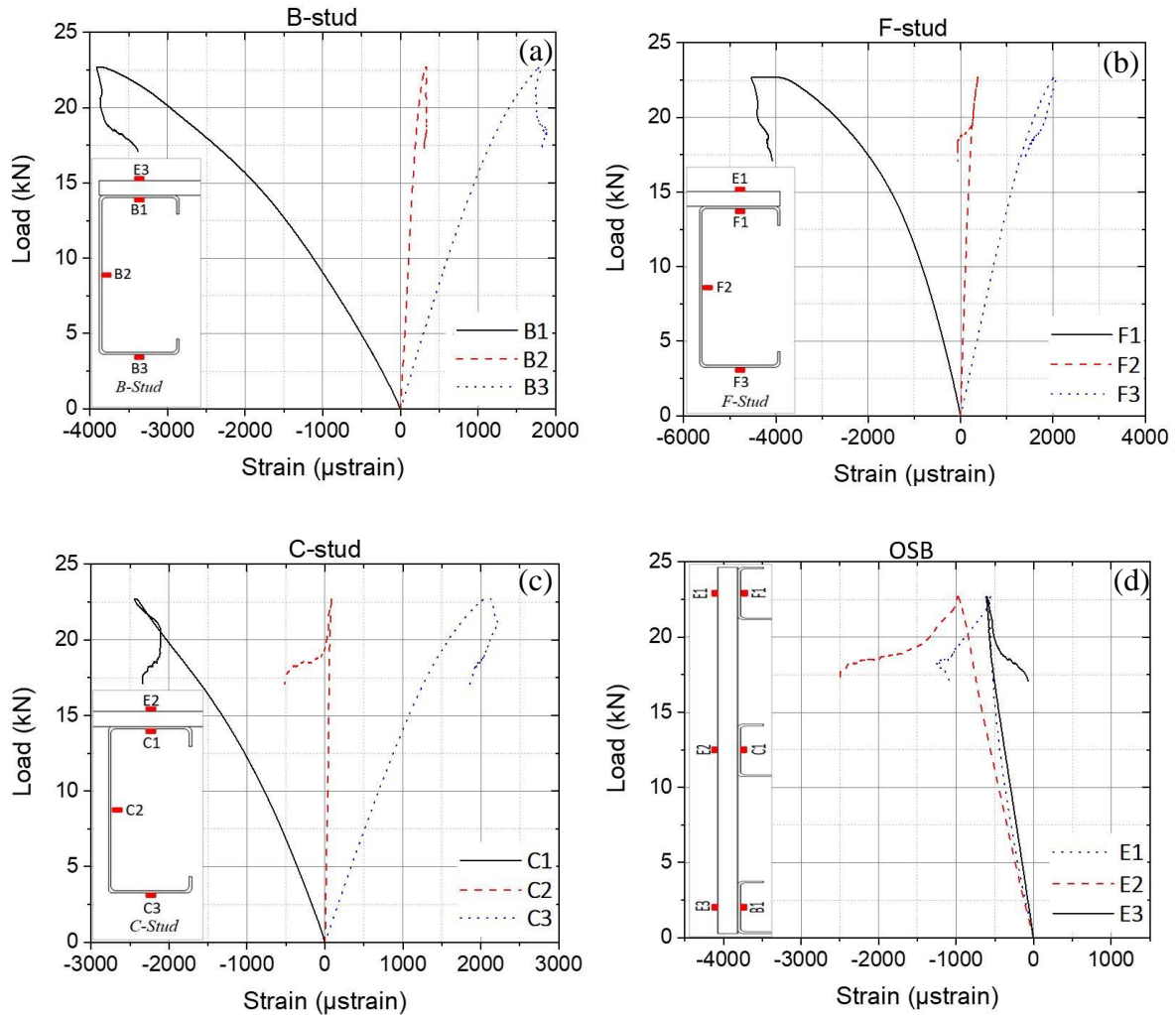
Figure 4.35 Load-strain curve for (a) B-stud, (b) C-stud, (c) F-stud and (d) OSB of S300 specimen

4.7.3. Materials and thicknesses

As shown in Fig. 4.36, in general increasing the thickness of the material could significantly improve the out-of-plane performance of the stud wall panels. It can be resulted that the out-of-plane strength of the stud wall was increased by 33% from 29.2 kN to 38.9 kN by doubling the thickness of the board. This also showed a major effect on the failure mechanism of the system, in which the failure of the OSB board was prevented, and alternatively one of the boundary studs (B-stud) experienced lateral-torsional buckling (Figs. 4.37 (a) and (b)). Interestingly, thickening of CFS elements from 1.2 mm to 2 mm was found to be more beneficial in improving the out-of-plane performance than using a thicker OSB board. The out-of-plane strength and stiffness of the stud wall with thicker CFS elements were enhanced by 86% and 45%,

respectively, compared to the key specimen, which is attributed to preventing distortional buckling in the studs of the system (Figs. 4.37 (c) and (d)). Compared to the OSB material, using plywood boards with the same thickness (i.e. 9 mm) resulted in a more ductile behaviour before the peak capacity while it causes a negligible change in the out-of-plane strength and stiffness of the system, as shown in Fig. 4.36. However, unlike the OSB, a fracture of the plywood was observed along the edge of the wall close to the boundary B-stud (Fig. 4.37 (e)). The results of strain gauges versus the applied load were reported in Figs. 4.38, 4.39 and 4.40 for the OSB18, CFS2 and P9 specimens, respectively. In general, it could be seen that the strains developed in the studs and the OSB board were in good agreement before the initiation of the buckling at a load of approximately 40 kN. In addition, almost similar stresses were developed in the stud walls with different thicknesses and board materials.
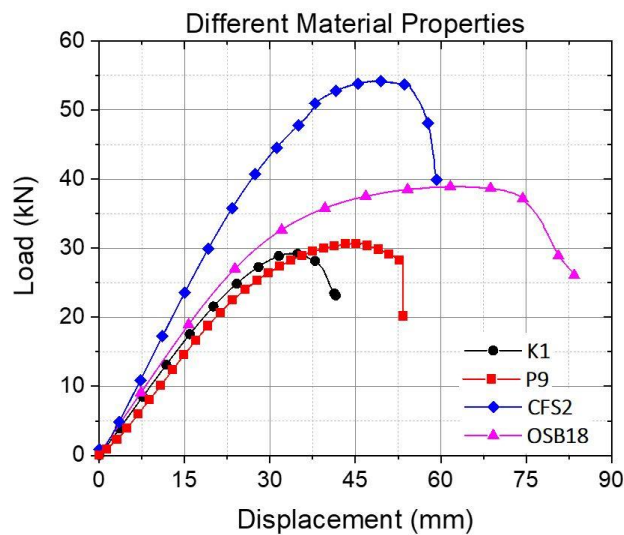
Figure 4.36 Load-displacement responses of stud walls with different material properties
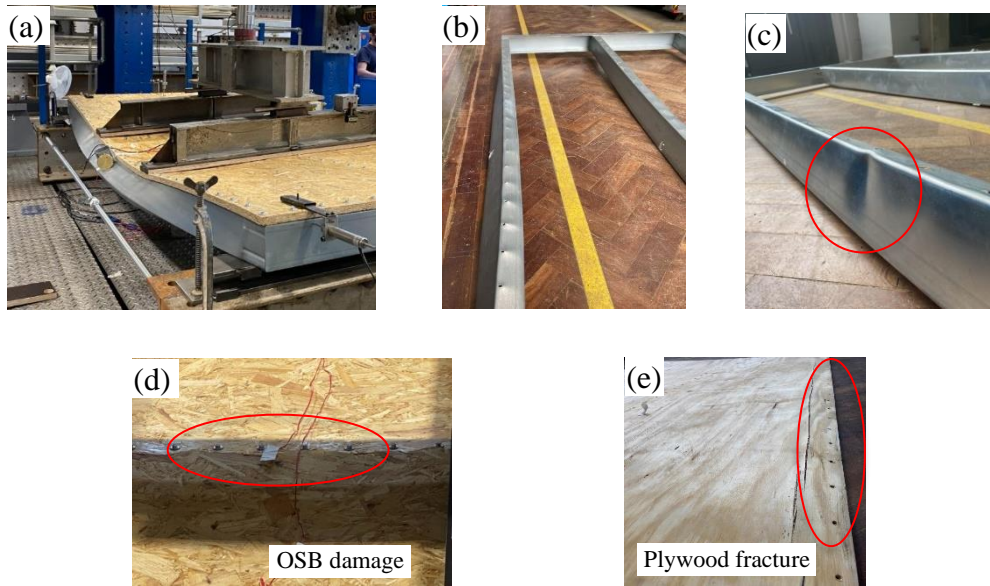
Figure 4.37 Failure modes of (a), (b) OSB18, (c), (d) CFS2-1 and (e) P9 specimens

Figure 4.38 Load-strain curve for (a) B-stud, (b) C-stud, (c) F-stud and (d) OSB of OSB18 specimen

Figure 4.39 *Load-strain curve for (a) B-stud, (b) C-stud, (c) F-stud and (d) OSB of CFS2 specimen*

***Figure 4.40** Load-strain curve for (a) B-stud, (b) C-stud, (c) F-stud and (d) Plywood of P9 specimen*

4.7.4. Board configurations

Fig. 4.41 compares the load-displacement responses of the key specimen with the same specimen but with different board scenarios. By comparing out-of-plane load-displacement responses of unsheathed stud wall (UB) with the single sheathed key specimen (K1), it was revealed that removing the OSB board resulted in a significant reduction in out-of-plane strength of the system from 30 kN to 8 kN whilst as expected the ductility of the system was considerably improved (see Fig. 4.41). As illustrated in Fig. 4.42 (a) and (b), the unsheathed system failed in a lateral-torsional buckling of the studs (B- and C-studs), which was then interacted by the local buckling at the final stage of the loading. This is attributed to the lack of lateral-resisting contribution from the OSB board to the compressive flanges of the studs. Using CFS stud walls sheathed on both sides (DB1 and DB2) was found to be more effective in

improving the out-of-plane stiffness rather than strength. The out-of-plane initial stiffness and strength of the stud wall with double-sheathed OSB were enhanced by 16% and 45% compared to the key specimen due to providing restraint on both flanges of the studs. Hence, while distortional buckling was prevented, local buckling occurred in the middle of the CFS studs (Figs. 4.42 (c, d)). Moreover, the top compressive OSB board was crushed in mid-height of the wall, however, no crack was observed in the bottom tensile OSB board. The results also demonstrated that the out-of-plane strength and initial stiffness of the stud wall remained almost constant by decreasing the centre spacing (drift ratio) from 610 to 305 mm (Fig. 4.41). However, the load-displacement responses of the stud walls after the peak load showed that reducing centre spacing resulted in more brittle behaviour. The failure mechanism of the stud wall system with reduced drift ratio was found almost similar, where the distortional buckling of studs along with the localised failure of their webs was combined with some damage in the OSB as depicted Figs. 4.42 (e-g). The results of strain gauges versus the applied load were reported in Figs. 4.43, 4.44 and 4.45 for the UB, DB1, and DR specimens, respectively. In general, it can be seen that the strains developed in the studs and the OSB board at the same locations were in good agreement before the initiation of the buckling at a load of maximum loading.
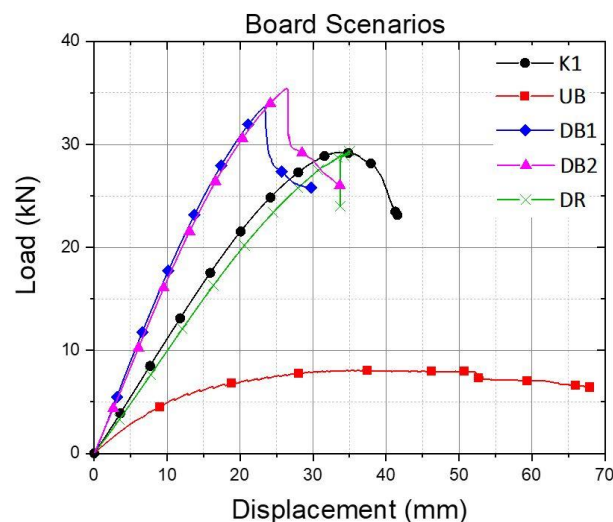
Figure 4.41 Load-displacement responses of stud walls with different board scenarios
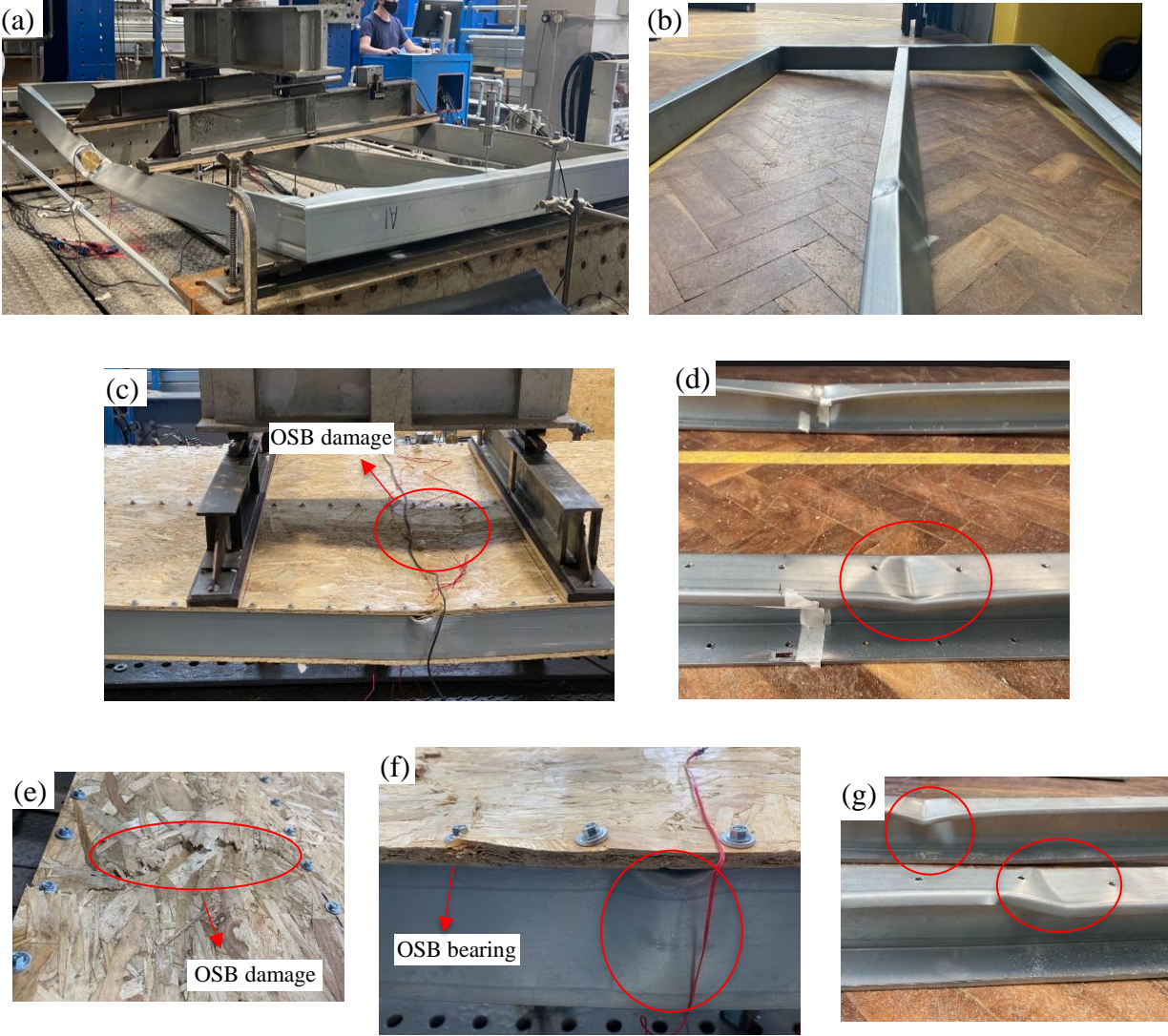
Figure 4.42 Failure modes of (a), (b) UB, (c), (d) DB1, (e), (f) and (g) DR specimens
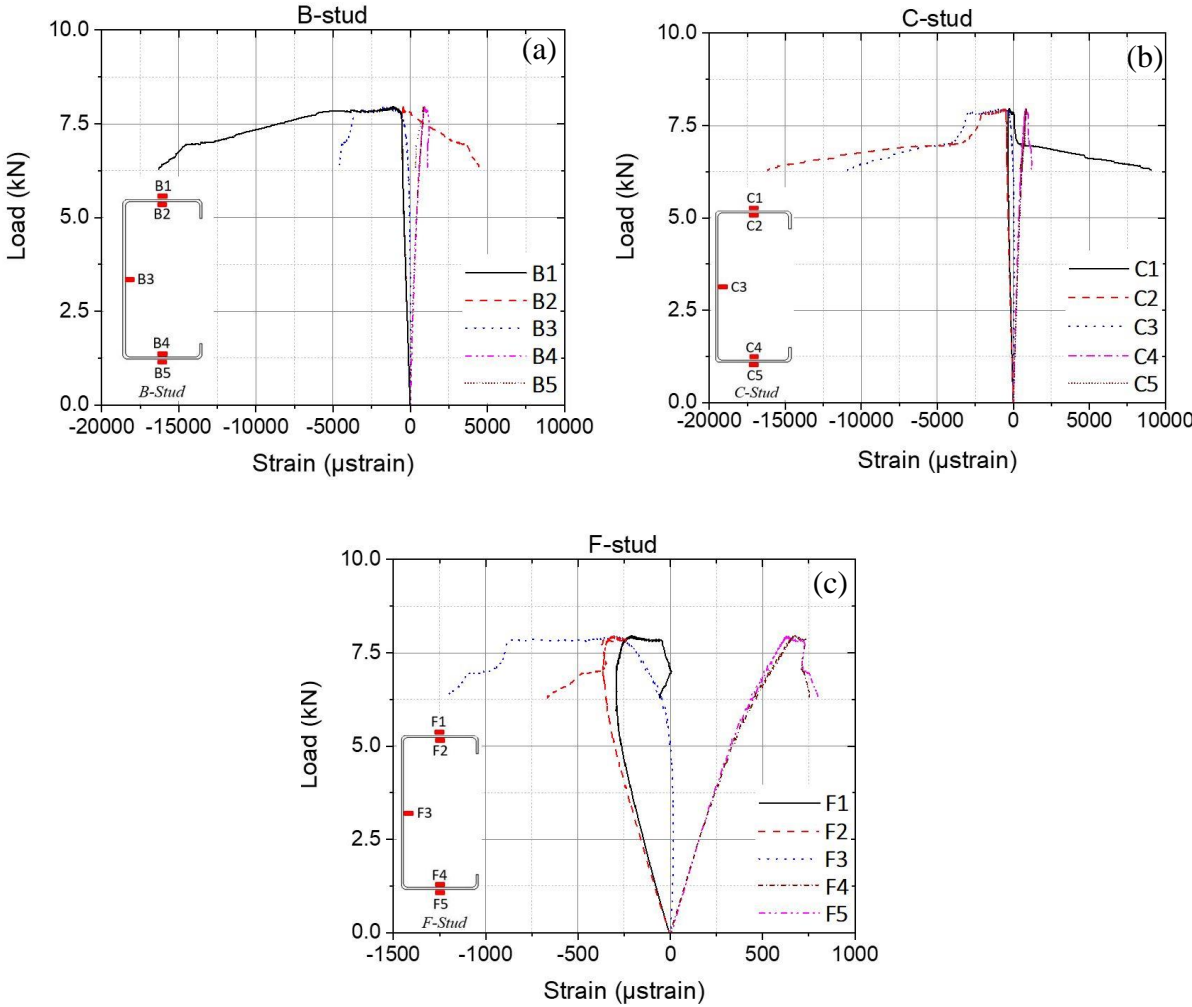
Figure 4.43 Load-strain curve for (a) B-stud, (b) C-stud and (c) F-stud of UB specimen
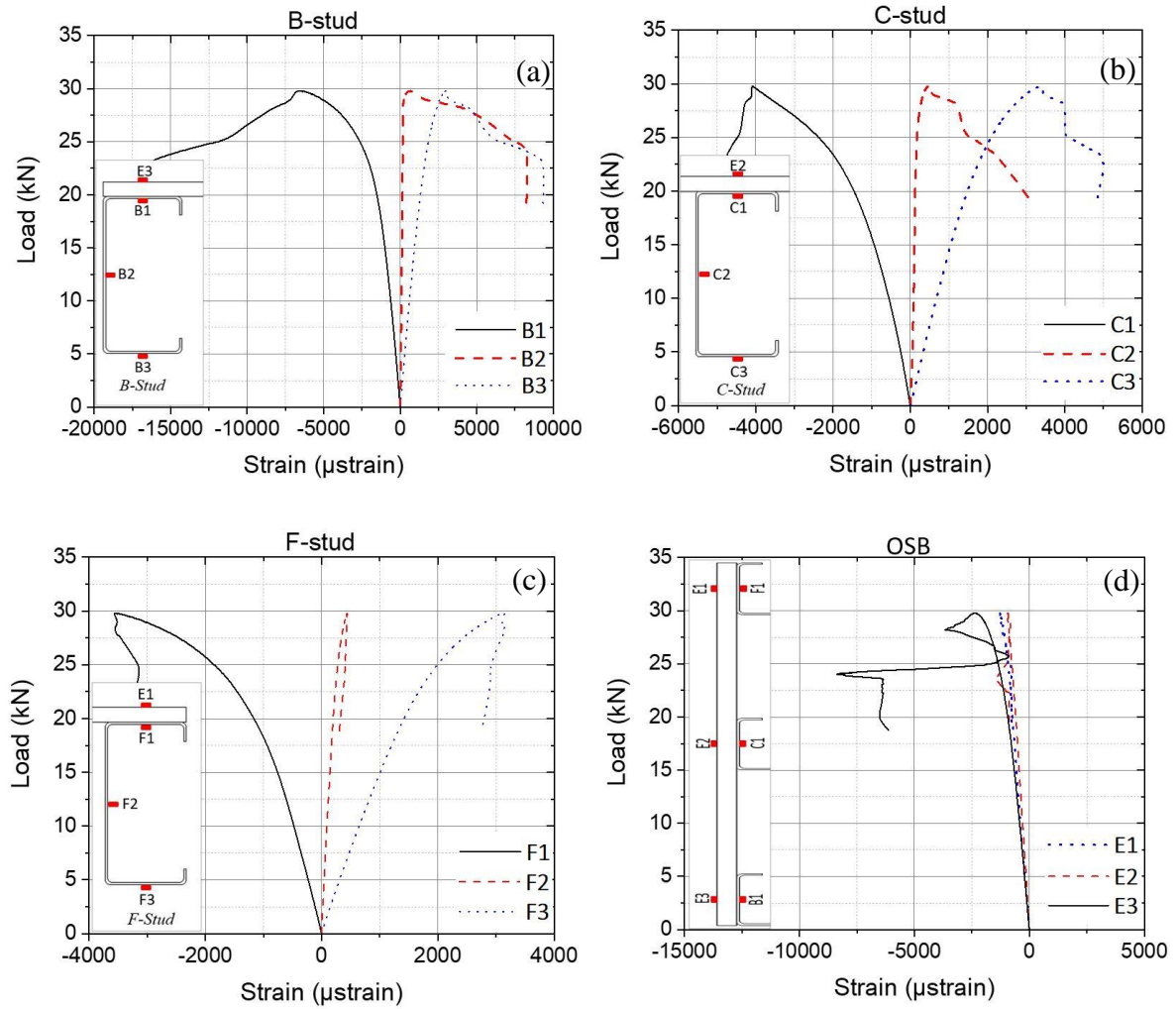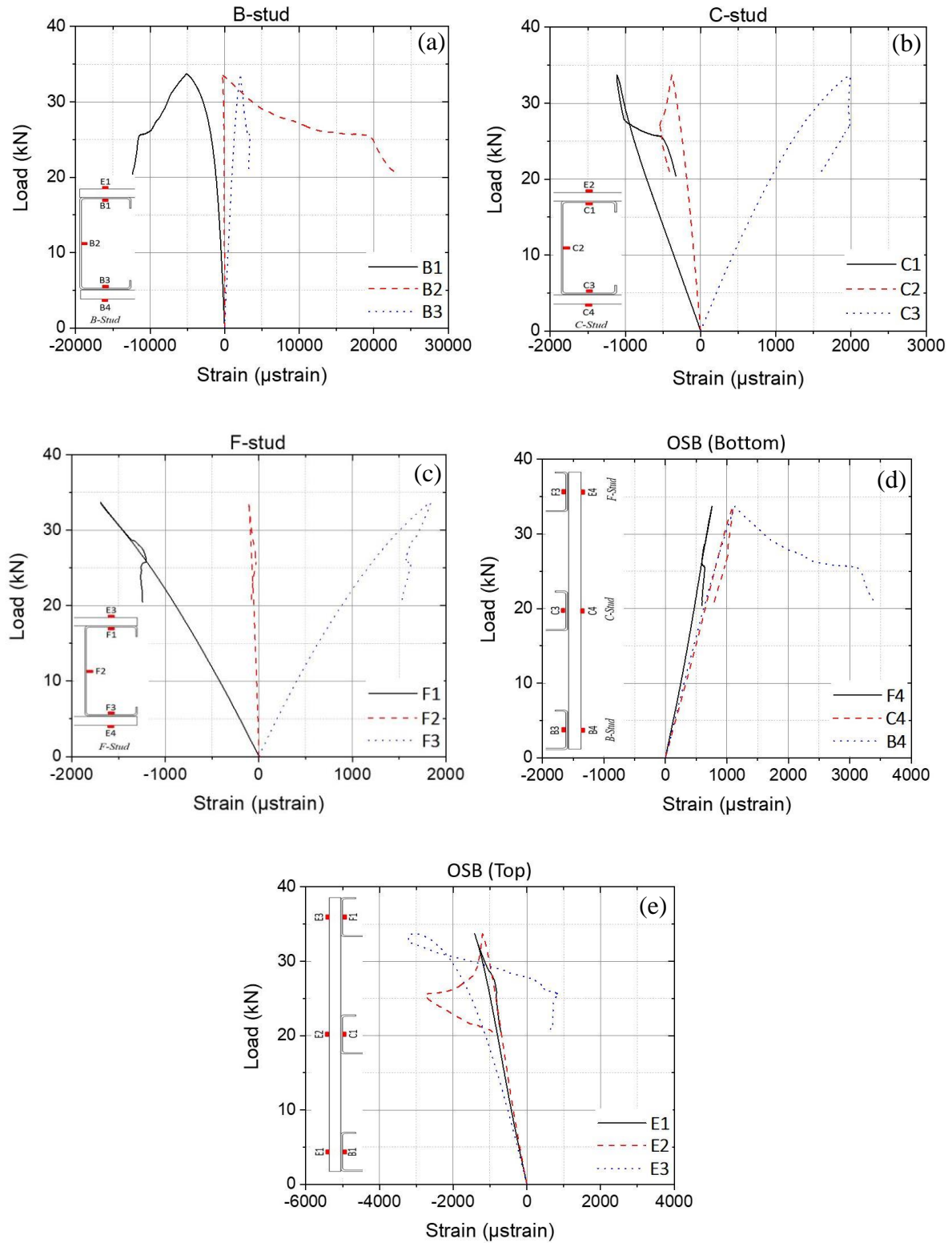
***Figure 4.44** Load-strain curve for (a) B-stud, (b) C-stud, (c) F-stud (d) OSB (bottom) and (e) OSB (top) of DB1 specimen*
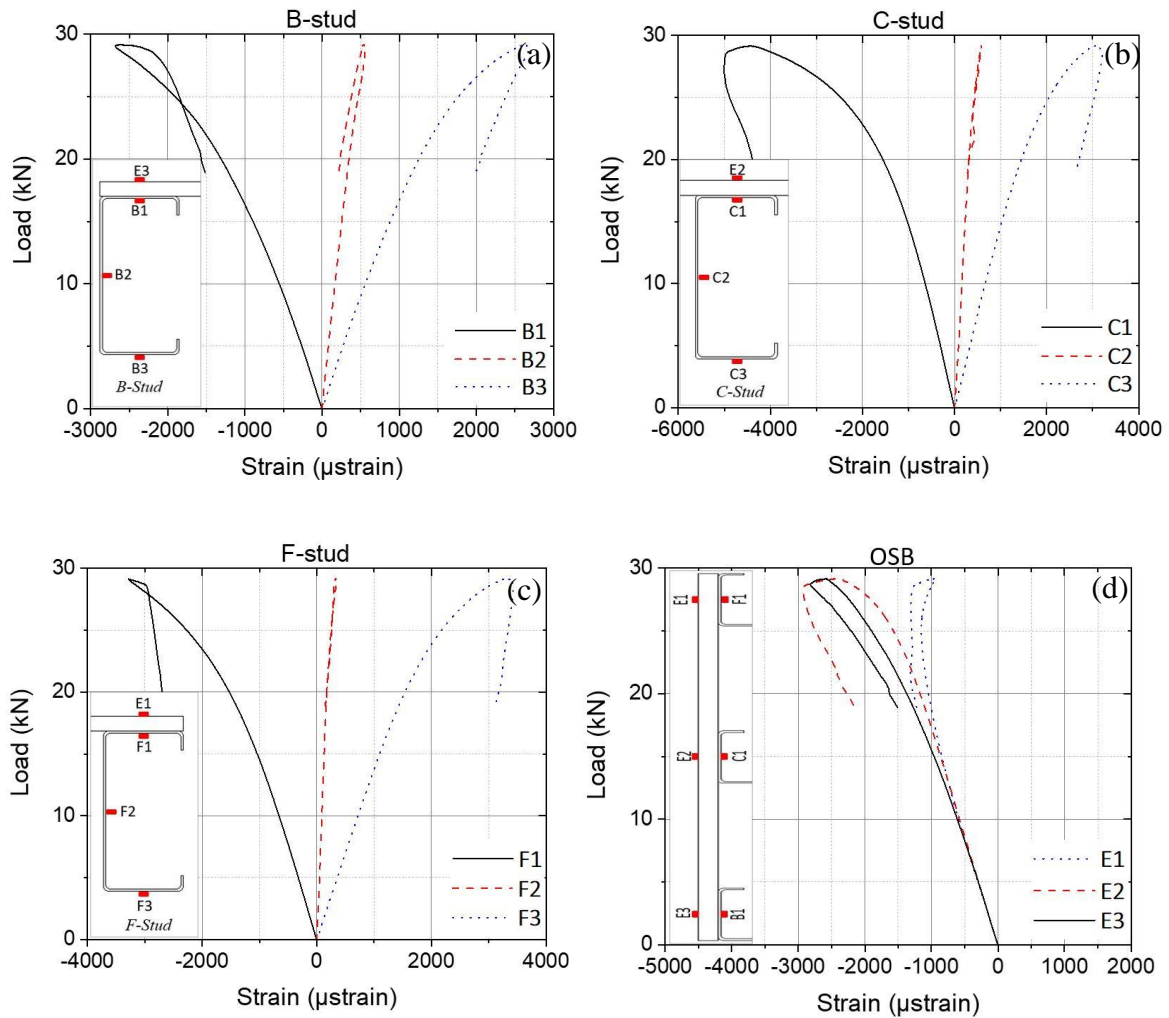
Figure 4.45 Load-strain curve for (a) B-stud, (b) C-stud, (c) F-stud and (d) OSB of DR specimen

4.7.5. Main/auxiliary components

Fig. 4.46 compared the responses of the key specimen K1 with the same specimens however in the absence/presence of main/auxiliary components of the system. It was observed that the absence of the pinned track (PT) and the presence of the seam (S) have a negligible effect on the out-of-plane stiffness of the stud wall panels. On the contrary, using nogging elements (N) in the CFS stud wall improved the stiffness of the system by 18%. Furthermore, while incorporating either noggings or seam provided slight enhancements in the out-of-plane strength of the system by 7%, the absence of the pinned track led to a 12% reduction in the out-of-plane capacity of the stud wall (see Table 4.11). By comparing the failure mechanism of the S and N stud wall specimens with that of the key specimen, it can be concluded that the

existence of the seam and nogging elements has no effect on the dominant failure mode as shown in Fig. 4.47 (a-c). Based on the readings of stud rotations, while noggin elements exhibited a noticeable effect in reducing the rotation of studs (see Fig. 4.48 (a) and (b)), on the contrary, the presence of the seam increased the rotational flexibility of studs (see Fig. 4.48 (a) and (c)). With respect to the PT specimen, due to the lack of lateral restraint at both ends of the studs, lateral-torsional buckling happened along with some OSB damage at the locations of the supports (Fig. 4.47 (d)). As expected, the rotation of studs was diminished when the pinned track elements were omitted from the stud wall specimen (see Fig. 4.48 (a) and (d)). It should be noted that the end-slip measurements of the stud-wall showed that the presence/absence of the main/auxiliary components has negligible effects on the out-of-plane torsional behaviour of the system (see Fig. 4.4). The results of strain gauges versus the applied load were reported in Figs. 4.48-4.50 for the S, N and PT specimens, respectively.
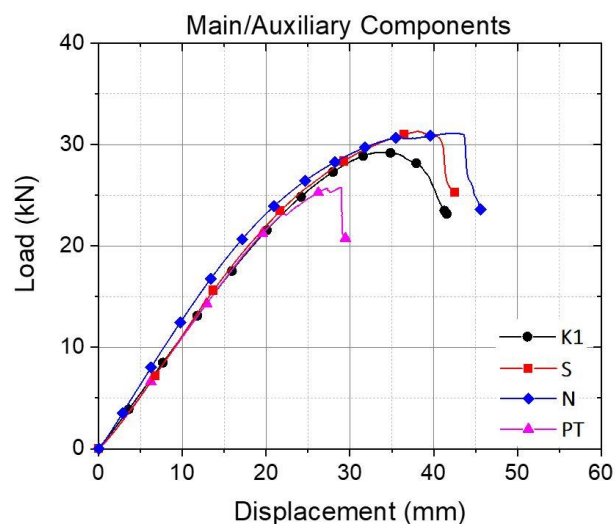
Figure 4.46 Load-displacement responses of CFS stud walls considering the effects of main/auxiliary components
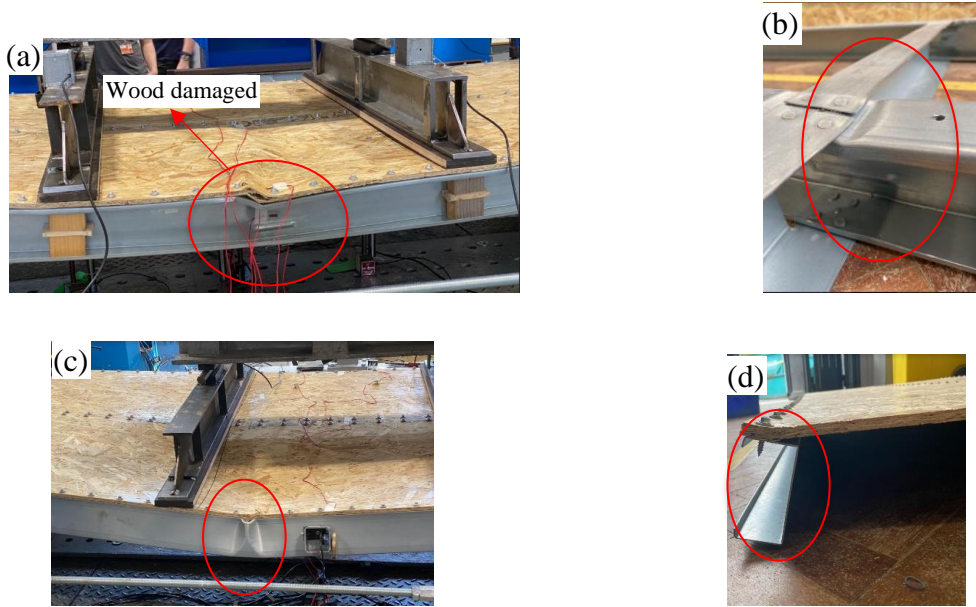
Figure 4.47 Failure modes of (a), (b) N, (c) S and (d) PT specimens
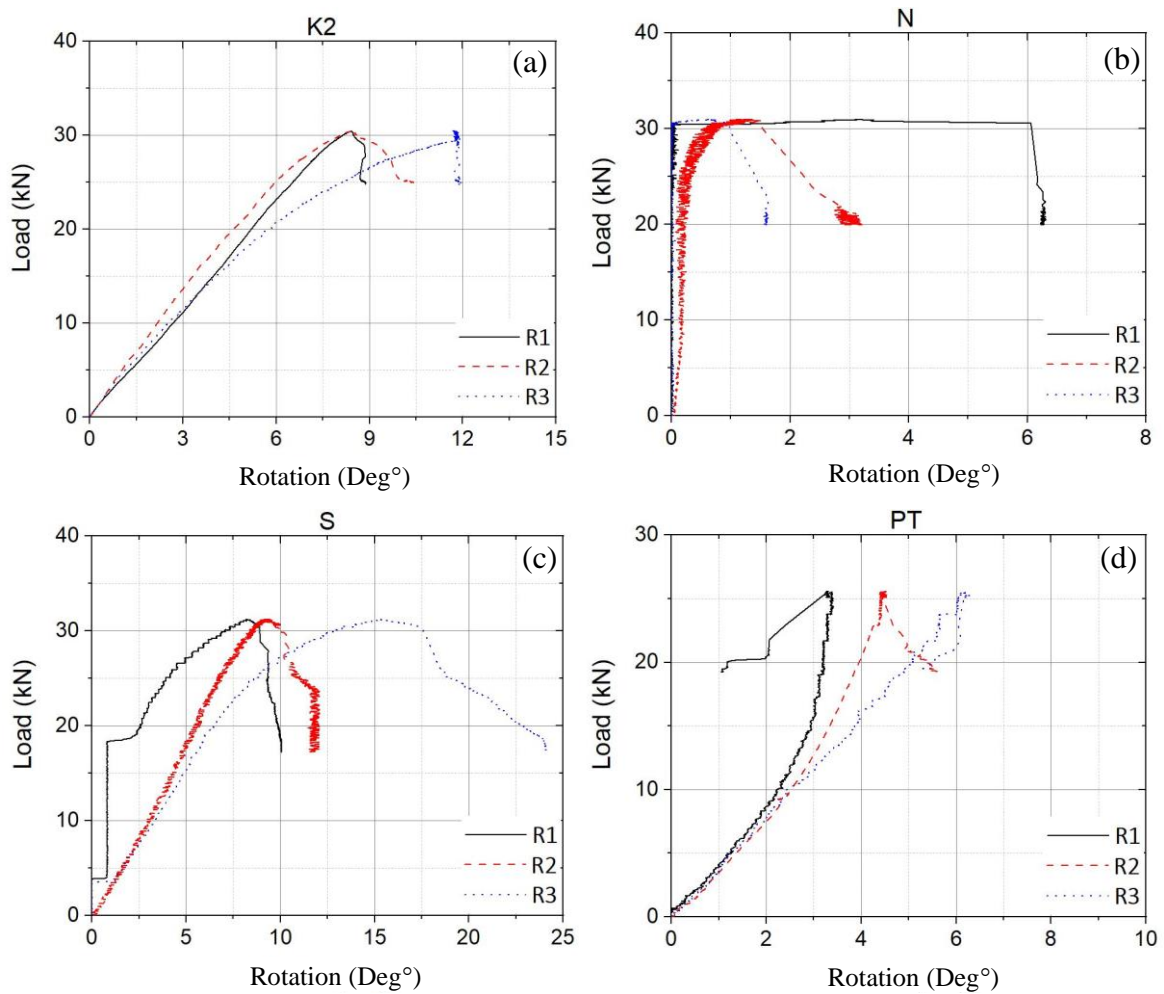
Figure 4.48 Rotation of studs along their major axis for: (a) K2, (b) N, (c) S and (d) PT specimen
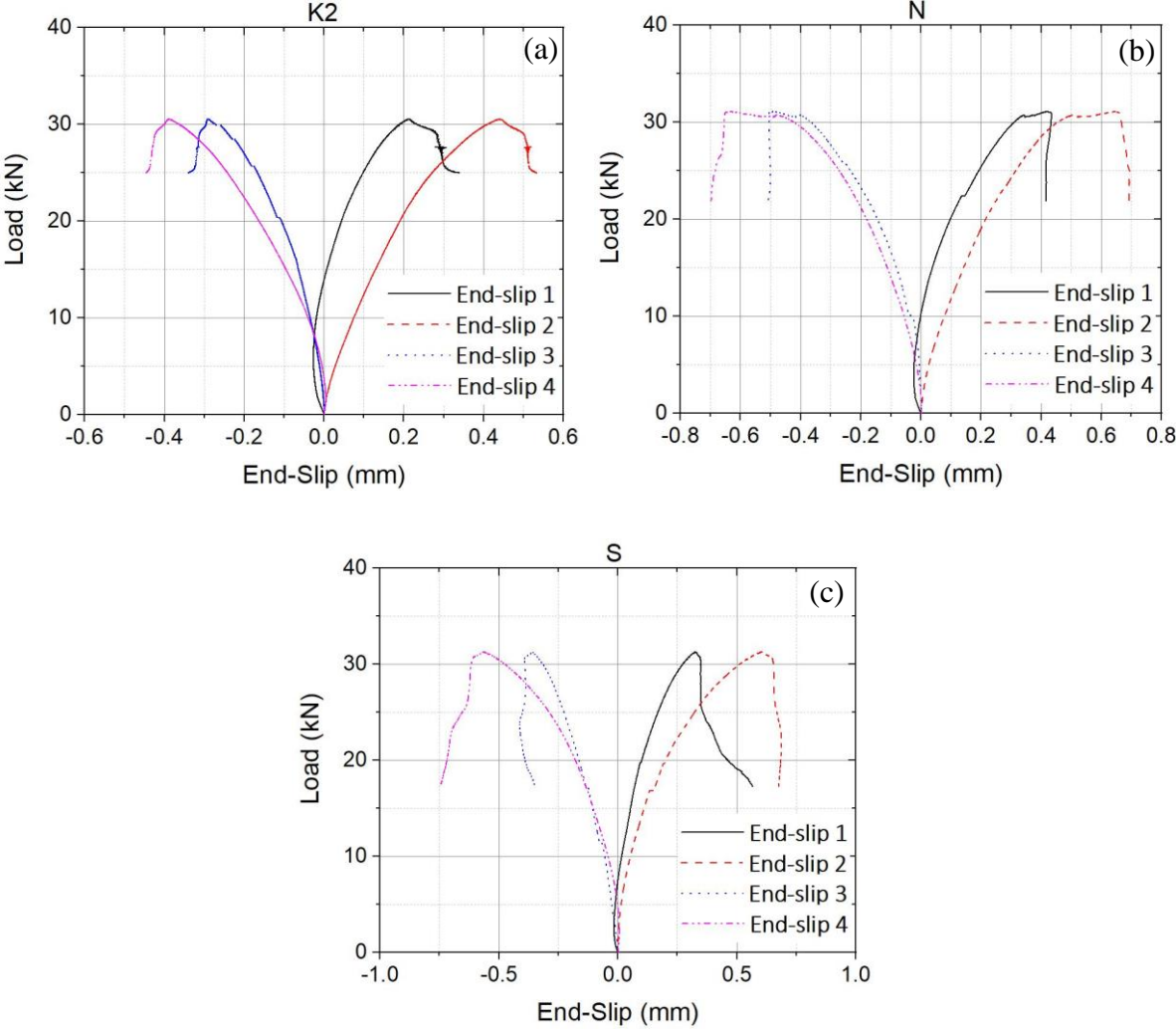
Figure 4.49** **End-slip measurement histories of: (a) K2, (b) N and (c) S specimen
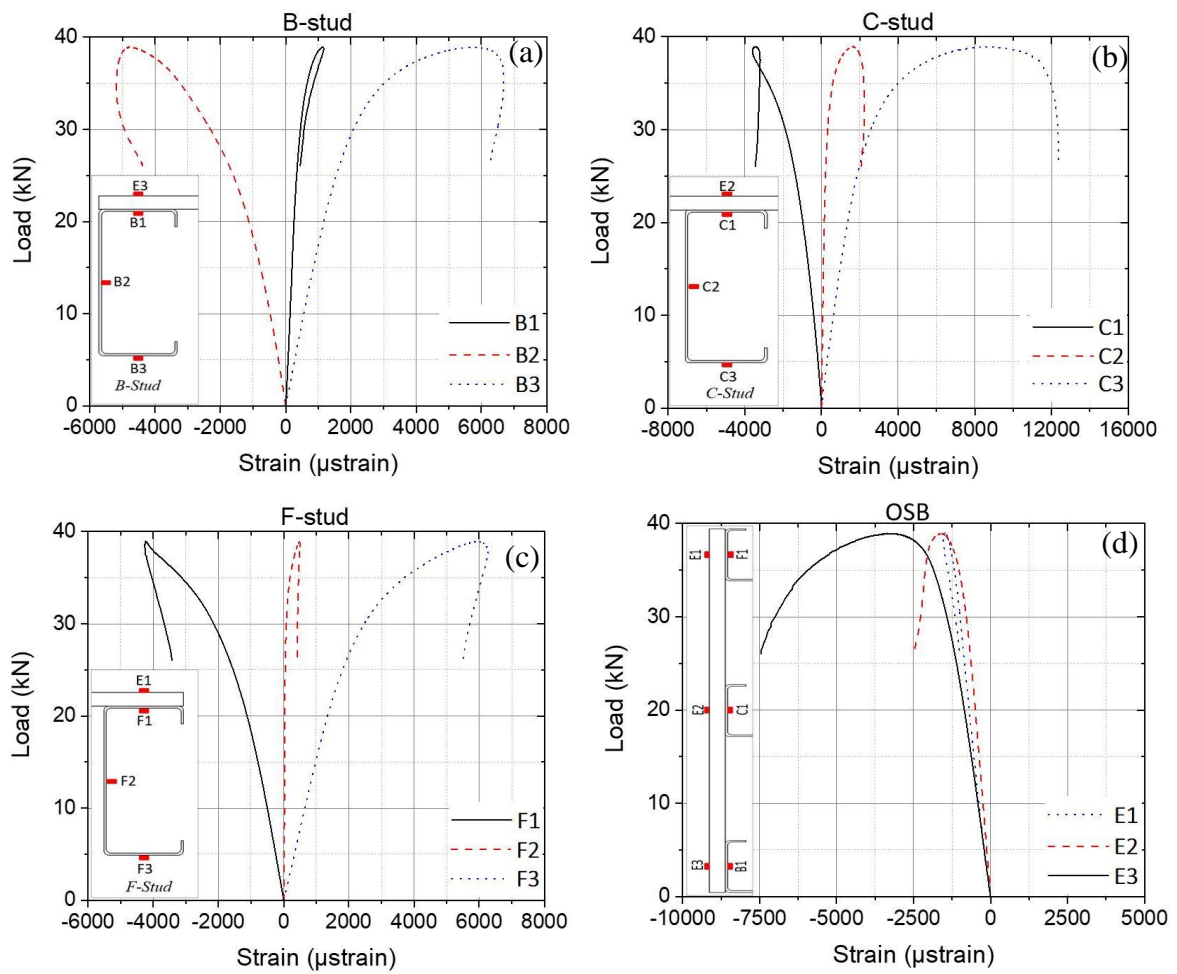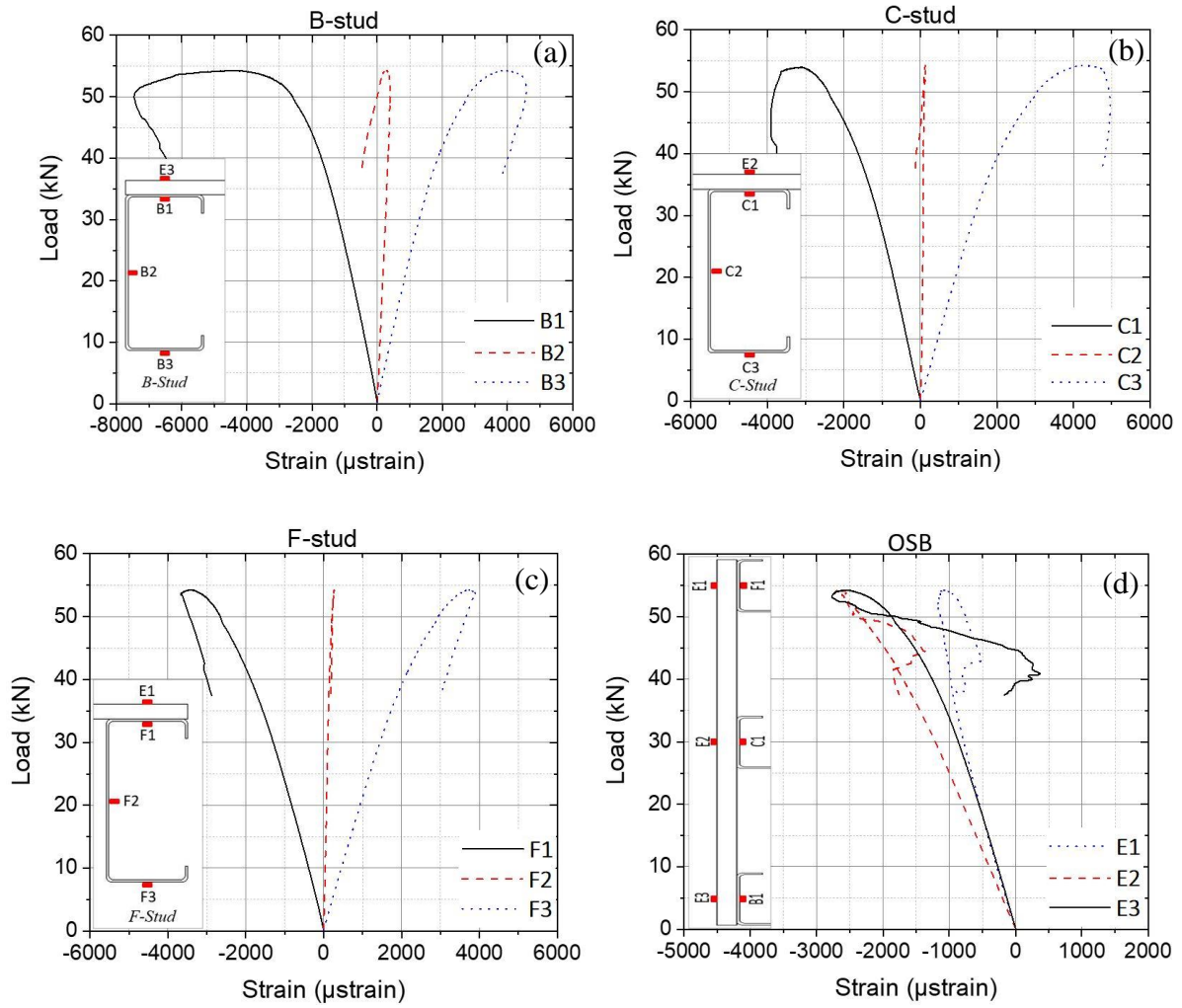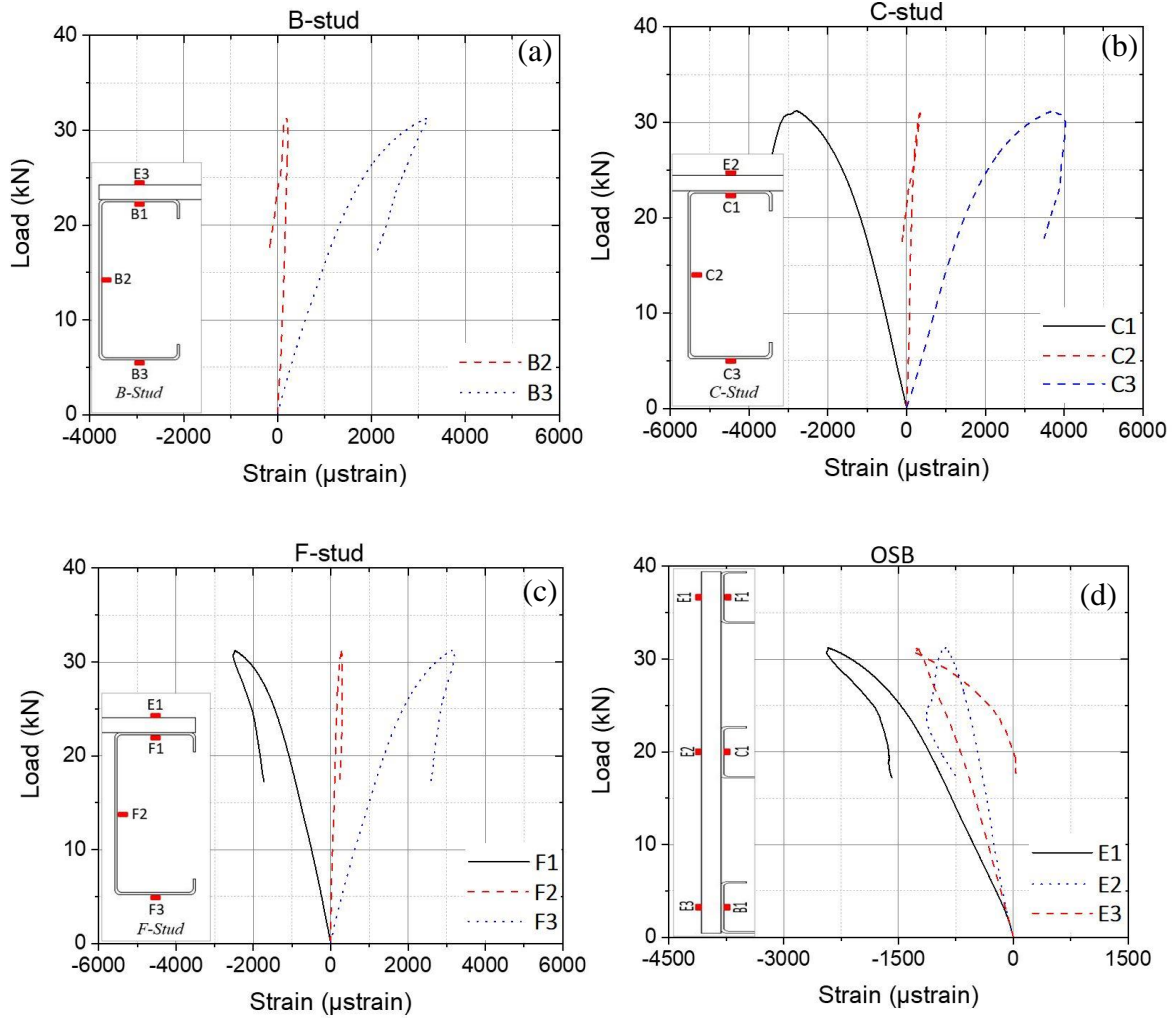
***Figure 4.50** Load-strain curve for (a) B-stud, (b) C-stud, (c) F-stud and (d) OSB of S specimen*

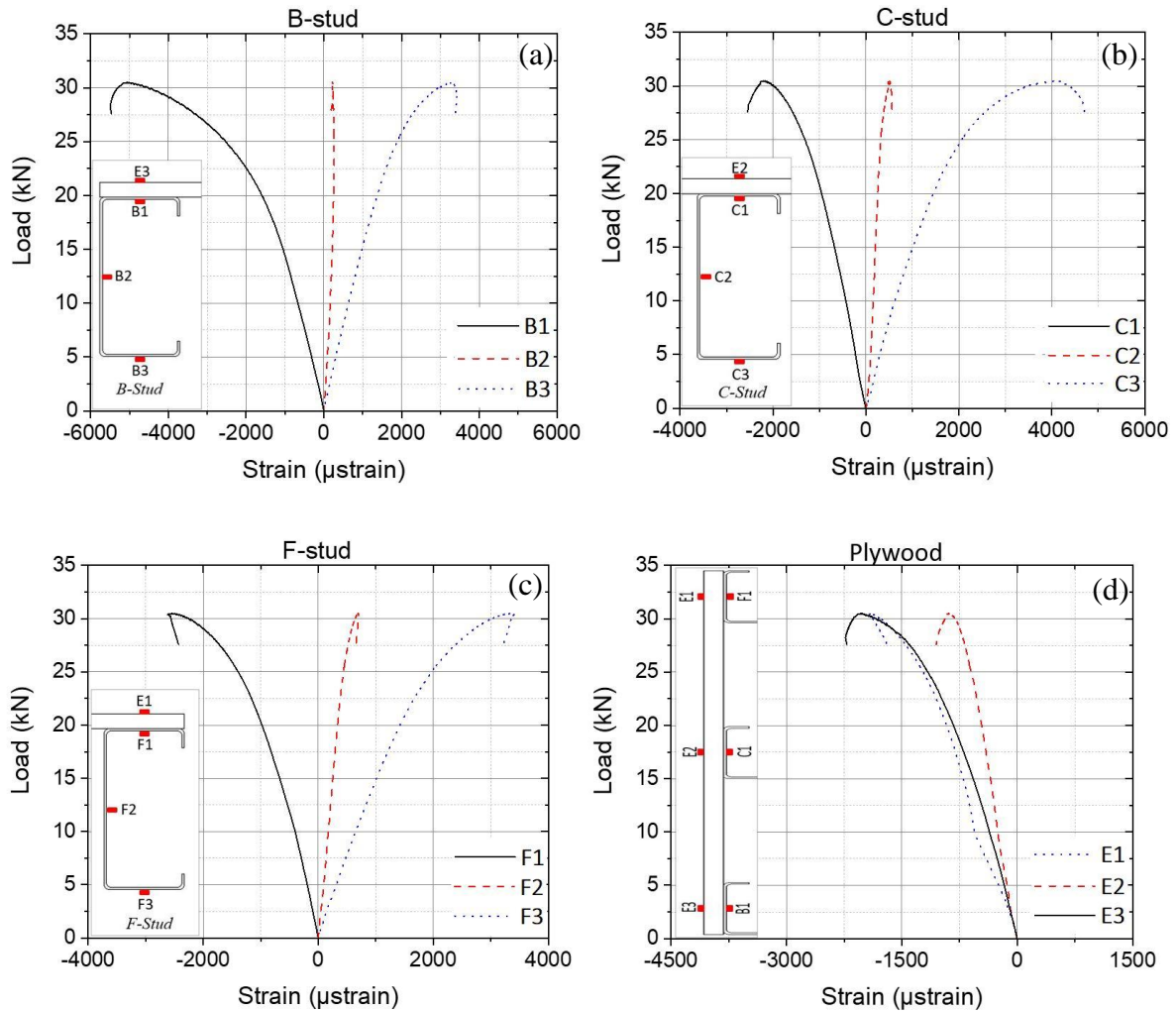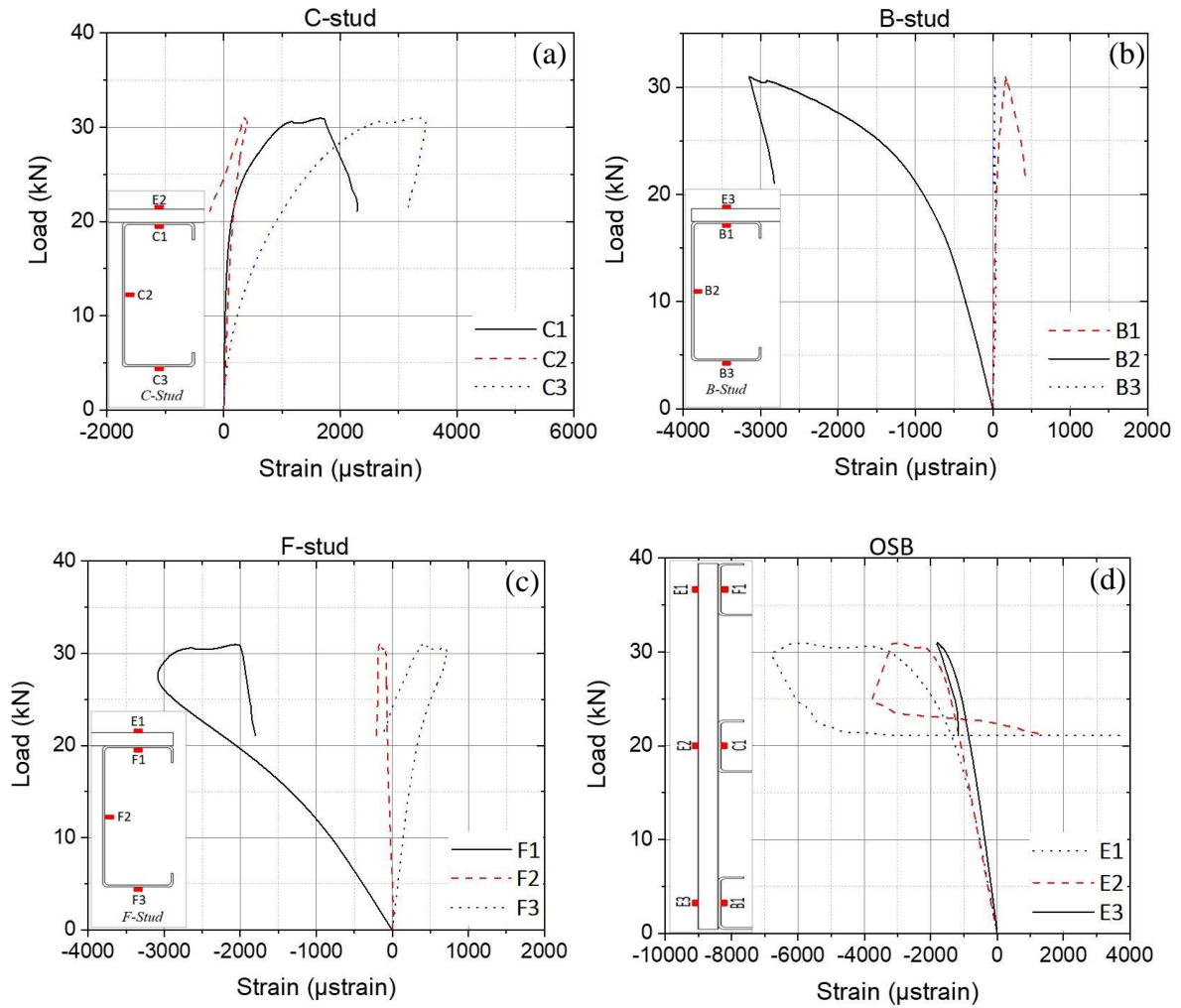**Figure 4.51 Load-strain curve for (a) B-stud, (b) C-stud, (c) F-stud and (d) OSB of N specimen**
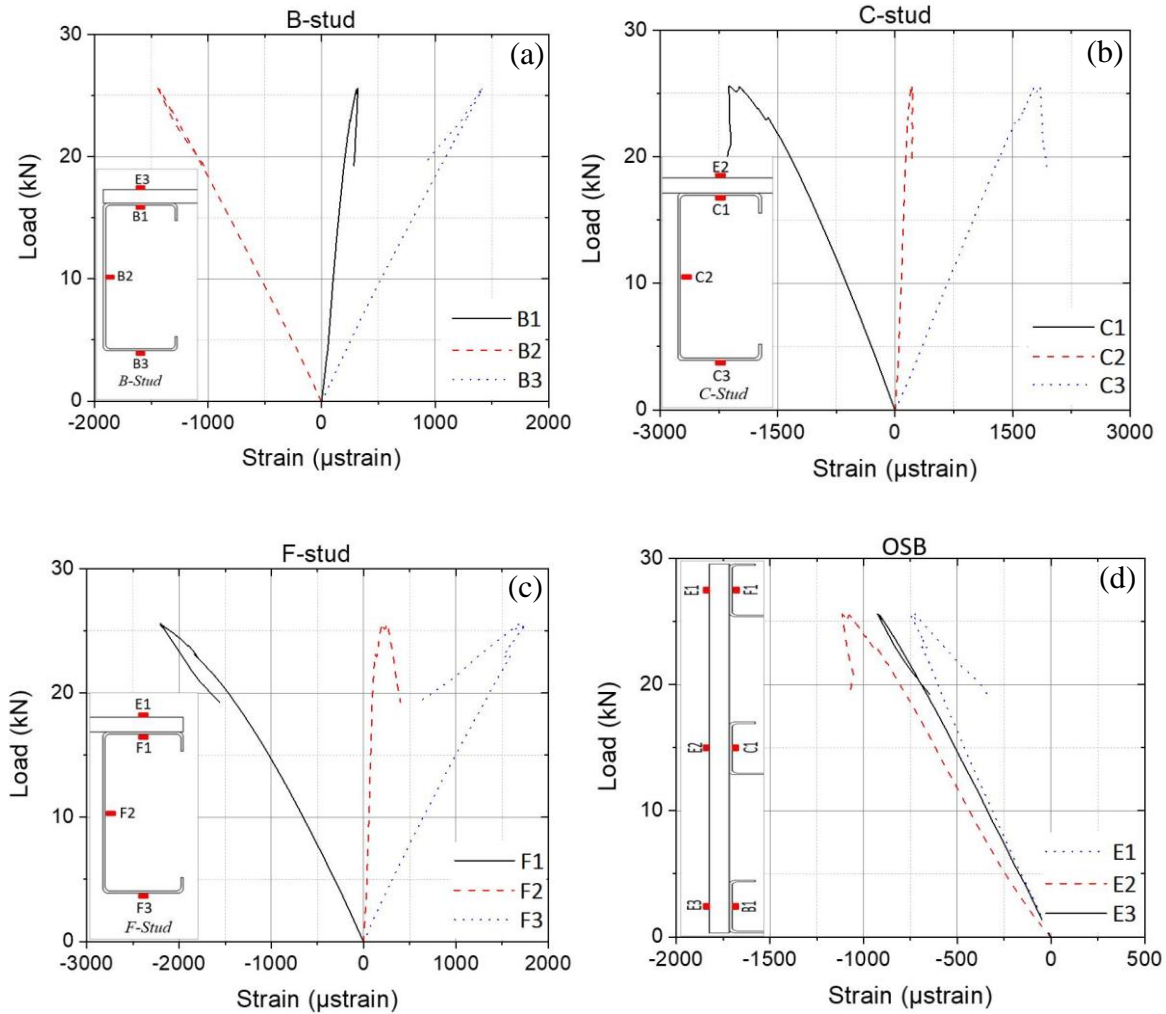
Figure 4.52 Load-strain curve for (a) B-stud, (b) C-stud, (c) F-stud and (d) OSB of PT specimen

4.8. Summary and conclusions

This chapter investigated the bending behaviour and capacity of CFS stud wall panels sheathed with the wood-based board by considering the effects of key design parameters on the performance of these systems as one of the emerging systems used in modern modular construction. For this purpose, a comprehensive experimental programme was conducted on the sheathed stud wall systems by systematically varying key design parameters, including the screw spacing, the thickness of the CFS studs and the boards, the board material (i.e. OSB and plywood), the board scenarios (unsheathed, single- and double-sheathed) and the effects of main/auxiliary components (i.e. seam, nogging and no pinned track). The results were used to investigate the main structural performance parameters (i.e. bending load capacity, initial stiffness) and failure mechanism of the tested specimens. A series of material coupon tests, as

well as small-scale push-out and pull-out tests, were conducted. Moreover, initial imperfections of the specimens were also measured for distortion and local buckling. The results of strain gauges versus the applied load for all specimens were reported in Appendix C.

Based on the presented results, the following conclusions can be drawn:

- Increasing the screw spacing from 75 to 300 mm resulted in a reduction in the out-of-plane strength of the stud wall by up to 75%, however, the initial out-of-plane stiffness of the wall remained almost constant by increasing the screw spacing. The results also demonstrated that increasing the screw spacing led to a more ductile stud-wall system. It was observed that the failure mechanism of the stud wall systems with various screw spacing was found almost similar, where the distortional buckling of studs along with the localised failure of their webs was combined with some damage in the OSB. However, for the stud wall system with the largest selected screw spacing (300 mm), an additional OSB bearing was observed at the corners of the wall.

- By doubling the thickness of the board from 9 mm to 18 mm, the out-of-plane strength of the stud wall was increased by 33%. This also showed a major effect on the failure mechanism of the system, in which the failure of the OSB board was prevented, and the boundary studs failed in the lateral-torsional buckling than the distortional buckling. In addition, thickening of CFS elements from 1.2 mm to 2 mm enhanced the out-of-plane strength and stiffness of the stud wall by 86% and 45%, respectively, which was attributed to preventing distortional buckling in the studs of the system. Compared to the OSB material, using plywood boards with the same thickness (i.e. 9 mm) resulted in a more ductile behaviour before the peak capacity while it causes a negligible change in the out-of-plane strength and stiffness of the system.

- Removing the OSB board resulted in a significant reduction in (over 3 times) out-of-plane strength of the system, however, the unsheathed system showed a considerably higher ductile behaviour. The out-of-plane initial stiffness and strength of the stud wall with double-sheathed OSB were enhanced by 16% and 45%

compared to the single-sheathed wall. In fact, the out-of-plane restraints were imposed by the OSB boards on both flanges of the studs, therefore, the distortional buckling was prevented, and subsequently local buckling occurred in the middle of the CFS studs. The results also demonstrated that the out-of-plane strength and initial stiffness of the stud wall remained almost constant by decreasing the centre spacing (drift ratio) from 610 to 305 mm. However, the load-displacement responses of the stud walls after the peak load showed that reducing centre spacing resulted in more brittle behaviour.

- It was observed that the absence of the pinned track and the presence of the seam have a negligible effect on the out-of-plane stiffness of the stud wall panels. On the contrary, using nogging elements in the CFS stud wall improved the stiffness of the system by 18%. Furthermore, while incorporating either noggings or seam provided slight enhancements in the out-of-plane strength of the system by 7%, the absence of the pinned track led to a 12% reduction in the out-of-plane capacity of the stud wall. While the existence of the seam and nogging elements has no effect on the dominant failure mode, for the no pinned track specimen, lateral-torsional buckling of studs happened along with some OSB damage at the locations of the supports due to the lack of lateral restraint at both ends of the studs.

Chapter 5: Out-of-plane bending behaviour and capacity of sheathed face-down CFS stud walls: experimental investigation

5.1. Introduction

A comprehensive experimental study was carried out with the aim of achieving the out-of-plane bending behaviour and capacity of cold-formed steel (CFS) face-down stud walls sheathed with wood-based boards in this chapter. The particular emphasis of this study is on the effects of the key design variables, including the thickness of materials (OSB and CFS), different board material (plywood), the drift ratio and the existence of the main and auxiliary components. A total of 10 stud walls sheathed with either Oriented Strand Board (OSB) or plywood specimens were tested under four-point bending loading which was applied directly to the board. To determine the stress-strain behaviour of the boards and CFS elements, a series of material coupon tests were carried out. Besides, the rotational connection tests were performed to investigate the composite action between light-gauge steel stud framing and wood-based materials under rotation loading. It was observed that the out-of-plane behaviour of the CFS stud-wall sheathed with wood-based materials can be varied by changing the key design

variables of the system. Based on the results and observations made during experiments, the structural performance parameters (i.e. bending load capacity, initial stiffness), failure mechanism, rotation of the C-shape studs and end-slips of the tested stud wall panels were investigated in detail for each parameter. The wall system was loaded in face-down directions, which means the face of the wooden board looked down. In the face-down specimens, the wood-based board was pushed down using four wood blocks to transfer the load from the hydraulic jack rather than pushing on the free flange of the CFS stud members. In this way, the stud wall systems were tested considering the more vulnerable condition.

5.2. Specimen geometry

The purpose of this experimental investigation is to determine the bending behaviour and capacity of sheathed CFS stud walls for various parameters. In this experimental test schedule, a total of 10 full-scale stud wall systems consisting of the CFS frame elements and a wood-based board were subjected to 4-point bending loading. In this study, the experimental program can be classified into three general design parameters (see Fig. 5.1);

- The specimens were designed to consider the effects of different thicknesses of materials; OSB 9 and 18 mm, Plywood 9 mm, CFS 1.2 and 2 mm.
- The effects of the drift ratio were examined by testing the panel specimens with two different centres spacing of 305 and 610 mm were considered.
- Effects of main/auxiliary components on the system were investigated through seam, noggins, pinned no track

A summary of the examined parametric test matrix was presented in Table 5.1.

OSB 9 and 18 mm,
Plywood 9 mm

CFS 1.2 and 2 mm

(a)

Drift Ratio (Centre spacing)
305 and 610 mm

(b)

Seam

(c)

Noggins

(d)

Pinned No Track

(e)
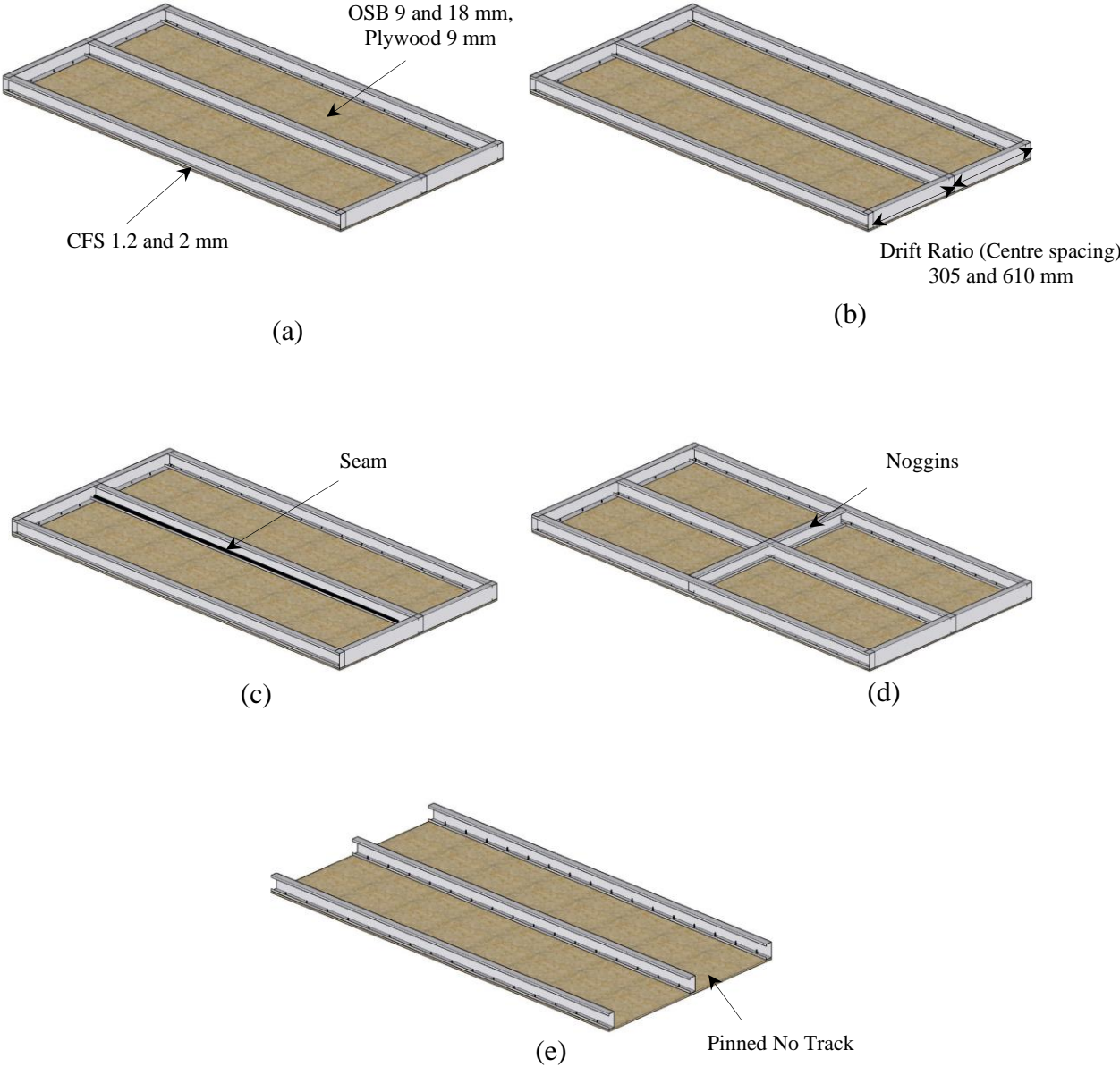
Figure 5.1 Design parameter; (a) materials and thicknesses, (b) drift ratio, (c), (d) and (e) effects of main/auxiliary components on the system

Table 5.1 The experimental parametric test matrix of the CFS shear wall panels

	Specimens	Test Code	Width x Length (mm x mm)	Test Numbers
Benchmark Test	Key Specimens	K3 K4 K5	1220 × 2440 1220 × 2440 1220 × 2440	3 Tests
Materials and thicknesses	Plywood (9 mm) OSB (18 mm) CFS (2 mm)	P9-2 OSB18-2 CFS2-2	1220 × 2440 1220 × 2440 1220 × 2440	3 Tests
Drift Ratio	Centre Spacing (305mm)	DR2	610 × 2440	1 Tests
Effects of main/auxiliary components on the system	Seam Noggings Pinned no track	S2 N2 PT2	1220 × 2440 1220 × 2440 1220 × 2440	3 Tests

The overall dimensions of the face-down stud wall specimens were 1220×2440 mm^2. The CFS framing elements were composed of the C-lipped channel and the C-unlipped channel for stud and track elements, respectively, as illustrated in Fig. 5.2. To accurately measure the dimensions and thickness of the wall components, the micro millimetre calliper was used. The average out-to-out cross-sectional dimensions of all 1.2 and 2 mm CFS members were reported in Table 5.2. Moreover, the average thickness of the wood-based board at three different locations; top, middle and bottom (see Fig. 5.3); were listed in Table 5.3.

(a) (b) (c)
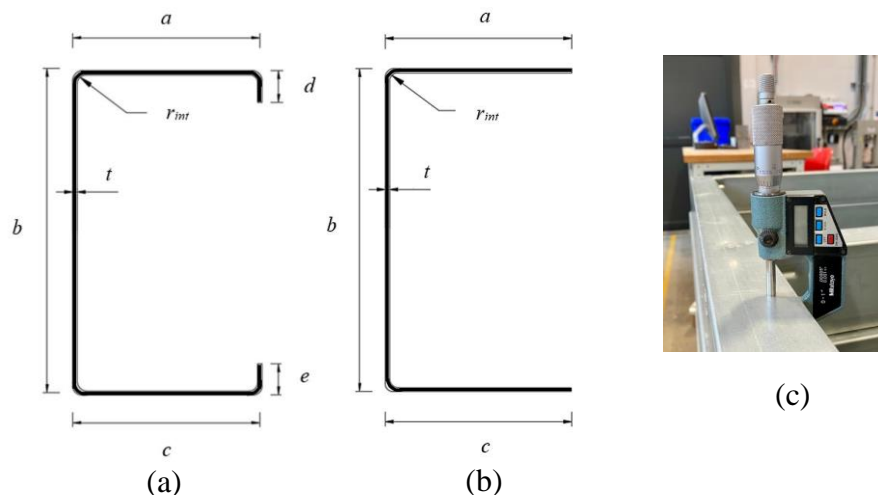
Figure 5.2 Cross-sectional (a) C-lipped channel stud, (b) C-unlipped channel track with the labelling of dimensions of tested CFS members and (c) micrometre calliper

Table 5.2 Average dimensions (out-to-out) of the tested CFS members (in mm)

Specimen Batch	t	r_{int}	C-lipped channel CFS (studs)					C-unlipped channel CFS (tracks)		
			a (flange)	b (web)	c (flange)	d (lip)	e (lip)	a (flange)	b (web)	c (flange)
1.2 mm CFS	1.19	2.8	50.75	99.72	50.36	8.59	11.13	57.66	99.62	57.22
2 mm CFS	1.92	3.2	49.17	100.88	49.22	13.94	15.15	56.93	103.18	57.48
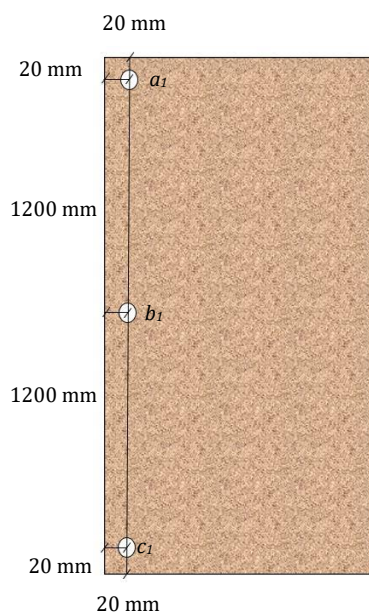
Figure 5.3 Three points for average thickness of tested wood-based boards

Table 5.3 Average thickness of the tested wood-based boards (in mm)

Specimen Batch	The thickness of the wood-based board			
	a_1	b_1	c_1	Average thickness
9 mm OSB	8.85	8.95	8.65	8.82
18 mm OSB	17.61	17.66	17.67	17.65
9 mm Plywood	9.54	9.32	9.46	9.44

In this study, the benchmark test specimen is called 'key specimen' which was used to evaluate the behaviour of the other tested specimens with different design variables. The tests were repeated three times and labelled K3, K4 and K5. The key specimens consisted of 1.2 mm CFS framing members (i.e. studs and tracks) with stud spacing of 75 mm connected to 9 mm thick single OSB sheathing using 6.3 mm diameter self-drilling screws with a bonded washer screw (see Fig. 5.4). It should be noted that the seam and noggins were not incorporated in the key specimen.

Figure 5.4 The 6.3 mm diameter of the self-drilling screws with a bonded washer

5.3. Material tests

The material characteristics (basic stress-strain behaviour) of the main components of experimental test materials (CFS members and OSB panels) were identified by carrying out the tensile coupon and compression tests by using regulation procedures. Material tests were not performed in the Section 5.3. Since only the test setup was changed for face-up specimens in Chapter 5, the results of the material tests (i.e. CFS and OSB) at Chapter 4 were used in herein.

5.3.1. CFS members

In total, six CFS tensile coupon specimens were tested to determine the material characteristics. Two flat coupons of these were cut from 1.2 mm stud and track webs of the actual wall specimens after the test. Then, the remaining four flat coupons were cut from 1000 mm length intact 1.6 mm thick C-shape stud element, where the two coupons were taken along the midline of the web, and the other two were sampled along the midline of the bottom and top flanges of the section. The 1.6 mm thick tensile coupon specimens and detailed drawing of the tensile coupons are given in Fig. 5.5 (a) and (b), respectively. The dimensions of all tensile coupons were the same with a nominal gauge width of 12.5 mm as recommended by EN ISO 6892-1 regulations (CEN, 2009). Each flat coupon was instrumented using two 10 mm strain gauges on both sides to accurately record longitudinal strains in the early stages of testing and a 50 mm extensometer attached to the middle of the specimen. An extensometer machine with a 50 mm gauge length was used to apply the tensile loads on the coupons, as depicted in Fig. 5.5 (c). In order to capture the realistic values of the strain gauge data, the zinc coating was removed from the coupons before attaching strain gauges. The width and thickness of each coupon were measured using a digital micrometre calliper, which is listed in Table 5.4.
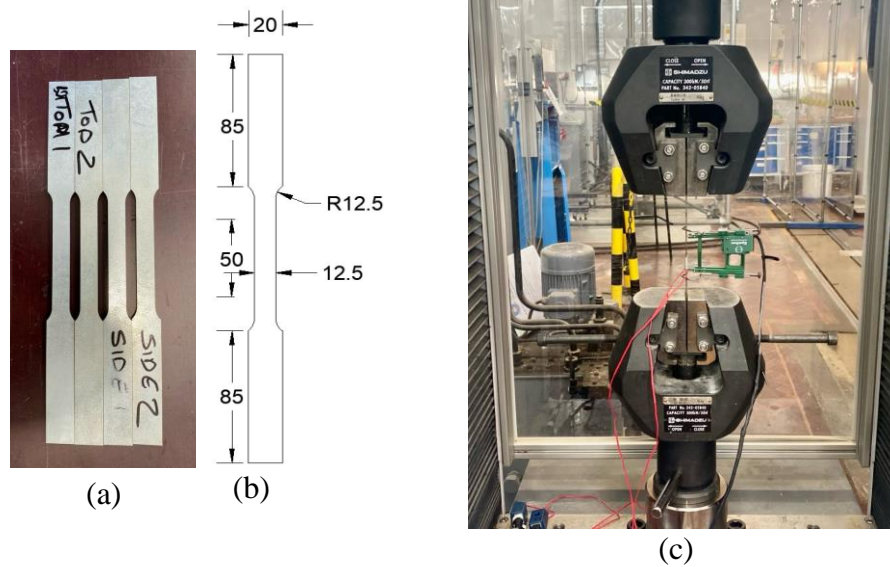
Figure 5.5 (a) Tensile CFS coupons, (a) dimensions of coupon (in mm) and (c) test set-up

Table 5.4 Measured dimensions of the tested coupon specimens

Specimen Batch	Width (mm)	Thickness (mm)	Area (mm2)
CFS-1	12.51	1.19	14.89
CFS-2	12.48	1.20	14.98
Top	12.54	1.61	20.19
Bottom	12.54	1.60	20.06
Side-1	12.52	1.60	20.03
Side-2	12.55	1.62	20.33

The tensile tests were conducted according to EN ISO 6892-1 (CEN, 2009) in a displacement control manner using a 300 kN Shimadzu testing machine. The loading protocol was applied with a displacement rate of 0.50 mm/min. To eliminate the effect of the loading/strain rate on the mechanical properties of the CFS (Huang and Young, 2014), the tensile test was halted two times; once the yield was reached, and when the ultimate strength was almost achieved. The test results of all six CFS flat coupons are presented in Table 5.5, which lists Young's modulus (E_{CFS}), yield stress ($f_{y,CFS}$), ultimate strength ($f_{u.CFS}$), ultimate strain ($\varepsilon_{u.CFS}$) and strain at fracture ($\varepsilon_{f.CFS}$). The static curve was obtained by reducing the stress values to be consistent with the levels observed during the pauses of loading illustrated in Fig. 5.6. The static curve was obtained by reducing the stress values to be consistent with the levels observed during the pauses of loading.

Table 5.5 Measured material properties of the CFS

Coupons	$E_{,CFS}$ (GPa)	$f_{y,CFS}$ (Mpa)	$f_{u,CFS}$ (Mpa)	$\varepsilon_{u,CFS}$ (%)	$\varepsilon_{f,CFS}$ (%)
CFS-1	182	410	525	15	24
CFS-2	210	415	517	12	19
Top	214	480	520	8	13
Bottom	239	480	520	5	7
Side-1	226	490	529	7	13
Side-2	235	504	536	7	7
Average	218	463	525	9	14

Figure 5.6 Stress-strain curve for CFS-2 and Top coupon specimens

5.3.2. OSB boards

Since the material properties of OSB are different in tension and compression, separate experiments were conducted to determine its tensile and compressive properties. The tests were conducted according to EN 789 (CEN, 2004). For each loading condition, three compression and tensile coupons were cut from the OSB board in three different directions, α = 0°, 45°, and 90°, as shown in Fig. 5.7.
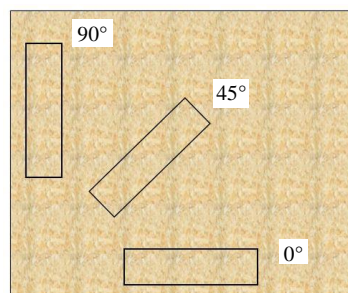
Figure 5.7 Direction of the cut made on the OSB board

5.3.2.a. Tensile coupon test

The dimensions of the 9 mm thick tensile coupons were chosen according to EN 789 (CEN, 2004), as presented in Fig. 5.8. The load was applied using a 300 kN Shimadzu universal testing machine employed in a displacement control manner with a constant axial rate of 0.25 mm/min, obeyed EN 789 (CEN, 2004). Each tensile coupon was instrumented using four 10 mm strain gauges mounted to the middle of the specimen. Table 5.6 lists the measured module of elasticity ($E_{t,OSB}$), ultimate tensile stress ($f_{t,osb}$) and its corresponding ultimate strain ($\varepsilon_{t,osb}$) for the tensile coupons. The stress-strain curves of the tensile tests for all specimens were presented in Fig. 5.9.

(a)   (b)
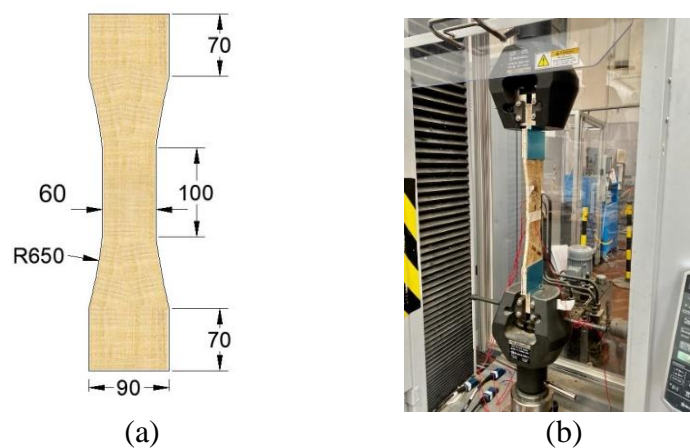
Figure 5.8 (a) OSB tensile coupons dimensions in mm and (b) test set-up

Table 5.6 Measured material properties of the OSB obtained from tensile coupon tests

Specimens	$E_{t,OSB}$ (GPa)	$f_{t,OSB}$ (Mpa)	$\varepsilon_{t,OSB}$
OSB-1$_{ten}$ (α=0)	2.1	13.1	0.009
OSB-2$_{ten}$ (α=45)	2.2	10.18	0.005
OSB-3$_{ten}$ (α=90)	2.1	11.30	0.008
Average	2.1	11.53	0.007
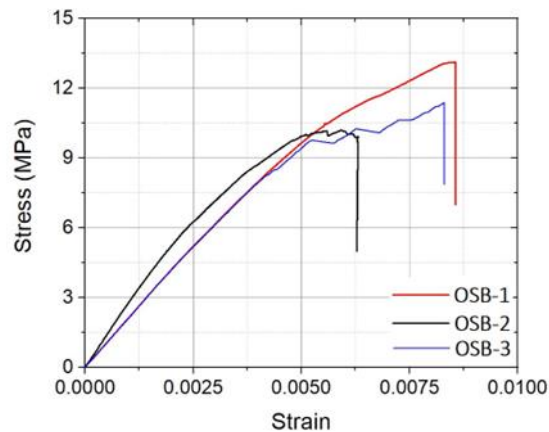
Figure 5.9 The stress-strain curves of the tensile tests for OSB board

5.3.2.b. Compression test

Compressive coupons were extracted from the 9 mm OSB in order to obtain its compressive mechanical properties in the direction parallel to the faces. Each compressive coupon consisted of five rectangular pieces of the board with the dimensions of 50 mm × 240 mm (see Fig. 5.10 (a)), in line with BS EN 789 (CEN, 2004). To form the compressive coupon, the five pieces were glued together using outdoor epoxy adhesive and subsequently, as shown in Fig. 5.10 (a). It should be noted that each coupon was cut from the OSB board in three different directions (α = 0°, 45°, and 90°).

According to EN ISO 789 (CEN, 2004), the compressive load was applied using a 300 kN Shimadzu universal testing machine in a displacement control manner. A constant displacement rate of 0.50 mm/min was applied until failure. In addition, each specimen was instrumented using four 10 mm strain gauges, as depicted in Fig. 5.10 (b).
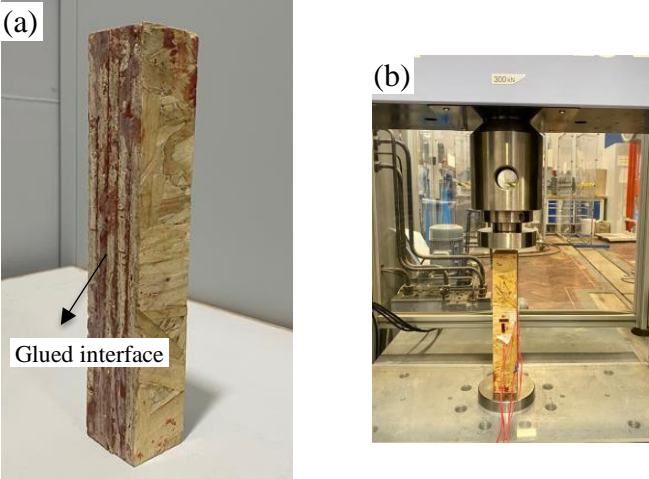
Figure 5.10 (a) OSB compressive coupons and (b) test set-up

The measured properties of the OSB material for compressive coupons are presented in Table 5.7, where $E_{c,OSB}$ represents the module of elasticity of the OSB in compression, and $f_{c,OSB}$ and $\varepsilon_{c,OSB}$ are the ultimate compressive stress and strain of the OSB material. The stress-strain curves of the compression tests for all specimens were presented in Fig. 5.11.

Table 5.7 Measured material properties of the OSB obtained from compressive coupon tests

Specimens	$E_{c,OSB}$ (GPa)	$f_{c,OSB}$ (MPa)	$\varepsilon_{c,OSB}$
OSB-1$_{com}$ (α=0)	2.3	14.4	0.009
OSB-2$_{com}$ (α=45)	2.4	13.6	0.007
OSB-3$_{com}$ (α=90)	2.3	14.5	0.006
Average	2.3	14.17	0.007
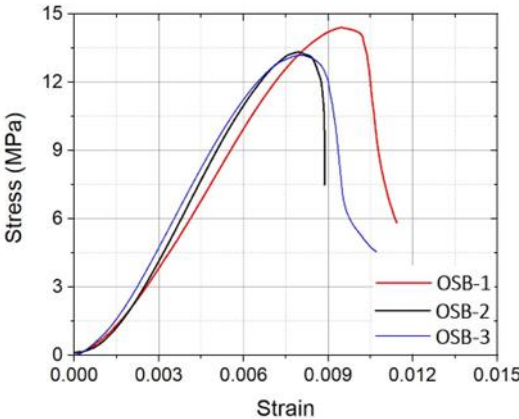
Figure 5.11 The stress-strain curves of the compression tests for OSB boards

5.4. Rotational tests

It was shown in the literature that the capacity and failure mode of the sheathed CFS stud wall systems are mainly dependent on the behaviour of the fasteners. To obtain an insight into the behaviour and load-slip response of the CFS-to-sheathing under rotational loading, connection tests were conducted on a total of 7 small-scale board-to-CFS connection subassemblies. The summary of the parametric test matrix is presented in Table 5.8. As an instance, $K1_{Rot}$ represents the rotation test on the key specimen connections, where seven self-drilling screws with the spacing of 75 mm were used to connect the 9 mm thick OSB board on each flange of 1.2 mm CFS stud. The load was applied on the middle of the web C-stud using a 150 kN hydraulic jack employed in displacement control mode, and the loading protocol applied a displacement rate of 1 mm/min. The data acquisition system was controlled by the National Instrument LabView software, which produced data with a sampling rate of 1 Hz. The rotational tests were discussed in more detail in Chapter 6.

Table 5.8 Rotation connection test matrix

	Specimen representation	Test Code	Width × Length (mm x mm)	Number of tests
Rotation Tests	Key specimens Plywood (9 mm) OSB (18 mm) CFS (2 mm) Washer effect	$K1_{Rot}$-$K2_{Rot}$-$K3_{Rot}$ $P9_{Rot}$ $OSB18_{Rot}$ $CFS2_{Rot}$ UW_{Rot}	600×600	7

Fig. 5.12 showed the schematic view of the rotation test arrangement in which flange of the CFS section were connected to the wood-based boards. Each specimen in this test schedule basically consisted of a 600 mm CFS stud member with an OSB panel (600×600 mm^2) screwed into the flange by seven self-drilling screws. The parametric studies including various design parameters, including different wood-based boards (i.e. OSB and plywood), OSB and CFS thicknesses, and washer effect, were tested under rotation loading to identify the load-slip behaviour.
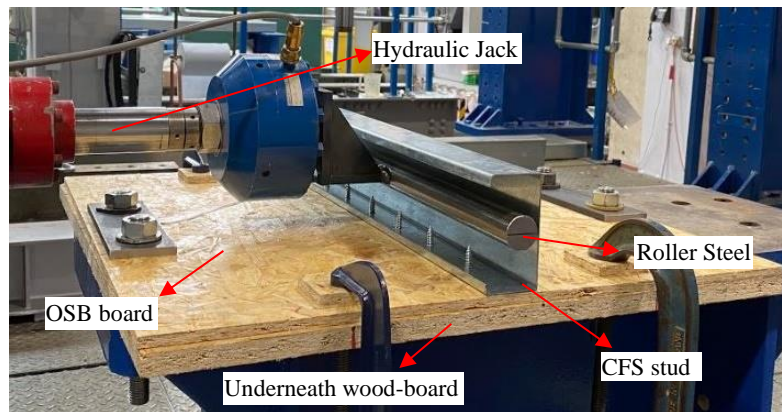
Figure 5.12 Test set-up of the rotation tests

The moment-displacement (M-Δ) responses for all specimens were presented in Fig. 5.13, where M was the moment per screw and Δ was the horizontal displacement at mid-height of the web. A summary of the ultimate moment capacity per fastener (M_u) and the web displacement at the ultimate moment (Δ_u) was reported in Table 5.9. It can be summarised that all rotation test specimens failed by the significant bend C-stud except CFS2$_{Rot}$ specimen, as shown in see Fig. 5.14 ((a) and (b)). The deformation of the system is dominated by the bending C-shape stud. It can be seen from Fig. 5.13 that increasing the CFS from 1.2 to 2 mm resulted in significantly higher stiffness and strength in connection by up to nearly double. This also showed a major effect on the failure mechanism of the system, in which pull-thought and crushing occurred at the connection point in the CFS2 specimen instead of bending the C-stud member. For this reason, it could be concluded that the thickness of CFS plays an essential role in determining the behaviour of the fastener under rotation loading. On the contrary, while increasing the OSB thickness had a negligible influence on the rotation strength and initial stiffness of the connection. The results also demonstrated that the presence of a washer in the connection can slightly decrease the load-slip response obtained from the rotation test, dropped by 2%. Furthermore, by comparing the response of plywood and OSB in the same connection configuration, it can be concluded that using plywood provides lower strength and stiffness for the connection.

Table 5.9 Main performance parameters in rotation test results

Specimen Batch	M_u (kN)	Δ_u (mm)
K1$_{Rot}$	16.78	19.95
K2$_{Rot}$	16.93	20.58
K3$_{Rot}$	17.95	19.95
P9$_{Rot}$	16.61	21.61
OSB18$_{Rot}$	18.76	19.27
CFS2$_{Rot}$	33.11	16.21
UW$_{Rot}$	16.71	21.02
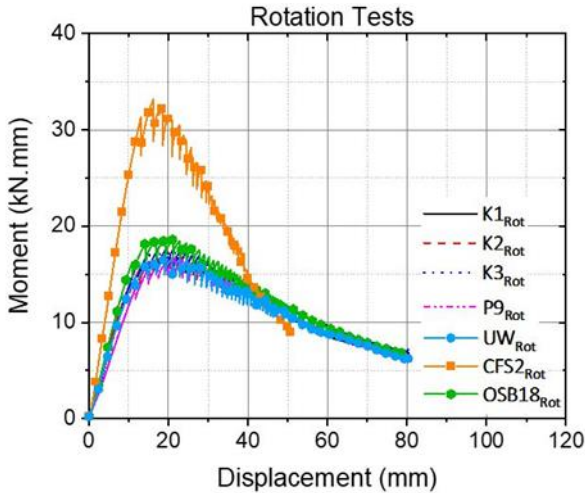
Figure 5.13 The moment-displacement (M-Δ) response of the rotation tests
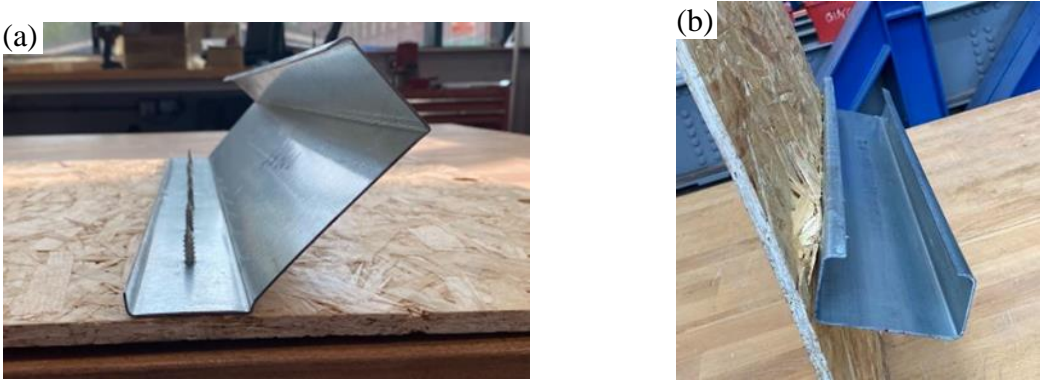
Figure 5.14 Typical failure mode of: (a) K1$_{Rot}$ and (b) CFS2$_{Rot}$ captured from the rotation tests

5.5. Initial imperfection measurements

Imperfections have an important impression on structure stability, especially on thin-walled structural members when coupled instabilities are involved (van der Neut, 1969; Becque, 2014). For this reason, the geometric imperfections of initial C-shape studs were measured using a

specially designed imperfection measuring rig, as shown in Fig. 5.15. The rig consisted of a traverse system with two electric motors in order to move a Keyence LK-G82 laser sensor in two orthogonal (X- and Y-axis) directions. The laser sensor was moved longitudinally at a speed of 5 mm/s while readings were taken at a sampling rate of 5 Hz resulting in one reading every millimetre. Based on the sensitivity assessment conducted on the frame, it was found that the accuracy of the frame is in the order of ±0.07 mm. Geometric imperfections were not measured in this chapter. Since only the test setup was changed for the face-up specimens, the results of initial imperfection measurements performed in Chapter 4 were used in herein.
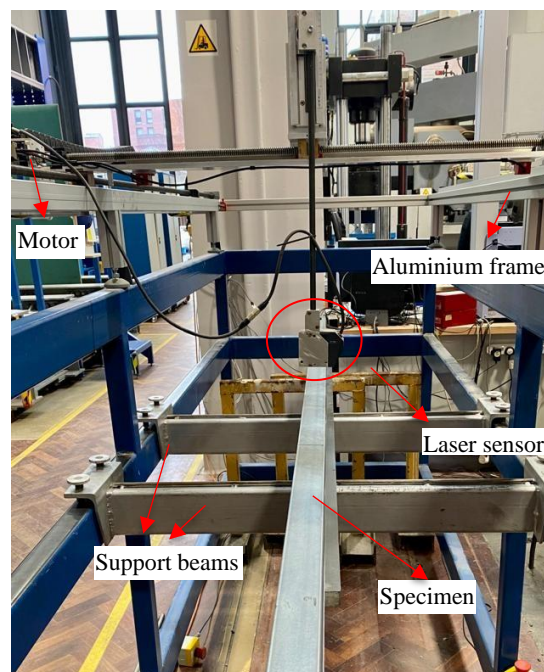
Figure 5.15 Test set-up

The imperfections were measured along seven longitudinal lines of CFS members, as shown in Fig. 5.16, where three lines were recorded on the web and two lines on both flanges. The imperfection data was further employed to determine representative magnitudes of the cross-sectional out-of-plane imperfections. To this end, the out-of-plane imperfections along the centre line of the web (δ_{web}) and the flange edge (δ_{flange}) were measured relative to their corners. While the readings along lines 1, 2, 6 and 7 were used to identify the distortional imperfections, lines 3, 4 and 5 provided information about the imperfections in overall flexural buckling and local buckling of the web. The distortional imperfection was calculated by subtracting reading

along lines 1 to 2, 6 to 7, while the local imperfection was calculated by subtracting the average reading along lines 3 and 5 from the readings taken along line 4 (see *Eq.1, Eq.2 and Eq.3*).
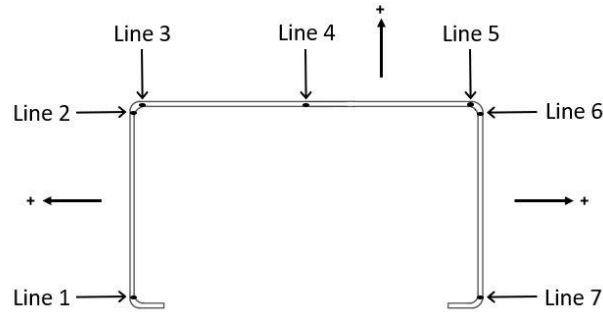
Figure 5.16 Location lines of the C-shape imperfection measurements

$$\text{Local} = \delta_{web}(x) = \text{Line 4} - \left(\frac{\text{Line 3} - \text{Line 5}}{2}\right) \qquad (5.1)$$

$$\textit{Distortional-1} = \delta \textit{ flange } (x) = \textit{Line 1} - \textit{Line 2}$$

$$\textit{Average } \delta \textit{ flange } (x) = 0 \qquad (5.2)$$

$$\textit{Distortional-2} = \delta \textit{ flange } (x) = \textit{Line 7} - \textit{Line 6}$$

$$\textit{Average } \delta \textit{ flange } (x) = 0 \qquad (5.3)$$

The maximum amplitudes of the recorded local and distortional imperfections in the six initial C-shaped elements are provided in Table 5.10. The results indicate that the maximum out-of-plane imperfections encountered in the flange of the C-lipped channels exhibited imperfections of up to 0.36 mm, while the webs of the channels were of the order of 0.81 mm (see Table 5.10). Fig. 5.17 presents the result of the recorded imperfections in the lipped channel members.

Table 5.10 Maximum amplitudes of local, distortional-1 and distortional-2 (in mm)

Specimen	Local	Distortional-1	Distortional-2
C1	0.35	0.07	0.17
C2	0.58	0.14	0.22
C3	0.34	0.11	0.24
C4	0.49	0.17	0.36
C5	0.81	0.26	0.13
C6	0.36	0.22	0.21
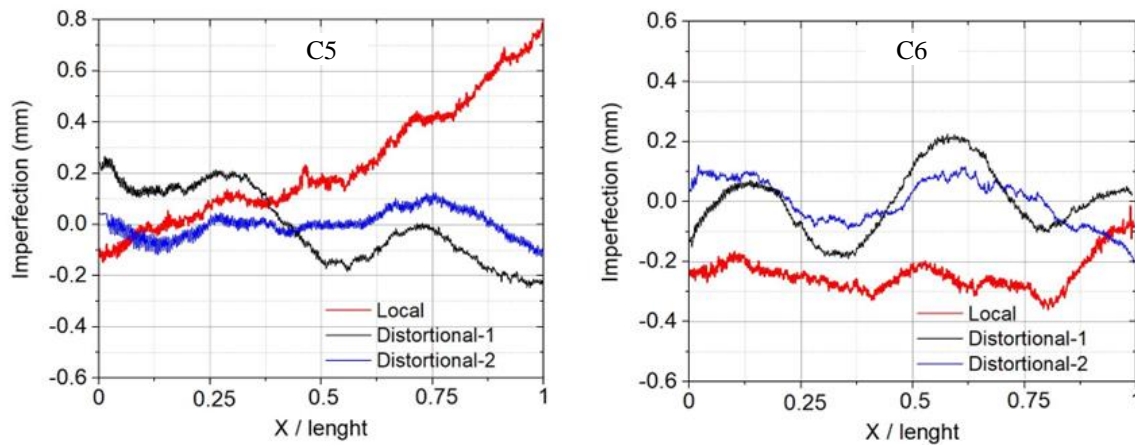
***Figure 5.17** Typical recorded imperfections for two different CFS lipped channel members*

5.6. Four-point bending test set-up

CFS sheathed wall panel specimens were tested under a specially designed four-point bending loading protocol to obtain their out-of-plane bending behaviour. All specimens were lied down in a way that the loading was applied directly to the board of the wall panels. Indeed, the wood-based board was pushed down using four wood-blocks (450 mm × 200 mm) to transfer the load from the hydraulic jack; rather than pushing on the free flange of the CFS stud members. The stud wall systems tested considering the more vulnerable condition and the test set-up is as illustrated in Fig. 5.18. Four woodblocks were used to transfer the load from the 150-kN hydraulic jack through-loading plates to two loading tubes running across the width of the wood-based board. The distance between the two intermediate loading points was fixed as equal to 746.67 mm, which was one-third of the total span, with a 100 mm overhanging from each support point (see Fig. 5.19). The data acquisition system was controlled by the National Instrument LabView software, which produced data with a sampling rate of 1 Hz. The loading protocol applied a displacement rate of 2 mm/min. To provide interpretation of the results, the CFS studs were denoted by "B" and "F" for the boundary elements and "C" for the middle one.
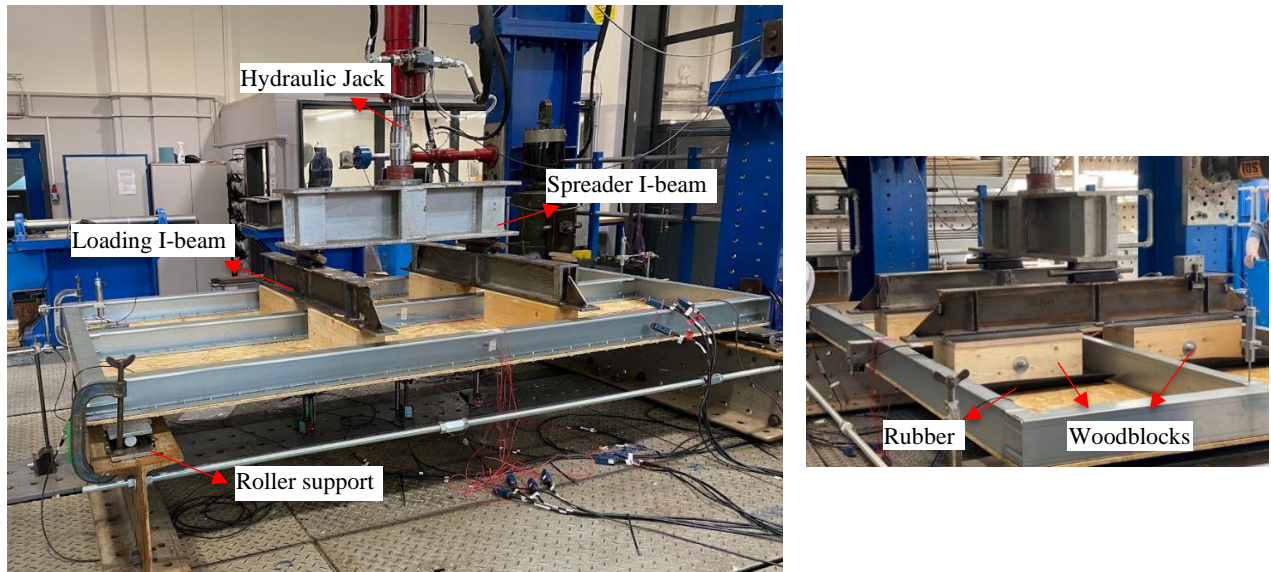
Figure 5.18 (a) Test set-up for face-down specimens, (b) woodblocks
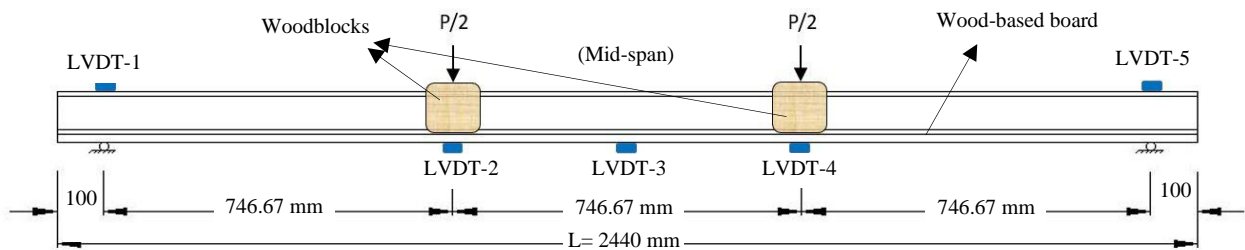
Figure 5.19 Employed instrumentation for 4-point bending test

In general, all the elements of the test setup from the face-up test setup were also used in this face-down set-up. Strain gauges were attached to the board and CFS sections at the mid-span of the shear wall panel, as shown in Fig. 5.20. It should be noted that these strain gauge readings were employed to determine the position of the neutral axis within the CFS elements. To determine the rotation of each CFS stud where one of their flanges was restrained by the wood-based board, an inclinometer was installed to the CFS web at the mid-span of the system (see Fig. 5.20). An extra two inclinometers were also mounted to each loading tube in order to measure the longitudinal rotation of the stud wall system, as illustrated in Fig. 5.21. To measure out-of-plane deformations of the wall panels, five LVDTs were installed on top of the supports and along the length of the mid-stud bottom flange at the locations of mid-span and loading points (see Figs. 5.19 and 5.22). In addition, the end-slip between the CFS tracks and wood-

based board at the four corners of the specimens was measured using other four LVDTs readings placed horizontally at four corners of the wall panel (End-slip 1, End-slip 2, End-slip 3 and End-slip 4), as shown in Fig. 5.23.
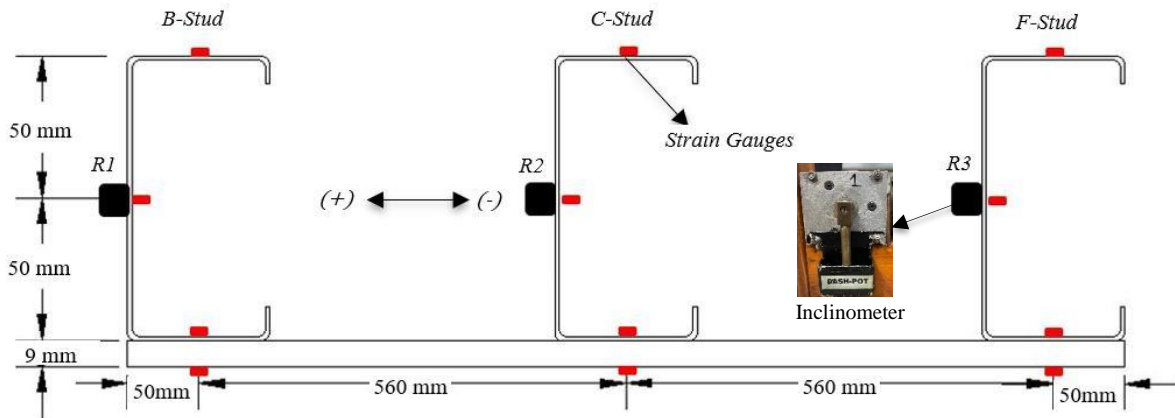
Figure 5.20 Positions of inclinometers and strain gauges in the midspan of the panel
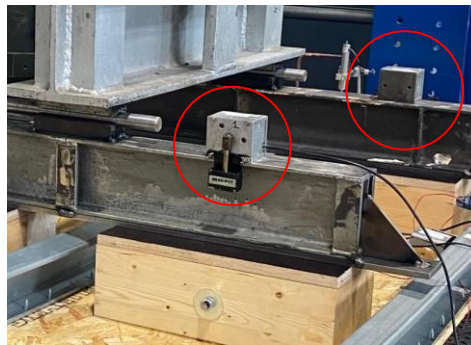
Figure 5.21 Position of inclinometers on the loading tubes
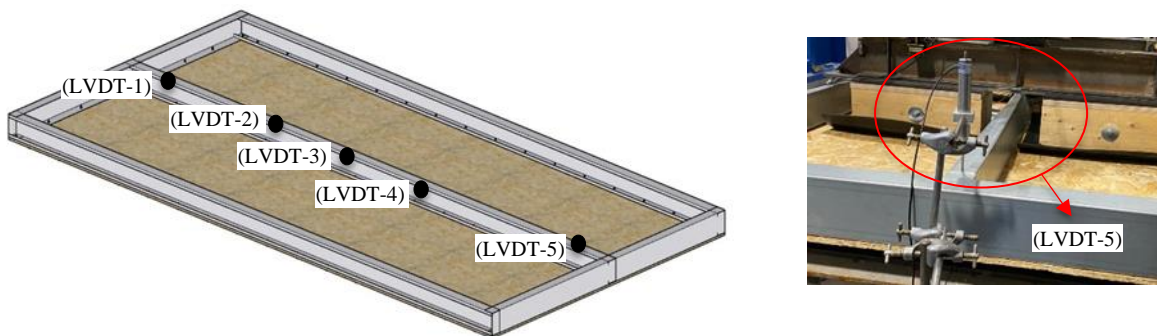
Figure 5.22 Positions of five LVDTs at mid-stud of the system
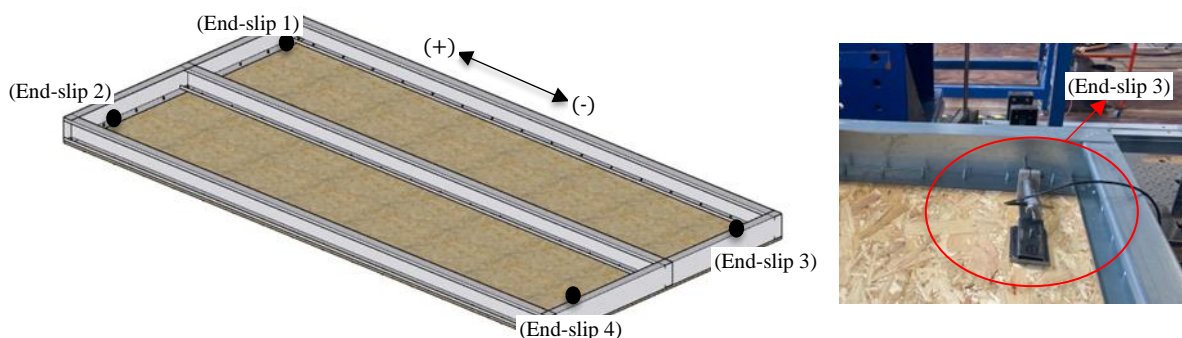
Figure 5.23 Positions of four LVDTs for end-slip measurement

5.7. Four-Point test results

A summary of the main structural performance parameters obtained from four-point bending tests on the face-down CFS stud wall panels was listed in Table 5.11, including maximum out-of-plane load capacities and their corresponding displacements, ultimate displacements at which the out-of-plane capacity of the wall was dropped by 20% and the dominant failure modes. In addition, Tables 5.12 and 5.13 reported a series of complementary results consisting of the values of end-slip measured at four corners of the wall in the longitudinal direction and the rotation of the studs for each tested specimen, respectively.

Table 5.11 Main structural performance parameters and failure mode for each specimen

Specimens	Maximum load capacity (kN)	Displacement at peak load (mm)	Ultimate displacement (mm)	Out-of-plane stiffness (kN/mm)	Failure modes
K3	15.5	36.9	47.9	0.7	Lateral torsional buckling-wood crushing
K4	13.5	52.9	56.2	0.6	Lateral torsional buckling-wood crushing
K5	14.2	58.6	62.8	0.6	Lateral torsional buckling-wood crushing
P9-2	14.2	51.6	53.9	0.6	Lateral torsional buckling-wood tilting/bearing
OSB18-2	16.6	35.4	43.5	0.8	Lateral torsional buckling
CFS2-2	23.9	26.0	33.4	1.0	Wood crushing
DR2	12.1	39.4	43.4	0.6	Lateral torsional buckling-wood crushing
S2	14.1	55.8	58.6	0.8	Lateral torsional buckling-wood crushing
N2	15.7	49.0	52.9	1.0	Lateral torsional buckling-wood crushing
PT2	15.6	32.5	58.8	0.6	Lateral torsional buckling-wood crushing

Table 5.12 End-slip readings measured in the longitudinal direction at four corners of each tested specimen (in mm)

Specimens	At Peak Load				At Ultimate Displacement			
	End-slip 1	End-slip 2	End-slip 3	End-slip 4	End-slip 1	End-slip 2	End-slip 3	End-slip 4
K3	2.57	1.44	1.97	2.53	2.66	1.44	2.06	2.55
K4	2.27	1.55	1.86	1.88	2.57	1.67	2.19	2.06
K5	2.46	2.17	3.37	2.38	2.52	2.18	3.39	2.39
P9-2	2.19	2.15	2.80	2.24	2.20	2.16	2.84	2.26
OSB18-2	1.30	1.65	1.50	1.65	1.31	1.67	1.52	1.68
CFS2-2	2.62	2.38	3.28	2.45	2.64	2.45	3.30	2.76
DR2	1.30	1.11	1.08	1.13	1.35	1.11	1.14	1.13
S2	2.35	1.77	2.05	2.01	2.35	1.77	2.05	2.01
N2	2.13	1.75	2.12	2.43	2.13	1.75	2.12	2.43

Table 5.13 Measured rotation at the three studs of each tested specimen (in Deg$^\bullet$)

Specimens	At Peak Load			At Ultimate Displacement		
	R1 (Deg°)	R2 (Deg°)	R3 (Deg°)	R1 (Deg°)	R2 (Deg°)	R3 (Deg°)
K3	-11.31	-	-	-11.75	-	-
K4	-12.08	-12.22	-23.12	-12.33	-20.09	-23.13
K5	-11.75	-21.92	-18.80	-13.34	-21.93	-21.02
P9-2	-19.41	-14.79	-13.84	-29.15	-21.60	-14.04
OSB18-2	-22.16	-20.95	-13.61	-22.80	-22.29	-13.82
CFS2-2	-9.57	-4.73	-16.66	-13.54	-11.84	-19.72
DR2	-8.51	-19.48	-12.13	-23.90	-20.51	-12.15
S2	-12.31	-15.65	-12.28	-16.90	-22.92	-12.47
N2	-1.21	-0.85	-1.63	-1.37	-1.82	-3.02
PT2	-1.84	-16.73	-10.09	-2.16	-18.81	-11.17

*Some data was not recorded due to the sudden drop of the inclinometers

5.7.1. Key specimens (benchmark specimens)

Fig. 5.24 illustrates the load versus vertical displacement measured at the centre of the wall (LVDT-3) for the key specimens (K3, K4 and K5). The maximum load capacity reached 15.5, 13.5 and 14.2 kN, and the out-of-plane deflection of the wall centre point at the peak load recorded 36.9, 52.9 and 58.6 mm, respectively. The reason why two peaks were seen in each load-displacement response was due to the buckling of the studs in order, mid-stud than B- or F-studs. As expected, the K3, K4 and K5 key specimens exhibited remarkably similar failure mechanism. At the maximum capacity of the specimens, the lateral distortional buckling of the top flange, and by further increasing the load again a distortional buckling started to happen in the top flanges of the F-stud for K3 specimens, as shown in Fig. 5.25. In addition, the OSB material was damaged mainly at the loading point of the wall where the board experienced pressure due to loading. However, the lateral distortional buckling of the top flange occurred the K4 and K5 specimens before reached to the maximum load capacity. The results of strain

gauges versus the applied load were reported in Fig. 5.26 for the key specimen K3. It can be illustrated that the strains developed in the studs and the OSB board were in good agreement before the initiation of the buckling at a load of approximately 15 kN. Besides, while almost similar stresses were developed at locations of the strain gauges attached to the boundary CFS studs (i.e. B- and F-studs), the strain gauges attached to the OSB showed different stress behaviour. This implies that the out-of-plane bending behaviour of the system was unsymmetric. This was confirmed by extracting the results of inclinometers mounted on the loading tubes, in which the stud wall system was found rotated towards the F-stud in the order of 3 degrees. Also, it was noticed that the B-stud of all key specimens did not face any buckle during test time due to this rotation. Based on the results, the behaviour of the CFS stud walls was discussed in the following sub-sections by considering various design variables.
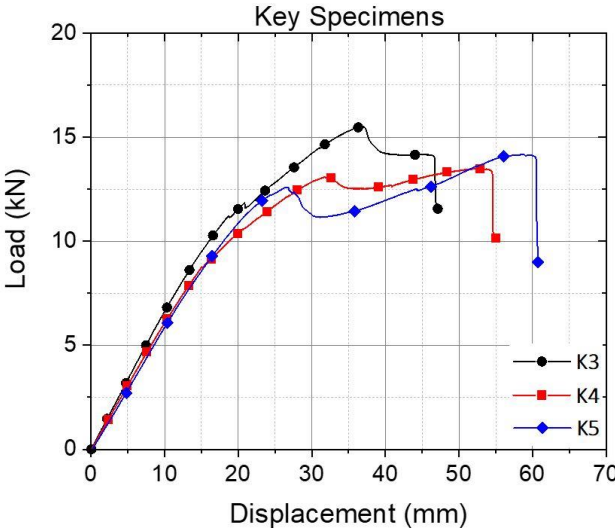
Figure 5.24 Load-displacement responses of key specimens

Figure 5.25 Failure modes of: (a) K3 and (b) K5 specimens
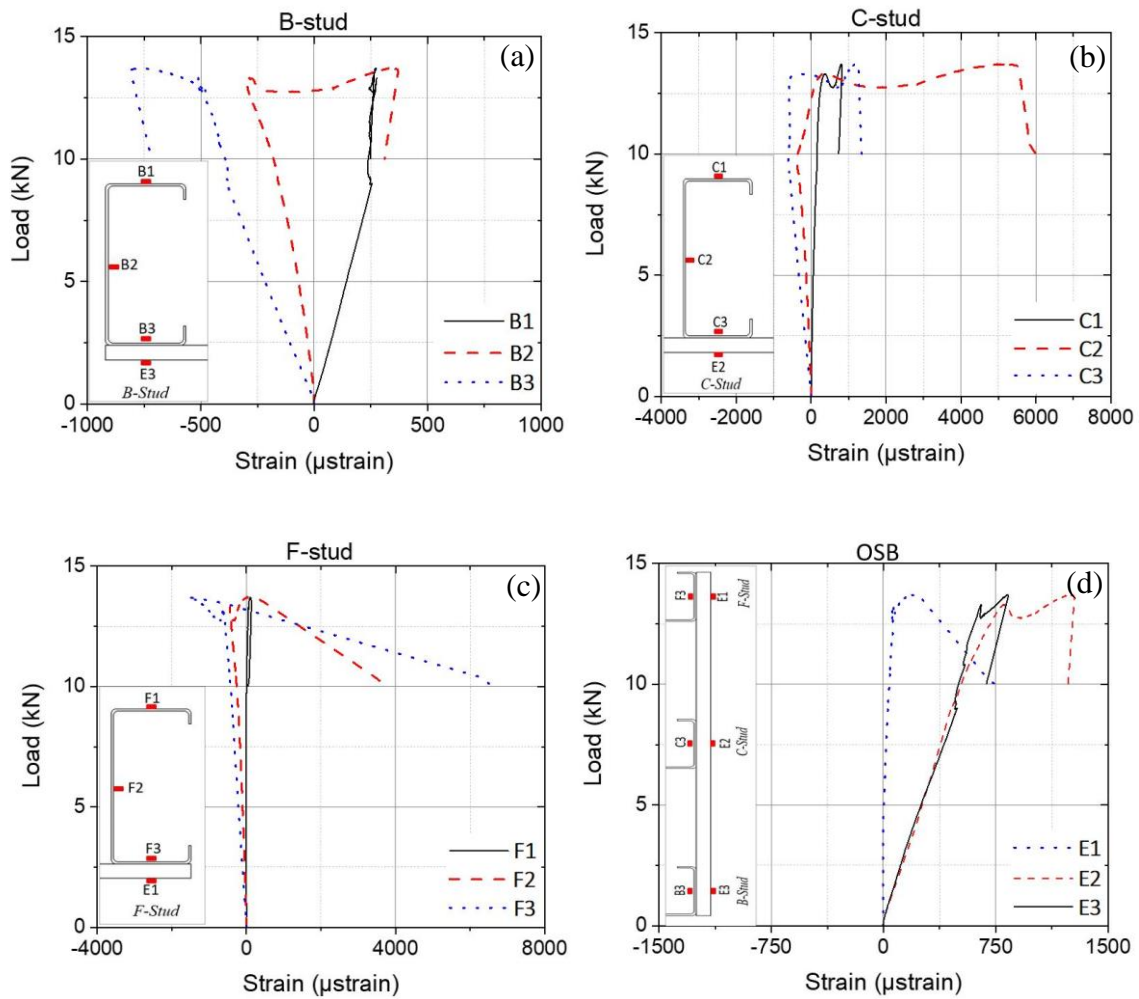
Figure 5.26 Load-strain curve for (a) B-stud, (b) C-stud, (c) F-stud and (d) OSB of K3 specimens

5.7.2. Materials and thicknesses

As shown in Fig. 5.27, in general increasing the thickness of the material (i.e. CFS and OSB) could significantly improve the out-of-plane performance of the stud wall panels. It was obviously showed that the out-of-plane strength of the stud wall was increased from 15.5 kN to 16.6 kN by doubling the thickness of the board. This also showed different effect on the failure mechanism of the system, in which the failure of the OSB board was prevented under out-of-plane loading. Also, the lateral distortional buckling of the top flange started to happen in the middle stud and B-stud at the maximum load capacity (Fig. 5.28 (a)). Interestingly, thickening of CFS elements from 1.2 mm to 2 mm was found to be more beneficial in improving the out-of-plane performance than using a thicker OSB board as like face-up specimens. The out-of-plane strength and stiffness of the stud wall with thicker CFS elements were enhanced compared

to the key specimen (K3) by 54% and 43%, respectively, which is attributed to preventing the lateral distortional buckling in the studs of the system (see Figs. 28 (b) and (c)). The CFS frame system of the CFS2-2 specimen did not face any buckle, while the OSB panel get damage mainly at the loading point of the wall. The test stopped due to the loading I-beam touch the top flange of the studs. Using plywood boards with the same thickness (i.e. 9 mm) resulted in a less ductile behaviour before the peak capacity compared to the OSB material, while it causes a negligible change in the out-of-plane strength and stiffness of the system, as shown in Fig. 5.25. However, the wood crushing was not observed in the plywood board (Fig. 5.28 (d)). The end-slips readings were shown in Fig. 5.29 for K3 and OSB18-2 stud walls. It can be concluded that increasing thickness of the OSB materials can significantly decrease the end-slips of the stud wall system and consequently decreased the torsional flexibility of the wall. However, the thickness of the OSB material and plywood has a negligible influence on the rotation of studs, while CFS thickness has slight decrease on the rotation (see Fig. 5.30). The results of strain gauges versus the applied load were reported in Figs. 5.31, 5.32 and 5.33 for the OSB18-2, CFS2-2 and P9-2 specimens, respectively. In general, it can be concluded that the strains developed in the studs and the OSB board were in good agreement before the initiation of the buckling at a load point.
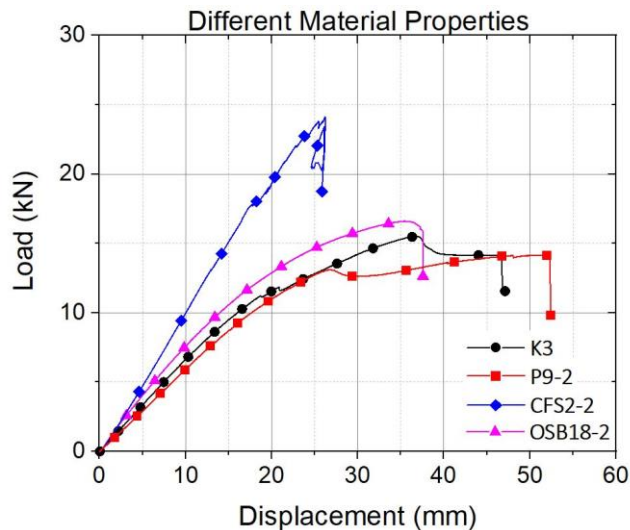
Figure 5.27 Load-displacement responses of stud walls with different material properties
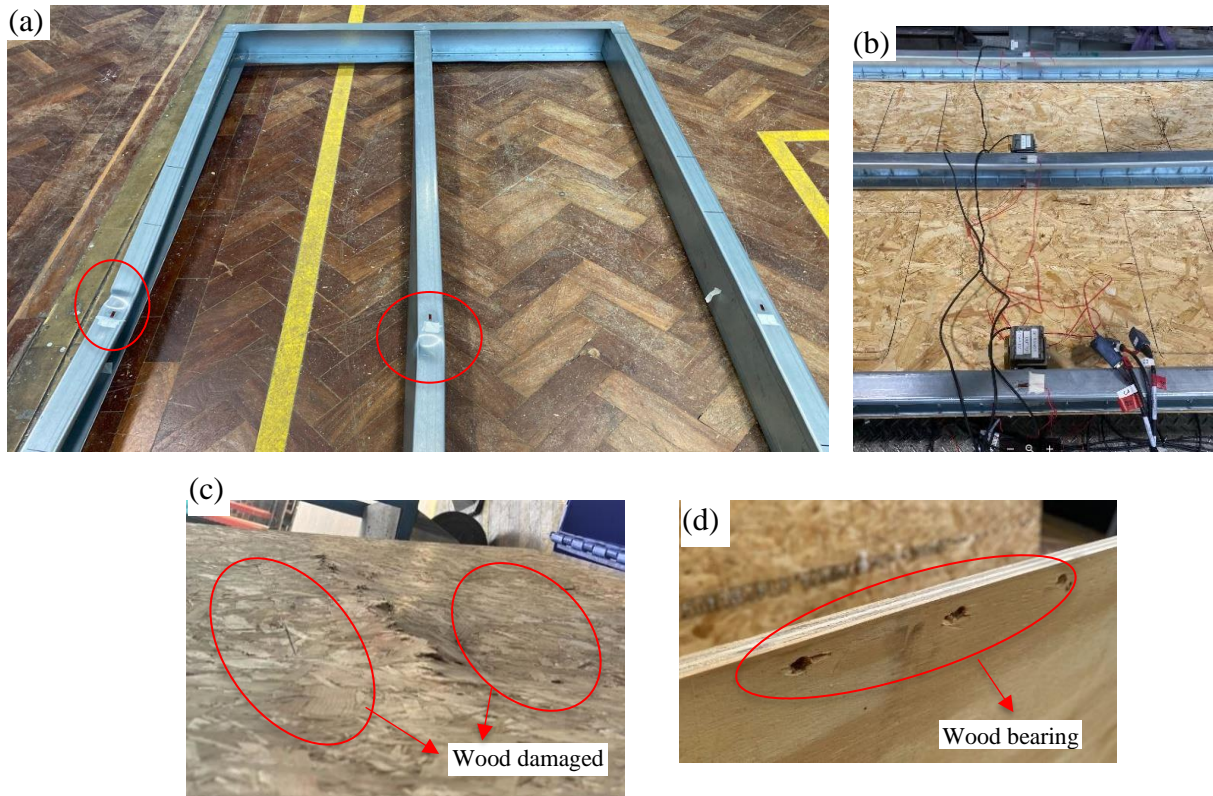
Figure 5.28 Failure modes of (a) OSB18-2, (b), (c) CFS2-2 and (d) P9-2 specimens
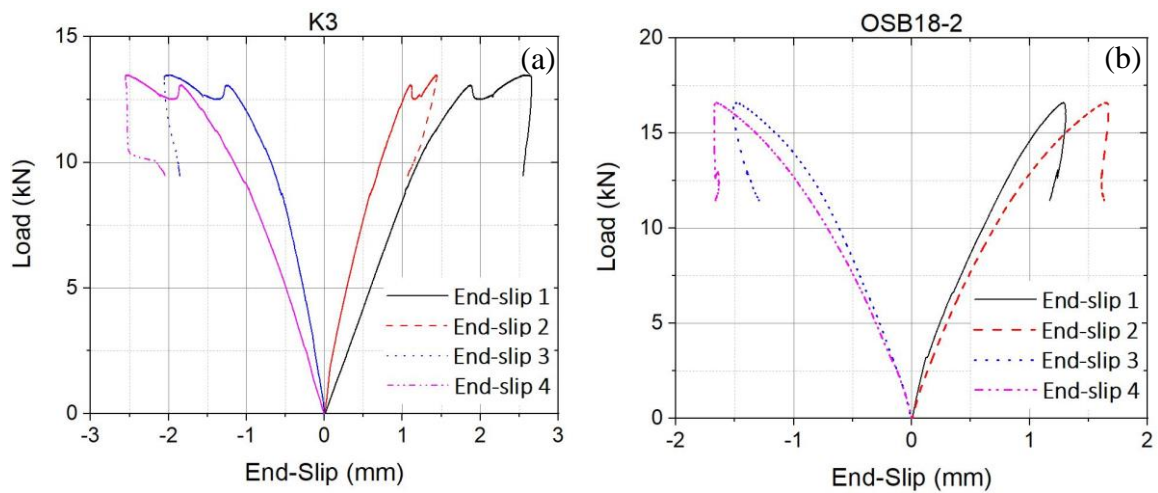
Figure 5.29 End-slip measurement histories of: (a) K3 and (b) OSB18-2 specimens
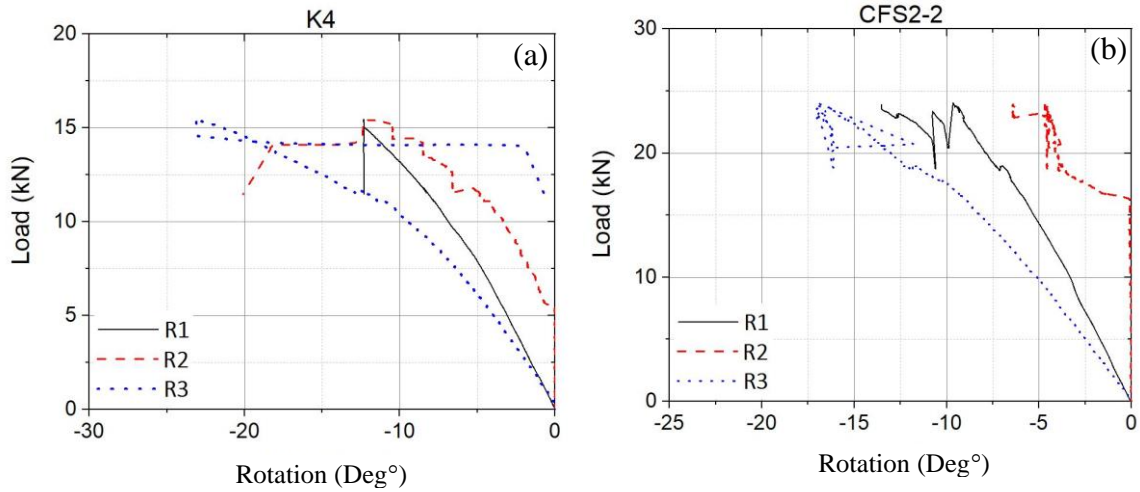
Figure 5.30 Rotation of studs along their major axis for: (a) K4 and (b) CFS2-2 specimens

Figure 5.31 Load-strain curve for (a) B-stud, (b) C-stud, (c) F-stud and (d) OSB of OSB18-2 specimen

Figure 5.32 Load-strain curve for (a) B-stud, (b) C-stud, (c) F-stud and (d) OSB of CFS2-2 specimen

Figure 5.33 Load-strain curve for (a) B-stud, (b) C-stud, (c) F-stud and (d) Plywood of P9-2 specimen

5.7.3. Drift ratio (centre spacing)

Fig. 5.34 compares the load-displacement responses of the key specimen with the different the drift ratio of the system. By comparing out-of-plane load-displacement responses of drift ratio specimen (DR2) with the single sheathed key specimen (K3), it was revealed that reducing the drift ratio resulted in a significant reduction in out-of-plane strength of the system dropped by 22%. However, the load-displacement responses of the stud walls after the peak load showed that reducing centre spacing resulted in more brittle behaviour. The ductility of the system was considerably reduced compared to key specimen (K3). The results also demonstrated that the initial stiffness of the stud wall remained almost constant by decreasing the centre spacing (drift ratio) from 610 to 305 mm compared to key specimens (see Fig. 5.34). As illustrated in Fig. 5.35, the failure mechanism of the stud wall system with reduced drift ratio was found almost

similar, where the lateral distortional buckling of the top flange started to in the middle stud, and by further increasing the load again a distortional buckling started to happen in the top flanges of the F-stud. The results of strain gauges versus the applied load were reported in Fig. 5.36 for the DR2 specimens. In general, it could be concluded that the strains developed in the studs and the OSB board at the same locations were in good agreement before the initiation of the buckling at a load of maximum loading.
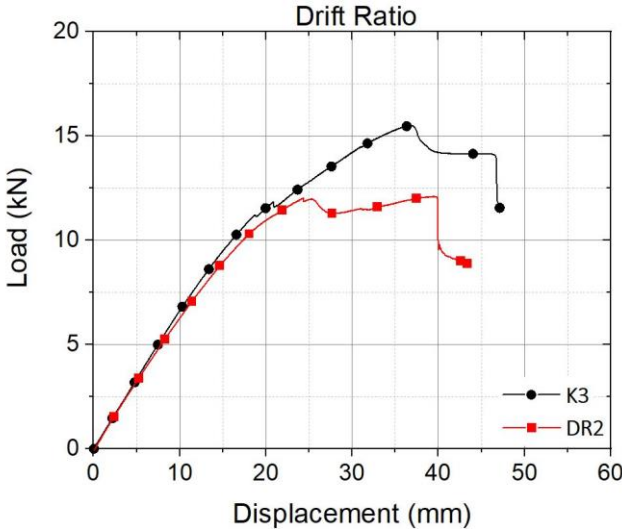
Figure 5.34 Load-displacement responses of stud walls with different drift ratio

Figure 5.35 Failure modes of DR2 specimen
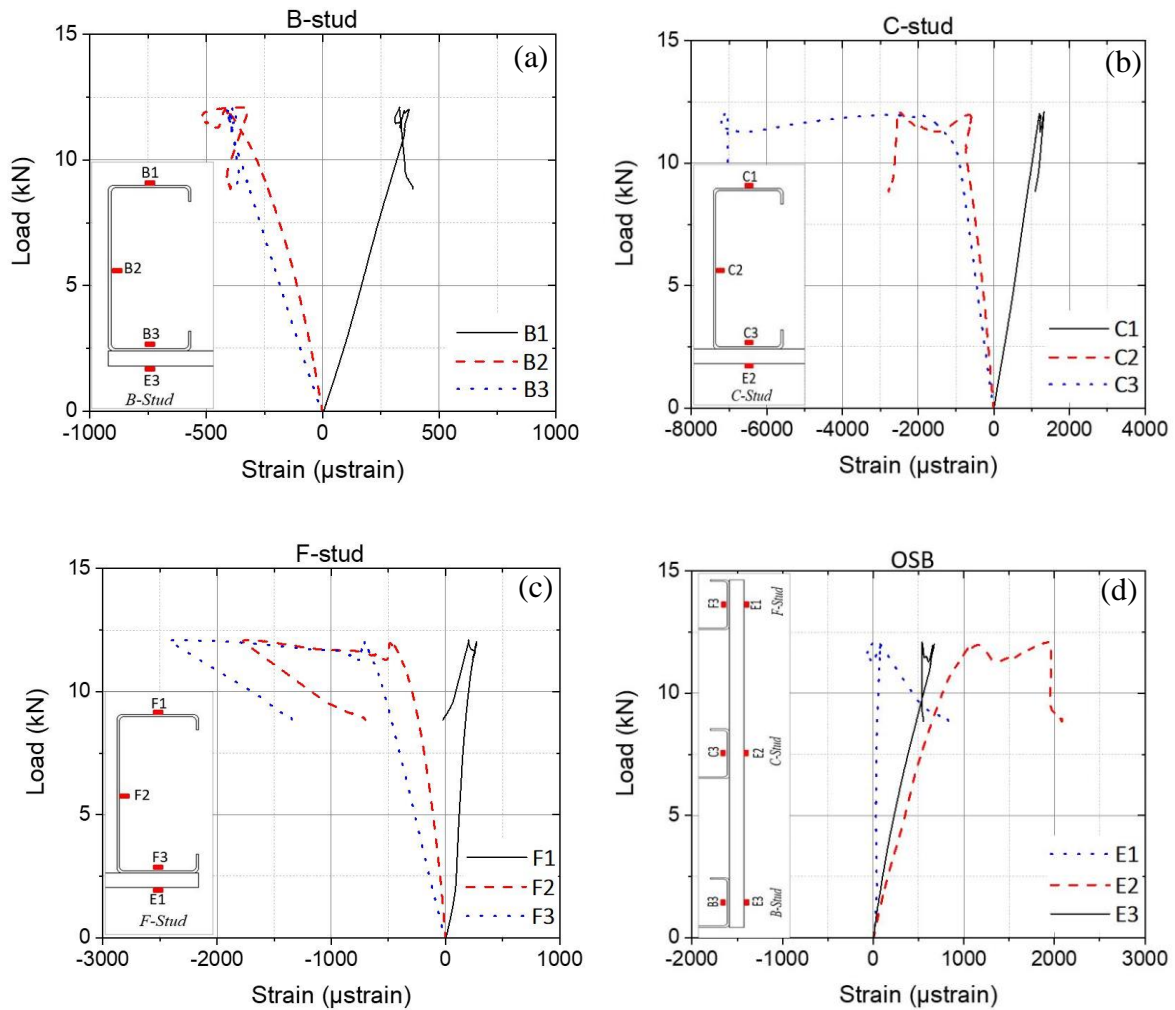
Figure 5.36 Load-strain curve for (a) B-stud, (b) C-stud, (c) F-stud and (d) OSB of DR2 specimen

5.7.4. Main/auxiliary components

Fig. 5.37 compared the responses of the key specimen K3 with the same specimens however in the absence/presence of main/auxiliary components of the system. It was observed that the presence of the nogging (N2) and the absence of the pinned track (PT2) have a negligible effect on the out-of-plane strength of the stud wall panels. On the contrary, using seam elements (S2) in the CFS stud wall dropped the strength of the system by 9%. Furthermore, while incorporating either noggings or seam provided notably enhancements in the initial out-of-plane stiffness of the system by 42% and 14%, respectively, the absence of the pinned track led to a 14% reduction the initial out-of-plane stiffness of the stud wall (see Fig. 5.37). By comparing the failure mechanism of the S2 and N2 stud wall specimens with that of the key specimen (K3), it can be concluded that the existence of the seam and nogging elements has no effect on

the dominant failure mode as shown in Fig. 5.38 (a-c). However, the PT2 specimen was occurred the lateral distortional buckling of the top flange interaction with local buckling started to happen in the web of the middle studs but by further increasing the load again not started to happen in the top flanges of in the F-stud or B-stud (see Fig. 5.38 (d)). Based on the readings of stud rotations, while noggin elements exhibited a considerable effect in reducing the rotation of studs (see Fig. 5.39 (a) and (b)), the presence of the seam and the absence of the pinned track has slightly the rotational flexibility of studs (see Fig. 5.39 (c) and (d)). It should be noted that the end-slip measurements of the stud-wall showed that the presence/absence of the main/auxiliary components has negligible effects on the out-of-plane torsional behaviour of the system (see Fig. 5.40). The results of strain gauges versus the applied load were reported in Figs. 5.41-5.43 for the S2, N2 and PT2 specimens, respectively.
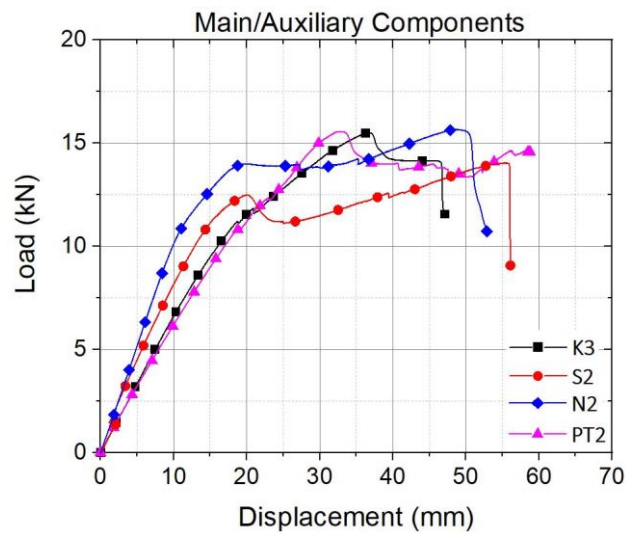
Figure 5.37 Load-displacement responses of CFS stud walls considering the effects of main/auxiliary components
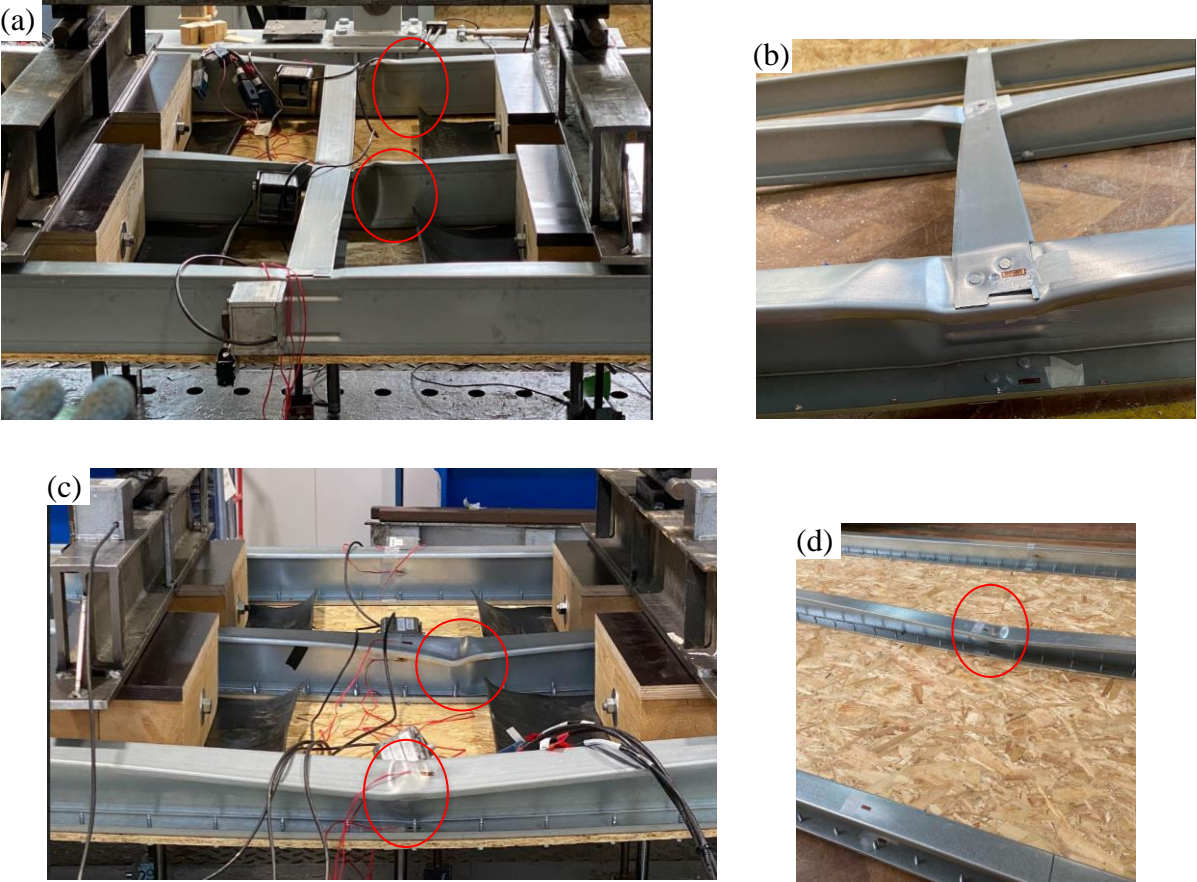
Figure 5.38 Failure modes of (a), (b) N2, (c) S2 and (d) PT2 specimens
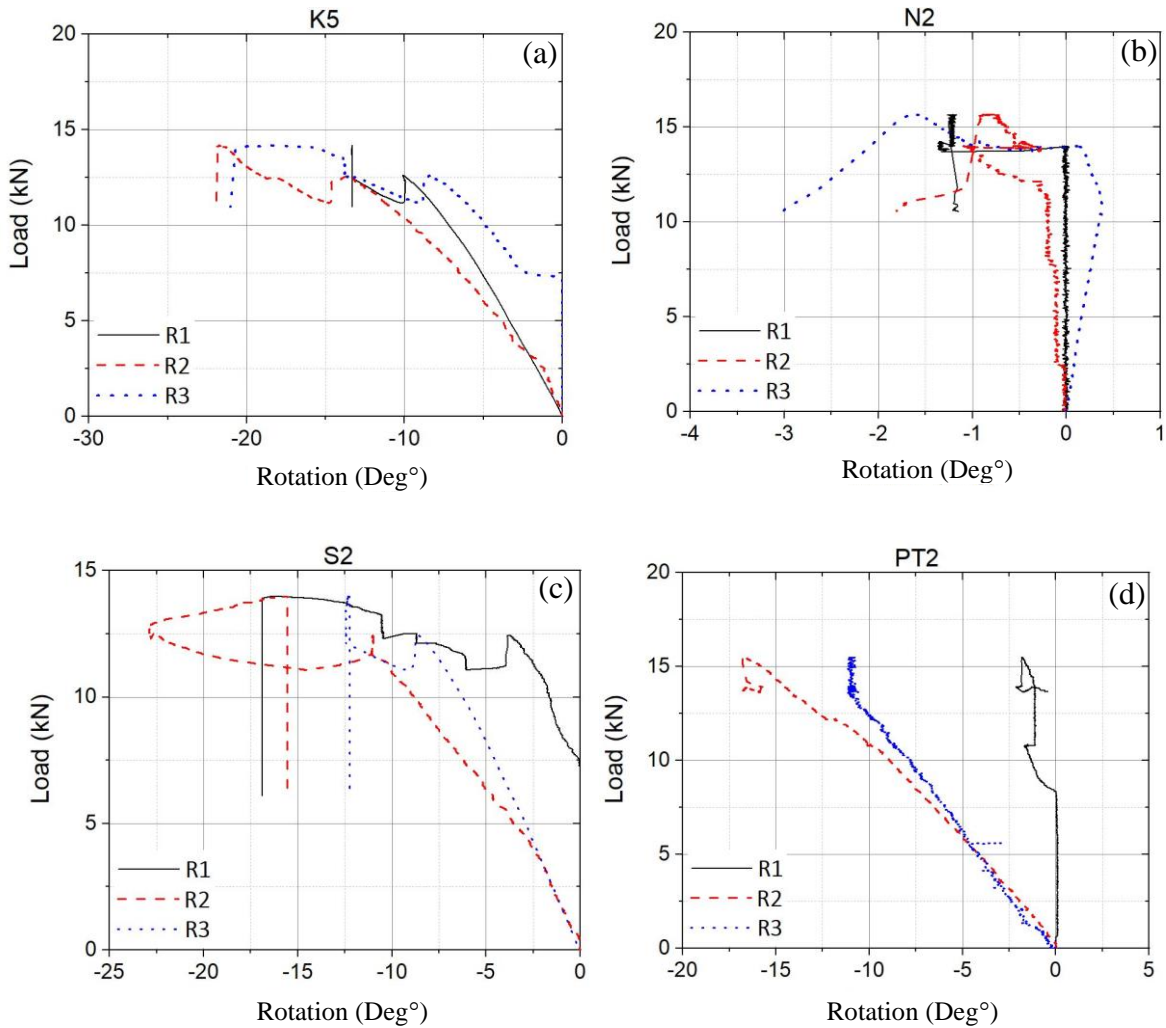
Figure 5.39 Rotation of studs along their major axis for: (a) K5, (b) N2, (c) S2 and (d) PT2 specimen
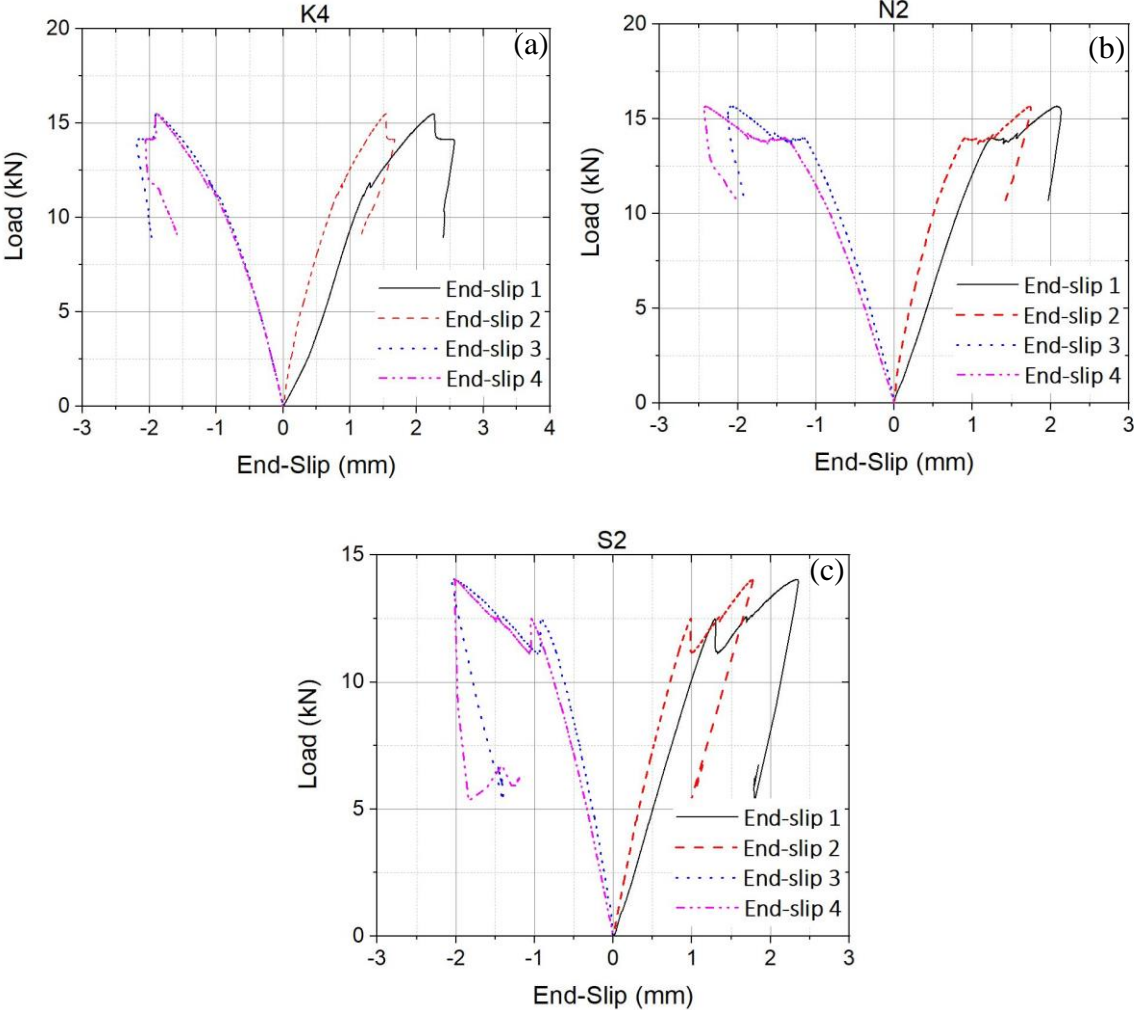
Figure 5.40 End-slip measurement histories of: (a) K4, (b) N2 and (c) S2 specimen
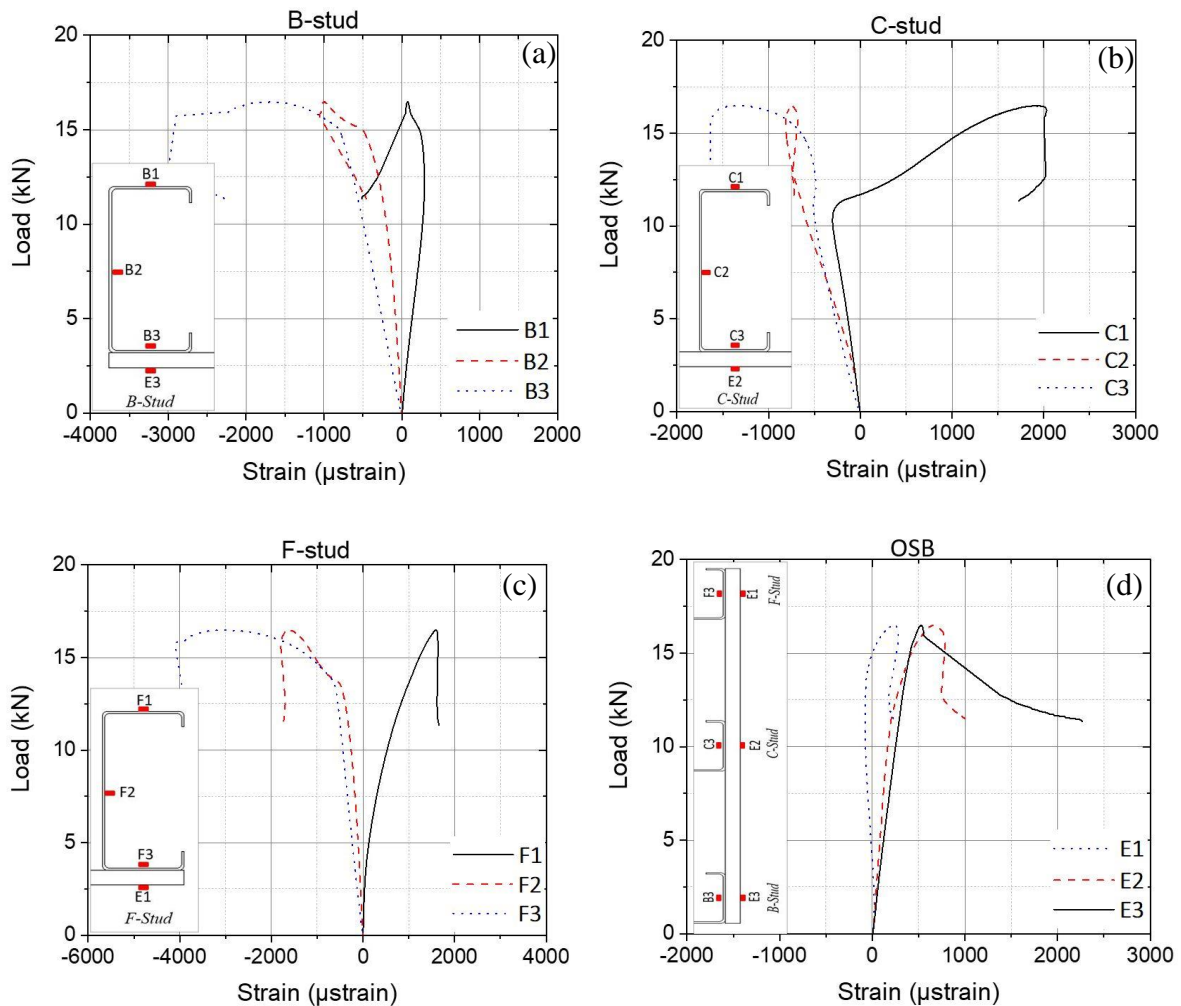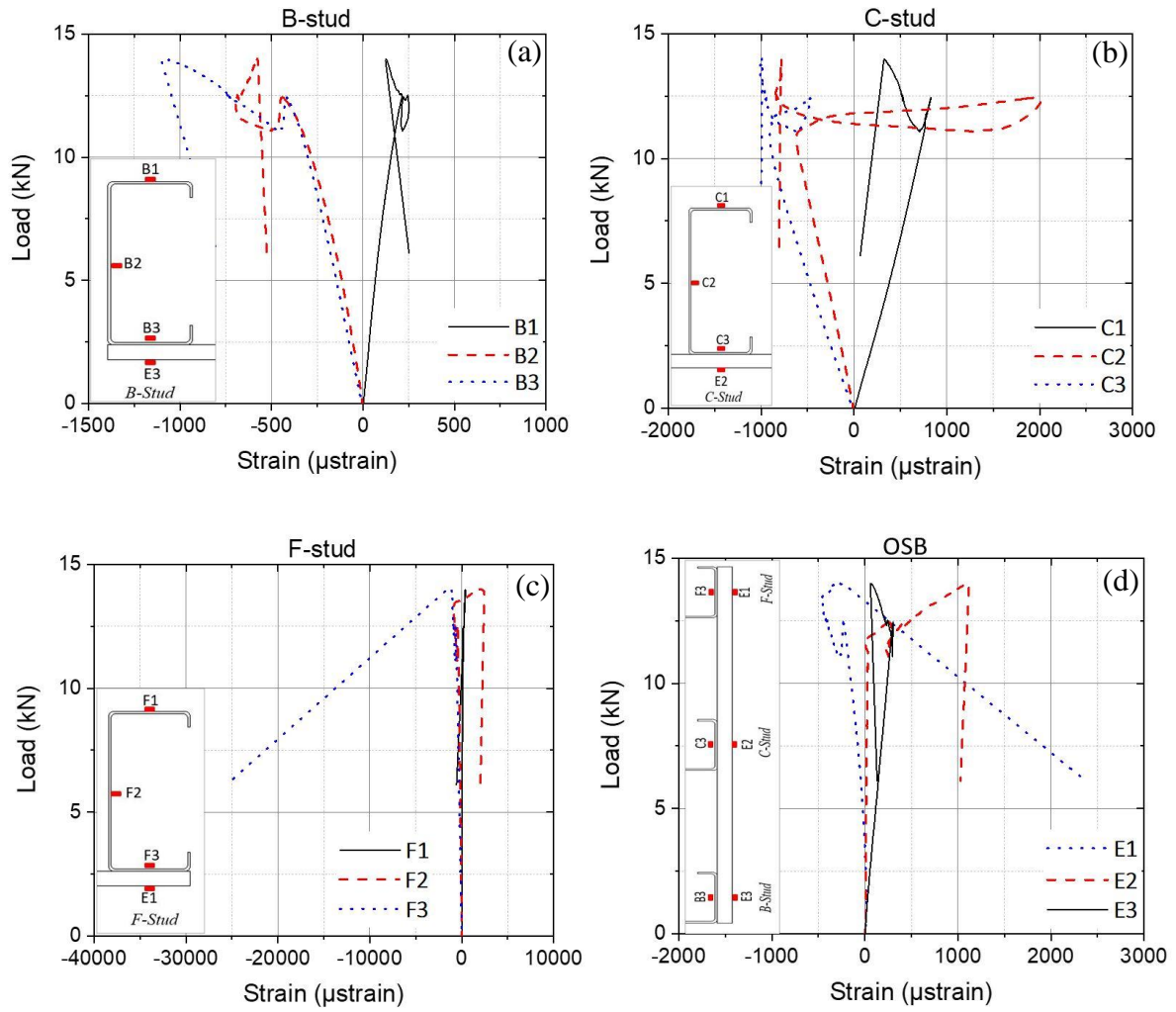
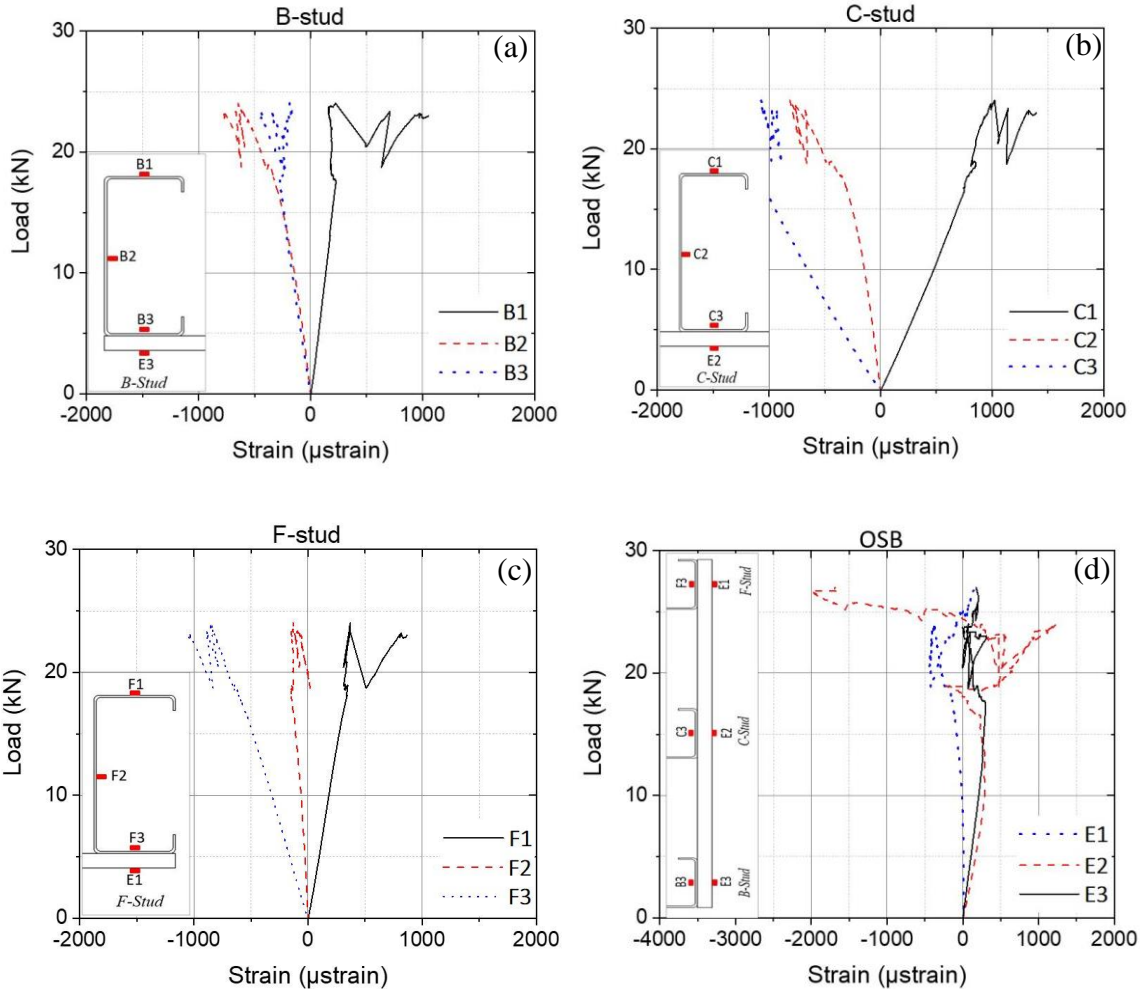***Figure 5.41 Load-strain curve for (a) B-stud, (b) C-stud, (c) F-stud and (d) OSB of S2 specimen***

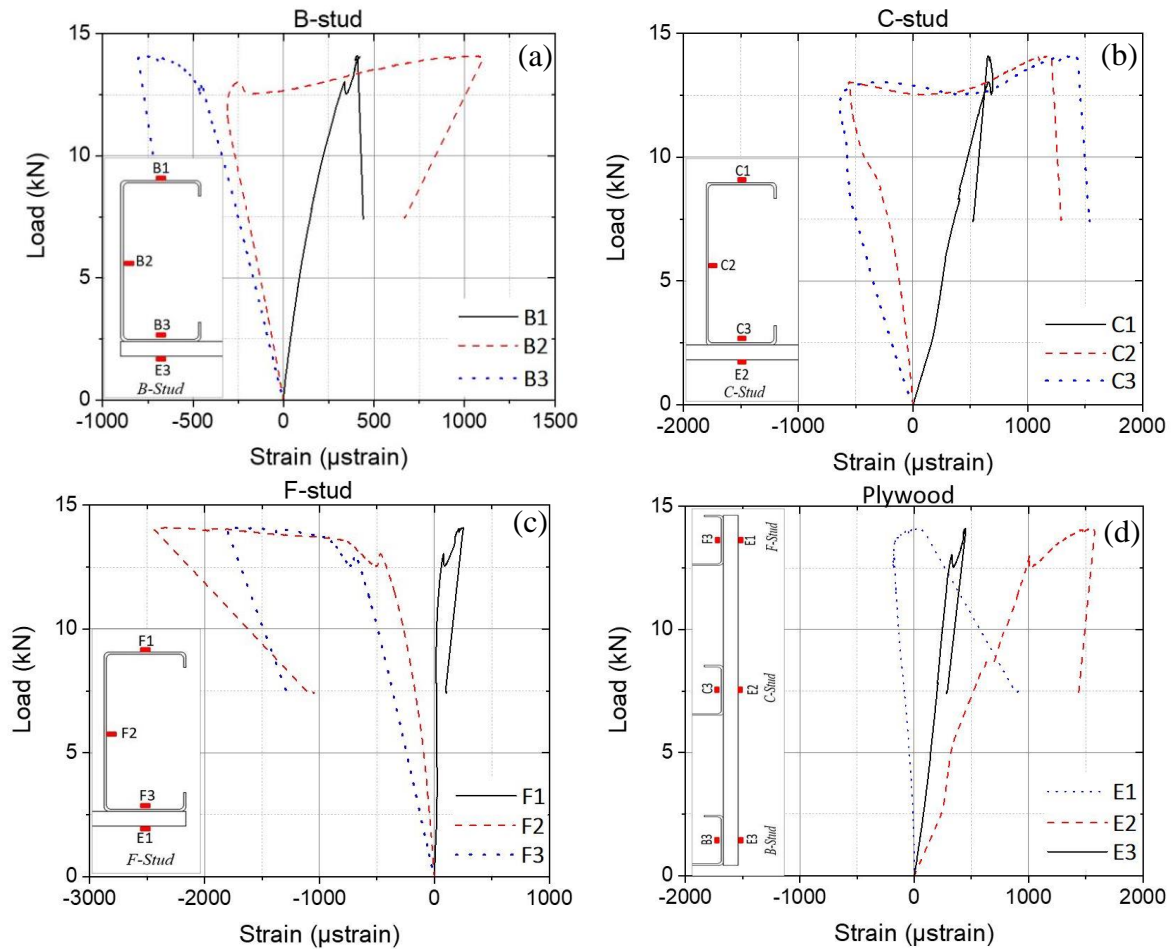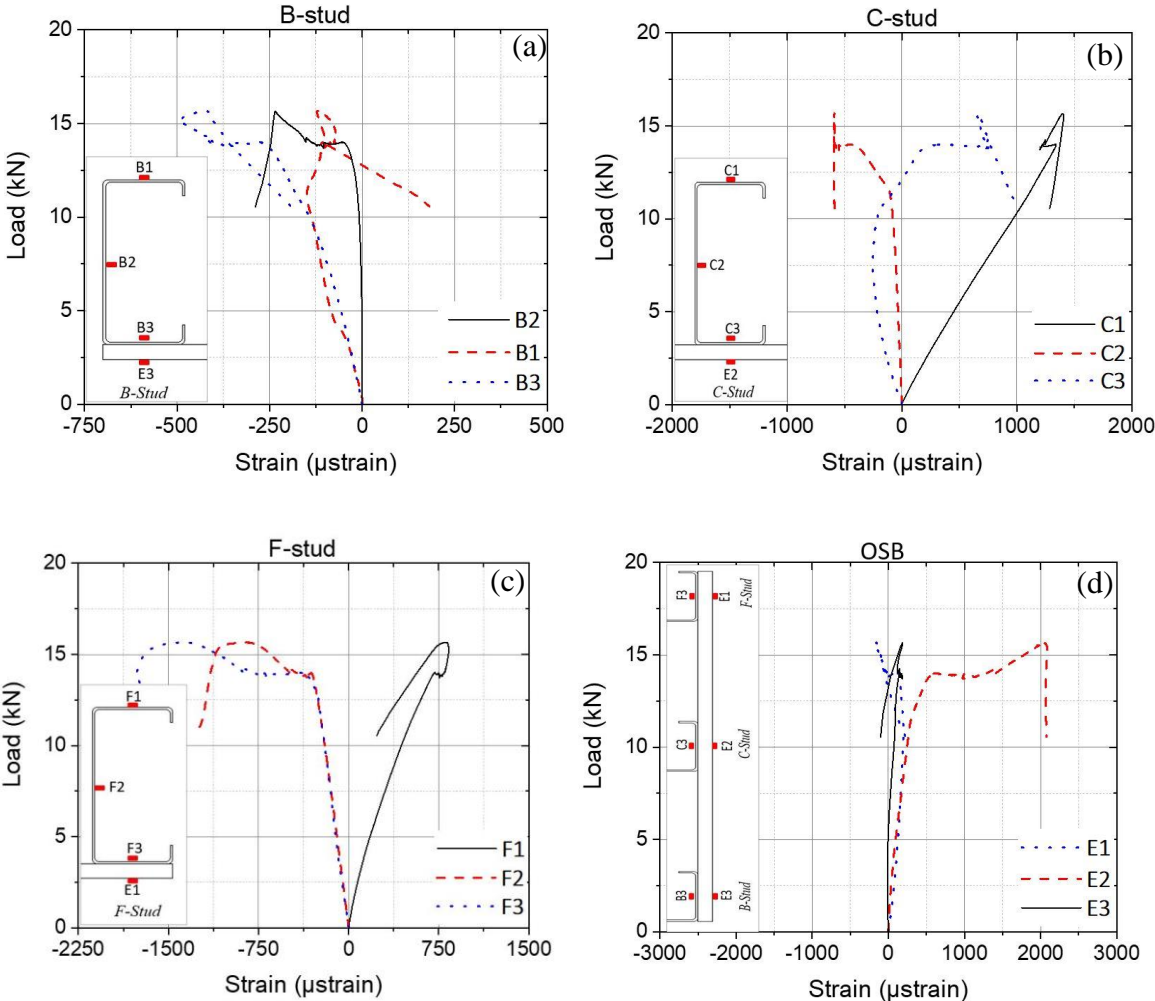**Figure 5.42 Load-strain curve for (a) B-stud, (b) C-stud, (c) F-stud and (d) OSB of N2 specimen**
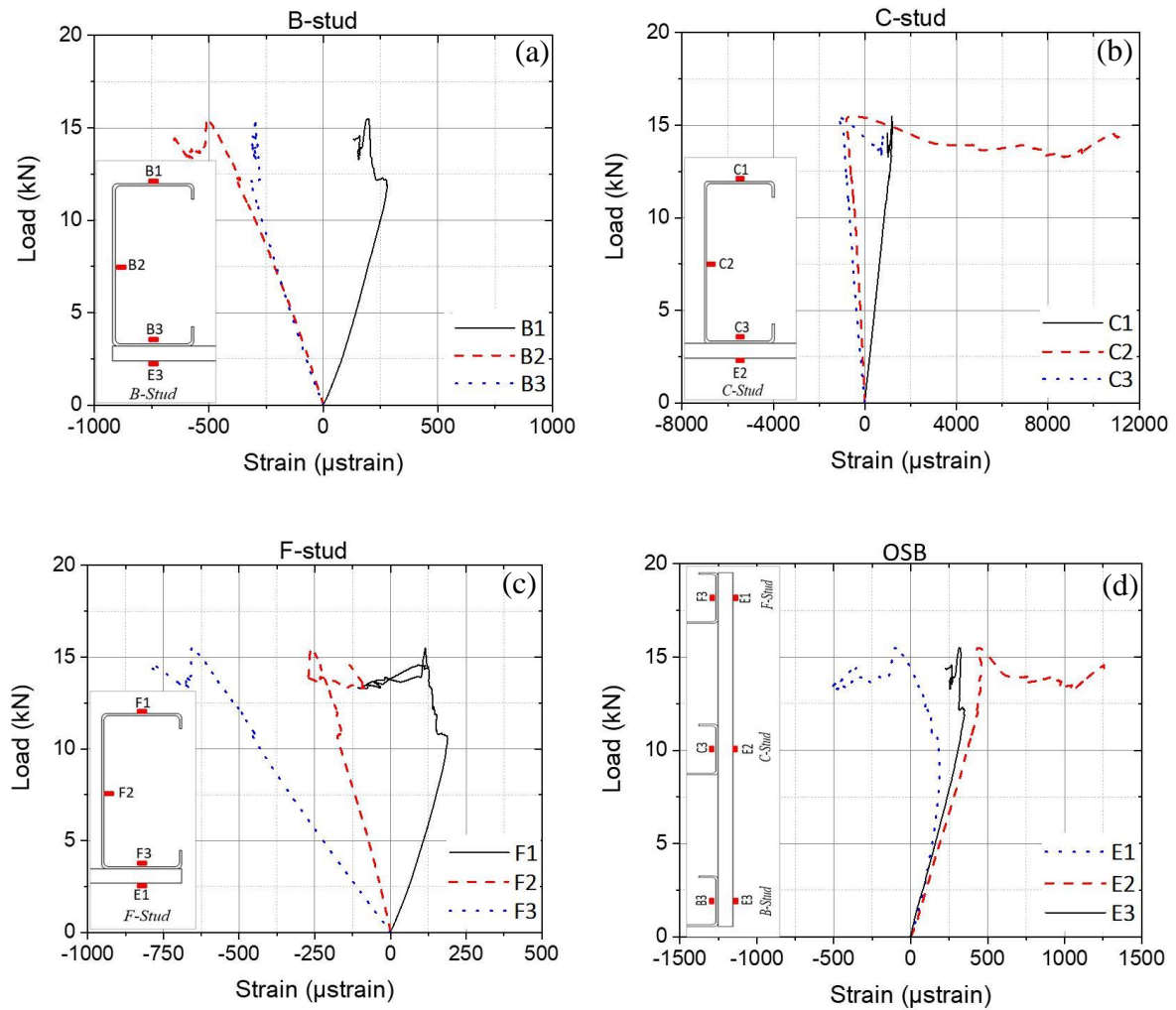
Figure 5.43 Load-strain curve for (a) B-stud, (b) C-stud, (c) F-stud and (d) OSB of PT2 specimen

5.8. Summary and conclusions

This chapter investigated the bending behaviour and capacity of face-down CFS stud wall panels sheathed with the wood-based board by considering the effects of key design parameters on the performance of these systems as one of the emerging systems used in modern modular construction. For this purpose, a comprehensive experimental programme was conducted on the sheathed stud wall systems by systematically varying key design variables, including the thickness of the CFS studs and the boards, the board material (i.e. OSB and plywood), the drift ratio and the effects of main/auxiliary components (i.e. seam, nogging and no pinned track).

The results were used to investigate the main structural performance parameters and failure mechanism of the tested specimens.

Based on the presented results, the following conclusions can be drawn:

- By doubling the thickness of the board from 9 mm to 18 mm, the out-of-plane strength of the stud wall was increased by 7%. This also showed a major effect on the failure mechanism of the system, in which the failure of the OSB board was prevented, and alternatively F-stud experienced the lateral distortional buckling instead of B-stud. In addition, increasing thickness of CFS elements from 1.2 mm to 2 mm enhanced the out-of-plane strength and stiffness of the stud wall by 54% and 43%, respectively, attributed to preventing the lateral distortional buckling in the studs of the system. Compared to the OSB material, using plywood boards with the same thickness (i.e. 9 mm) resulted in a more ductile behaviour before the peak capacity while it causes a negligible change in the out-of-plane strength and stiffness of the system.

- The results also demonstrated that the initial stiffness of the stud wall remained almost constant by decreasing the drift ratio (centre spacing) from 610 to 305 mm. However, the reducing the centre spacing resulted in a significant reduction in out-of-plane strength of the system dropped from 15.5 kN to 12.1 kN and it was revealed that the ductility of the system was considerably reduced. The failure mechanism of the stud wall system with reduced drift ratio was found almost similar, in which the lateral distortional buckling of the top flange interaction started to happen in middle stud, and by further increasing the load again a distortional buckling started to happen in the top flanges of the F-stud.

- It was observed that the presence of the nogging and the absence of the pinned track have a negligible effect on the out-of-plane strength of the stud wall panels. On the contrary, using seam elements in the CFS stud wall dropped the strength of the system by 9%. Furthermore, incorporating either noggings or seam provided notably enhancements in the initial out-of-plane stiffness of the system by 42% and 14%, respectively, while the absence of the pinned track led to a 14% reduction the initial out-of-plane stiffness of the stud wall. Indeed, the existence of the seam and nogging

elements has no effect on the dominant failure mode, however; the lateral distortional buckling of the top flange started to happen of the middle studs in the no pinned track specimen.

Chapter 6: Behaviour of fasteners in sheathed CFS studs under push-out, pull-out and rotational actions

6.1. Introduction

It was shown in the previous chapters that the overall performance of sheathed CFS wall structural systems was significantly dependent on the behaviour of fasteners because one of the critical components of the composite systems was connection point under in-plane and out-plane monotonic loading. Therefore, this experimental investigation was performed to determine behaviour of fasteners in sheathed CFS studs under push-out, pull-out and rotational actions. In this research, small-scale specimens consisting of cold-formed steel (CFS) stud segments attached to wood-based boards were tested to identify the response of fasteners under push-out (shear), pull-out (tension) and rotational actions. The experimental programme was designed to investigate the effects of key design parameters, namely the thickness of the CFS studs and the wood-based boards, the board material (OSB vs. plywood), absence washers and screw spacing. Extensive studies show that the connection point in this composite structure plays a vital role because of that the capacity of sheathed cold-formed steel stud wall systems

is directly dependent on the behaviour of the fasteners. The experimental schedule includes a series of connection tests conducted to describe the characterise the behaviour of the load-slip response at the connection point and provides insight into the connection failure mechanism by taking into account the effects of key design parameters, which as the thickness of CFS and OSB, different material (plywood), absence washer (un-washer) and screw spacing. It was obviously observed that such failure modes (i.e. screw tilting, pull-thought, wood-bearing) occurred, which predominantly affect the performance of the system. It can be summarised that while the deformation of the systems for push-out and pull-out tests are dominated by the wood-based board, the results of the rotation test are dominated by CFS stud members. The key results of the experimental tests (push-out, rotation and pull-out) are summarised herein to better understand the behaviour of fasteners and use further analytical research in the analysis of such type of construction.

6.2. Push-out tests

Eight push-out tests were conducted to determine the load-slip responses of the fastenings under shear loading. The tests considered two wood-based board materials (OSB and plywood), two thicknesses of the OSB board (9 and 18 mm), two CFS thicknesses (1.2 and 2 mm), the presence/absence of a washer and two different screw spacings (75 and 300 mm). A detailed summary of the parametric test matrix was presented in presented in Table 6.1.

Table 6.1 Push-out connection test matrix

	Specimen representation	Test Code	Width x Length (mm x mm)	Test Numbers
Push-out (Shear) Tests	Key specimens	$K1_{Push}$-$K2_{Push}$-$K3_{Push}$		
	Plywood (9 mm)	$P9_{Push}$		
	OSB (18 mm)	$OSB18_{Push}$	200 x 500	8
	CFS (2 mm)	$CFS2_{Push}$		
	Absence Washer	UW_{Push}		
	Screw Spacing (300mm)	$S300_{Push}$		

6.2.1. Push-out test set-up

The schematic view of the push-out test arrangement in which both sides of wood-based boards were sheathed on C-shaped steel sections to ensure a stable system during testing is shown in Fig. 6.1. Each specimen in this work consisted of a CFS stud member with two wood-based

panels screwed onto each of the flanges using self-drilling screws. Five self-drilling screws were used to connect the OSB sheathing on each side to the C-shape CFS, a total of ten screws. It should be also noted that the benchmark test specimen is repeated three times in this study to provide a reference response against which the remaining systems could be compared. The benchmark specimen tested used to 6.3 mm diameter of the self-drilling screws with a bonded washer (see Fig. 6.2) to connect the 9 mm thick single OSB sheathing to the 1.2 mm CFS C-shape stud spacing at 75 mm.
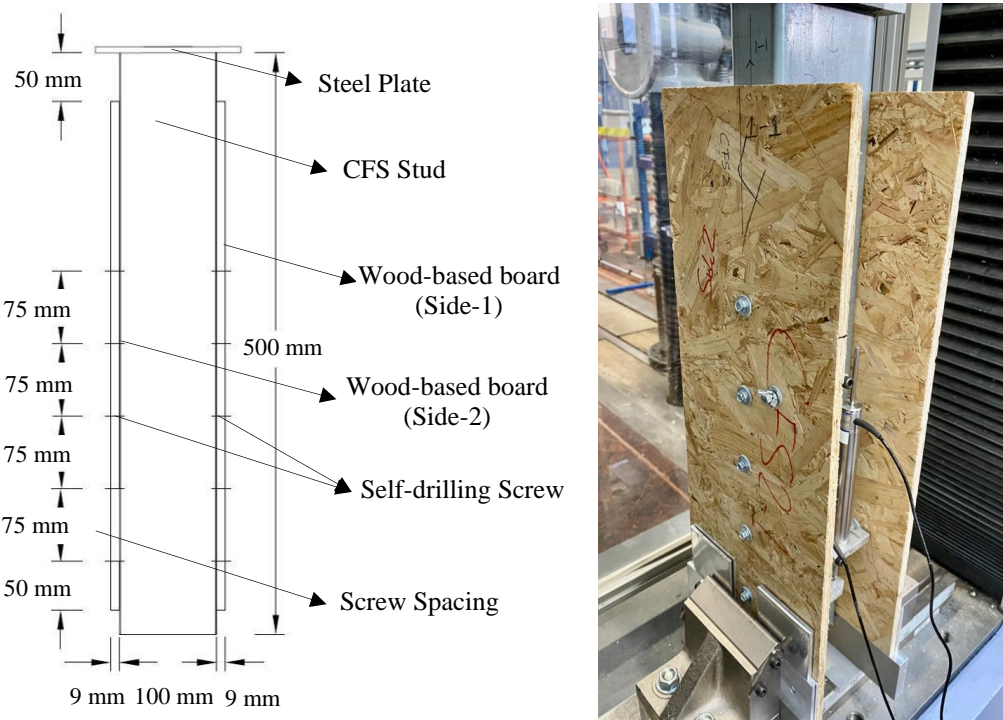
Figure 6.1 Test set-up of the Push-out tests

Figure 6.2 The 6.3 mm diameter of the self-drilling screws with a bonded washer

The 500 mm long lipped-C CFS stud segments had the cross-sectional dimensions of $100 \times 50 \times 10$ (in mm). Both flanges of the lipped channel stud were connected to 200×425 mm^2 wood-based boards using 6.3 mm diameter self-drilling screws with bonded washers (see Fig. 6.2). The actual thicknesses of the CFS stud segments and the wood-based boards were measured by a micrometre tool and reported in Table 6.2.

Table 6.2 Thickness of the CFS and wood-based boards (in mm)

Specimen Batch	CFS	Wood-based board (Side-1)	Wood-based board (Side-2)
K1$_{Push}$	1.26	9.04	8.96
K2$_{Push}$	1.24	8.93	9.06
K3$_{Push}$	1.24	9.19	8.91
P9$_{Push}$	1.25	9.11	8.96
OSB18$_{Push}$	1.26	18.02	18.04
CFS2$_{Push}$	1.96	9.00	9.14
UW$_{Push}$	1.26	8.95	9.03
S300$_{Push}$	1.25	8.96	8.93

The load was applied using a 300 kN Shimadzu testing machine, employed in a displacement-controlled manner with a rate of 1.00 mm/min. Two linear variable displacement transducers (LVDTs) were employed to measure the slip for both sides between wood-based boards and CFS stud flanges (see Fig. 6.3). The data acquisition system was controlled by a LabView script, which imposed a sampling rate of 1 Hz.
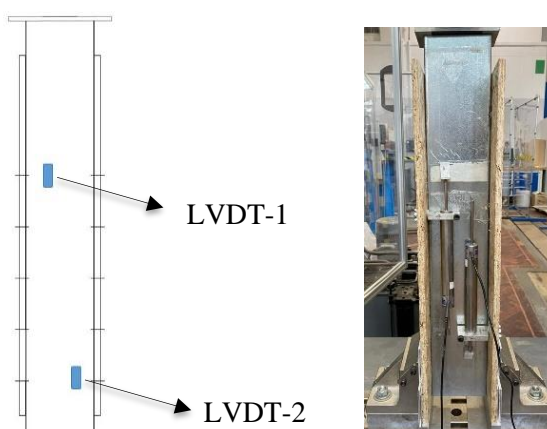
Figure 6.3 The Positions of the two LVDTs

6.2.2. Push-out test results

The load-slip (*P-s*) responses for all specimens were given in Fig. 6.4, where *P* is the load per screw and s_u is the average slip that was calculated by averaging the values measured from the two LVDTs readings. Besides, a summary of the ultimate load per connector (P_u), the slip at the ultimate load (s_u) and the initial stiffness of each connection (R_i) were reported in Table 6.3.

Figure 6.4 The load-slip (P-s) response of the push-out tests

Table 6.3 Main performance parameters in push-out test results

Specimen Batch	Pu (*kN*)	Su (*mm*)	Ri (*kN/mm*)
K1$_{Push}$	3.42	13.70	2.39
K2$_{Push}$	3.48	12.67	2.16
K3$_{Push}$	2.85	7.25	2.20
P9$_{Push}$	2.61	18.04	1.95
OSB18$_{Push}$	5.79	18.77	2.36
CFS2$_{Push}$	3.69	19.18	2.18
UW$_{Push}$	2.59	8.26	2.22
S300$_{Push}$	2.73	12.30	2.05

All specimens exhibited a similar failure mechanism, where tilting of the screws as well as bearing failure of the screws against the wood-based boards was observed (see Fig. 6.5). It can be seen from Table 7 that increasing the OSB thickness from 9 to 18 mm resulted in roughly twice the fastening strength. When comparing the responses of plywood and OSB fastenings for the same fastening configuration (i.e. thickness and screw spacing), it can also be concluded

that using plywood provided slightly lower stiffness and strength (with reductions of 19% and 24%, respectively). Increasing the CFS thickness, on the other hand, showed statistically negligible influence on the connection strength (with only an 8% increase, compared to a COV of 11% for the key test results). The results also demonstrated that the presence of washers slightly improved the fastening strength. While increasing the screw spacing from 75 mm to 300 mm appeared to decrease both the strength and stiffness of the fastenings by 14% and 9%, respectively, these variations, observed in a single test, might not be statistically meaningful.
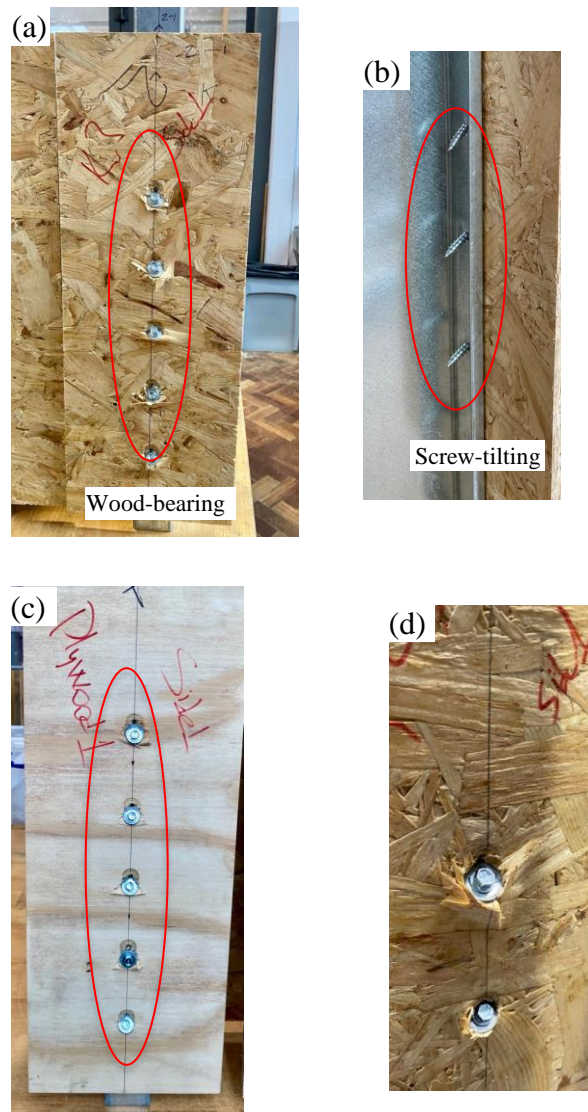
Figure 6.5 Typical failure mode captured from the push-out tests

6.3. Pull-out Tests

The load-slip response of the fasteners under vertical loading was determined through a series of experimental monotonic pull-out tests. Each specimen consisted of a CFS stud (500 mm) with an OSB panel (300×300 mm^2) screwed onto the flange using a self-drilling screw. The summary of the detailed parametric test matrix is presented in Table 6.4.

Table 6.4 Pull-out connection test matrix

	Specimens	Test Code	Width x Length (mm x mm)	Test Numbers
Pull-out Tests	Key specimens	K1$_{Pull}$-K2$_{Pull}$-K3$_{Pull}$	500 x 300	3

6.3.1. Pull-out test set-up

The load-slip response of the fasteners under tensile loading in the out-of-plane direction was determined through a series of monotonic pull-out tests. Each specimen consisted of a 300×300 mm^2 OSB board, connected to the flange of a 500 mm long CFS stud segment. The actual measured thicknesses of the CFS stud segments and the OSB panels are reported in Table 6.5.

Table 6.5 Thickness of the tested the CFS and wood-based boards (in mm)

Specimen Batch	CFS	Wood-based board
K1$_{Pull}$	1.25	8.87
K2$_{Pull}$	1.26	8.98
K3$_{Pull}$	1.25	8.85

The schematic view of the pull-out test arrangement was shown in Fig. 6.6. A U-shaped steel yoke was used to transfer the load from the testing machine directly to the wood-based board and load the screw in tension. The load was applied using a 300 kN Shimadzu testing machine, employed in a displacement-controlled manner with a rate of 0.50 mm/min.
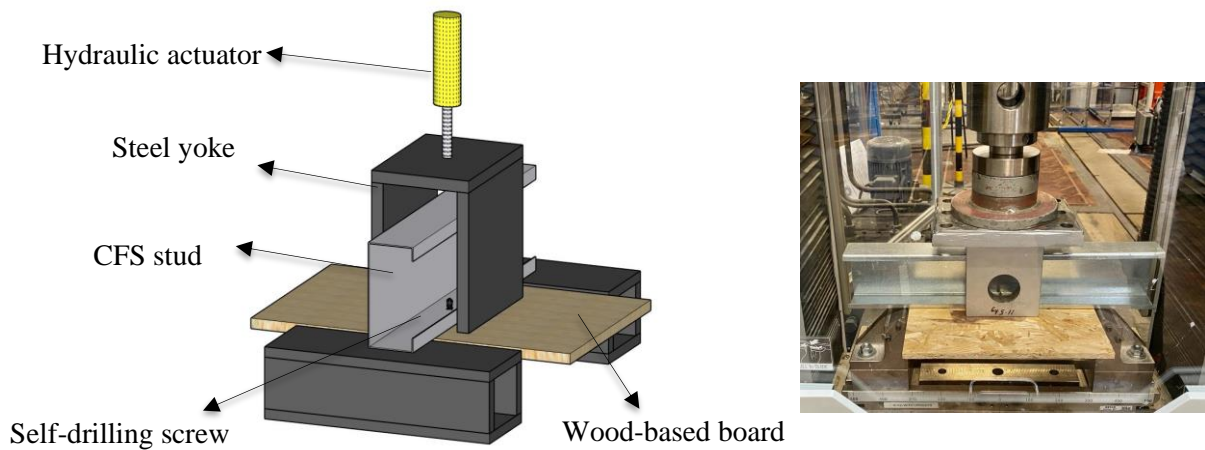
Figure 6.6 Test set-up of the pull-out tests

6.3.2. Pull-out test results

The load-slip (*P-s*) responses for all specimens were given in Fig. 6.7, where *P* is the load per screw and S_u is the average slip. Moreover, a summary of the main performance parameters was reported in Table 6.6, where P_u is the ultimate load per connector, s_u is the slip at the ultimate load and R_i is the initial stiffness.
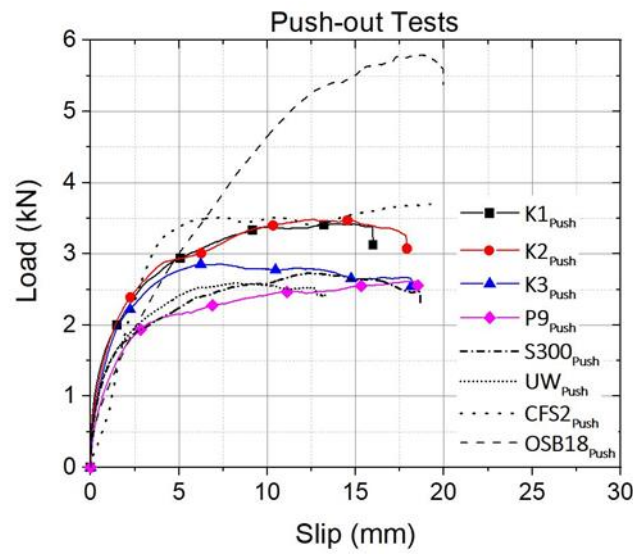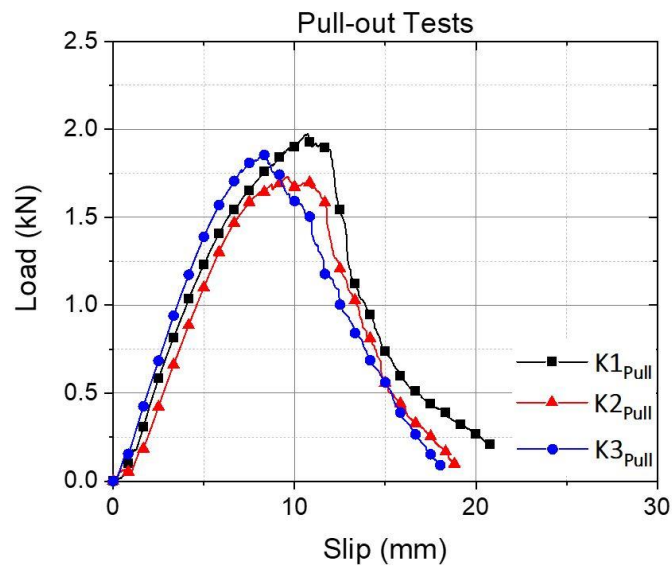

Figure 6.7 The load-slip (P-s) response of the pull-out tests

Table 6.6 Main performance parameters in pull-out test results

Specimen Batch	Pu (kN)	Su (mm)	Ri (kN/mm)
K1$_{Pull}$	1.98	10.74	0.24
K2$_{Pull}$	1.73	9.60	0.21
K3$_{Pull}$	1.86	8.45	0.26

As expected, all pull-out specimens showed a similar load-slip response over the whole range of loading (see Fig. 6.7). Pull-thought of screws were observed as a dominant failure mode in all three specimens, as shown in Fig. 6.8. In general, less ductile behaviour was observed when the screws were loaded in tension, compared to shear.

Figure 6.8 Typical failure mode captured from the pull-out tests

6.4. Rotational Tests

A series of rotational tests were conducted to determine the rotational behaviour of the fasteners containing four various design parameters, including different wood-based panels (OSB and plywood boards), the thickness of OSB board (9 and 18 mm) and CFS member (1.2 and 2 mm) and absence of washers. Seven specimens were tested to determine the rotational behaviour of the stud wall panel connection subassemblies. The summary of the detailed parametric test matrix for rotation tests was presented in Table 6.7.

Table 6.7 A detailed test matrix for rotation connection

	Specimens	Test Code	Width x Length (mm x mm)	Test Numbers
Rotation Tests	Key specimens Plywood (9 mm) OSB (18 mm) CFS (2 mm) Washer effect	$K1_{Rot}$-$K2_{Rot}$-$K3_{Rot}$ $P9_{Rot}$ $OSB18_{Rot}$ $CFS2_{Rot}$ UW_{Rot}	600 x 600	7

6.4.1. Rotation test set-up

The test setup arrangement as well as a detailed drawing showing the locations of screws were depicted in Figs. 6.9 (a) and (b). Each specimen consisted of an OSB board (600×600 mm2) screwed to one flange of a 600 mm CFS stud member using seven 6.3 mm self-drilling screws. It should be noted that similar to the push-out tests, a certain arrangement of the specimens was selected as benchmark specimens (key specimens). Key specimens included a 9 mm thick single OSB and a 1.2 mm CFS stud with screw spacing of 75 mm and bonded washers ($K1_{Rot}$ $K2_{Rot}$-$K3_{Rot}$).
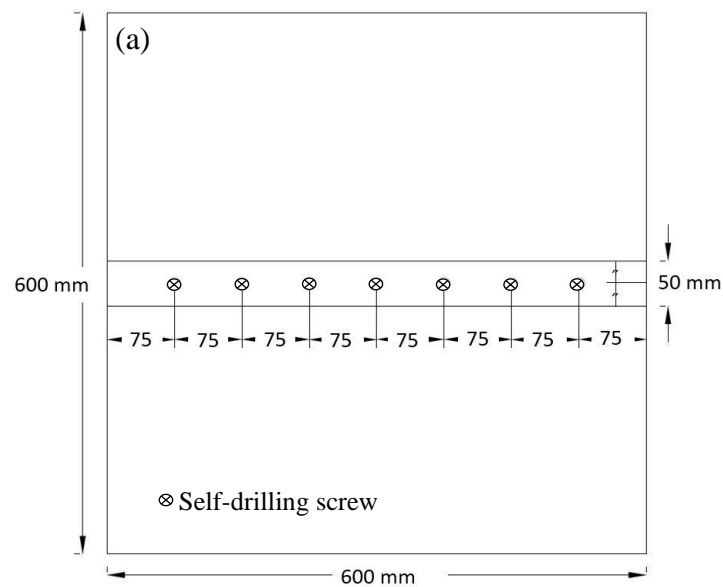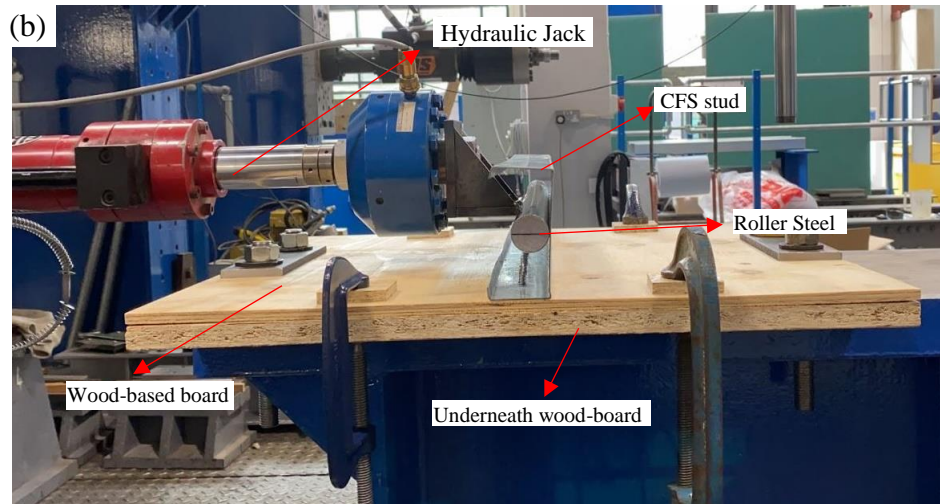
Figure 6.9 (a) Location of self-drilling screws and (b) test set-up of the rotation tests

The load was uniformly applied along the web middle line of the stud element using a solid bar connected to a 150 kN hydraulic jack. The grease was generously applied to the stud's web and the solid bar in order to eliminate the friction. The loading was imposed in a displacement control manner with a rate of 1 mm/min. The data acquisition system was controlled by the National Instrument LabView software, which produced data with a sampling rate of 1 Hz.

Table 6 reported the measured distance from the first (D1) and second (D2) screws to the edge of the stud flange before testing, as illustrated in Fig. 6.10. In addition, the actual thickness of the CFS studs and the wood-based boards were measured and listed in Table 6.8.
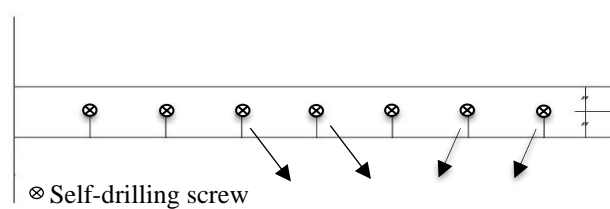
Figure 6.10 Distance from the screws to edge of C-stud flange

Table 6.8 Average thickness of the tested the CFS and wood-based boards and distance from the screws to C-stud (in mm)

Specimen Batch	CFS	Wood-based board	Average distance from screws to edge of flange
K1$_{Rot}$	1.26	8.96	25.6
K2$_{Rot}$	1.26	8.97	25.1
K3$_{Rot}$	1.25	8.91	25.4
P9$_{Rot}$	1.24	8.76	25.3
OSB18$_{Rot}$	1.24	18.08	25.2
CFS2$_{Rot}$	1.96	9.05	25.4
UW$_{Rot}$	1.27	8.84	23.8

6.4.2. Rotational test results

The moment-displacement (M-Δ) responses of all specimens are shown in Fig. 6.11, where M is the load per screw and Δ is the horizontal displacement at mid-height of the web. A summary of the ultimate moment capacity per fastener (M_u) and the web displacement at the ultimate moment (Δ_u) was reported in Table 6.9.
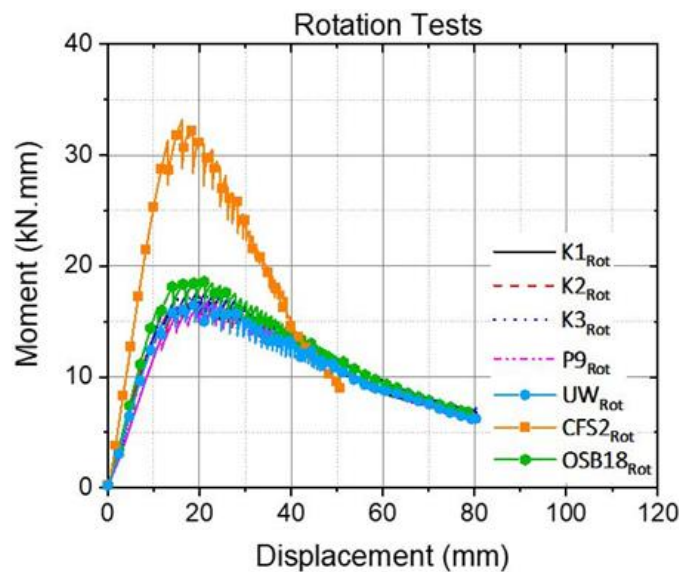
Figure 6.11 Moment-displacement (M-Δ) responses in the rotational tests

Table 6.9 Main performance parameters in rotation test results

Specimen Batch	M_u (kN)	Δ_u (mm)
K1$_{Rot}$	16.78	19.95
K2$_{Rot}$	16.93	20.58
K3$_{Rot}$	17.95	19.95
P9$_{Rot}$	16.61	21.61
OSB18$_{Rot}$	18.76	19.27
CFS2$_{Rot}$	33.11	16.21
UW$_{Rot}$	16.71	21.02

Fig. 6.12 shows the typical failure modes encountered in the rotational tests. It was observed that the CFS thickness had an important effect on the rotational behaviour and the failure mechanism. All specimens with a thickness of 1.2 mm failed by the formation of a yield line at the web-flange junction (Fig. 6.12a, b) and the fastenings did not participate in failure. When increasing the CFS thickness from 1.2 mm to 2.00 mm (CFS2Rot), the fastenings failed by pull-through, accompanied by localized failure of the board material around the screws (See Fig. 6.12 (c), (d) and (e)). This increase in thickness was accompanied by the moment capacity roughly doubling. Increasing the OSB thickness from 9 mm to 18 mm while keeping the thickness at 1.2 mm, however, did not provide significant enhancements in strength, as failure occurred in the CFS channel. For the same reason, the presence of a washer had a negligible effect on the rotational behaviour and using OSB or plywood both led to a similar moment capacity.
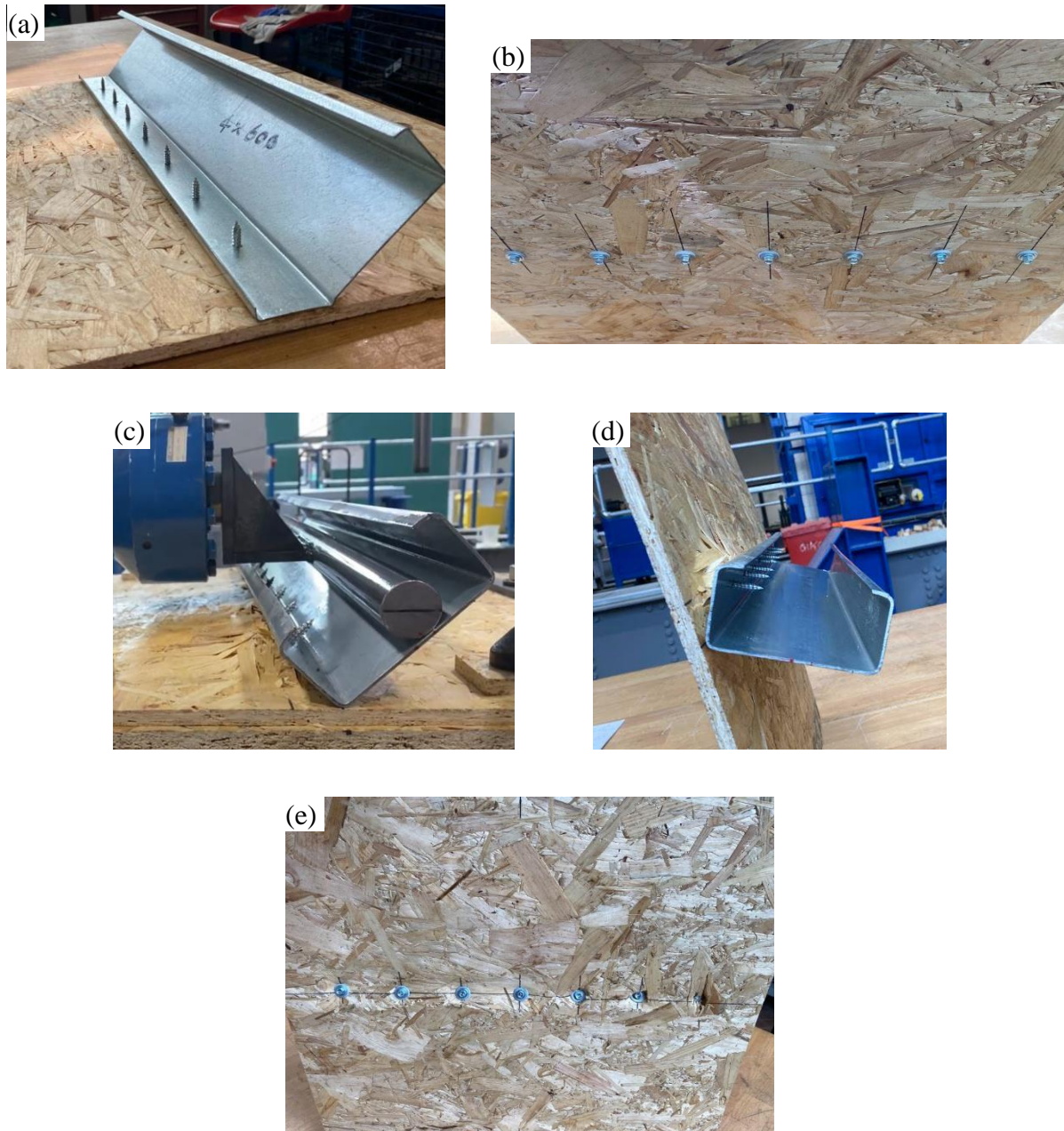
Figure 6.12 Typical failure mode of: (a), (b) K1$_{Rot}$ and (c), (d), (e) CFS2$_{Rot}$ captured from the rotation tests

6.5. Summary and conclusions

A comprehensive experimental programme was conducted on small-scale test samples in order to investigate the behaviour of the fastenings between CFS studs and wood-based sheathing. The in-plane (shear) and out-of-plane (tensile) behaviour were examined, and the rotational restraint provided by the fastening to the stud was quantified. The effects of different key design parameters were systematically studied, including the type of wood-based board material, the

thickness of the board, the CFS thickness, the presence/absence of washers and the screw spacing. Based on the results, the following conclusions were drawn:

- All specimens in the push-out tests experienced tilting of the screws, as well as bearing failure in the wood-based boards. The CFS thickness had a negligible effect on the fastening behaviour, while increasing the OSB thickness from 9 to 18 mm resulted in roughly twice the strength. The results also showed that using plywood provided 19% lower stiffness and 24% lower strength. The presence of washers slightly improved the fastening strength.

- The specimens under pull-out loading all failed by pull-through of the screws. Very limited ductility was observed in this case.

- Two distinct failure modes were observed in the rotational tests. All test specimens with a thickness of 1.2 mm failed by the formation of a yield line along the web-flange junction. When increasing the CFS thickness from 1.2 mm to 2.00 mm, failure occurred instead by pull-through and localized crushing of the wood-based board, while the moment capacity almost doubled. Conversely, increasing the OSB thickness from 9 mm to 18 mm, using a washer, or changing the board material to plywood did not significantly affect the moment capacity in the 1.2 mm thick specimens.

Chapter 7: Conclusions and future work

7.1. Conclusions

Sheathed CFS wall systems comprising CFS joists and wood-based boards have especially gained popularity in the modern construction industry due to their uniform quality, ease of mass production and prefabrication, lightweight designs, quick and straightforward installations and more accessible transportation and handling compared to other construction materials. The main purpose of this research aimed to develop a better understanding of the structural behaviour and capacity of the sheathed stud wall panels under in-plane and out-of-plane loadings by considering the effects of key design parameters on the performance of these systems. Findings of this work can be grouped into four categories:

7.1.1. Behaviour and performance of OSB-sheathed cold-formed steel shear wall panels under combined vertical and seismic loading (objectives 1-3)

The lateral structural performance parameters and behaviour of sheathed CFS wall systems (i.e. maximum lateral load capacity, initial stiffness and failure mechanism) under in-plane loading were studied for each design parameter (i.e. screws spacing, the thickness of the OSB and CFS, board configuration, gravity load ratio, and board single- and double-sheathed system) by

developing detailed FE models. The more efficient design of these systems then provided by considering the influence of various key design variables. An efficient performance-based design methodology (EEEP) based on the numerical test results developed to assess the seismic characteristics (i.e. ultimate displacement, ductility and energy dissipation) of such type of structure to present the efficiency of these systems with various design variables leading to more efficient design solutions.

The following general conclusions can be drawn:

i.   Increasing the screw spacing could significantly reduce the maximum lateral load capacity and initial stiffness of the shear-wall panels by down to 58% and 45%, respectively. In addition, while using a short screw spacing can postpone the failure of the board at the location of the screws, increasing screw spacing results in significant deformation of the OSB and consequently failure in the board. The results demonstrated that increasing screw spacing resulted in an increase the ductility of the shear wall panel as long as no failure occurred in the board element.

ii.   The overall load-displacement responses of the CFS wall panels were significantly influenced by the thickness of the OSB sheathing board. Using thinner OSB panel in the structure could decrease the initial stiffness and maximum load capacity of the shear wall systems almost proportionally. While the thinner OSB provided higher ductility and ultimate displacement for the system, energy dissipation was increased by increasing the board thickness.

iii. It was concluded that the contribution of CFS thickness to the lateral strength and stiffness of shear wall panels was found to be negligible (less than 10%). In general, increasing the thickness of CFS elements can potentially result in the development of failure in the board element. The results showed that using thicker CFS elements could always improve the seismic characteristics of the OSB sheathed shear wall panels.

iv.   The existence of the horizontal/vertical seam in the shear wall panels resulted in a significant reduction in both lateral strength and stiffness of the system, while without horizontal/vertical seam could present the highest initial stiffness and maximum lateral load capacity. The failure mechanism demonstrated that the boards

and the vertical elements in the shear wall panel experienced localised failure at the location of the horizontal seam, which significantly decrease the seismic characteristics of the shear wall panel by up to approximately 5 times.

v. Interestingly, the effects of gravity load on the initial stiffness of the system were negligible regardless of the amount of gravity load. In addition, the influence of gravity load on the lateral strength was found to be negligible for loads of up to 40% of the total compressive capacity of the stud cross-sections. However, when the vertical load was increased from 40% to 60% of the total compressive capacity, the lateral strength of the shear wall panel was significantly reduced, which was due to localised buckling of the compressive chord stud.

vi. As expected, the lateral capacity and stiffness of the unsheathed system were negligible, leading to low energy dissipation. The double-sheathed wall panel outperformed the single-sheathed wall in terms of energy dissipation capacity by 36%. However, the single-sheathed wall panel displayed around 22% more deformation capacity and 30% more ductility.

7.1.2. Out-of-plane bending behaviour and capacity of sheathed face-up cold-formed steel stud walls: experimental investigation (objectives 4-6)

The bending structural performance parameters (i.e. maximum bending load capacity, initial stiffness and failure mechanism) of sheathed face-up CFS wall systems were examined by conducting comprehensive experimental programme under out-of-plane loading. The influence of various key design variables, including by taking into account the effects of screw spacing, the thickness of CFS and sheathing, different board material, the board scenarios (unsheathed, single-sheathed and double sheathed), drift ratio and the main/auxiliary components (seam, noggins, pinned no track) were considered. The rotation of the CFS studs and end-slip between stud and wood-based board were consider for each parameter.

From these experiments, the following general conclusions can be drawn:

i. Increasing the screw spacing resulted in a reduction in the out-of-plane strength of the stud wall by up to 75%; however, the initial out-of-plane stiffness of the wall remained almost constant by increasing the screw spacing. The results also

demonstrated that increasing the screw spacing led to a more ductile stud-wall system. It was observed that the failure mechanism of the stud wall was found almost similar for systems various screw spacing, however; an additional OSB bearing was observed at the corners of the wall for the stud wall system with the largest selected screw spacing (300 mm).

ii. Unlike the OSBs, using plywood boards with the same thickness (i.e. 9 mm) resulted in a more ductile behaviour before the peak capacity while it causes a negligible change in the out-of-plane strength and stiffness of the system. In addition, thickening of CFS elements from 1.2 mm to 2 mm enhanced the out-of-plane strength and stiffness of the stud wall by 86% and 45%, respectively, which was attributed to preventing distortional buckling in the studs of the system. By doubling the thickness of the board from 9 mm to 18 mm, the out-of-plane strength of the stud wall was increased by up to 33%. This also showed prevented the failure of the OSB board.

iii. The test results showed that removing the OSB board resulted in a significant reduction in out-of-plane strength of the system which dropped to nearly 67%, however, the unsheathed specimen had a considerably higher ductile behaviour. Besides, the out-of-plane strength and initial stiffness of the stud wall with double-sheathed OSB were increased by up to 45% and 16% compared to the single-sheathed wall. The results also showed that the out-of-plane strength and initial stiffness of the stud wall remained almost similar with decreasing the centre spacing (drift ratio) from 610 to 305 mm. However, brittle behaviour was observed after the peak load in 305 mm centre spacing specimen.

iv. It was observed that the presence of the seam and the absence of the pinned track have a negligible effect on the out-of-plane stiffness of the stud wall panels. In addition, the use of nogging elements in the CFS stud wall enhanced the stiffness of the system. While incorporating either noggings or seam provided slight enhancements in the out-of-plane strength of the system (7%), the absence of the pinned track led to a 12% reduction in the out-of-plane capacity of the stud wall.

7.1.3. Out-of-plane bending behaviour and capacity of sheathed face-down cold-formed steel stud walls: experimental investigation (objectives 4-6)

The comprehensive experimental programme was conducted to assess bending structural performance parameters (i.e. maximum bending load capacity, initial stiffness and failure mechanism) of sheathed face-down CFS wall systems under out-of-plane loading. The influence of various key design variables was taken into account the effects of screw spacing, the thickness of CFS and sheathing, different board material, the board scenarios (unsheathed, single-sheathed and double sheathed), drift ratio and the main/auxiliary components (seam, noggins, pinned no track). The rotation of the CFS studs and end-slip between stud and wood-based board were consider for each parameter.

Based on the physical tests, the following general conclusions can be drawn:

i.   The use of plywood boards with the same thickness (i.e. 9 mm) resulted in a more ductile behaviour before the peak capacity when compared to the OSBs. However, it was observed a negligible difference in the out-of-plane strength and stiffness of the sheathed with plywood or OSB specimens. By doubling the thickness of the board from 9 mm to 18 mm, the out-of-plane strength of the stud wall was increased by 7%. This also showed a major effect on the failure mechanism of the system, in which the failure of the OSB board was prevented, and alternatively the left side stud experienced the lateral distortional buckling of the top flange instead of right side. In addition, increasing thickness of CFS elements from 1.2 mm to 2 mm enhanced the out-of-plane strength and stiffness of the stud wall by 54% and 43%, respectively. This can be attributed to the prevention of the lateral distortional buckling in the studs of the system.

ii. It was demonstrated that the initial stiffness of the stud wall systems remained almost constant when decreasing the drift ratio of the specimen (centre spacing) from 610 to 305 mm. However, the reducing the centre spacing resulted in a significant reduction in out-of-plane strength of the system which dropped by 22%. Also, it was observed that the ductility of the system was considerably reduced. The failure mechanism of the stud wall system with reduced drift ratio was found almost similar, in which the lateral distortional buckling of the top flange interaction started

to happen in middle stud. If the load was further increased again, a distortional buckling started to happen in the top flanges of the F-stud.

iii. It was observed that the presence of the nogging and the absence of the pinned track had a negligible effect on the out-of-plane strength of the stud wall panels. However, seam elements in the CFS stud wall slightly dropped the strength of the system by 9%. In addition, incorporating either noggings or seam provided notably enhancements in the initial out-of-plane stiffness of the system by 42% and 14%, respectively, while the absence of the pinned track led to a 14% reduction the initial out-of-plane stiffness of the stud wall. The existence of the seam and nogging elements had no effect on the dominant failure mode, but the absence of the pinned track resulted in prevented to happen in the top flanges of in the F-stud or B-stud.

7.1.4. Behaviour of fasteners in sheathed cold-formed steel studs under push-out, pull-out and rotational actions (objective 7)

The small-scale specimens consisting of cold-formed steel (CFS) stud segments attached to wood-based boards were tested to identify the response of fasteners under push-out (shear), pull-out (tension) and rotational actions. The experimental programme was designed to investigate the effects of key design parameters, namely the thickness of the CFS studs and the wood-based boards, the board material (OSB vs. plywood), absence washers and the screw spacing.

The following general conclusions can be drawn:

i. Overall, all specimens exhibited very similar failure mechanism under lateral loading which was failed by tilting of their screws as well as the significant bearing of the wood-based boards Since the wood-based material was significantly softer than the CFS, the deformation was dominated by the wood board. For this reason, the wood-based board takes an important role in determining the behaviour of the fastener. It was clearly shown that increasing the OSB thickness from 9 to 18 mm has a nearly double capacity compared to other parameters. The load capacity of the fastener increased linearly with the increasing thickness of OSB under lateral loading. The results demonstrated that by comparing the response of plywood and

OSB materials in the same connection configuration (i.e. thickness and screw spacing), the plywood provides lower in-plane stiffness and strength for the connection by down to 19% and 24%, respectively. Interestingly, with increasing the CFS thickness had an almost negligible influence on the in-plane strength of the fastener, it is likely to increase the connection strength by up to 8%. It could be said that the presence of a washer in the connection can generally decrease the load-slip response obtained from the push-out test. In addition, the increasing the screw spacing from 75 to 300 mm decreased both in-plane strength and stiffness of the connections

ii. It was observed that the pull-thought failure mechanism happened in all tested pull-out specimens. Since the wood-based material is significantly softer than the CFS, the deformation is dominated by the wood board.

iii. Apart from other connection actions, the thickness of CFS played an essential role in determining the behaviour of the fastener under rotation loading. The failure deformation of the tested specimens is dominated by the bending C-shape stud. For this reason, it was clearly shown that with increasing the thickness of CFS, the stiffness and load capacity. For this reason, increasing the CFS from 1.2 to 2 mm resulted in significantly higher stiffness and strength in connection by up to nearly double. This also showed a major effect on the failure mechanism of the system, in which pull-thought and crushing occurred at the connection point. However, the increasing the OSB thickness had a negligible influence on the rotation strength and initial stiffness of the connection compared to thickness of CFS stud. The results also demonstrated that the presence of a washer in the connection and using plywood board instead of OSB in the same configuration decreased lower strength and stiffness for the connection

7.2. Recommendations for future work

This research can be further developed to cover the following subjects;

i. The findings were provided detail information about the structural behaviour and capacity of the sheathed wall panels considering the various key design parameters

under in-plane and out-of-plane loadings herein. However, further advances could be achieved for the sheathed wall structures by considering another different key design parameters, apart from the used parameters in this study.

ii. Though a good agreement was captured between numerical and experimental test results to assess lateral structural performance (i.e. maximum lateral load capacity, initial stiffness and failure mechanism) of sheathed CFS wall system under monotonic in-plane loading, a comprehensive numerical study can be conduct to simulate lateral behaviour of sheathed CFS wall systems under reversed cyclic loading. The detailed non-linear FE models numerical model could be included micro-modelling approach (material and geometric nonlinearity) and hysteretic behaviour of fasteners. were

iii. The detailed FE models of CFS stud wall panel structures can be also developed to validate using the results of experiment. The detailed numerical model should be comprised material and geometric nonlinearity, initial material (i.e. CFS and OSB) imperfections. In addition, the load-slip response of the fasteners obtained from the connection test results can be used to define the interaction between the CFS frame system and the wood-based panel.

iv. The behaviour of fasteners can be further improved by using different type of fasteners. The bolt and nut connections could be outperformed self-drilling screws (stiffness and strength). Besides, deformation mechanism of the structure (i.e. crushed, tilting) can be prevented using these types of fasteners as well as they could be proposed easy installation.

v. The hysteretic response of fasteners can be examined under cyclic loading conducting experimental study. The enlargement of fastener hole could be defined due to bearing damage in sheathing board. Since the connection played a vital role due to the capacity of sheathed cold-formed steel stud wall systems in this composite structure, the hysteretic behaviour response results and failure modes can be used for further analytical research.

vi. The further improvements could be achieved by using optimisation method for the employed CFS frame cross-sectional shape to determinate of the optimal cross-sectional geometry of the CFS members. Optimising the non-symmetric cross-

sectional geometry of CFS frames could be provided more efficient performance and reduced material usage.

References

Accorti, M., Baldassino, N., Zandonini, R., Scavazza, F. & Rogers, C.A. (2016). "Reprint of Response of CFS Sheathed Shear Walls". *Structures*. 8, 318–330. doi:10.1016/j.istruc.2016.07.002.

Alaee, S.A.M., Sullivan, T., Rogers, C.A. & Nascimbene, R. (2012). "Semi-empirical method to predict the displacement capacity and resistance of cold formed steel frame wood-panel shear walls". *World Conference on Timber Engineering 2012, WCTE 2012*. 5 (January), 450–455.

Allen, D. (2006). "History of Cold Formed Steel". *Structure Magazine*. 11 (November), 28–32. http://www.structuremag.org/wp-content/uploads/2014/09/C-BB-History-AllenLowndes-Nov061.pdf.

American Iron and Steel Institute (2016). "*AISI S400-15 w/S1-16, North American Standard for Seismic Design of Cold-Formed Steel Structural Systems*" *(with Supplement 1)*. 73.

American Iron and Steel Institute (2002). "Standard for Cold-Formed Steel Framing Design Provisions Lateral Resistance", Feb. 2002 Draft, Washington, DC, USA.

Attari, N.K.A., Alizadeh, S. & Hadidi, S. (2016). "Investigation of CFS shear walls with one and two-sided steel sheeting". *Journal of Constructional Steel Research*. 122, 292–307. doi:10.1016/j.jcsr.2016.03.025.

Badr, A.R., Elanwar, H.H. & Mourad, S.A. (2019). "Numerical and experimental investigation on cold-formed walls sheathed by fi ber cement board". *Journal of Constructional Steel Research*. 158, 366–380. doi:10.1016/j.jcsr.2019.04.004.

Bagheri Sabbagh, A., Petkovski, M., Pilakoutas, K. & Mirghaderi, R. (2013). "Cyclic behaviour of bolted cold-formed steel moment connections: FE modelling including slip". *Journal of Constructional Steel Research*. 80, 100–108. doi:10.1016/j.jcsr.2012.09.010.

Bagheri Sabbagh, A., Petkovski, M., Pilakoutas, K. & Mirghaderi, R. (2012). "Development of cold-formed steel elements for earthquake resistant moment frame buildings". *Thin-Walled Structures*. 53, 99–108. doi:10.1016/j.tws.2012.01.004.

Balh, N., Dabreo, J., Ong-Tone, C., El-Saloussy, K., Yu, C. & Rogers, C.A. (2014). "Design of steel sheathed cold-formed steel framed shear walls". *Thin-Walled Structures*. 75, 76–86. doi:10.1016/j.tws.2013.10.023.

Baran, E. & Alica, C. (2012). "Behavior of cold-formed steel wall panels under monotonic horizontal loading". *Journal of Constructional Steel Research*. 79, 1–8. doi:10.1016/j.jcsr.2012.07.020.

Becque, J. (2014). "Local-overall interaction buckling of inelastic columns: A numerical study of the inelastic Van der Neut column". *Thin-Walled Structures*. 81, 101–107. doi:10.1016/j.tws.2013.07.010.

Bian, G., Buonopane, S.G., Ngo, H.H. & Schafer, B.W. (2014). "Fastener-based computational models with application to cold-formed steel shear walls". *22nd International Specialty Conference on Recent Research and Developments in Cold-Formed Steel Design and Construction*. (January), 825–840.

Blais, C. and Rogers A. (2006). "Testing and Design of Light Gauge Steel Frame 9mm OSB Panel Shear Walls". *Eighteenth International Specialty Conference on Cold-Formed Steel Structures Orlando, Florida, U.S.A, October 26 & 27, 2006*. 637–662.

Branston, A.E., Chen, C.Y., Boudreault, F.A. & Rogers, C.A. (2006). "Testing of light-gauge steel-frame - wood structural panel shear walls". *Canadian Journal of Civil Engineering*. 33 (5), 561–572. doi:10.1139/l06-014.

Brière, V., Santos, V. & Rogers, C.A. (2018). "Cold-formed steel centre-sheathed (mid-ply) shear walls". *Soil Dynamics and Earthquake Engineering*. 114 (February), 253–266. doi:10.1016/j.soildyn.2018.07.008.

Buonopane, S.G., Tun, T.H. & Schafer, B.W. (2014). "Fastener-based computational models for prediction of seismic behavior of CFS shear walls". *NCEE 2014 - 10th U.S. National Conference on Earthquake Engineering: Frontiers of Earthquake Engineering*. doi:10.4231/D3ZW18S94.

DaBreo, J., Balh, N., Ong-Tone, C. & Rogers, C.A. (2014). "Steel sheathed cold-formed steel framed shear walls subjected to lateral and gravity loading". *Thin-Walled Structures*. 74, 232–245. doi:10.1016/j.tws.2013.10.006.

Dubina, D., Ungureanu, V. and Landolfo, R. (2012). Design of Cold-Formed Steel Structures - *Eurocode 3: design of Steel Structures Part 1-3: Design of Cold-formed Steel Structures,* ECCS - European Convention for Constructional Steelwork.

Esmaeili Niari, S., Rafezy, B. & Abedi, K. (2015). "Seismic behavior of steel sheathed cold-formed steel shear wall: Experimental investigation and numerical modeling". *Thin-Walled Structures*. 96, 337–347. doi:10.1016/j.tws.2015.08.024.

Fiorino, L., Macillo, V. & Landolfo, R. (2017a). "Shake table tests of a full-scale two-story sheathing-braced cold-formed steel building". *Engineering Structures*. 151, 633–647. doi:10.1016/j.engstruct.2017.08.056.

Fiorino, L., Pali, T., Bucciero, B., Macillo, V., Teresa Terracciano, M. & Landolfo, R. (2017b). "Experimental study on screwed connections for sheathed CFS structures with gypsum or cement based panels". *Thin-Walled Structures*. 116 (March), 234–249. doi:10.1016/j.tws.2017.03.031.

Fiorino, L., Pali, T. & Landolfo, R. (2018a). "Out-of-plane seismic design by testing of non-structural lightweight steel drywall partition walls". *Thin-Walled Structures*. 130 (March), 213–230. doi:10.1016/j.tws.2018.03.032.

Fiorino, L., Shakeel, S., Macillo, V. & Landolfo, R. (2018b). "Seismic response of CFS shear walls sheathed with nailed gypsum panels: Numerical modelling". *Thin-Walled Structures*. 122 (September 2017), 359–370. doi:10.1016/j.tws.2017.10.028.

Gao, W.C. & Xiao, Y. (2017). "Seismic behavior of cold-formed steel frame shear walls sheathed with ply-bamboo panels". *Journal of Constructional Steel Research*. 132, 217–229. doi:10.1016/j.jcsr.2017.01.020.

Gioncu, V. (2000). "Framed structures. Ductility and seismic response: General Report". *Journal of Constructional Steel Research*. 55 (1–3), 125–154. doi:10.1016/S0143-974X(99)00081-4.

Hancock, G.J., Celeban, M., Healy, C., Georgiou, P.N. & Ings, N.L. (1990). "Tests of purlins with screw fastened sheeting under wind uplift". *International Specialty Conference on Cold-Formed Steel Structures*. 393–419.

Huang, Y. & Young, B. (2014). "The art of coupon tests". *Journal of Constructional Steel Research*. 96, 159–175. doi:10.1016/j.jcsr.2014.01.010.

Javaheri-Tafti, M.R., Ronagh, H.R., Behnamfar, F. & Memarzadeh, P. (2014). "An experimental investigation on the seismic behavior of cold-formed steel walls sheathed by thin steel plates". *Thin-Walled Structures*. 80, 66–79. doi:10.1016/j.tws.2014.02.018.

Karabulut, B. & Soyoz, S. (2017). "Experimental and analytical studies on different configurations of cold-formed steel structures". *Journal of Constructional Steel Research*. 133, 535–546. doi:10.1016/j.jcsr.2017.02.027.

Karki, D., Al-hunaity, S., Far, H. & Saleh, A. (2022). "Composite connections between CFS beams and plywood panels for flooring systems : Testing and analysis". *Structures*. 40 (February), 771–785. doi:10.1016/j.istruc.2022.04.064.

Kyprianou, C., Kyvelou, P., Gardner, L. & Nethercot, D.A. (2021a). "Characterisation of

material and connection behaviour in sheathed cold-formed steel wall systems – Part 1: Experimentation and data compilation". *Structures*. 30 (February), 1184–1199. doi:10.1016/j.istruc.2020.12.052.

Kyprianou, C., Kyvelou, P., Gardner, L. & Nethercot, D.A. (2021b). "Characterisation of material and connection behaviour in sheathed cold-formed steel wall systems – Part 2: Analytical modelling". *Structures*. 30 (January), 1184–1199. doi:10.1016/j.istruc.2020.12.052.

Kyprianou, C., Kyvelou, P., Gardner, L. & Nethercot, D.A. (2020). "Numerical study of sheathed cold-formed steel columns". *Proceedings of the 9th International Conference on Advances in Steel Structures, ICASS 2018*. (December). doi:10.18057/ICASS2018.P.090.

Kyvelou, P., Gardner, L. and Nethercot, D.A., (2018). "Finite element modelling of composite cold-formed steel flooring systems". *Engineering Structures*, 158, pp.28-42.

Kyvelou, P., Gardner, L. & Nethercot, D.A. (2017). "Testing and Analysis of Composite Cold-Formed Steel and Wood−Based Flooring Systems". *Journal of Structural Engineering*. 143 (11), 04017146. doi:10.1061/(asce)st.1943-541x.0001885.

Lange, J. & Naujoks, B. (2007). "Behaviour of cold-formed steel shear walls under horizontal and vertical loads". *Thin-Walled Structures*. 44 (12), 1214–1222. doi:10.1016/j.tws.2007.01.007.

Macillo, V. & Fiorino, L. (2017). "Seismic response of CFS shear walls sheathed with nailed gypsum panels : Experimental tests". *Thin-Walled Structures*. 120 (September), 161–171. doi:10.1016/j.tws.2017.08.022.

McCreless, C.S. (1977). "Shear Resistance Tests of Steel-Stud Wall Panels", Master's Thesis, Department of Civil Engineering, Vanderbilt University, Nashville, TN, USA.

McCreeless, C.S. & Tarpy, T. (1978). "Experimental Investigation of Steel Stud Shear Wall Diaphragms". *Proceedings - Annual Public Water Supply Engineers' Conference*. 2, 647–672.

Mohebbi, S., Mirghaderi, R., Farahbod, F. & Bagheri Sabbagh, A. (2015). "Experimental work on single and double-sided steel sheathed cold-formed steel shear walls for seismic actions". *Thin-Walled Structures*. 91, 50–62. doi:10.1016/j.tws.2015.02.007.

Mojtabaei, S.M., Hajirasouliha, I. & Ye, J. (2021). "Optimisation of cold-formed steel beams for best seismic performance in bolted moment connections". *Journal of Constructional Steel Research*. 181, 106621. doi:10.1016/j.jcsr.2021.106621.

Mowrtage, W., Hasan Yel, N., Pekmezci, B. & Atahan, H.N. (2012). "Load carrying capacity enhancement of cold formed steel walls using shotcreted steel sheets". *Thin-Walled Structures*. 60, 145–153. doi:10.1016/j.tws.2012.06.010.

van der Neut, A. (1969). *The interaction of local buckling and column failure of thin-walled compression members BT - Applied Mechanics*. In: M. Hetényi & W.G. Vincenti (eds.). 1969 Berlin, Heidelberg, Springer Berlin Heidelberg. pp. 389–399.

Nguyen, V.B., Pham, C.H., Cartwright, B. and English, M.A. (2017). "Design of new cold rolled purlins by experimental testing and Direct Strength Method". *Thin-Walled Structures*, *118*, pp.105-112.

Nithyadharan, M. & Kalyanaraman, V. (2012). "Behaviour of cold-formed steel shear wall panels under monotonic and reversed cyclic loading". *Thin-Walled Structures*. 60, 12–23. doi:10.1016/j.tws.2012.05.017.

Pan, C.L. & Shan, M.Y. (2011). "Monotonic shear tests of cold-formed steel wall frames with sheathing". *Thin-Walled Structures*. 49 (2), 363–370. doi:10.1016/j.tws.2010.10.004.

Papargyriou, I. & Hajirasouliha, I. (2021). "More efficient design of CFS strap-braced frames under vertical and seismic loading". *Journal of Constructional Steel Research*. 185 (July), 106886. doi:10.1016/j.jcsr.2021.106886.

Papargyriou, I., Hajirasouliha, I., Becque, J. & Pilakoutas, K. (2021). "Performance-based assessment of CFS strap-braced stud walls under seismic loading". *Journal of Constructional Steel Research*. 183, 106731. doi:10.1016/j.jcsr.2021.106731.

Papargyriou, I., Mojtabaei, S.M., Hajirasouliha, I., Becque, J. & Pilakoutas, K. (2022). "Cold-formed steel beam-to-column bolted connections for seismic applications". *Thin-Walled Structures*. 172 (January), 108876. doi:10.1016/j.tws.2021.108876.

Pehlivan, B.M., Baran, E. & Topkaya, C. (2020). "An energy dissipating hold down device for cold-formed steel structures". *Journal of Constructional Steel Research*. 166, 105913. doi:10.1016/j.jcsr.2019.105913.

Pehlivan, B.M., Baran, E. & Topkaya, C. (2018). "Testing and analysis of different hold down devices for CFS construction". *Journal of Constructional Steel Research*. 145, 97–115. doi:10.1016/j.jcsr.2018.02.007.

Peterman, K.D. & Schafer, B.W. (2013). "Hysteretic shear response of fasteners connecting sheathing to cold - formed steel studs". (January). http://www.ce.jhu.edu/bschafer/sheathedwalls/.

Pourabdollah, O., Farahbod, F. & Rofooei, F.R. (2017). "The seismic performance of K-braced cold-formed steel shear panels with improved connections". *Journal of Constructional Steel Research*. 135 (October 2016), 56–68. doi:10.1016/j.jcsr.2017.04.008.

Qadir, S.J., Nguyen, V.B., Hajirasouliha, I., Ceranic, B., Tracada, E. and English, M.A. (2022). "Shape optimisation of cold roll formed sections considering effects of cold working". *Thin-Walled Structures*, *170*, p.108576.

R Park (1989). "Structural Assemblages From Laboratory Testing". *Bulletin of the New Zealand National Society for Earthquake Engineering*. 22 (3), 155–166.

Ringas, N., Huang, Y. & Becque, J. (2021). "Fastener behaviour in sheathed light-gauge steel stud walls under cyclic and monotonic actions". *Ce/Papers*. 4 (2–4), 517–524. doi:10.1002/cepa.1324.

Schafer, B.W., Ayhan, D., Leng, J., Liu, P., Padilla-Llano, D., Peterman, K.D., Stehman, M., Buonopane, S.G., Eatherton, M., Madsen, R., Manley, B., Moen, C.D., Nakata, N., Rogers, C. & Yu, C. (2016). "Seismic Response and Engineering of Cold-formed Steel Framed Buildings". *Structures*. 8, 197–212. doi:10.1016/j.istruc.2016.05.009.

Schafer, B.W. & Peköz, T. (1998). "Computational modeling of cold-formed steel: Characterizing geometric imperfections and residual stresses". *Journal of Constructional Steel Research*. 47 (3), 193–210. doi:10.1016/S0143-974X(98)00007-8.

Selvaraj, S. & Madhavan, M. (2019). "Investigation on sheathing effect and failure modes of gypsum sheathed cold-formed steel wall panels subjected to bending". *Structures*. 17 (September 2018), 87–101. doi:10.1016/j.istruc.2018.09.013.

Selvaraj, S. & Madhavan, M. (2020). "Structural behaviour and design of plywood sheathed cold-formed steel wall systems subjected to out of plane loading". *Journal of Constructional Steel Research*. 166, 105888. doi:10.1016/j.jcsr.2019.105888.

Selvaraj, S. & Madhavan, M. (2018). "Studies on Cold-Formed Steel Stud Panels with Gypsum Sheathing Subjected to Out-of-Plane Bending". *Journal of Structural Engineering*. 144 (9), 04018136. doi:10.1061/(asce)st.1943-541x.0002069.

Shamim, I., DaBreo, J. & Rogers, C.A. (2013). "Dynamic Testing of Single- and Double-Story Steel-Sheathed Cold-Formed Steel-Framed Shear Walls". *Journal of Structural Engineering*. 139 (5), 807–817. doi:10.1061/(asce)st.1943-541x.0000594.

Shamim, I. & Rogers, C.A. (2013). "Steel sheathed/CFS framed shear walls under dynamic loading: Numerical modelling and calibration". *Thin-Walled Structures*. 71, 57–71. doi:10.1016/j.tws.2013.05.007.

Tarpy, T.S. (1980). "Shear Resistance of Steel-Stud Walls Panels", Proc., Fifth International Specialty Conference on Cold-Formed Steel Structures, StLouis, MO, USA, 331 - 348.

Tarpy, T.S., Girard, J.D. (1982). "Shear Resistance of Steel-Stud Wall Panels", Proc., Sixth International Specialty Conference on Cold-Formed Steel Structures, St-Louis, MO, USA, 449 - 465.

Tarpy, T.S., Hauenstein, S.F. (1978). "Effect of Construction Details on Shear Resistance of Steel-Stud Wall Panels", Project No. 1201-412 sponsored by the AISI, Department of Civil Engineering, Vanderbilt University, Nashville, TN, USA.

Tarpy, T.S., McBrearty, A.R. (1978). "Shear Resistance of Steel-Stud Wall Panels with Large Aspect Ratios", Report No. CE-USS-2, Department of Civil Engineering, Vanderbilt University, Nashville, TN, USA.

Tarpy, T.S., McCreless, C.S. (1976). "Shear Resistance Tests on Steel-Stud Wall Panels", Department of Civil Engineering, Vanderbilt University, Nashville, TN, USA.

TS 498, Turkish code for Design Loads for Buildings (2003). "Turkish Standard Insitute." Necatibey caddesi No. 112 Bakanliklar/Ankara-Turkey

Vieira, L.C.M. & Schafer, B.W. (2012). "Lateral stiffness and strength of sheathing braced cold-formed steel stud walls". *Engineering Structures*. 37, 205–213. doi:10.1016/j.engstruct.2011.12.029.

Wang, J., Wang, W., Xiao, Y. & Yu, B. (2019). "Cyclic test and numerical analytical assessment of cold-formed thin-walled steel shear walls using tube truss". *Thin-Walled Structures*. 134 (November 2018), 442–459. doi:10.1016/j.tws.2018.09.038.

Wang, X. & Ye, J. (2015). "Reversed cyclic performance of cold-formed steel shear walls with reinforced end studs". *Journal of Constructional Steel Research*. 113, 28–42. doi:10.1016/j.jcsr.2015.05.012.

Wu, H., Chao, S., Zhou, T. & Liu, Y. (2018). "Cold-formed steel framing walls with infilled lightweight FGD gypsum Part II: Axial compression tests". *Thin-Walled Structures*. 132 (July 2017), 771–782. doi:10.1016/j.tws.2018.06.034.

Xie, Z., Yan, W., Yu, C., Mu, T. & Song, L. (2018). "Experimental investigation of cold-formed steel shear walls with self-piercing riveted connections". *Thin-Walled Structures*. 131 (October 2017), 1–15. doi:10.1016/j.tws.2018.06.028.

Yanagi, N. & Yu, C. (2014). "Effective Strip Method for the Design of Cold-Formed Steel Framed Shear Wall with Steel Sheet Sheathing". *Journal of Structural Engineering*. 140 (4), 04013101. doi:10.1061/(ASCE)ST.1943-541X.0000870.

Ye, J., Feng, R., Chen, W. & Liu, W. (2016). "Behavior of cold-formed steel wall stud with sheathing subjected to compression". *Journal of Constructional Steel Research*. 116, 79–91. doi:10.1016/j.jcsr.2015.08.028.

Ye, J., Wang, X., Jia, H. & Zhao, M. (2015). "Cyclic performance of cold-formed steel shear walls sheathed with double-layer wallboards on both sides". *Thin-Walled Structures*. 92, 146–159. doi:10.1016/j.tws.2015.03.005.

Ye, J., Wang, X. & Zhao, M. (2016). "Experimental study on shear behavior of screw connections in CFS sheathing". *Journal of Constructional Steel Research*. 121, 1–12. doi:10.1016/j.jcsr.2015.12.027.

Yu, C. & Chen, Y. (2011). "Detailing recommendations for 1.83 m wide cold-formed steel shear walls with steel sheathing". *Journal of Constructional Steel Research*. 67 (1), 93–101. doi:10.1016/j.jcsr.2010.07.009.

Zhang, W., Mahdavian, M. & Yu, C. (2018). "Lateral strength and deflection of cold-formed steel shear walls using corrugated sheathing". *Journal of Constructional Steel Research*. 148, 399–408. doi:10.1016/j.jcsr.2018.06.009.

Zhu, E.C., Guan, Z.W., Rodd, P.D. & Pope, D.J. (2005). "A constitutive model for OSB and its application in finite element analysis". *Holz als roh-und werkstoff*. 63 (2), 87–93.

Appendix A

The tensile tests for CFS members

The loading protocol was applied with a displacement rate of 0.50 mm/min. To eliminate the effect of the loading/strain rate on the mechanical properties of the CFS (Huang & Young, 2014), the tensile test was halted two times; once the yield was reached, and when the ultimate strength was almost achieved. The measured CFS material stress-strain curves of Side-1, Side-2 and bottom coupons are illustrated in Fig. A.1. The static curve was obtained by reducing the stress values to be consistent with the levels observed during the pauses of loading.
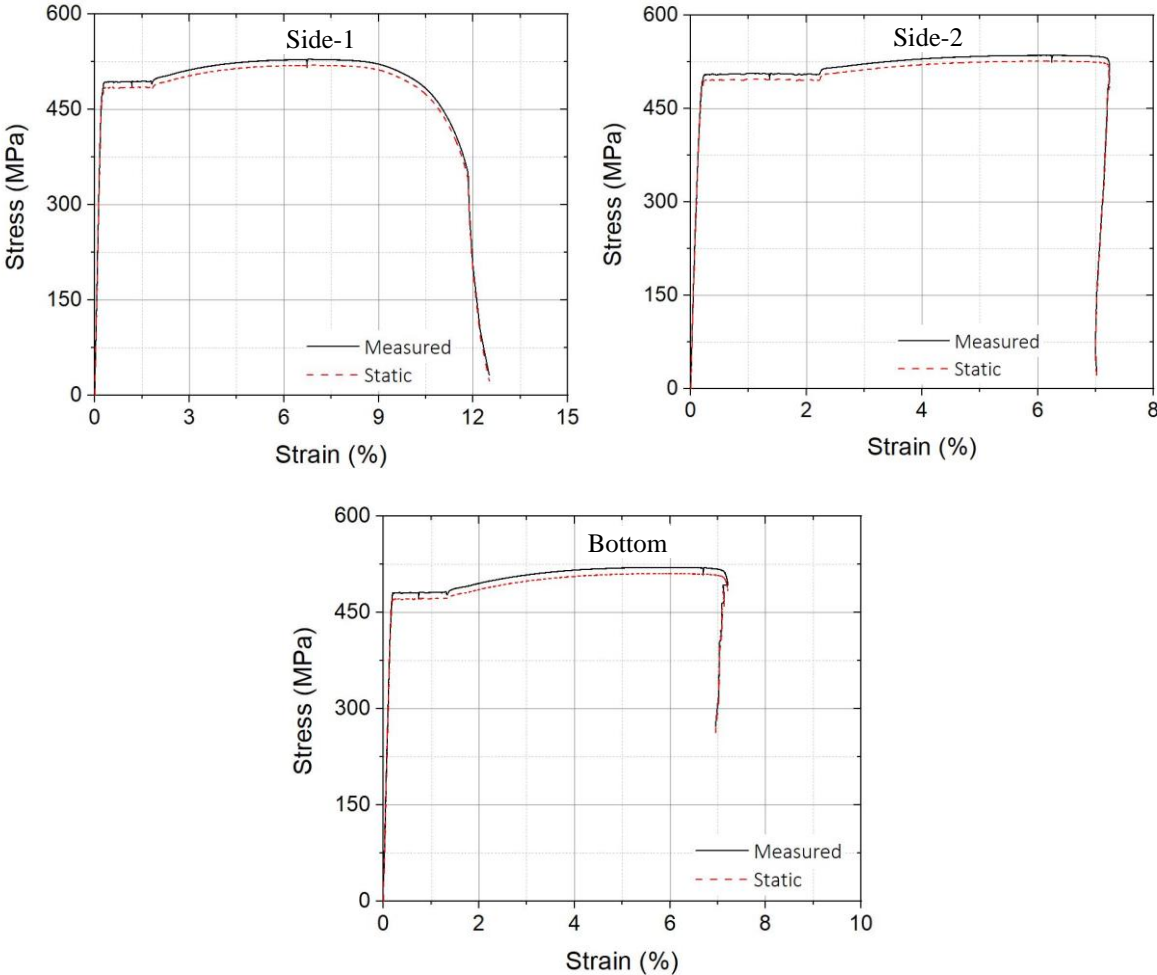
Figure A.1 Stress-strain curve for Side-1, Side-2 and Bottom coupons

Appendix B

The initial geometric imperfections

Fig. B.1 is represented the result of the recording imperfection at the C2 and C4 specimens. The maximum amplitudes of the recorded local and distortional imperfections in the six initial C-shaped elements were explained in Chapters 4-5. The results indicate that the maximum out-of-plane imperfections encountered in the webs of the channels were of the order of 0.6 mm, while the flange of the C-lipped channels exhibited imperfections of up to 0.36 mm.
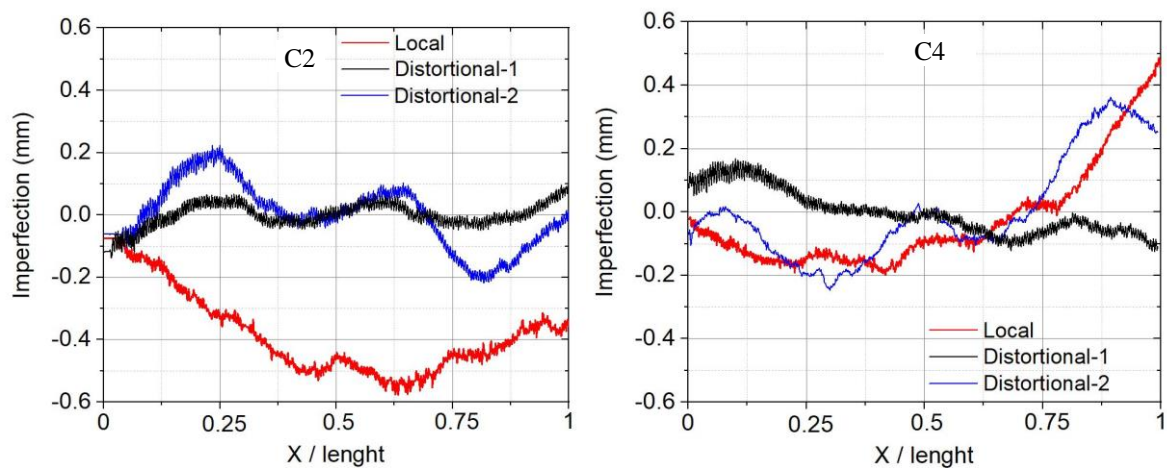
Figure B.1 Typical recorded imperfections for two different CFS lipped channel members

Appendix C

Sheathed Stud wall test data

All 25 face-up and face-down specimens test results was reported in Appendix-C. The results of strain gauges versus the applied load were reported in Figs. C.1-C.5 for the K2, S100 and DB2 face-up specimens and K4 and K5 face-down specimens.
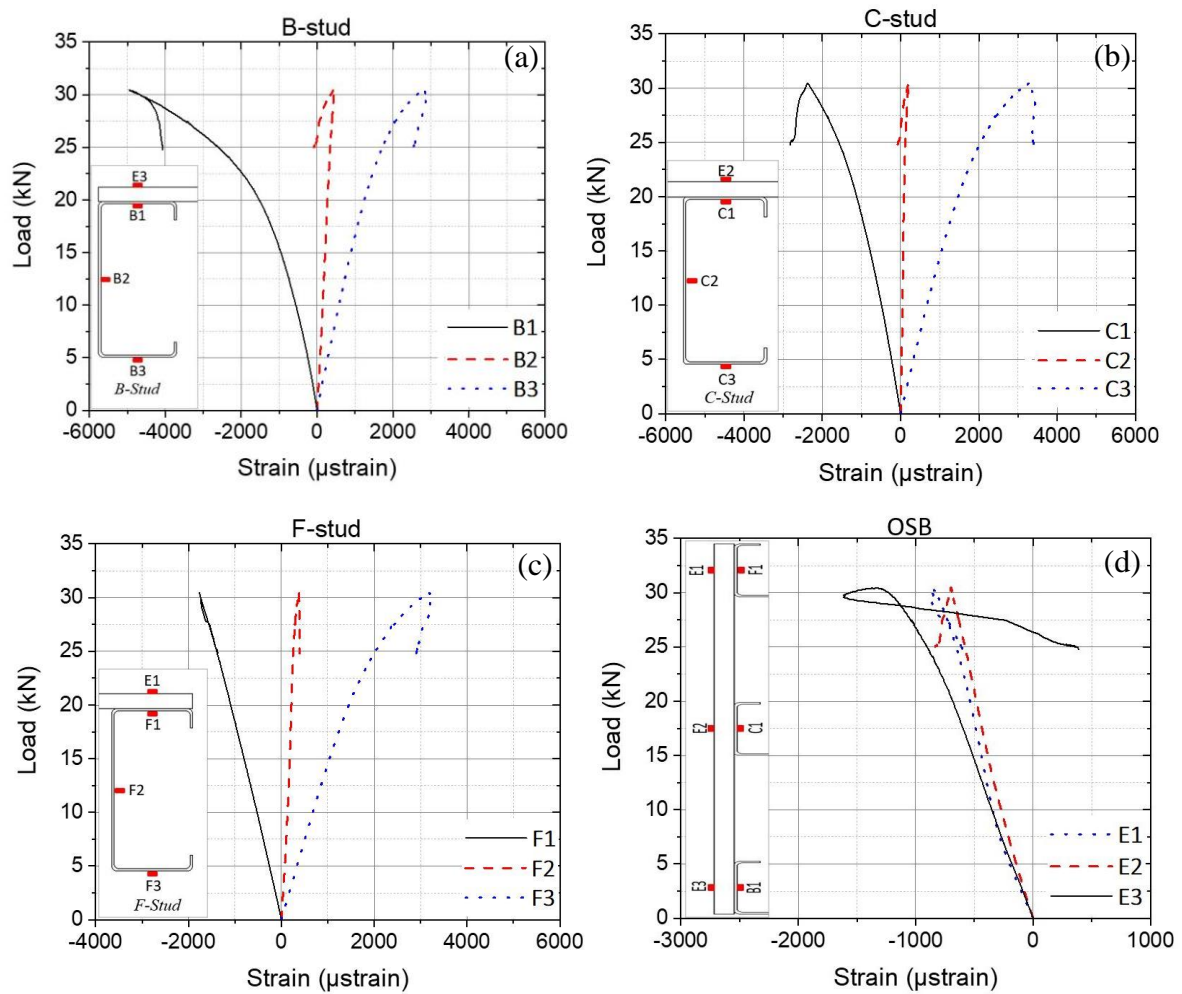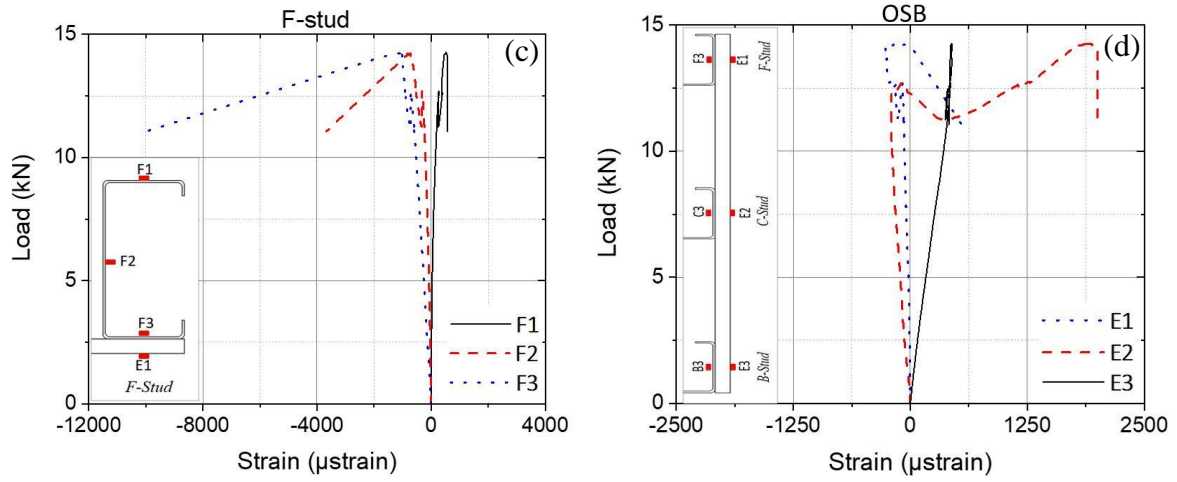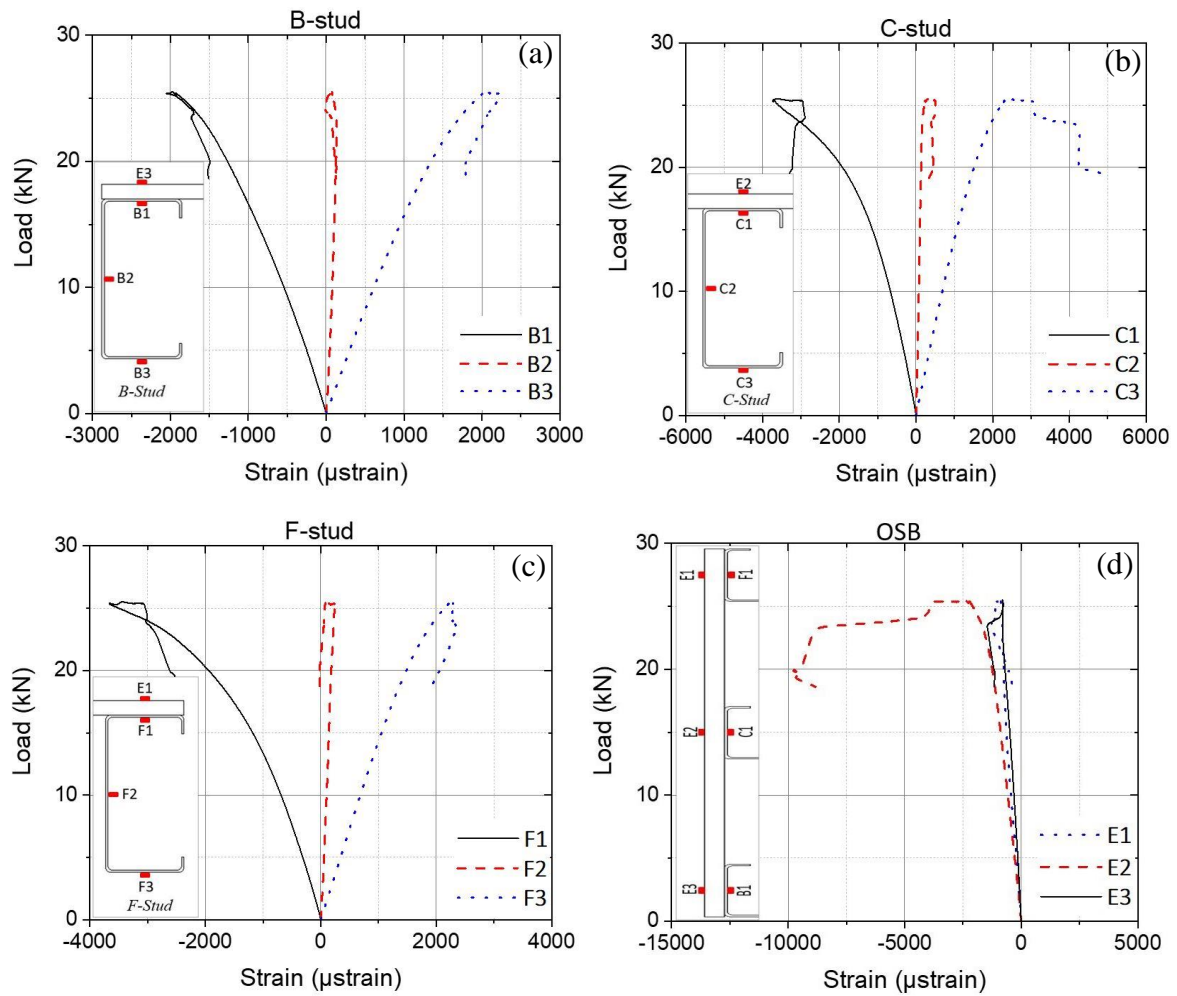

Figure C.1 Load-strain curve for (a) B-stud, (b) C-stud, (c) F-stud and (d) OSB of K2 specimens
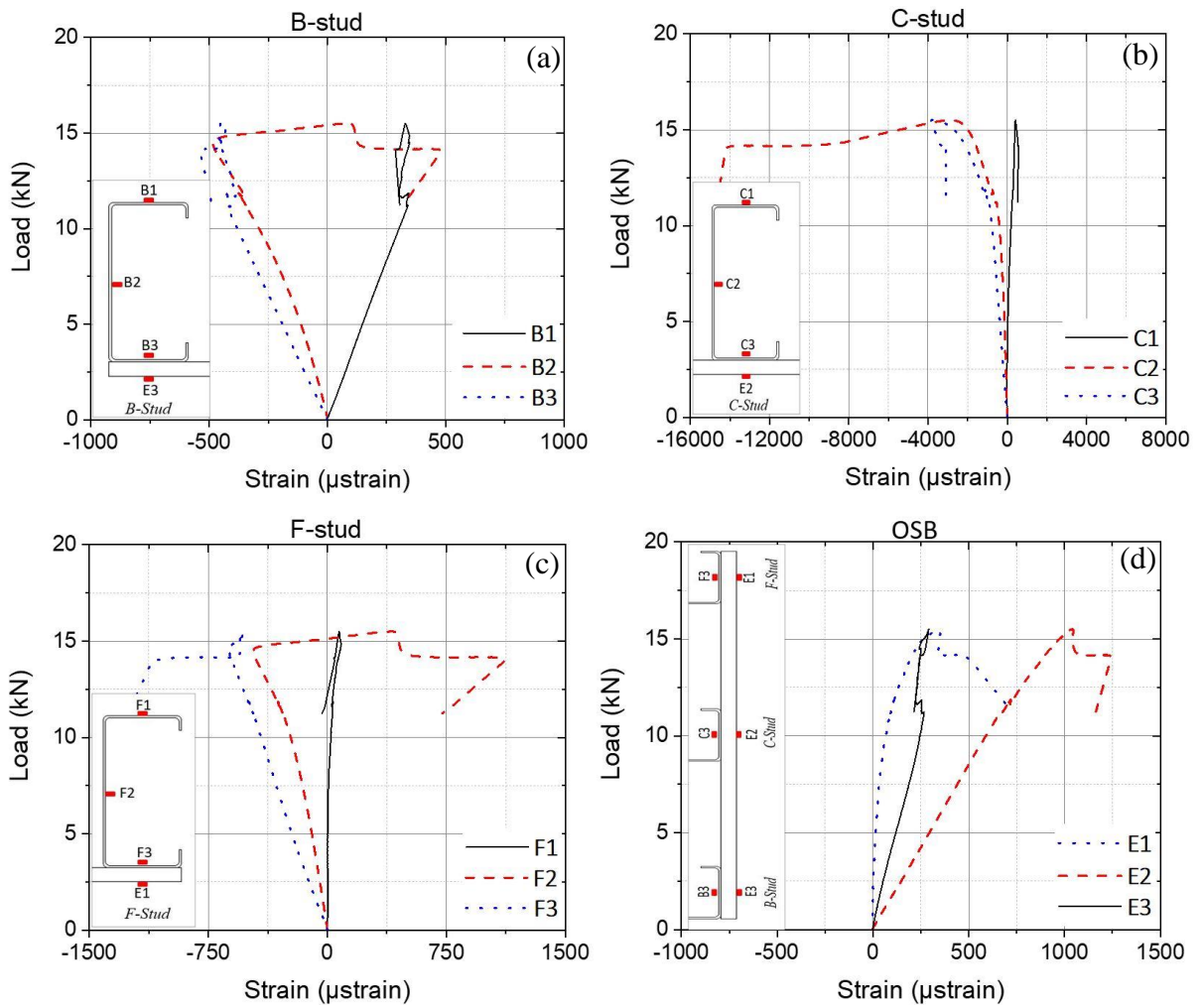
Figure C.2 Load-strain curve for (a) B-stud, (b) C-stud, (c) F-stud and (d) OSB of K4 specimens
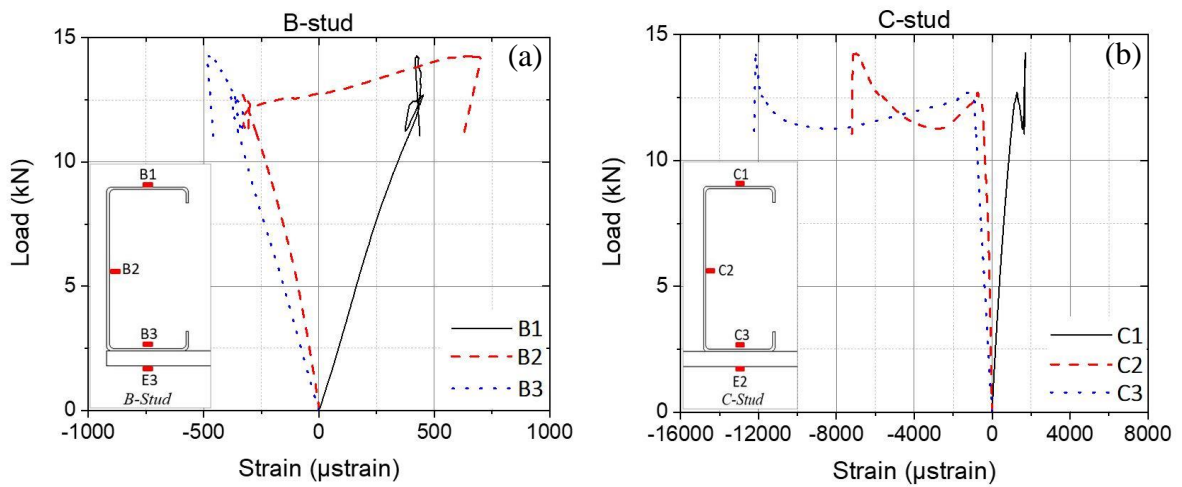
Figure C.3 Load-strain curve for (a) B-stud, (b) C-stud, (c) F-stud and (d) OSB of K5 specimens

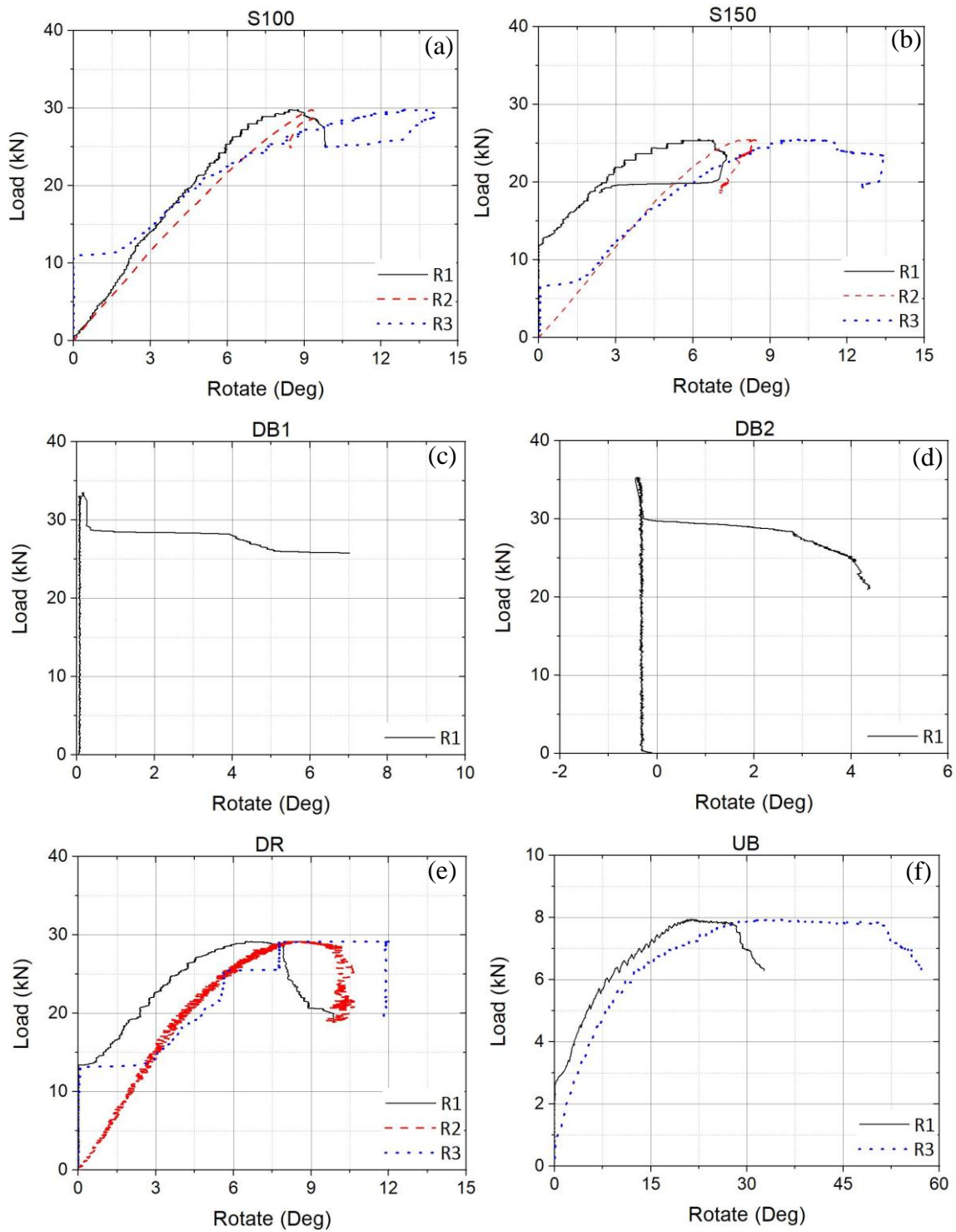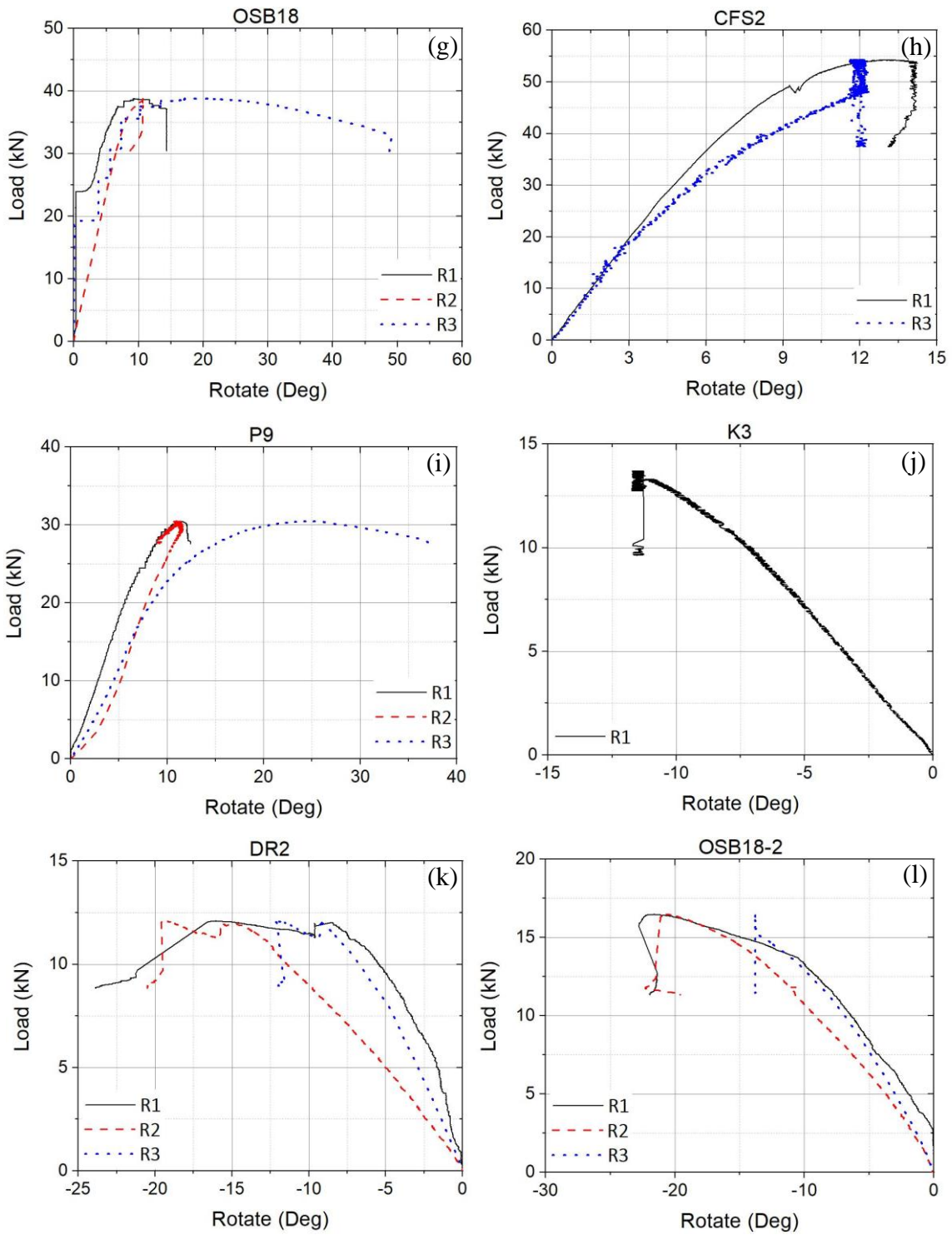*Figure C.4 Load-strain curve for (a) B-stud, (b) C-stud, (c) F-stud and (d) OSB of S100 specimens*
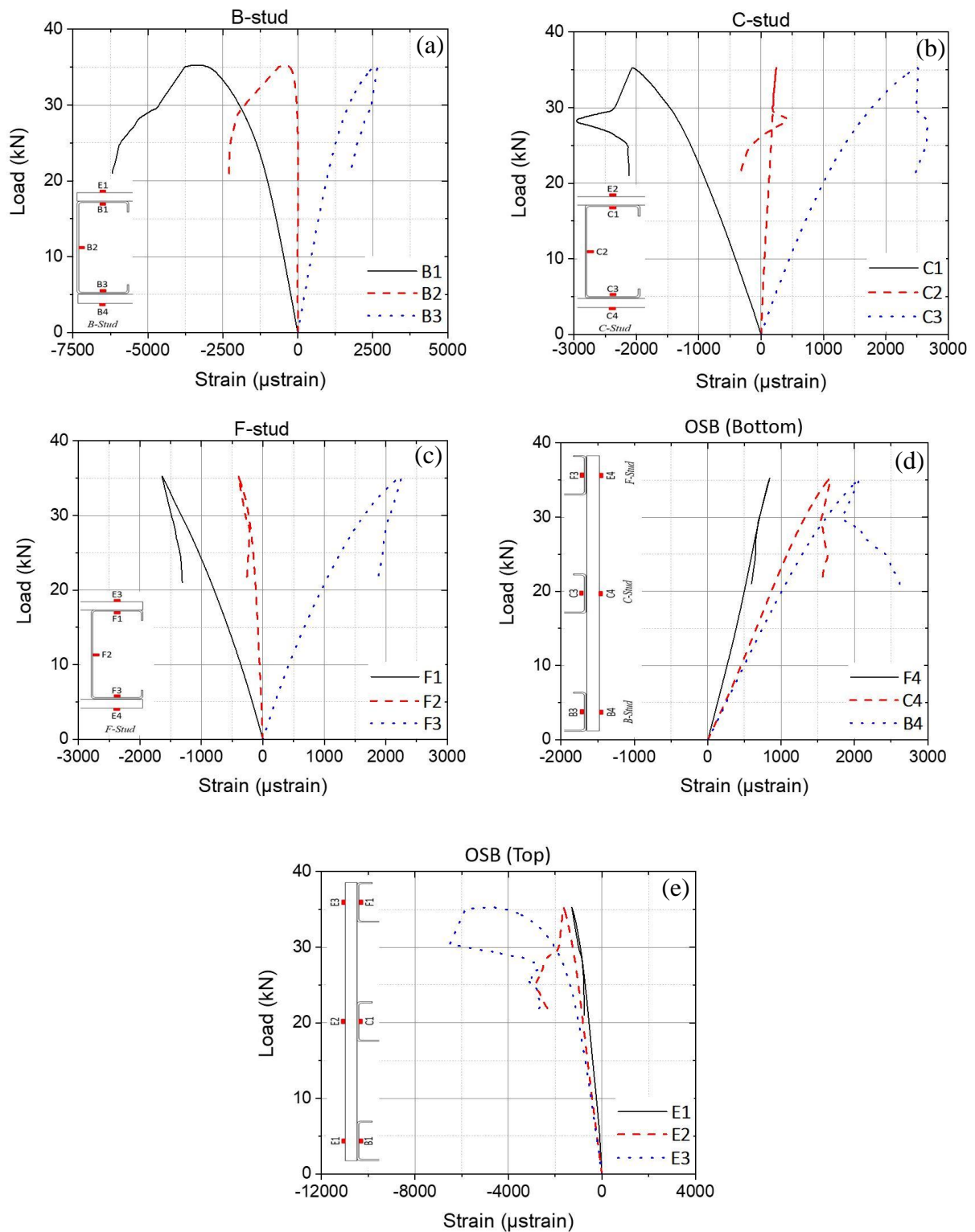
Figure C.5 Load-strain curve for (a) B-stud, (b) C-stud, (c) F-stud (d) OSB (bottom) and (e) OSB (top) of DB2 specimen

The results of rotation of the c-studs versus the applied load were reported in Figs. C.6 for the face-up and face-down specimens.
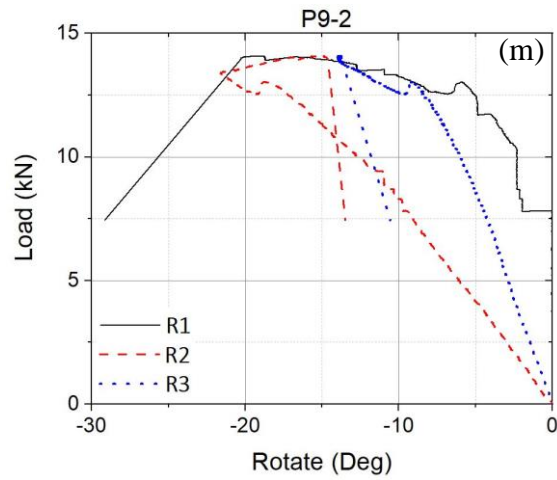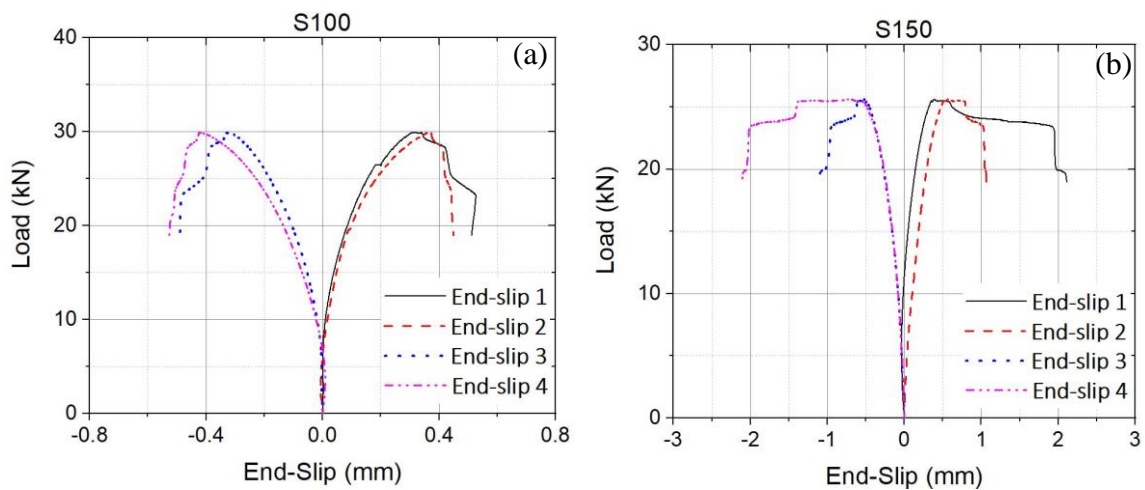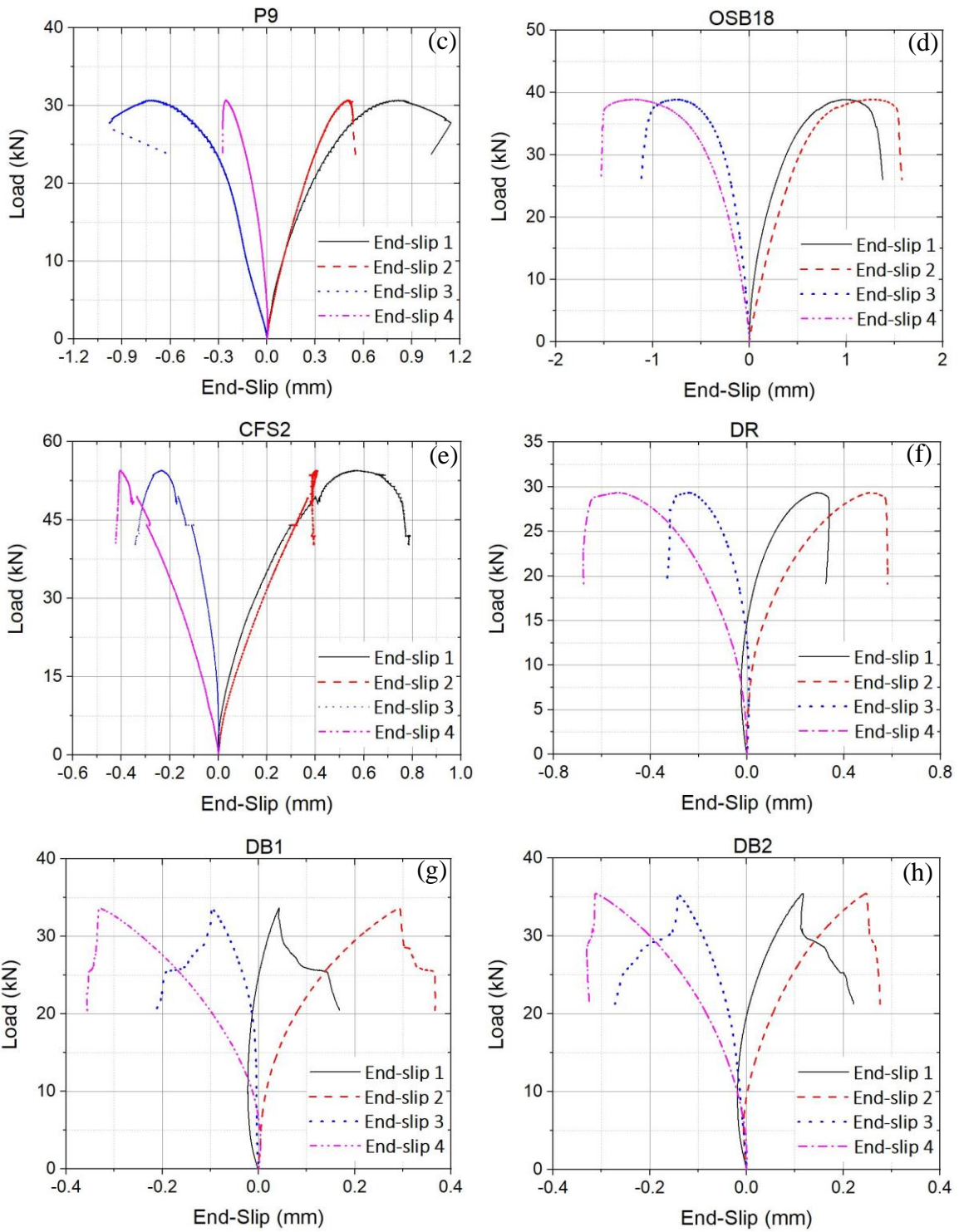
Figure C.6 Rotation of studs along their major axis for: (a) S100, (b) S150, (c) DB1, (d) DB2, (e) DR, (f) UB, (g) OSB18, (h) CFS2, (i) P9, (j) K3, (k) DR2, (l) OSB18 and (m) P9-2 specimens

The results of end-slip of the c-studs versus the applied load were reported in Figs. C.7 for the face-up and face-down specimens.
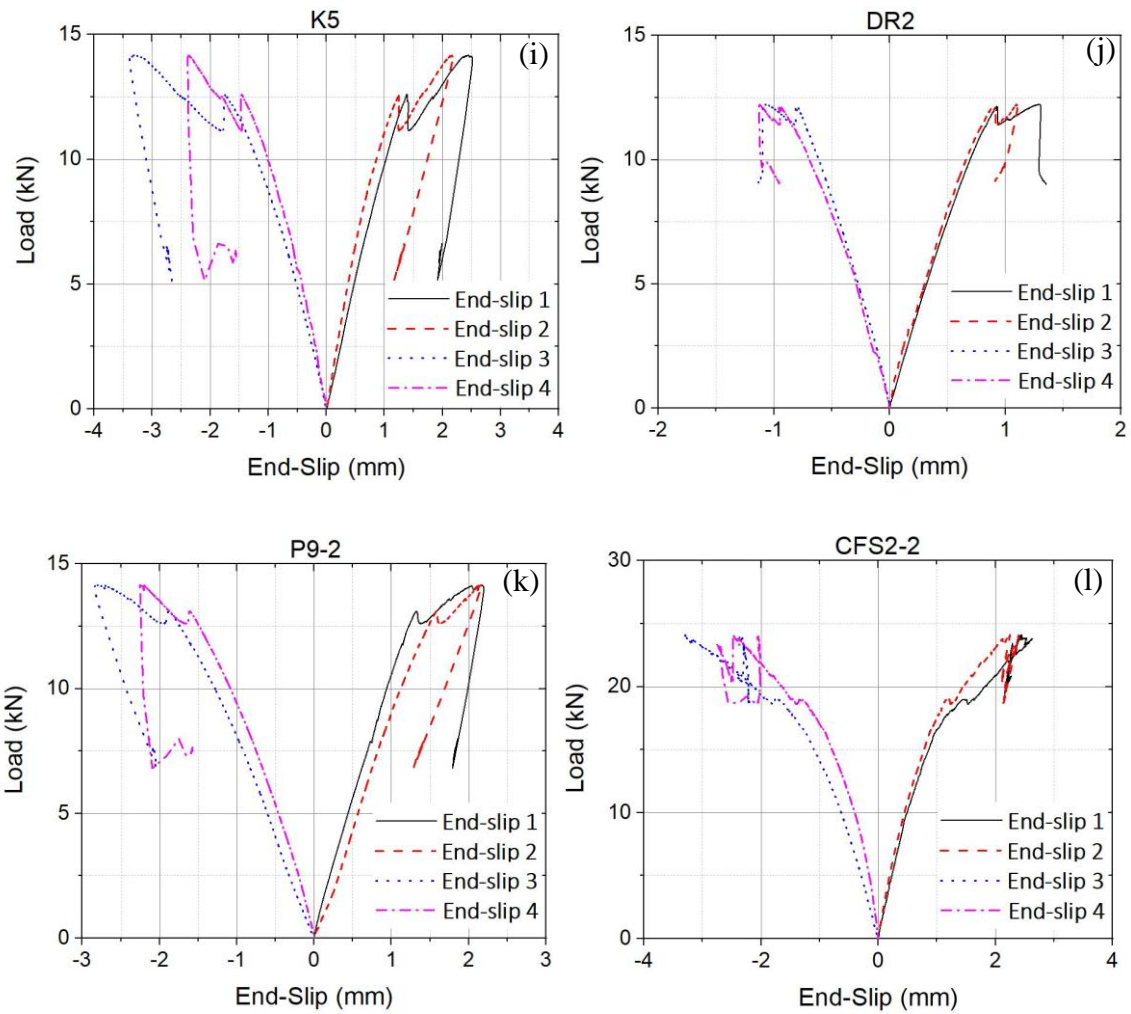
Figure C.7 End-slip measurement histories of: (a) S100, (b) S150, (c) P9, (d) OSB18, (e) CFS2, (f) DR, (g) DB1, (h) DB2, (i) K5, (j) DR2, (k) P9-2 and (l) CFS2-2 specimens

Appendix D

Tension Control Bolt (TCB) Tests

This appendix part presents the investigation into the slip load of 12M Tension Control Bolts (TCB) connecting 3 mm steel plates with galvanized surfaces in a double shear configuration. The technical provisions of Annex G of EN 1090-2 (BSI 2018) were taken as a guidance document. The test specimens were produced according to the dimensions given in Annex G of EN 1090-2. It should be noted that the test specimens differ from this configuration in two respects; the 12M bolts were used, rather than 16M bolts as well as all plate elements had a thickness of 3 mm, rather than the 8 mm/16 mm thicknesses specified in EN 1090-2.

Five nominally identical specimens were tested in a 1000 kN capacity ESH universal testing machine. The loading procedure was displacement controlled. In the first test an initial displacement rate of 0.2 mm/min was imposed, which was increased once the test had progressed well past the slip plateau to 1 mm/min. This resulted in a test duration well beyond 1 hour (and well beyond the duration recommended by EN 1090-2). In the three subsequent tests the displacement rates were therefore increased to 0.5 mm/min and 3 mm/min, before and after the slip plateau, respectively. Four separate LVDTs (Linear Voltage Differential Transducers) were used to monitor the four slip planes, numbered S1-S4 in Figure D.1. In addition, a speckle pattern was applied to the specimens in order to use DIC (Digital Image Correlation) as a second, independent measurement method. In the DIC procedure photographs are taken of the specimen at regular intervals during the test (in this case every 10 seconds) and a GOM software is used to determine the specimen displacements by tracking the speckles. This provides a complete map of the displacement field and an arbitrary amount of measuring points.
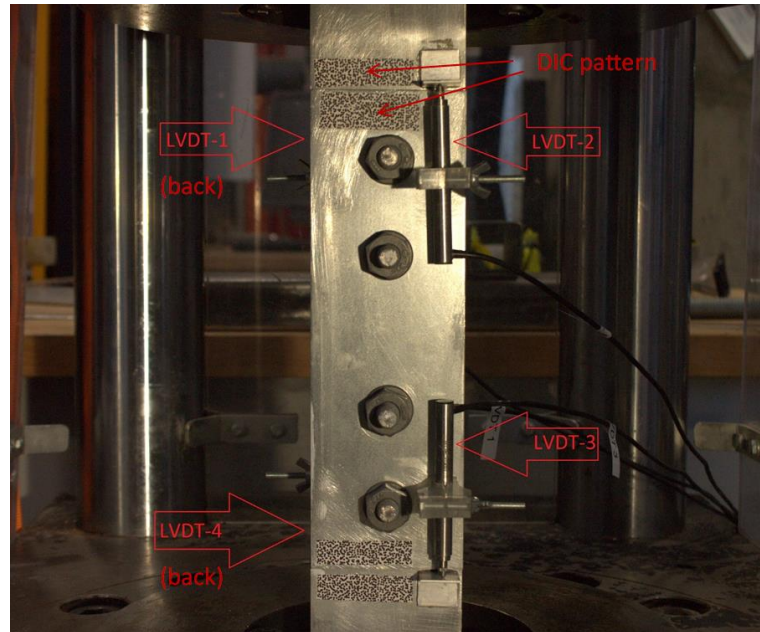
Figure D.1 Test set-up

When increasing the loading slip was first observed in two out of the four slip planes. These were typically located either both at the top (i.e. slip planes S1 and S2 were activated) or both at the bottom (i.e. slip planes S3 and S4 were activated). Fig. D.2 shows an example of the processed DIC data, where the relative displacement of speckles on either side of the outer plate edge is compared to the corresponding LVDT reading. Perfect agreement was obtained, instilling confidence in the results. Table D.1 lists the (peak) slip loads obtained from all 5 tests, with two results derived from each specimen (corresponding to the two slip events).
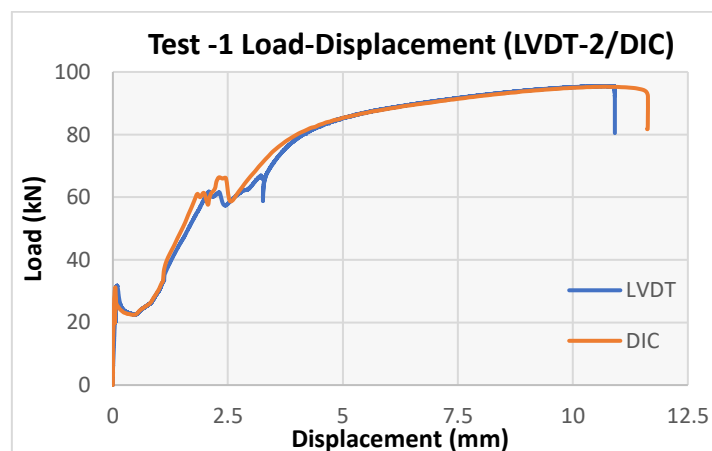

Figure D.2 Test result for Test 1

Table D.1 Main performance parameters for tension control bolts

	First slip		Second slip	
	Load (kN)	Slip planes	Load (kN)	Slip planes
Test 1	31.4	S1-S2	31.7	S3-S4
Test 2	31.6	S1-S2	31.8	S3-S4
Test 3	28.8	S1-S2	28.9	S3-S4
Test 4	36.6	S1-S2	36.4	S3-S4
Test 5	40.1	S1-S2	38.6	S3-S4

Appendix E

Eaves connection

E.1. Introduction

This chapter describes the experimental investigation into the structural performance and capacity as well as provides insight into the failure mechanism of the eaves bolted moment connection system under lateral loading. Although extensive experimental studies conducted for bolted moment connection, there is still a lack of comprehensive investigations on the structural behaviour of the system by considering the effects of key design parameters on the performance. Therefore, a detailed experimental investigation of bolted moment connection (eaves connection) is conducted by considering short/long beam, bolt configurations and different gusset plate scenarios. Based on the results and observations made during experiments, the structural performance parameters (i.e. lateral load capacity, displacement, initial stiffness), failure mechanism were investigated in detail for each parameter.

E.2. Specimen geometry

The main purpose of this experimental investigation is to determine the behaviour and capacity of bolted moment-connection for various parameters under lateral loading. In this experimental test schedule, a total of 5 full-scale eaves connection systems were subjected to lateral loading. The detailed drawing of the specimens is as illustrated in Fig. E.1. The bolted moment-connection is composed by using brackets bolted to the CFS sections (i.e. beam, column and gusset plate) are caused by in the particular area of load transfer from the bolts. The eaves bolted moment-connection specimens of the CFS members were composed of back-to-back C-lipped channel for beam and column members and gusset plate.
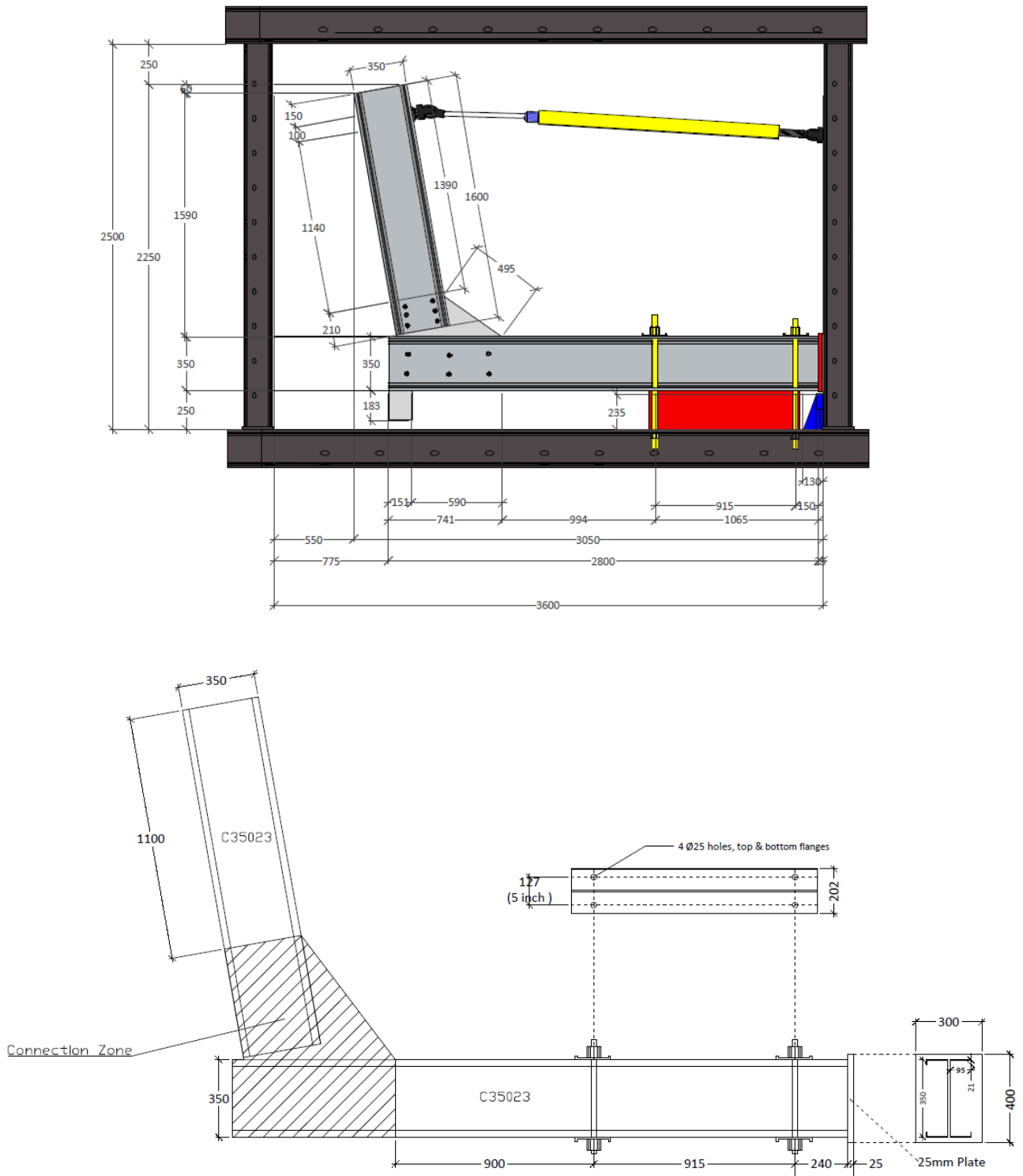
Figure E.1 The detailed drawing of the specimens (in mm)

E.3. Test set-up

Eaves connection specimens were tested under a specially designed monotonic in-plane loading protocol to obtain their lateral behaviour. The test set-up is illustrated in Fig. E.2. A clevis was used to transfer the load from the 150-kN hydraulic jack through pull to beams directly. The data acquisition system was controlled by the National Instrument LabView software, which produced data with a sampling rate of 1 Hz. The loading protocol applied a displacement rate of 1 mm/min.
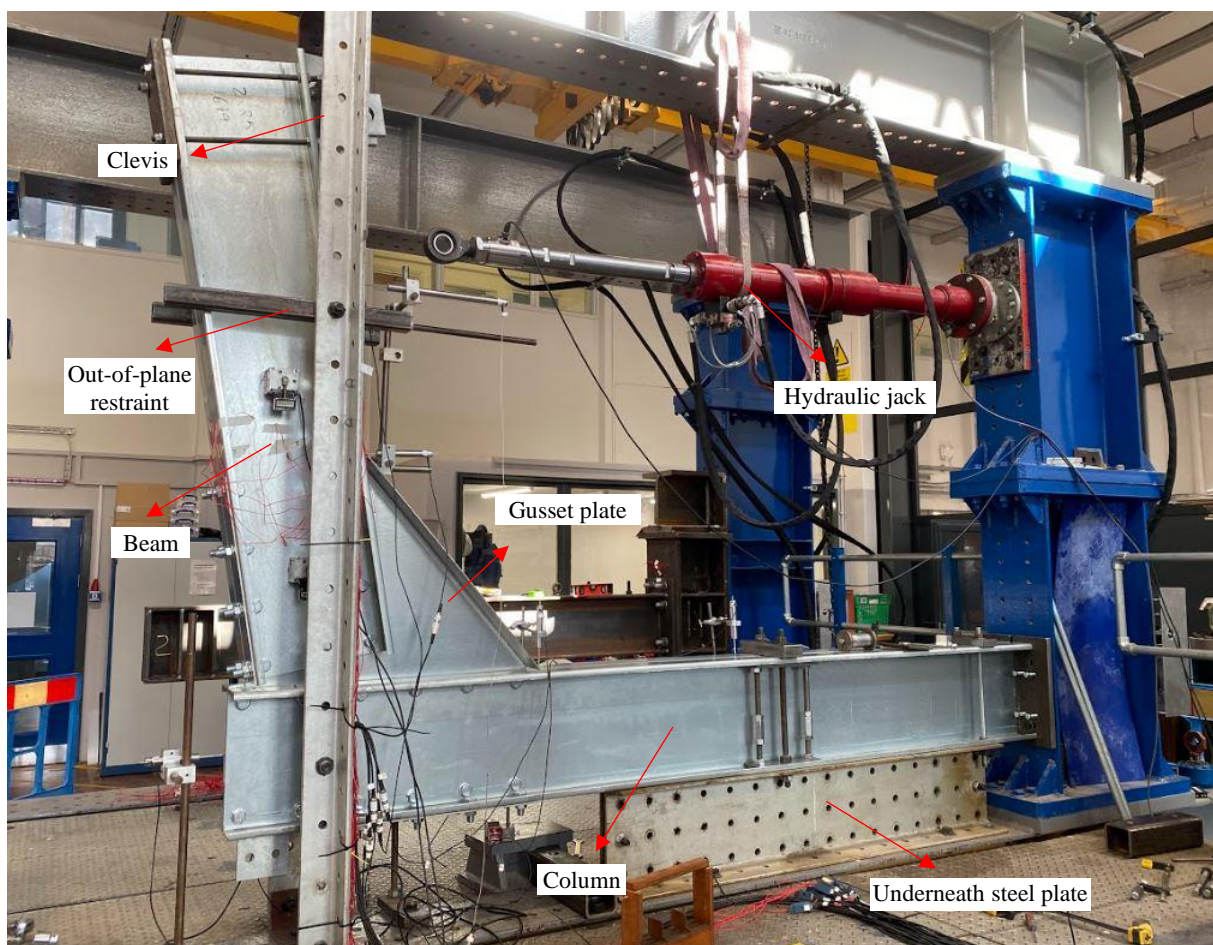

Figure E.2 Test set-up

Strain gauges were attached to the back-to-back C-section beam element close to the connection zone. However, it should be noted that these strain gauge readings were employed to monitor was transmitted consistently to beam members. In addition, to determine the rotation of beam and gusset plate, three inclinometers were installed to the CFS web of the beam and gusset plate

as well as to measure lateral deformations and vertical displacement of the system, ten LVDTs were installed on the eaves connection system.

E.4. Test result

Fig. E.3 illustrates the load versus vertical displacement measured at the centre of the wall for the specimens. The maximum load capacity reached approximately 100 kN and the lateral deflection of the wall centre point at the peak load was about 100 mm. It is noticed that the failure in the beam element close to the connection zone was captured in the specimens. it started with a bit of distortion of the compressive flange within the connection zone. As long as the load was increased, the flange distortion became more obvious and the back-to-back channels started to get separated (from the location of lateral restraint to the connection zone). At peak point, a localised failure happened in the compressive flanges and subsequently the compressive part of the web close to the connection zone, see Fig E.4.
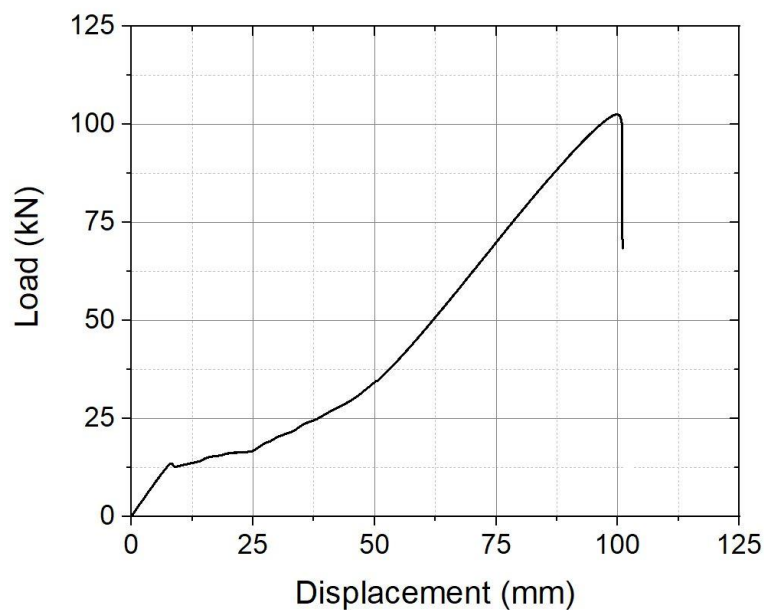
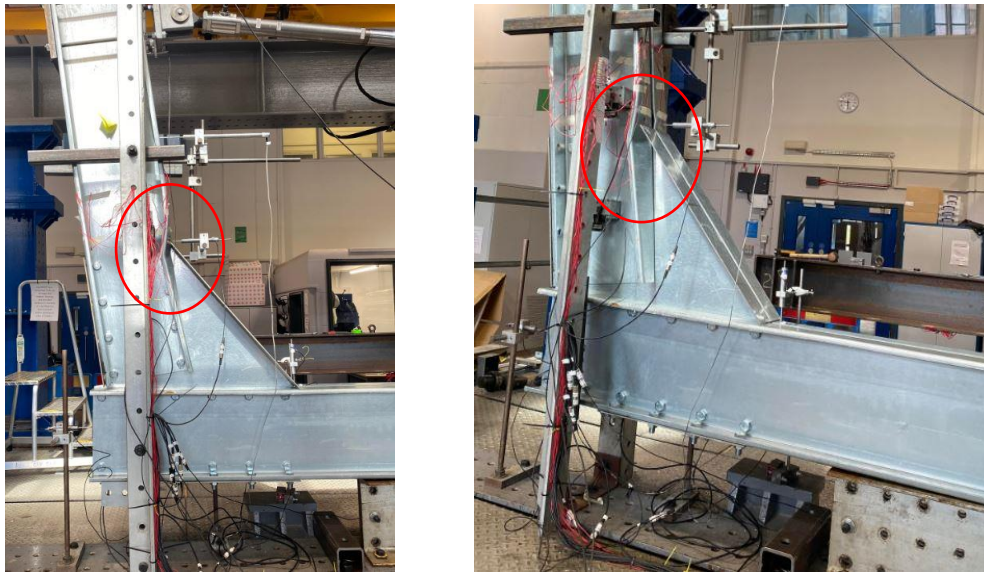

Figure E.3 Load-displacement responses of specimen

Figure E.4 Failure modes of specimens

E.5. Summary and conclusions

This chapter investigated the bending behaviour and capacity of bolted moment connection by considering the effects of key design parameters on the performance of these systems as one of the emerging systems used in modern modular construction. For this purpose, a comprehensive experimental programme was conducted on the eaves connection systems by systematically varying key design variables, including the short/long beam, bolt configurations and different gusset plate scenarios. The results were used to investigate the main structural performance parameters (i.e. lateral load capacity, stiffness) and failure mechanism of the tested specimens.